PROTEOMIC AND MICROARRAY IDENTIFICATION OF NOVEL CARDIAC SPECIFIC INDICATORS OF OXIDATIVE INJURY AND MECHANISM OF ACTION

By

Lifang Xie

A Dissertation Submitted to the Faculty of the

DEPARTMENT OF PHARMACOLOGY

In Partial Fulfillment of the Requirements
For the Degree of

DOCTOR OF PHILOSOPHY
WITH A MAJOR IN MEDICAL PHARMACOLOGY

In the Graduate College

THE UNIVERSITY OF ARIZONA

2007

THE UNIVERSITY OF ARIZONA
GRADUATE COLLEGE

As members of the Dissertation Committee, we certify that we have read the dissertation prepared by Lifang Xie

entitled "Proteomic and Microarray Identification of Novel Cardiac Specific Indicators of Oxidative Injury and Mechanism of Action"

and recommend that it be accepted as fulfilling the dissertation requirement for the Degree of Doctor of Philosophy.

_____ Date: 07-18-2007
Dr. Qin Chen

_____ Date: 07-18-2007
Dr. Marilyn Halonen

_____ Date: 07-18-2007
Dr. Robert Sloviter

_____ Date: 07-18-2007
Dr. Todd Vanderah

Final approval and acceptance of this dissertation is contingent upon the candidate's submission of the final copies of the dissertation to the Graduate College.

I hereby certify that I have read this dissertation prepared under my direction and recommend that it be accepted as fulfilling the dissertation requirement.

_____ Date: 07-18-2007
Dissertation Director: Dr. Qin Chen

STATEMENT BY AUTHOR

This dissertation has been submitted in partial fulfillment of requirements for an advanced degree at The University of Arizona and is deposited in the University Library to be made available to borrowers under rules of the Library.

Brief quotations from this dissertation are allowable without special permission, provided that accurate acknowledgement of source is made. Requests for permission for extended quotation from or reproduction of this manuscript in whole or in part may be granted by the head of the major department of the Dean of the Graduate College when in his or her judgement the proposed use of the material is in the interests of scholarship. In all other instances, however, permission must be obtained from the author.

SIGNED: Lifang Xie

ACKNOWLEDGEMENTS:

Although there is only one name as the author of this work, countless others are silent contributors to the successful completion of this Dissertation. One person that I will forever feel indebted to is my advisor, Dr. Qin Chen. Without her guidance, encouragement, patience, and support, I would never have accomplished a body of research so rich, exciting, and intellectually-rewarding. Not only did she light up the road of my studying abroad, she also taught me how to be a real scientist, and served as a role model of a successful woman with both family and career. I am also thankful to all of the members of my graduate advisory committee, Dr. Marilyn Halonen, Dr. Glenn Sipes, Dr. Robert Sloviter, Dr. Todd Vanderah, and Dr. Douglas Larson. Your thoughtful advice and comments on improving my research and dissertation over the years were very much appreciated. Special thanks also go to Dr. George Tsaprailis, Dr. George Watts and Dr. Ritu Pandey for helping me out with the proteomics and microarray data analyses. I am grateful for the help I received from past and present members of the Chen Laboratory. In particular, Beibei Xu has been invaluable in helping me finish my work, and Chunyi Tu, Tarrah Kirkpatrick, Jerome Terrand, Sally Elizabeth Purdom-Dickinson, Lena Sheveleva, Haipeng Sun and Steve Morrissey have all made my life easier in some way. Last but not least, I would thank my husband, Wenjian, for all your love and support.

DEDICATION:

I dedicate this dissertation to my family members in the USA and in China.

TABLE OF CONTENTS

TABLE OF CONTENTS-*Continued*

LIST OF FIGURES

LIST OF TABLES

ABSTRACT

Cardiovascular disease (CVD) is the leading cause of death in the United States. Oxidative stress plays an important role in the pathogenesis of CVD. Heart failure is the end point of many forms of CVD. The purpose of this study is to identify novel cardiac specific indicators of oxidative injury useful for early and convenient diagnosis of heart failure.

To determine the most suitable method for identification of non-invasive oxidative injury indicators in general, human diploid fibroblasts (HDFs) were treated with H_2O_2 for collection of mRNA, cell lysates and conditioned media to perform cDNA microarray and LC-MS/MS based Multidimensional Protein Identification Technology (MudPIT) analyses. Electron Spray Ionization (ESI)-LC-MS/MS analysis of the conditioned media led to the finding of IGFBP-6 as a non-invasive biomarker of cell oxidative injuy *in vitro* and *in vivo*. The data obtained from this study indicate that proteomic analysis of conditioned media is useful to identify non-invasive biomarkers valuable for diagnosis or management of diseases.

Cardiomyocyts (CMCs) and Cardiac fibroblasts (CFs) in culture were used to identify cardiac specific indicators of oxidative stress. Increased level of Cystatin C was detected in the conditioned medium of CMCs due to H_2O_2 treatment. In vivo models of oxidative stress were used to validate the increase of Cystatin C. Cystatin C levels increased in the plasma of mice with doxorubicin induced cardiomyopathy and coronary artery occlusion induced myocardial infarction (MI). These data indicate that Cystatin C can be a potential indicator of CMC oxidative injury *in vitro* and *in vivo*.

Cystatin C is a cysteine protease inhibitor. The finding that oxidative stress induces Cystatin C led us to investigate a novel pathway regulating cardiac extracellular matrix (ECM) with CFs in culture, increased levels of ECM protein and decreased levels of Cathepsin B (CTB) protein and activity were detected upon Cystatin C treatment. With coronary artery occlusion induced MI mouse model, increased levels of Cystatin C and ECM protein and decreased levels of CTB protein and activity were detected in the infarcted area of the myocardium. These data indicate that Cystatin C serves as a potential fibrotic factor during myocardial remodeling.

CHAPTER I: INTRODUCTION

Cardiovascular disease (CVD) is the Number one killer among all natural death worldwide (1). The mortality data show that CVD as the underlying cause of death accounted for 36.3% (871 517) of all 2 398 000 deaths in 2004, or 1 of every 2.8 deaths in the United States. Nearly 2400 Americans die of CVD each day, an average of 1 death every 36 seconds. CVD claims more lives each year than cancer, chronic lower respiratory diseases, and diabetes mellitus combined (2).

Autonomic control of the cardiovascular system

The autonomic nervous system (ANS) is part of the peripheral nervous system and controls contractile function of many organs such as the heart, stomach and intestines and muscles within the body. The ANS conveys sensory impulses from the blood vessels, the heart and all of the organs in the chest, abdomen and pelvis through nerves to other parts of the brain mainly the medulla, pons and hypothalamus. These impulses often do not reach our consciousness, but elicit largely automatic or reflex responses through the efferent autonomic nerves, thereby eliciting appropriate reactions of the heart, the vascular system, and all the organs of the body to variations in environmental temperature, posture, food intake, stress and many other changes.

The hypothalamus projects to the medulla, where the cells that drive the ANS are located. These include the parasympathetic vagal nuclei and a group of cells that descend to the sympathetic system in the spinal cord. The vasomotor medullary center located in the brainstem above the spinal cord, receives sensory input from different systemic and

central receptors (eg., baroreceptors and chemoreceptors) as well as signals from other brain regions (eg., hypothalamus) (Fig.1.1). The autonomic flow from the medulla center is divided principlely into two main branches: parasympathetic nervous system (PNS) and sympathetic nervous system (SNS).

The heart and blood vessels are innervated by both PNS and SNS. The cell bodies of the PNS are located in the spinal cord (sacral region) and in the medulla. In the medulla, the cranial nerves III, VII, IX and X form the preganglionic parasympathetic fibers. Other parasympathetic fibres emerge from the second, third, and fourth sacral segments of the spinal cord. The preganglionic fiber from the medulla or spinal cord projects to the ganglia close to target organs and makes a synapse. This synapse uses the neurotransmitter called acetylcholine (Ach). From this ganglion, the post-ganglionic neuron projects to and uses Ach again at the heart and blood vessels. Ach usually binds to muscarinic receptors (mAchRs) on these target organs to elicit "Rest and Digest" responses, such as decreasing the heart rate and blood pressure. The SNS originates in the spinal cord. Specifically, the cell bodies of the preganglionic neuron are located in the thoracic and first three segments of the spinal cord. Axons from these neurons project to a chain of ganglia located near the spinal cord. In most cases, this neuron makes a synapse with the post-ganglionic neuron in the ganglion. The synapse in the sympathetic ganglion also uses Ach as the neurotransmitter. The post-ganglionic neuron then projects to the heart and blood vessel and utilizes norepinephrine (NE) as the final transmitter at these target organs. NE binds to adrenoceptors (α_1-AR, β_1-AR and β_2-AR) on the heart and blood vessels to elicit "Fight or Flight" responses if necessary, such as rising in heart

beats and increasing blood pressure. A few preganglionic neurons act on other ganglia outside of the sympathetic chain and synapse there. The adrenal medulla is a modified sympathetic ganglion. It receives sympathetic preganglionic fibers via nictinic acetylcholine receptors (nAchR) and releases epinephrine into the bloodstream. The target tissue for epinephrine is mainly cardiac and skeletal muscles (Fig.1.1).

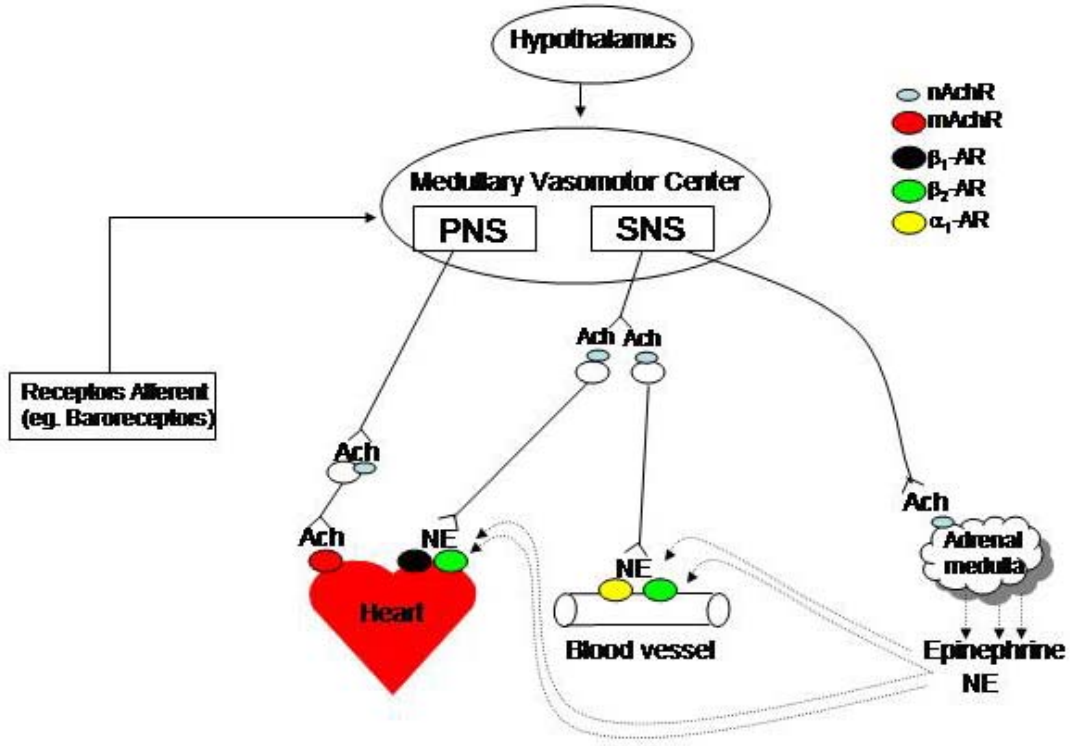

Fig.1.1 Proposed scheme of autonomic innervation of the heart and vasculature

The contractile function of the heart and blood vessels are regulated by both PNS and SNS (Fig.1.2). SNS innervation on the heart results in increased conduction velocity, increased heart rate, and increased contractility. In the blood vessels, sympathetic activation causes constriction of vascular smooth muscle via α_1-AR, resulting in an increase in peripheral resistance and consequently, an increase in the blood pressure. On the other hand, sympathetic activation of β_2-ARs located in skeletal muscle vascular beds, splanchnic vessels, and coronary vessels can cause relaxation of vascular smooth muscle, resulting in a decrease in peripheral vascular resistance and a drop in blood pressure. PNS innervation on the heart results in decreased heart rate and decreased conduction velocity. Most blood vessels in the body do not have PNS innervation. Physiologically, whenever the body activates the sympathetic system, it down regulates parasympathetic activity, and vice versa, so that the activites of these two branches of the autonomic nervous system respond reciprocally. For an example, both SNS and PNS are involved in the process of blood pressure regulation (Fig.1.2). An acute drop in blood pressure can be detected by the baroreceptors in the carotid arteries and in the aorta, resulting in an inhibition of firing rate. Inhibitory afferents from these structures are sensed and integrated by the vasomotor centers of the SNS, causing an increased sympathetic nervous stimulation. Sympathetic efferents flow to the heart, act onto β-ARs to increase myocardial contractility and heart rate, generating a greater cardiac output. Efferents to the blood vessels stimulate postsynaptic α-ARs, resulting in arteriolar vasoconstriction. Stimulation of venous α-ARs decreases venous capacitance, increases venous return to the heart and improves cardiac output. These changes collectively result in an increase in

the blood pressure. In contrast, increases in the blood pressure can be detected by the baroreceptors in the aorta and carotid arteries, resulting in an increase in the firing rate. Afferent excitatory impulses from these structures are integrated in the vasomotor centers of the sympathetic nervous system, resulting in a decreased sympathetic response consequently decreased vascular tone and decreased heart rate and a corresponding increased parasympathetic response. Parasympathetic efferents to the heart act mainly through mAchRs to decrease the heart rate and conduction velocity, resulting in decreased cardiac output. These changes collectively produce a feedback decrease in the blood pressure (Fig.1.2).

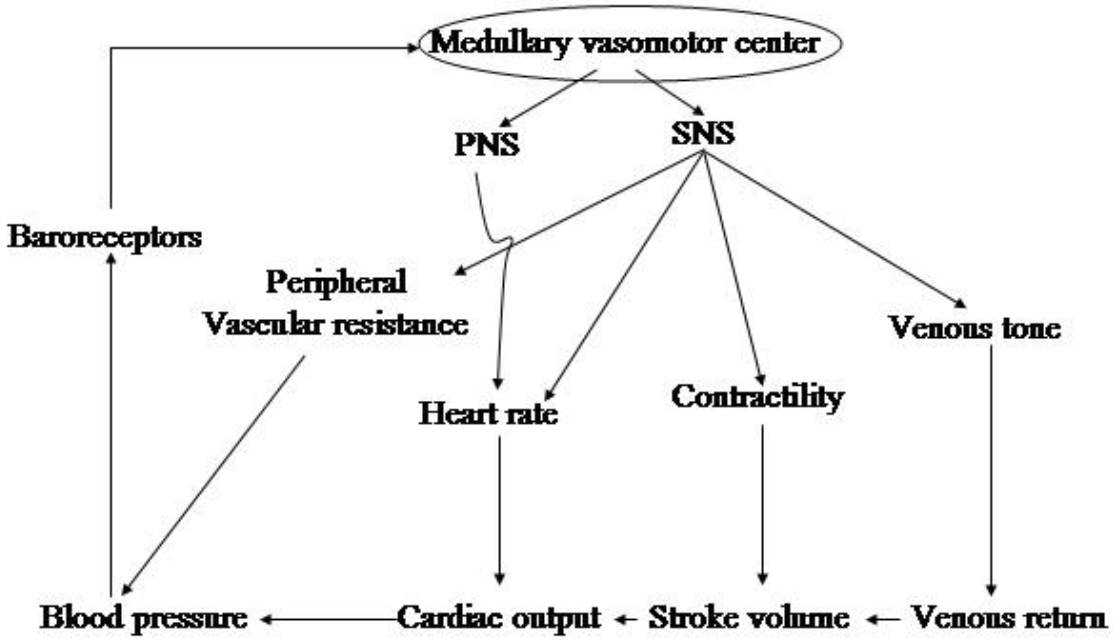

Fig.1.2. Proposed scheme of autonomic control of cardiovascular function

Atherosclerosis and myocardial infarction

What is atherosclerosis?

Atherosclerosis, derived from the Greek words athero (meaning gruel or paste) and sclerosis (hardness), is a general term for the thickening and hardening of arteries. The process of developing atherosclerosis involves deposition of fatty substances, cholesterol, cellular waste products, calcium and other substances in the inner lining of an artery, with a co-existent inflammatory response and proliferation of smooth muscle cells. This buildup, so called plaque, usually affects large and medium-sized arteries. Atherosclerosis is a pathologic condition that underlies several life threatening disorders including coronary artery disease, eg. myocardial infarction (MI or heart attack), cerebrovascular disease, eg. cerebral infarction or stroke, and peripheral artery disease.

Risk factors of atherosclerosis

Risk factors for atherosclerosis include smoking, high blood pressure, diabetes mellitus, obesity, dyslipidemia, physical inactivity, increased inflammatory reaction, infection and high blood levels of homocysteine. These risk factors can usually be modified. Risk factors that cannot be modified include having a family history of early atherosclerosis, advance age, and male sex. Men have a higher risk than women to develop atherosclerosis. Many of these risk factors such as smoking, hyperlipidaemia, diabetes mellitus, hypertension, obesity, and chronic systemic infection have been found to be associated with endothelial dysfunction.

The response to injury hypothesis of atherosclerosis

The endothelium is a continuous layer of cells that separate blood from the vessel wall. Several different factors, including elevated levels of LDL cholesterol and triglyceride in the blood, high blood pressure, smoking and diabetes, can cause injury to the endothelium, leading to endothelial cell dysfunction. Atherosclerotic plaques originate when the endothelium is injured. Injured endothelial cells express adhesion molecules such as vascular cell adhesion molecule-1 (VCAM-1) and intracellular adhesion molecule-1 (ICAM-1), which recruit circulating macrophages and T lymphocytes into the localized area of endothelium of the artery's wall. The earliest lesion of atheroscrosis is called the 'fatty streak', an aggregation of lipid-rich macrophages and T lymphocytes within the innermost layer of the artery wall, the intima (3). Activation of these monocytes results in production of inflammatory cytokines, which may cause smooth muscle cells underneath the endothelium to replicate. These vascular smooth muscle cells produce extracellular matrix proteins such as collagen and fibronectin, which form the substance of the fibrous cap of the mature lesion. Connective tissue, elastic tissue, cell debris and cholesterol crystals also accumulate within the fibrous cap. This accumulation of fat-laden cells, smooth muscle cells, and other materials form a patchy deposit called an atheroma or atherosclerotic plaque. As they grow, atheromas thicken the artery's wall and bulge into the channel of the artery. Over time, calcium accumulates in the atheromas, causing the atheroma to become fragile. Rupture of atheroma causes the spill of its fatty contents into the bloodstream. This fatty mass, i.e. fat embolus may travel through the bloodstream and block an artery in the body.

Atherosclerosis and myocardial infarction

Abnormal blood clotting is one of the causes of myocardial infarction. The rupture of an atherosclerotic plaque exposes the thrombotic core of the lesion to the circulating blood, initiating platelet aggregation and coagulation and triggering the formation of a blood clot, i.e. thrombus. The thrombus may occlude the artery at the site of formation or may detach (becoming an embolus), traveling through the blood stream, and block the blood vessel downstream. Thrombotic occlusion secondary to plaque disruption in a coronary artery is the most common cause of myocardial infarction (MI).

Acute Myocardial Infarction: Diagnosis

According to the World Health Organization, the diagnosis of myocardial infarction requires at least two of the following three criteria: (a) a clinical history of ischemic-type chest discomfort, (b) serial electrocardiographic tracings indicative of myocardial infarction, and (c) a rise and fall in serum cardiac markers (4). However, the advent and widespread adoption of novel diagnostic tools, including highly sensitive and specific serologic biomarkers and precise imaging techniques, have necessitated reevaluation of this established definition. The Joint European Society of Cardiology/American College of Cardiology Committee for the Redefinition of Myocardial Infarction has integrated these diagnostic modalities and published updated definitions of acute myocardial infarction. The basis of the new definition is the promotion of troponins to a pivotal role in the diagnosis of acute myocardial infarction,

coupled with the relegation of creatine kinase (CK-MB) to a secondary role; and, in the case of total CK, to the last of the consideration.

Classical symptoms of acute myocardial infarction include chest pain, shortness of breath, nausea, vomiting, palpitations, sweating and anxiety. The severity of an MI is dependent on three factors: the level of the occlusion in the coronary artery, the length of time of the occlusion, and the presence or absence of collateral circulation. Generally speaking, the more proximal the coronary occlusion, the more extensive is the amount of myocardium at risk of necrosis. The larger the MI, the greater is the chance of death due to a mechanical complication or pump failure. The longer the time period of vessel occlusion, the greater the chances of irreversible myocardial damage distal to the occlusion.

Therapy for atherothromobotic disease

Therapy for atherothrombotic disease includes: 1) Control of modifiable risk factors(5, 6), such as cessation of smoking and increased exercise. 2) Lipid lowering drugs, such as statins, can reduce the plasma level of low density lipoprotein (LDL). Treatment with statins can decrease the incidence and motality of MI(7, 8). 3) Antiplatelet drug therapy, such as aspirin. Aspirin interferes with function of cyclooxygenase and inhibits the formation of thromboxane A2. Within minutes, aspirin prevents additional platelet activation and interferes with platelet adhesion and cohesion. This effect benefits all patients with acute coronary syndromes, including those with a MI. So Immediate administration of Aspirin is recommended upon recognition of MI signs

and symptoms. 4) Anticoagulants, such as heparin and warfarin. Heparin can form a chemical complex with antithrombin III. This complex inactivates both free thrombin and factor Xa, therefore inhibits the additional formation and propagation of thrombi. 5) Angiotensin-converting enzyme inhibitors (ACEI) can decrease myocardial afterload through vasodilatation. 6) Beta blockers can decrease the rate and force of myocardial contraction and decrease overall myocardial oxygen demand. So it is recommended within 12 hours of MI symptoms and what is continued indefinitely. Treatment with a beta-blocker reduces MI mortality.

Oxidants, antioxidants and tissue injury

Reactive oxygen species (ROS) are constantly formed in biological systems. The steady-state formation of ROS in cells and organs is balanced by a similar rate of their consumption by antioxidants (enzymatic and/or nonenzymatic). “Oxidative stress” results from an increased formation of ROS, and/or a decreased antioxidant defense. Oxidative stress has been shown to play an important role in the pathology of many diseases, such as cancer, neurodegenerative disease and cardiovascular disease (CVD) (Fig.1.3).

ROS can be generated endogenously or exogenously within our body (Fig.1.3). The presence of an unpaired electron is a certain common feature of ROS, so called free radicals. ROS are highly reactive entities that can readily participate in a variety of chemical and biochemical reactions. Molecular oxygen (O_2) contains 2 unpaired electrons in its outermost shell of the atomic orbital. A full reduction of oxygen to water as a terminal event in the electron transport chain of the mitochondria requires 4 electrons.

The sequential donation of electrons to oxygen during the process of respiration can generate ROS as intermediates due to "electron leakage" (9-11). Donation of a single electron to molecular oxygen results in the formation of the superoxide radical ($O2•^-$). Hydrogen peroxide (H_2O_2) can be generated by the donation of a second electron. Donation of a third electron, such as occurs in the Fenton reaction ($Fe^{2+} + H_2O_2 \rightarrow Fe^{3+} + •OH + OH^-$), results in production of the highly reactive hydroxyl radical (•OH). Hydrogen peroxide is not a free radical itself, but is usually included under the general heading of reactive oxygen species (ROS). It is a weak oxidizing agent that might directly damage proteins and enzymes containing reactive thiol groups. However, its most vital property is the ability to cross cell membranes freely, which superoxide generally cannot do (12). Therefore, hydrogen peroxide formed in one location might diffuse a considerable distance before decomposing to yield the highly reactive hydroxyl radicals. Hydroxyl radicals mediate the toxic effects of hydrogen peroxide under most circumstances. Therefore, hydrogen peroxide acts as a medium to transmit free radical induced damage across cell compartments and between cells.

The hydroxyl radical ($^{\cdot}OH$) is a mediator of most free radical induced tissue damage(13). Both $O2^{\cdot -}$ and H_2O_2 exert their pathological effects by giving rise to hydroxyl radicals. The hydroxyl radical reacts, with extremely high rate constants, with almost every type of molecule found in living cells including sugars, amino acids, proteins, lipids, and nucleic acids . These reactions can cause cell or tissue injury, which plays an important role in the pathogenesis of cancer, neurodegenerative diseases and cardiovascular disease (Fig.1.3).

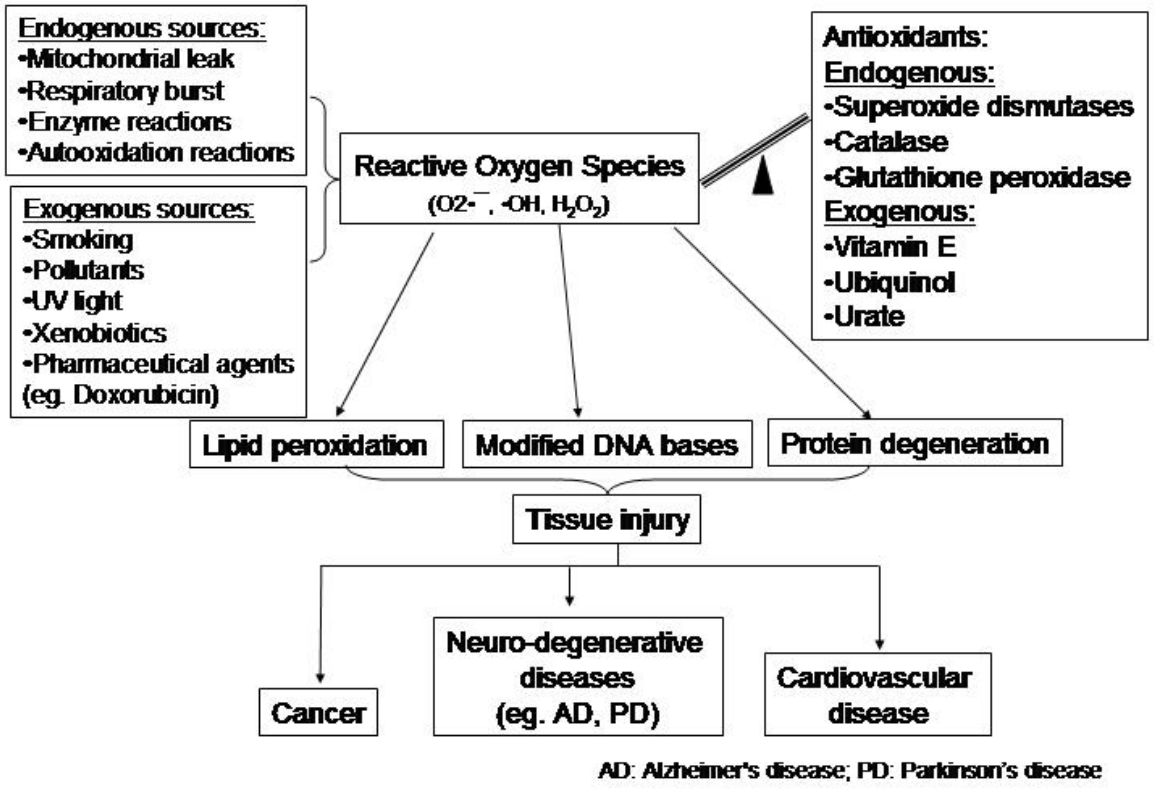

Fig.1.3. Proposed scheme of ROS induced cell or tissue injury

Oxidative stress and cardiovascular disease

Over the past five decades, a great deal of research work has been carried out to seek understanding of the role of oxygen toxicity as well as reactive oxygen species (ROS) in cardiac dysfunction under a wide variety of pathophysiological conditions(14, 15). Likewise, a large body of information is available in literature which implicates Reactive oxygen species (ROS) in the genesis of vascular abnormalities(14). The increased formation of ROS, and ROS-induced oxidative stress in cardiac and vascular myocytes has been linked with cardiovascular tissue injury (16). ROS-induced oxidative stress also plays a role in various cardiovascular diseases such as atherosclerosis, ischemic heart disease, hypertension, cardiomyopathies, cardiac hypertrophy and congestive heart failure(14).

ROS generation and counterbalancing in the heart

ROS are intermediates of the reduction of O_2 to water and include superoxide anion ($O2^{\bullet-}$), hydroxyl radical (•OH) and hydrogen peroxide (H_2O_2). ROS play a critical role in many disorders of the cardiovascular system (e.g.(17-19)), such as ischemia–reperfusion injury, myocardial stunning, apoptosis, inflammation and arteriosclerosis. ROS can be formed in the heart by a variety of mechanisms, including generation during oxidative phosphorylation in the mitochondria as a byproduct of normal cellular aerobic metabolism(20, 21). Thus, the major process from which the heart derives sufficient energy can also result in the production of ROS(21).

A major endogenous source of ROS is the leakage of electrons from the electron transport chain in mitochondria, which then react with nearby oxygen to form superoxide

radicals (22). In tissues with a high density of mitochondria such as cardiac muscle cells, this normal mitochondrial leakage can result in a significant amount of intracellular superoxide. Other sources of ROS in the heart include xanthine oxidase (XO), cytochrome P450-based enzymes, NAD(P)H oxidase, autooxidation of catecholamines and uncoupling of NO synthase (NOS)(22-26). Under certain conditions accumulation of ROS can trigger a burst of ROS production (‘‘ROS induced ROS release’’) by mitochondria that can lead to apoptotic cell death(27).

There are several cellular mechanisms that counterbalance the production of ROS, including enzymatic and nonenzymatic pathways(28). Among the best-characterized enzymatic pathways are catalase and glutathione peroxidase, which coordinate the catalysis of H_2O_2 to water, and the superoxide dismutases (SODs), which facilitate the formation of H_2O_2 from O2•–(29-32). Thioredoxin and thioredoxin reductase together form an additional enzymatic antioxidant and redox regulatory system that has been implicated in a wide variety of ROS-related processes(28). Thioredoxin and thioredoxin reductase can catalyze the regeneration of many antioxidant molecules, including ubiquinone (Q10), lipoic acid, and ascorbic acid, and as such constitute an important antioxidant defense against ROS. Deletion of thioredoxin reductase results in developmental heart abnormalities and in cardiac death secondary to a severe dilated cardiomyopathy(33). Nonenzymatic mechanisms include intracellular antioxidants such as the vitamins E, C, and β-carotene (a precursor to vitamin A), ubiquinone, lipoic acid, and urate(28). Therefore, for normal functioning of the cell, the control of the balance between ROS production and elimination is pivotal.

Oxidative stress and antioxidant enzymes in the failing myocardium

Oxidative stress is usually associated with increased formation of ROS. It has been reported that ROS are increased in the failing heart. Three major ROS, O2•–, H_2O_2 and •OH, are responsible for oxidative stress in heart failure. Cells also contain different mechanisms against oxidative stress(34, 35). The main intracellular enzymatic mechanisms are SOD, catalase, and glutathione peroxidase(34, 35). A decrease in the antioxidant defense mechanisms in myocytes can be seen to promote oxidative stress. In this sense, Dhalla and Singal(36) have shown that the level of superoxide in cardiac tissue is increased as a consequence of the reduced antioxidant reserve in heart failure. The usefulness of antioxidant therapy, especially vitamin E, in attenuating the progression of heart failure has also been reported(37). Similarly, the ROS scavenger DMTU (dimethylthiourea) prevented chamber dilation and pump dysfunction in the mouse post-MI(38).

Several clinical studies have suggested increased ROS in patients with heart failure(39-42). The plasma and pericardial fluid of patients with heart failure contain elevated levels of thiobarbituric acid–reactive substances, which are markers of ROS activity(43, 44). Ellis et al(45) have also recently shown, by electron paramagnetic resonance spectroscopy, that lipid-derived ROS were significantly higher in patients with chronic heart failure than in control subjects. ROS may contribute in an important manner to the pathophysiology of heart failure by initiating myocyte apoptosis through nuclear factor (NF)-κB and exerting direct negatively inotropic effects through depressed calcium uptake and reduced calcium-stimulated magnesium dependent adenosine triphosphate

activity of the cardiac sarcoplasmic reticulum(46, 47). Oxidative stress may also contribute to endothelial dysfunction in heart failure.

ROS and cardiac myocyte remodeling

Contractile function

In-vitro studies have shown that ROS impair contractile function by disrupting excitation–contraction coupling processes, notably trans-sarcolemmal calcium fluxes and intracellular calcium cycling(48). ROS also depress mitochondrial respiration and reduce the ability of the myocyte to generate ATP, thereby causing a rise in resting tension and contractile dysfunction in isolated muscle preparations(49). These contractile changes can be ameliorated by antioxidant treatment(49).

Hypertrophy

Mounting evidence has strongly implicated ROS signaling in the genesis of cardiac hypertrophy(50-54). Many extracellular factors are capable of inducing hypertrophy of cardiomyocytes, and many of the various downstream signaling pathways that mediate the hypertrophic growth response to these factors can be activated directly or indirectly by ROS. Angiotensin II, tumor necrosis factor-α and α-adrenergic receptor stimulation have been shown to cause myocyte hypertrophy through a ROS-dependent pathway(55, 56), leading to disproportionate changes in the shape of individual CMCs. For instance, patients with dilated cardiomyopathy present with eccentric hypertrophy, or a lengthening of CMCs. This causes the heart as a whole to have a larger volume, but thinner walls than normal. The opposite problem may also occur: patients with pressure overload can present with concentric hypertrophy, or a thickening of individual CMCs

(57). In this case the heart has a larger overall mass, but the chamber walls are thicker without enlarging the diameter of the heart, leading to a loss of interior volume. There is also evidence shown that ROS may be involved as intracellular ignaling molecules in some of the subcellular pathways involved in the development of cardiac hypertrophy(58). These include PKC; the MAPKs p38, JNK, apoptosis-signaling kinase 1 (ASK-1), and ERK1/2; PI3K; Akt; several tyrosine kinases (e.g., src and FAK); NF-κB; and calcineurin(59, 60).

Apoptosis

Recent data from in Vitro and experimental studies in the heart suggest that oxidative stress plays an important role in CMC cell death by way of apoptosis or necrosis(61, 62). Myocyte death induced by oxidative stress is associated with the standard structural and biochemical changes indicative of apoptosis, distinct from necrosis. Mmyocyte apoptosis induced by chronic exposure to ROS can be inhibited experimentally by antioxidants(55, 58). Recently oxidative stress was shown to trigger CMC apoptosis in myocardial infarction, ischemia/reperfusion injury, cardiomyopathy, atherosclerosis, and heart failure(63, 64).

In human myocardial infarction, both apoptosis and necrosis have been observed(65), and apoptosis has been considered the predominant form of myocyte cell death in the border zone compared with noninfarcted and remote areas(65). After myocardial infarction in humans, as well as animals, transmural translocation of cells has been observed in both the border zone and in remote areas of the left ventricle(66). It has been shown that the slippage of cells is greater in the border zone(66) and parallels the

extent of apoptosis. Myocardial apoptosis has been suggested as the initiating factor in postinfarction leftventricular remodeling(67).

ROS regulation of interstitial matrix turnover by cardiac fibroblasts

Interstitial matrix proteins connect cardiac myocytes with one another, maintain overall tissue architecture, and play an integral role in coordinating the force generated by individual myocytes. The turnover of the interstitial matrix is regulated by proteases and the protein synthetic machinery of the cardiac cells (68). As in other tissues, fibroblasts play an important role in regulating the turnover, composition and quantity of cardiac interstitial matrix proteins. Collagen is the major component of the interstitium that contributes to the structural integrity of the myocardium. Myocardial collagen content is regulated by the balance between synthesis and degradation, the latter primarily due to the action of Matrix metalloproteinases (MMPs) (69).

MMPs are an endogenous family of zinc-dependent enzymes that are responsible for matrix remodeling in physiological conditions and in several disease states(70). MMPs are regulated at multiple levels including transcription, secretion, and activation of inactive zymogens, while their tissue activity is under the strict control of specific inhibitors, i.e., tissue inhibitors of metalloproteinases (TIMPs)(70). Several studies suggest that ROS play a major role in the activation of MMPs(71, 72), and that NAD(P)H oxidase activation, a major source of ROS, is a key event in this process(73, 74). The cardiac content of MMP-2 andMMP-9 is increased in both experimental and clinical forms of heart failure(75, 76). When MMP activity is increased with insufficient

quenching activity by TIMPs, progressive disruption of the collagen network occurs, thus leading to progressive dilation and remodeling of the left ventricle(77, 78).

Based on the available data, the role of free radicals in the pathogenesis of cardiomyopathies and heart failure is illustrated in Fig.1.1. Any acute or chronic cardiac stress conditions, resulting in a relative deficit in the myocardial 'antioxidant reserve', are associated with an increase in myocardial 'oxidative stress'. The latter is capable of causing subcellular abnormalities, leading to cardiomyocyte hypertrophy, contratile dysfunction or apoptosis. Concomitant changes in cardiac fibroblasts include increased fibroblast proliferation as well as accelerated and aberrant remodeling of extracellular matrix and net accumulation of ECM, resulting in cardiac fibrosis. The ultimate results of these changes are systolic and diastolic dysfunction. In this regard, the occurrence and importance of free radicals in cardiac pathophysiological conditions is now well established. Furthermore, the available evidence from animal and human studies illustrates that different antioxidants constituting an antioxidant reserve offer protection against oxidative stress-mediated myocardial changes. An understanding of the molecular basis of antioxidant changes will help to develop newer therapies for modulating the pathogenesis of heart failure.

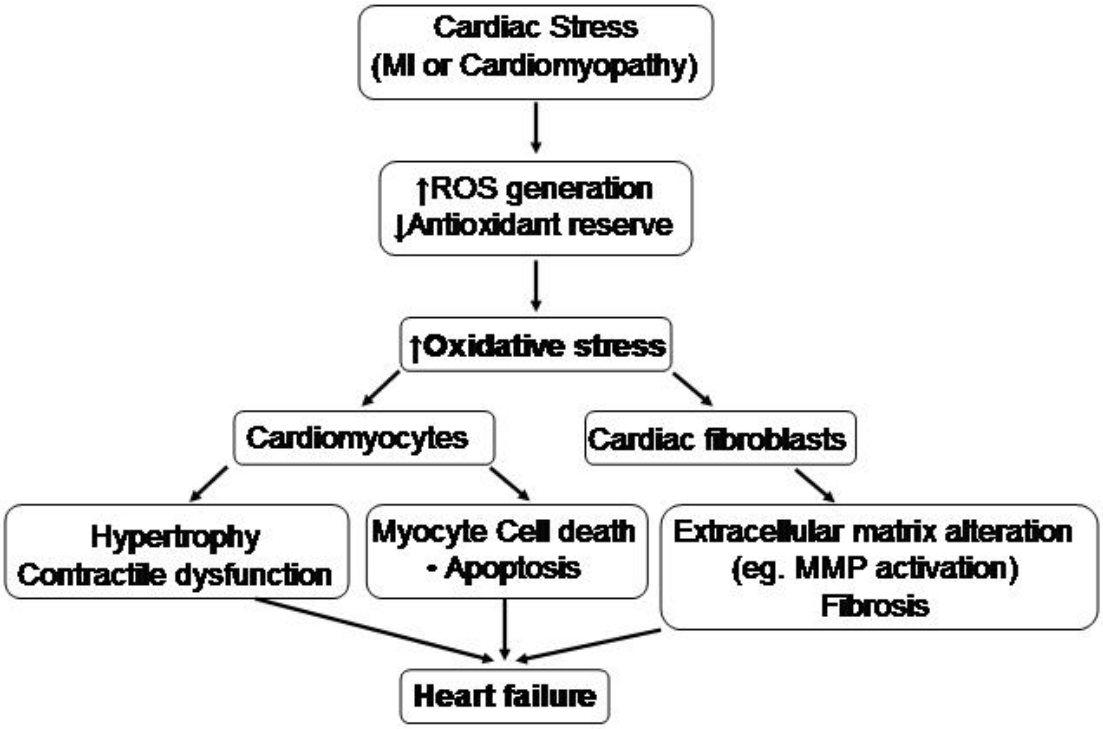

Fig. 1.4. Proposed scheme for the role of oxidative stress in the development of heart failure.

Biomarkers of heart failure

Heart failure is an end point of many forms of CVD. It is the only cardiovascular disorder with an increasing incidence and prevalence(1). On average, one in five patients die within 1 year of heart failure diagnosis (79). The estimated cost of heart failure in the United States for 2007 is $33.2 billion (1). Given the adverse morbidity, mortality and high cost of heart failure, research has intensified in developing biomarkers to predict susceptibility and aid in the early diagnosis and management of this disease.

Strategies for developing biomarkers of heart failure

Biological marker (biomarker) is defined as a characteristic that is objectively measured and evaluated as an indicator of normal biological processes, pathogenic processes, or pharmacologic responses to a therapeutic intervention(80). Biomarkers can indicate a variety of health or disease characteristics, including the level or type of exposure to an environmental factor, genetic susceptibility, genetic responses to exposures, markers of subclinical or clinical disease, or indicators of response to therapy. Thus, a simplistic way to think of biomarkers is as indicators of disease trait (risk factor or risk marker), disease state (preclinical or clinical), or disease rate (progression)(81). Accordingly, biomarkers can be classified as antecedent biomarkers (identifying the risk of developing an illness), screening biomarkers (screening for subclinical disease), diagnostic biomarkers (recognizing overt disease), staging biomarkers (categorizing disease severity), or prognostic biomarkers (predicting future disease course, including recurrence and response to therapy, and monitoring efficacy of therapy)(80).

Biomarkers have been useful in improving the diagnosis as well as identification of individuals with higher risk for developing coronary syndromes such as angina and acute myocardial infarction(82). In fact, the very way that acute coronary syndrome is diagnosed has been profoundly impacted by biomarkers. Perhaps biomarkers for congestive heart failure (CHF) will ultimately lead to new criteria for the diagnosis of heart failure. Biological markers can also be useful for the prediction and earlier diagnosis of heart failure in asymptomatic or minimally symptomatic patients(83).

Genomic approach

With the emergence of microarray technology, it is now possible to simultaneously assess the expression of tens of thousands of gene transcripts, providing a resolution and precision of phenotypic characterization not previously possible. In the field of cardiomyopathy, many microarray studies have focused on gene discovery. Some studies involved small sample sizes and binary comparisons such as failing and nonfailing hearts(84-91), dilated and hypertrophic cardiomyopathy (92), and before and after left ventricular assist device (LVAD) placement(93-96). Other studies have used more sophisticated techniques, focusing on three-way comparisons: comparing the differential gene expression of ischemic and nonischemic cardiomyopathy relative to nonfailing hearts (88, 97) or failing and LVAD-supported hearts relative to nonfailing hearts(98). These studies have provided insights into novel genetic pathways and therapeutic targets, and they also serve as the basis for studies involving molecular signature analysis.

Proteomic approach

Proteomics is a new systems biological approach to study proteins and protein variation on a large scale as. The field of proteomics is undergoing a dramatic transformation, owing to the completion and annotation of the human genome as well as technological advancement. The new science of proteomics can potentially yield novel biomarkers reflecting cardiovascular disease, establish earlier detection strategies, and monitor responses to therapy.

Gel-based proteomic approaches. In cardiovascular proteomics, much of the work to date has been performed through high-quality two-dimensional (2-D) gel-based electrophoresis of tissue or blood samples (99-101). The principles of the gel-based technique involve separation of proteins in the first dimension according to their charge properties (isoelectric point [pI]) under denaturing conditions, followed by their separation in the second dimension according to their relative molecular mass by sodium dodecylsulfate polyacrylamide gel electrophoresis (SDS-PAGE) (102-104).

Studies using gel-based technologies have yielded novel insights into the mechanisms of ischemic myocardial disease, particularly the post-translational modifications of abundant proteins, such as troponin(100). Gel-based techniques have additional advantages in terms of the ease and cost efficiency. However, the technique is constrained by theselectivity of protein coverage. Staining 2-D gels only detects abundant proteins that are visible, and the efficiency of protein recovery from the polyacrylamide gel is often a rate-limiting step that prohibits detection of proteins at low abundance.

Gel-free "shotgun" proteomic techniques with tandem mass spectrometry.

The more recent use of gel-free systems, which couple high-efficiency liquid chromatography separation procedures with automated tandem mass spectrometry, allows for large-scale "shotgun" sequencing of a complex mixture (105-107). The archetypal approach, termed MudPIT (multidimensional protein identification technology)(108), has proven to be effective for investigating global changes in protein expression as a function of development and disease(109-111). In contrast to 2-D electrophoretic techniques in which high-abundance protein species predominate, the gel-free "shotgun" profiling procedures provide much more extensive coverage with orders of magnitude increase in resolution. The tandem approach permits peptide species identification and also semi-quantitative estimation of the relative abundance. Current efforts are focused on adapting data mining algorithms, which can be trained to find specific features to distinguish between samples. Shotgun techniques require typically rigorous statistical approaches to evaluate the significance of any predicted patterns, owing to the volume of data analyzed and the hazards of multiple comparisons. Shotgun tandem mass spectrometry technique currently provides the greatest depth of protein coverage and widest dynamic range of size of proteins identified. Once the candidates are identified, validation can be done with gel-based approaches or dedicated protein arrays.

Current biomarkers for heart failure diagnosis and prognosis

Based on the growing amount of data, heart failure biomarkers are mainly classified as neurohormonal mediators, markers of myocyte injury, markers of ECM remodeling, inflammatory markers, markers of oxidative stress, markers of sodium pump

activity, and a separate group of other peptides associated with heart failure whose significance in pathophysiology is somewhat less understood (Table 1.1).

Table1.1: Current biomarkers in chronic heart failure

Neurohormonal activation	Brain natriuretic peptide (BNP) [Reviewed in (112)] Atrial natriuretic peptide (ANP) NT-proBNP(113-117) Pro-ANP(83, 118) Plasma norepinephrine (PNE)(119-121)
Myocyte injury	Troponin T (cTnT)(122-128) Troponin I (cTnI)(129-131) Heart-type fatty acid-binding protein (H-FABP)(132, 133) Myosin light chain-1 (MLC-1)(134, 135)
Remodeling of extracellular matrix	Matrix metalloproteinases (MMPs)(76, 78, 136-138) Tissue inhibitors of metalloproteinases (TIMPs)(139)
Inflammation	C-reactive protein (CRP)(140, 141) Interleukin-6 (IL-6)(140, 141) Tumor necrosis factor-α (TNF- α)(140, 141) ST2(142, 143) Interleukin-2 receptors(144) CD40-CD154(145, 146) Adhesion molecules Intracellular adhesion molecule-1 (ICAM-1)(147) P-selectin(148)
Oxidative stress	Urinary byopyrrins(149) Urinary isoprostanes(150) Plasma malonyldialdehyde (MDA)(40)
Sodium pump activity	Cardiotonic steroids DLIFs (digoxin-like immunoreactive factors)(151) OLFs (oubain-like factors)(152)
Others	CA 125(153, 154) Urocortin(155) Adrenomedullin(156-158) Cardiotropin-1 (member of IL-6 family)(159)

Functional role of heart failure biomarkers

Biomarkers of heart failure play an important role in the diagnosis, prognostic assessment, and management of patients with suspected heart failure. In additon, several biomarkers identify different components of biochemical pathways in the pathophysiology of heart failure. For instance, natriuretic peptides reflect neurohormonal activation and hemodynamic stress. The appearance of troponins in the blood indicates myocyte necrosis. MMPs participate in the ECM remodeling during the process of heart failure.

To date, only natriuretic peptides have been studied sufficiently as biomarkers with a practical level of sensitivity and specificity for diagosis and monitering heart failure. The structure and function of natriuretic peptides have been studied over the years. Functionally, natriuretic peptides are neurohormones that regulate body fluid retension, natriuresis, and diuresis, acting as an intrinsic counterregulatory system that responds to excessive rennin angiotensin aldosterone (RAAS) and vasopresin activation. In addition, they have relevant vasodilator and antifibrotic properties and play a major role in endothelial vascular function. Three recombinant natriuretic peptides are currently used for the management of acutely decompensated heart failure: nesiritide, i.e.recombinant brain type natriuretic peptide (BNP),; carperitide, i.e.recombinant atrial natriuretic peptide, or ANP, which is not yet approved in the United States but is used in Japan; and a third recombinant peptide, ularitide, a synthetic version of urodilatin (a newly identified analogue of human atrial natriuretic factor) found to be beneficial and safe in patients with acute decompensated heart failure in Europe(160).

Statement of the problem

Although the heart failure literature is extensive with examples of circulating biochemical markers that predict poor outcomes in patients with heart failure, to date, only natriuretic peptides have been sufficiently studied as biomarkers with a high level of sensitivity and specificity for the current diagnosis, management and prognosis of heart failure (161). Among the natriuretic peptide family, most clinicians are acquainted with ANP and BNP. Both are synthesized by cardiac myocytes and released from the atria and entricles under increased hemodynamic pressure or cardiac volume and wall stress. ANP and BNP are the only biomarkers approved by FDA for the diagnosis and management of heart failure. Strong evidence exists for use of BNP in the diagnosis of acute heart failure and for improved clinical outcomes. However, the use of BNP as a screening tool for asymptomatic left ventricular systolic dysfunction, or to distinguish systolic from diastolic heart failure, is not supported by current data (162). Therefore, identification of novel indicators prior to the clinical onset of heart failure symptoms will be valuable in early diagnosis or management of heart failure.

Organization of the dissertation

This dissertation attempts to address the strategies used for identifying cardiac specific indicator mediating oxidative injury in the heart, which could be potential indicators for early diagnosis of heart failure, and to examine the functional role of the indicator in cardiac remodeling. Specifically, this dissertation contains the following sections: 1) Introduction (Chapter I); 2) Identification of techniques most suitable for

finding novel targets mediating oxidative injury (Chapter II & Chapter III); 3) Identification of novel cardiac specific indicator associated with oxidative stress using ESI-LC-MS/MS based shotgun approach of proteomics (Chapter IV); 4) Functional study of Cystatin C in cardiac extracellular matrix (ECM) remodeling (Chapter V); 5) Summary statements (Chapter VI); 6) References.

CHAPTER II: GENOMIC AND PROTEOMIC PROFILING OF OXIDATIVE STRESS RESPONSE IN HUMAN DIPLOID FIBROBLASTS

Introduction:

Oxidative stress has been linked to aging and many aging associated diseases. Several common sources of oxidants include: 1) mitochondrial respiration generating reactive oxygen species (ROS) as byproducts; 2) saturation of antioxidant defenses, such as inactivation of antioxidant enzymes and depletion of sulfhydryls by xenobiotics; 3) activation of oxidases, for example cytochrome p450 during drug metabolism, xanthine oxidases during ischemic reperfusion, and membrane associated NAD(P)H oxidase by angiotensin II binding to its receptor. Under most circumstances, the level of oxidants produced inside our body is relatively low and not sufficient to kill the majority of cells. Cellular maladaptation to oxidants contributes to various disease states, including diabetes, cardiovascular disease, cancer, and neurodegenerative disease (16, 163-165). Despite the fact that oxidative stress is known to be associated with many diseases, epidemiological studies and clinical trials with antioxidant vitamins have generated controversial data(166). These controversies argue for the importance of systematic reevaluation on the cellular response to oxidants at the molecular level.

Recent developments in genomic and proteomic technologies provide an opportunity to study the biological consequence of oxidative stress without the bias of prior knowledge. The sequence information of the human genome provides a needed database for profiling genes and proteins using microarray technology and LC-MS/MS

based proteomics. Microarray technologies allow the examination of gene expression on the scale of a genome when an organism or cells experience a changing status. Despite the advancement in microarray technologies, the question remains unanswered as how many genes showing changes at the mRNA level also change their expression at the protein level. Complementary technologies, such as LC-MS/MS based proteomics, provide an opportunity to profile proteins appearing with different states of cells. Since proteins ultimately denote the function of genes, it is important to reveal the identities of the proteins showing changes with oxidative stress.

Multidimensional chromatography coupled with mass spectrometry is an emerging technique for profiling proteins in a complex mixture. To improve the resolution for LC-MS/MS based proteomics, MudPIT employs biphasic or triphasic microcapillary columns for high-performance liquid chromatography(167, 168). With tandem mass spectrometer, peptides eluted from liquid chromatography can be identified in combination with sequence database searching tools. Although technology improvement remains as a main focus of proteomics, current MudPIT and mass spectrometry based techniques have been shown promise in finding new targets and pathways by profiling proteins in a complex mixture such as biological fluids, tissue extracts, cell lysates, and subcellular organelles(169-171). These techniques allow us to profile changes at the protein level when cells experience oxidative stress.

Fibroblasts are the most abundant cell types within our body. Fibroblasts or fibroblast-like cells are present in most if not all organs, serving as a scaffold for proper functions of organ specific cells. Normal human diploid fibroblasts (HDFs) can be

isolated from certain tissues, for example the skin, and remain viable under tissue culture condition. Unlike human tumor cells or immortalized rodent cells, HDFs have a limited replicative potential in culture(172-175). Fibroblasts from newborn forskin generally replicate about 50 – 80 population doublings before reaching replicative senescence. On the other hand, early passage of HDFs develop a phenotype resembling premature senescence following the exposure to low or mild dose of oxidants(176-178). Differing from tumor cells, HDFs from individuals with normal genetic background retain genomic integrity in culture, allowing us to profile changes relevent to human health at the level of genes and proteins following oxidative stress. In this study, we compare the outcome of proteomics with that of microarray using current available technologies after stressing HDFs with a mild dose of H_2O_2.

Materials and methods:

Chemicals and Reagents—Chemicals were purchased from Sigma unless otherwise indicated. Stabilized H_2O_2 (H-1009, Sigma) was used and the concentration of the stock was verified by absorbency at 240 nm.

Maintenance of Cell Culture—HCA_3 human dermal fibroblasts were obtained from Dr. Olivia Pereira-Smith at the population doubling level (PDL) 20. These cells typically reach replicative senescence after PDL 80 and were used for this study at PDL 26–40. HCA_3 cells were subcultured weekly in 10 ml of Dulbecco's modified Eagle's medium (DMEM) containing 10% (v/v) fetal bovine serum (FBS), 50 units/ml penicillin, and 50 μg/ml streptomycin (Invitrogen) at a seeding density of $1x10^6$ cells/100-mm Falcon dish. Under these conditions, the cells reached confluence 6–7 days after subculture.

Treatment with H_2O_2—HCA_3 cells were seeded at a density of $2x10^6$/100-mm dish 5 days before treatment. At the time of H_2O_2 treatment, cells have reached confluence, and the density of cells is $10.48\pm0.85x10^6$/100-mm dish. Confluent cells were treated with 600 μM H_2O_2 in a 100-mm dish containing 10 ml of medium. This dose is equivalent to ~0.6 pmol of H_2O_2/cell. The dose less than 0.85 pmol/cell has been shown to be non-lethal and induce premature senescence in early passage HDFs (179-182). After 2-h incubation in the presence of H_2O_2, cells were placed in fresh DMEM containing 10% (v/v) FBS and were allowed to recover for 3 days before harvesting RNA or proteins.

MudPIT and LC-MS/MS analysis of cell lysates—Three days after H_2O_2 treatment, HDFs cells were washed twice with ice-cold PBS and scraped in 200 μl of EB lysis buffer (1% Triton X-100, 10 mM Tris, pH 7.4, 5 mM EDTA, 50 mM NaCl, 50 mM NaF, and freshly added 2 mM DTT, 1 mM Na_2VO_3, 1 mM phenylmethylsulfonyl fluoride, 100 μg/ml leupeptin, and 10 μg/ml aprotinin). Each sample was diluted by and dialyzed against 0.01 N NH_4HCO_3, passed through a 0.45-μm filter to remove insoluble cell debris, and concentrated down using a speed vacuum concentrator. Protein concentration in each sample was determined by the Bradford method according to the manufacturer's instruction (Bio-Rad, Hercules, CA). Protein mixtures from whole cell lysates were digested overnight with trypsin at a 50:1 ratio (protein:trypsin) (180, 183). A microbore HPLC system (Paradigm MS4, Michrom, Auburn, CA) was used with two separation columns: a reverse phase (RP) column as a 100 μm I.D. capillary packed with 10 cm of 5 μm Vydac C18 reversed phase resin, and a strong cation exchange (SCX) column with 250 μm I.D. capillary packed with 8 cm of 5 μm Partisphere strong cation exchanger resin (Whatman, Clifton, NJ). The sample (23 μg) was acidified using TFA and manually injected onto the SCX column, with the effluents going through RP column. A twelve-step fractionation analysis was performed with the solvents of: 10% methanol/0.1% formic acid, 0.01%TFA (buffer A), 95% methanol/0.1% formic acid, 0.01% TFA (buffer B), 10% methanol/0.1% formic acid, 0.01% TFA (buffer C) and 500 mM ammonium acetate/10% methanol/0.1% formic acid, 0.01% TFA (buffer D). Step 1 consists of a 5 min equilibration step at 100% buffer A, followed by another equilibration step for 5 min at 25% buffer B (75% buffer A), followed by a 40 min gradient from 25%

buffer B to 65% buffer B, followed by a 10 min 65% buffer B and 10 min of 100% buffer A. Chromatography steps 2 to 12 follow the same pattern: 15 min of the appropriate % of buffers C & D followed by a 2 min 100% buffer C wash, a 5 min wash with 100% A, equilibration with 25% buffer B for 5 min, followed by a gradient from 25% buffer B to 65% buffer B in 40 min, followed by a 10 min 65% buffer B and 10 min of 100% buffer A. The buffer C/D percentages used were 95/5%, 90/10%, 85/15%, 80/20%, 70/30%, 60/40%, 40/60%, 20/80%, 0/100%, 0/100%, 0/100% respectively, for the 11 salt steps. The flow rate is approximately 350 nl/min, with elution directly into the electrospray ionization source of a ThermoFinnigan LCQ-Deca XP Plus ion trap mass spectrometer (ThermoFinnigan, San Jose, CA). Eluted peptides were electrosprayed into the mass spectrometer with a distally applied liquid junction spray voltage of 1.6 kV. Spectra are scanned over the range 380-2000 mass units. Automated peak recognition, dynamic exclusion, and daughter ion scanning of the most intense ion was performed using the Xcalibur software as described previously(184, 185).

MS/MS data were analyzed using Turbo SEQUEST(186). The criteria for a preliminary positive peptide identification for a doubly-charged peptide are a correlation factor (Xcorr) greater than 2.5, a delta cross-correlation factor (ΔXcorr) greater than 0.08, a minimum of one tryptic peptide terminus, and a high preliminary scoring. For triply- and singly-charged peptides the correlation factor threshold is set at 3.5 and 1.8, respectively(180). All spectra were searched against a non-redundant human protein sequence database from National Center for Biotechnology Information (NCBI).

cDNA Microarray Analysis—The microarray chips were generated as described by Watts et al.(187). The chips contain ~5300 human genes, with more than 3000 known genes and the remainders as expressed sequence tags (ESTs) determined by the UniGene. The cDNA sequences printed on the microarray are derived from cDNA clones produced by the IMAGE consortium. The clones were validated and distributed by the Research Genetics. A list of the clones on the arrays can be found at ftp://azccftp.arizona.edu/gwatts/GeneList/. Microarray analyses were performed as described by Crowley-Weber et al. (188). Briefly, total RNAs from H_2O_2 treated and control HDFs were isolated using a QIAGEN RNeasy kit (Qiagen, Valencia, CA). RNA samples were evaluated for integrity by electrophoresis in a 1.0% agarose gel with ethidium bromide staining. Cy3 or Cy5 labeled first strand cDNAs were made from 40 μg of total RNA with Micromax Direct cDNA Microarray System (NEN Life Sciences, Boston, MA) following manufacturer's protocol. Fluorescence labeled cDNAs from two reactions were hybridized to the cDNA array slides. The slides were scanned with Axon GenePix 4000 microarray reader (Axon Instruments, Foster City, CA) and quantified with GenePix software. The data were analyzed with GeneSpring 5.0 software (Silicon Genetics, Redwood, CA). Three independent experiments were performed with hybridization performed in triplicates. Changes in gene expression are judged by 1.5 fold or greater difference in Cy5 versus Cy3 signal strength and a P-value of <0.05 in a paired t-test among the triplicates. The up- versus down-regulated genes were classified and clustered by searching through the BioRag database generated by the Arizona Cancer

Center Bioinformatics Core (www.biorag.org) and categorization was verified individually by Unigene database search.

Functional Analysis and Gene Ontology networks— Cytoscape 2.4.0 (www.cytoscape.org) was used to generate the network of Gene Ontology (GO) terms. Differentially expressed genes and proteins found by cDNA microarray and LC-MS/MS based proteomics analyses were searched against BioRag database (www.biorag.org) for GO Molecular Function categories. The categories that had less than four genes were removed if the genes were also not represented in any other molecular function category for microarray data. For proteomic data, all the proteins found different between control versus treated groups and their GO categories were included for generating the network. Individual gene or protein is presented as a circular node and GO terms appear as squares. The edges are the links between gene/protein and the GO terms. The color shade in circular node reflects the fold change for up regulated (red) and down regulated (blue) genes for the network constructed from gene expression arrays. For the protein network, the node color indicates proteins found in control (green) or in H_2O_2 treated cells (red).

Semiquantitative RT-PCR—Total RNA was extracted from cells with TRIZOL (Invitrogen). Semiquantitative RT-PCR was performed using 2 μg of total RNA from each sample, 3 μl of the 35 μl RT reaction mixture was used for each PCR to measure the mRNA level of matrix metallopeptidase 3 (MMP3), serine/threonine kinase 15 (AURKA), thioredoxin reductase 1 (TXNRD1), Thioredoxin (TXN), Small inducible

cytokine A7 (CCL7), Small inducible cytokine subfamily A13 (CCL13), Tumor necrosis factor receptor superfamily member 12A (TNFRSF12A), ADP-ribosylation factor 4-like (ARF4L). Glyceraldehyde-3-phosphate dehydrogenase (GAPDH) was used as a reference gene and as an internal control. The Primer 3 Input Program (http://frodo.wi.mit.edu/cgi-bin/primer3/primer3.cgi) was used to design PCR primers and to calculate the optimal PCR annealing temperature (TempA, Table2.1). PCR products were detected by ethidium bromide staining after agarose gel electrophoresis.

Western Blot Analysis— HDFs cells were washed twice with ice-cold PBS and scraped in 200 μl of EB lysis buffer for protein concentration measurements as described above. Proteins (40 μg) from cell lysates were separated by 15% SDS-polyacrylamide gel electrophoresis before overnight transfer at 30 volts to a polyvinylidene difluoride (PVDF) membrane (Millipore, Bedford, MA). After eliminating non-specific binding with a minimal 1 hr incubation in 5% nonfat milk, the PVDF membrane was incubated overnight at 4 °C in the primary antibody against MMP-3 (1:2000 dilution, mouse monoclonal, MAB3306, Chemicon, CA), AURKA (1:2000 dilution, rabbit polyclonal, ab12324, abcam, MA), TXNRD1 (1:1000 dilution, rabbit polyclonal, 07-613, Upstate, NY), TXN (1:1000 dilution, mouse monoclonal, ab16965, abcam, MA), or GAPDH (1:2000 dilution; rabbit polyclonal, ab9485-100, Abcam, MA). The membranes were subsequently incubated 45 minutes in horseradish peroxidase-conjugated secondary antibodies (Zymed Laboratories Inc., South San Francisco, CA; 1:8000) for enhanced chemiluminescence (ECL) reaction.

Results:

Identification of Proteins in Cell Lysates by MudPIT

Cell lysates were collected from Control (Ctrl) and H_2O_2 treated HDFs for MudPIT and mass spectrometry to identify alterations in protein expression upon H_2O_2 treatment. Representative Total Ion Current (TIC) chromatograms from control and H_2O_2 treated cells are shown in Figure 2.1. The experimental tandem MS spectra obtained from mass spectrometry analyses were searched against NCBI human protein sequence database by the Turbo SEQUEST^{TM} algorithm. Confident protein identification relies mainly on two parameters: "Xcorr" and "Ions". In all cases, the value of Ions is greater than 50%, while Xcorr≥1.8 for +1 ions, Xcorr≥2.5 for +2 ions, and Xcorr≥3.5 for +3 ions (180). SEQUEST outputs were assembled and filtered into actual protein identifications by the DTASelect algorithm(189).

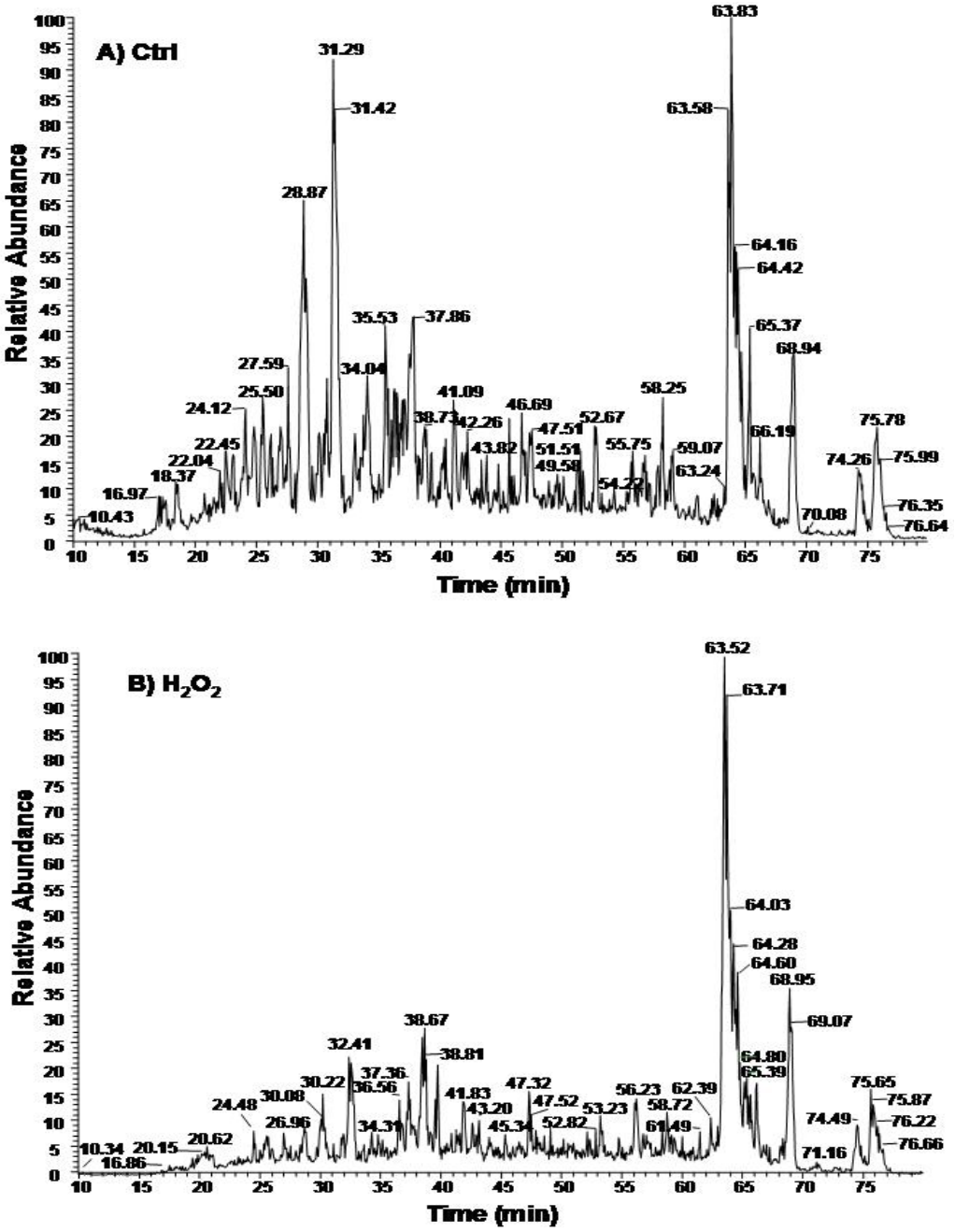

Fig.2.1. Total Ion Current (TIC) Chromatogram of the Whole Cell Lysate from Control or H2O2 Treated HDFs. HCA_3 fibroblasts (PDL26-40) were treated with 600 μM (~0.6 pmol/cell) of H_2O_2 for 2 hrs and were harvested 3 days later for dialysis, concentrating, tryptic digestion and LC-LC-MS/MS analyses. Each peak represents one parent peptide ion detected by the mass analyzer and the peak height reflects the abundance of the peptide ion.

The analyses found 109 proteins common among Ctrl and H_2O_2 treated HDFs (data not shown). There are 65 proteins unique to Ctrl group and 48 proteins unique to H_2O_2 treated HDFs (Table2.2). The network of changes in the proteins is shown in Figure 2.2. A cluster of metal ion binding proteins and several proteins in the oxidoreductase cluster have been found in H_2O_2 treated cells (Table2.2 and Fig.2.2). Among the list of proteins in H_2O_2 treated cells, the clusters of protein binding, RNA binding and structural constituents of ribosome stand out (Fig. 2.2).

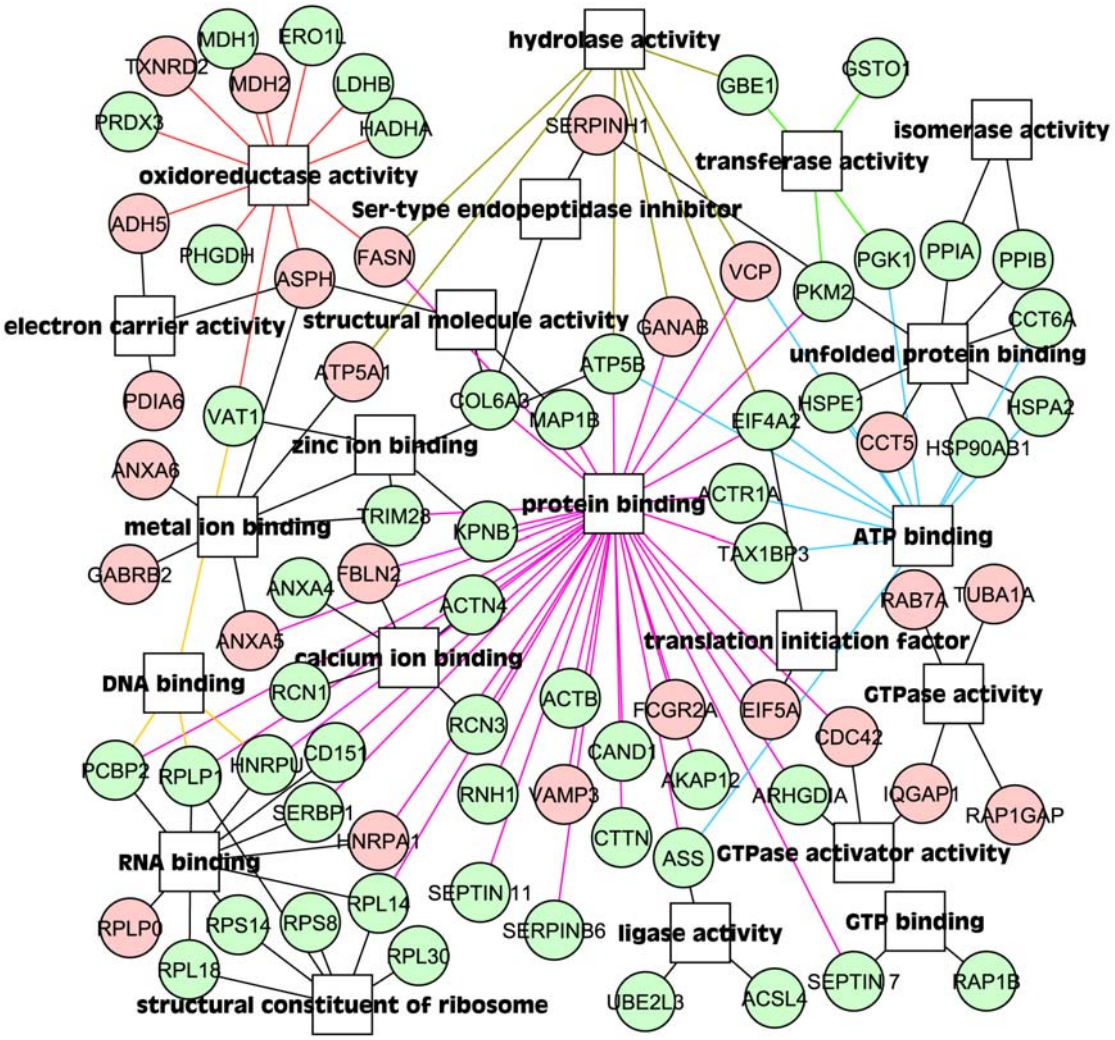

Fig.2.2. Display of the Proteomics Data by the Cytoscape Network. Proteins found unique to H_2O_2 treated group (red) or control group (green) were imported into the Cytoscape 2.4.0 software for building the network. The nodes represent individual proteins and squares indicate gene ontology terms. The colors of the edges enhance the view of corresponding gene ontology groups in the network of microarray data.

Thioredoxin (TXN) and thioredoxin reductase 1 (TXNRD1) are two examples of proteins found in H_2O_2 treated cells. The MS/MS spectra and SEQUEST Flicka protein information output on TXN and TXNRD1 are shown in Figures 2.3 and 2.4. Three peptides were identified from TXN protein by our mass spectrometer (Fig.2.3A-C). These peptides cover 37.1% of entire TXN protein sequence (Fig. 2.3D). The high percentage of sequence coverage, together with the acceptable Xcorr and Ions values give us the confidence in identification of this protein. Unlike TXN, the mass spectrometer only detected one peptide ion for TXNRD1 (Fig. 2.4A). However, the MS/MS spectrum (Fig. 2.4A), Xcorr value (3.11 for +2 ion) and Ions scores (67.9 %) all suggest the high quality of this protein identification. Western blot analyses were able to verify elevated levels of TXN and TXNRD1 with H_2O_2 treated HDFs (Fig. 2.5). These data suggest that H_2O_2 treated cells indeed elevate protein levels of TXN and TXNRD1.

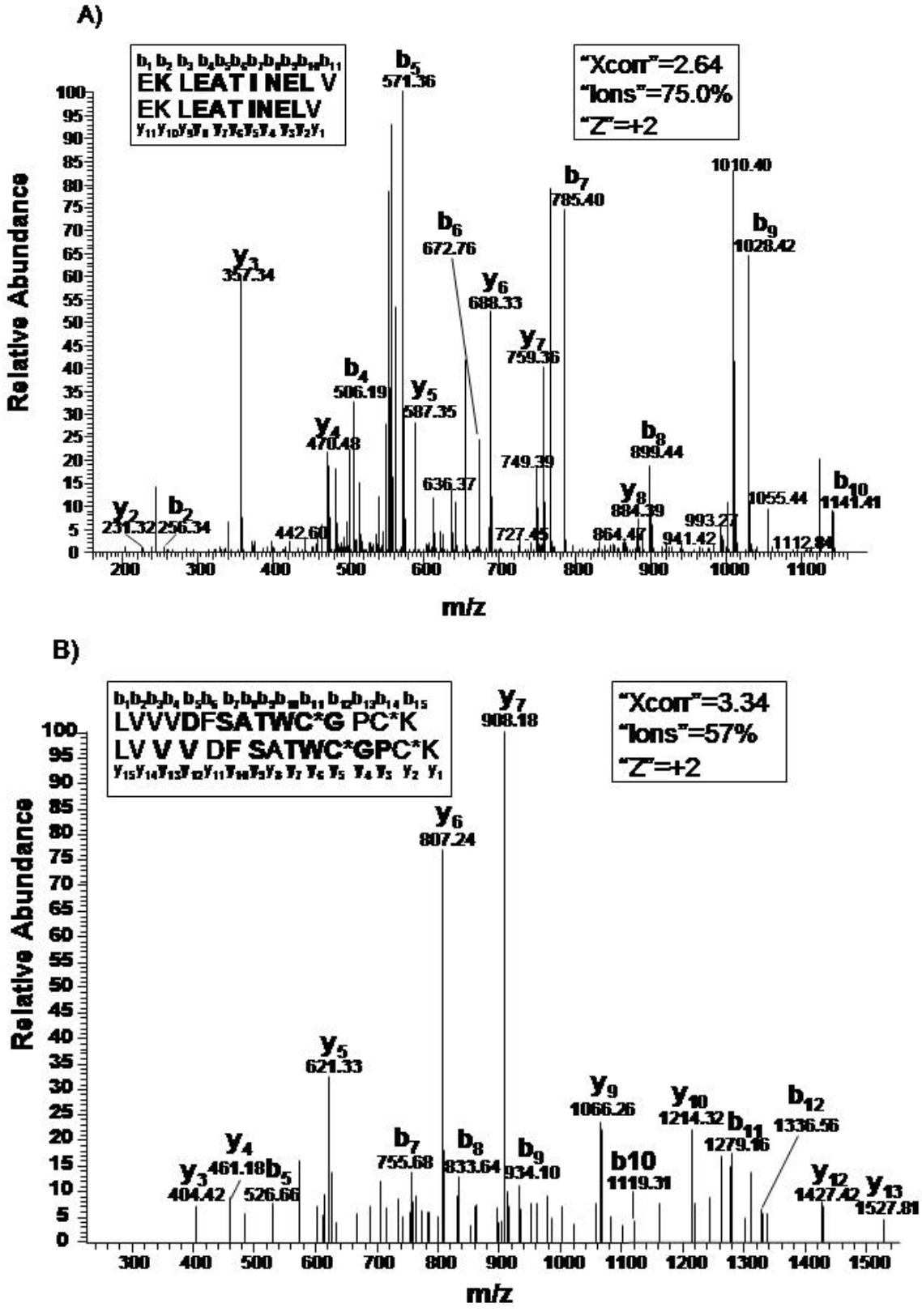
A)
EK LEAT I NEL V
EK LEAT INELV
"Xcorr"=2.64
"Ions"=75.0%
"Z"=+2
Relative Abundance
m/z
B)
LVVVDFSATWC*G PC*K
LV V V DF SATWC*GPC*K
"Xcorr"=3.34
"Ions"=57%
"Z"=+2
Relative Abundance
m/z

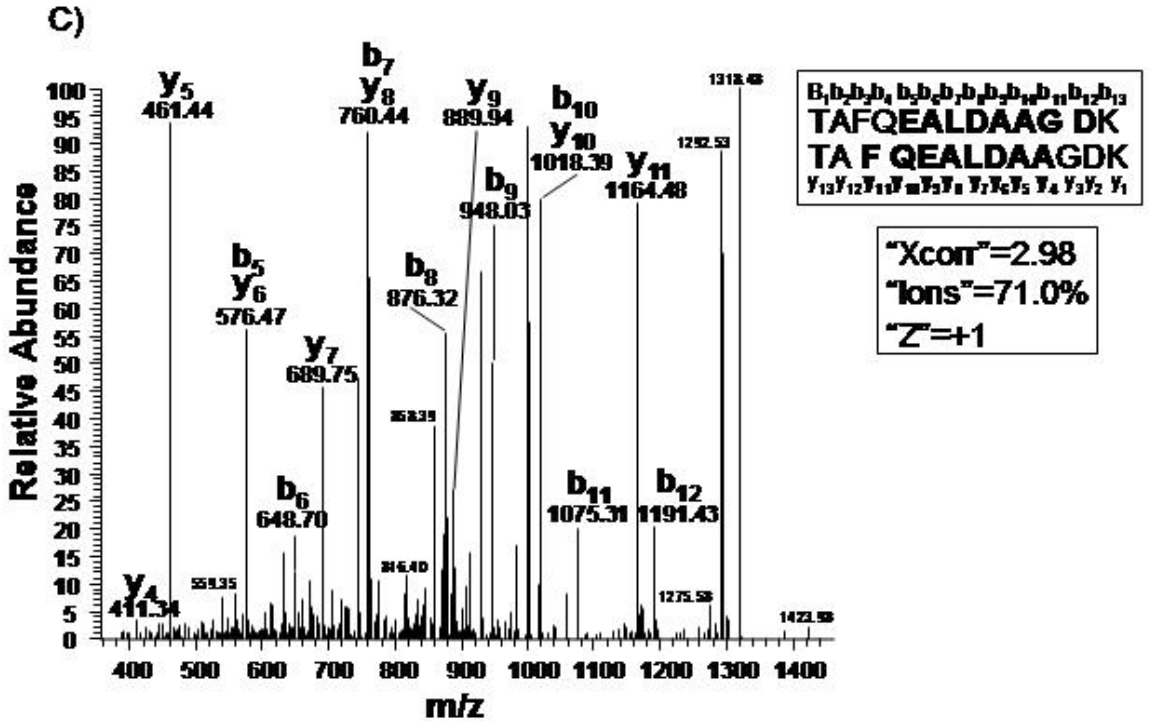

Fig.2.3. MS/MS Spectra of Thioredoxin Peptides Detected from H2O2 treated HDFs. The bolded letters indicate the detected b and y ions matching with the predicted ions in the protein sequence database (A-C). SEQUEST Flicka protein information shows the fragments detected relative to the complete sequence of thioredoxin protein (D).

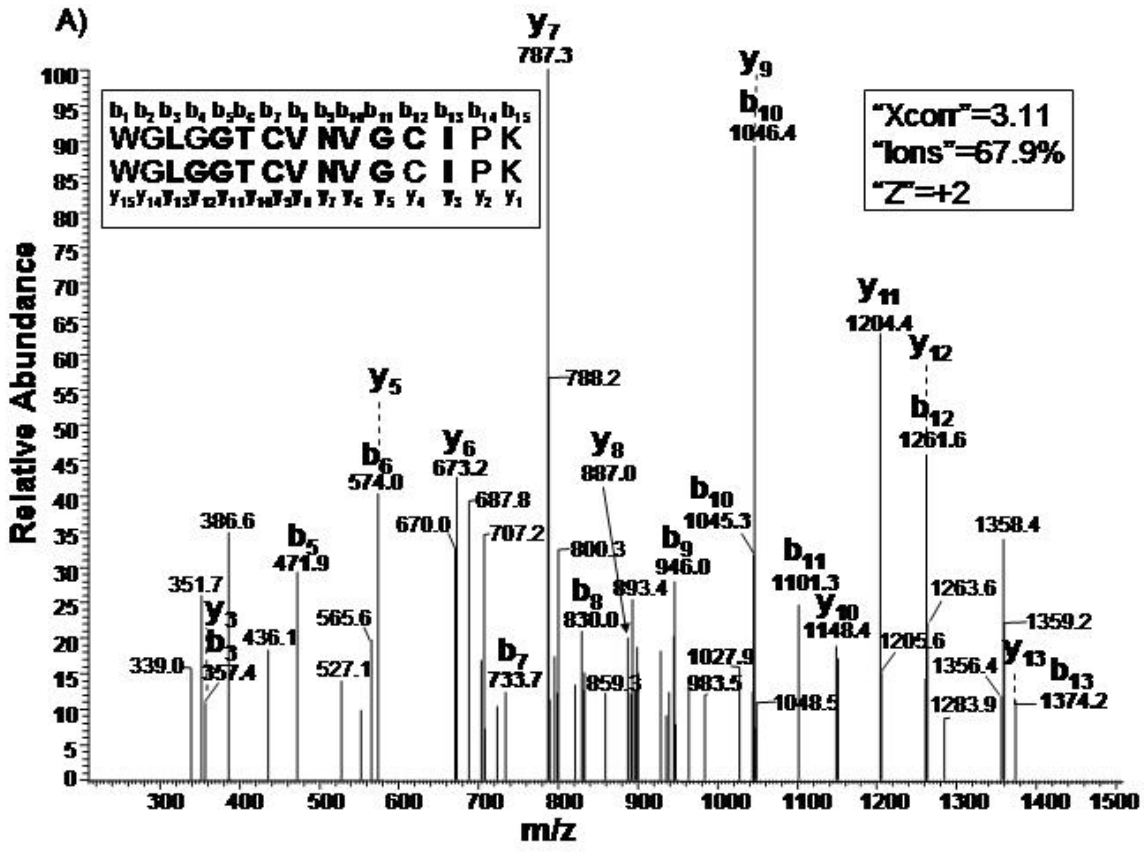

Fig.2.4. MS/MS Spectrum of Thioredoxin Reductase 1 Peptide Detected from H2O2-treated HDFs. The bolded letters indicate the detected b and y ions matching the predicted ion mass in the database (A). SEQUEST Flicka protein information shows the fragment detected relative to the complete sequence of thioredoxin reductase 1 protein (B).

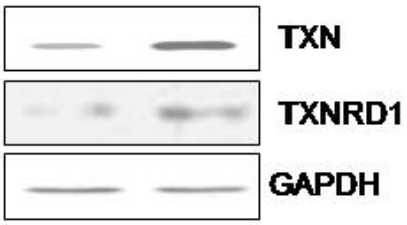

Fig.2.5. Increased TXN and TXNRD1 Protein Levels in the H2O2 Treated Cells. HDFs were treated with 600 μM H_2O_2 for 2 hrs. Cells were harvested 3 days after for SDS-PAGE and Western blot analyses to detect TXN and TXNRD1. GAPDH was used as a loading control to show equal amount of proteins between different groups of samples.

Alterations in gene expression profiles in HDFs upon H_2O_2 treatment

Microarray technology was adopted to address whether the proteins found unique to control or H_2O_2 treated cells show changes at the mRNA level. With RNA samples collected from Ctrl and H_2O_2 treated HDFs, we measured changes in gene expression by quantifying the binding of Cy5 versus Cy3 labeled cDNA to complementary strands of DNA immobilized to a microscopic chip. Since the goal here is to test whether the genes detected by proteomics also show changes at mRNA level, we used less stringent selection criteria by counting for the genes showing 1.5 fold or more changes in two out of three independent experiments, each of which has triplicates in hybridization. We found that 171 genes were up-regulated and 174 genes were down regulated by H_2O_2 treatment.

Functional genomics using BioRag program classified 17 up-regulated genes as related to antioxidant and detoxification responses (Table2.3). These 17 genes are TXNRD1, glutathione peroxidase 1 (GPX1), glutathione synthetase (GSS), Glutamate-cysteine ligase, modifier subunit (GCLM), Hydroxyacyl-Coenzyme A dehydrogenase, type II (HADH2), N-acetylglucosaminidase, alpha (NAGLU), Lysyl oxidase (LOX), Methylenetetrahydrofolate dehydrogenase (NADP+ dependent) 2 (MTHFD2), Prostaglandin-endoperoxide synthase 1 (PTGS1), Prostaglandin-endoperoxide synthase 2 (PTGS2) and 7 genes encoding different isoforms of metallothioneis (MTs), MT1A, MT1E, MT1G, MT1H, MT1M, MT1X and MT2A. Altered proteases, signaling molecules, kinases, and transcription regulators also stand out as a characteristic of H_2O_2

treated cells (Table2.3). In addition, H_2O_2 treated cells elevate the expression of a significant amount of cytokines or chemokines (Table2.3).

Cystoscape-based gene network sorting shows a significant portion of upregulated genes in the clusters of oxidoreductase, transferases, metal ion binding, protein Ser/Thr kinase, ATP binding, GTP binding, protein binding, and DNA binding (Fig. 6). Most of these clusters also contain downregulated genes (Fig.2.6). The clusters showing more decreased than increased genes include receptors and hydrolases (Fig.2.6).

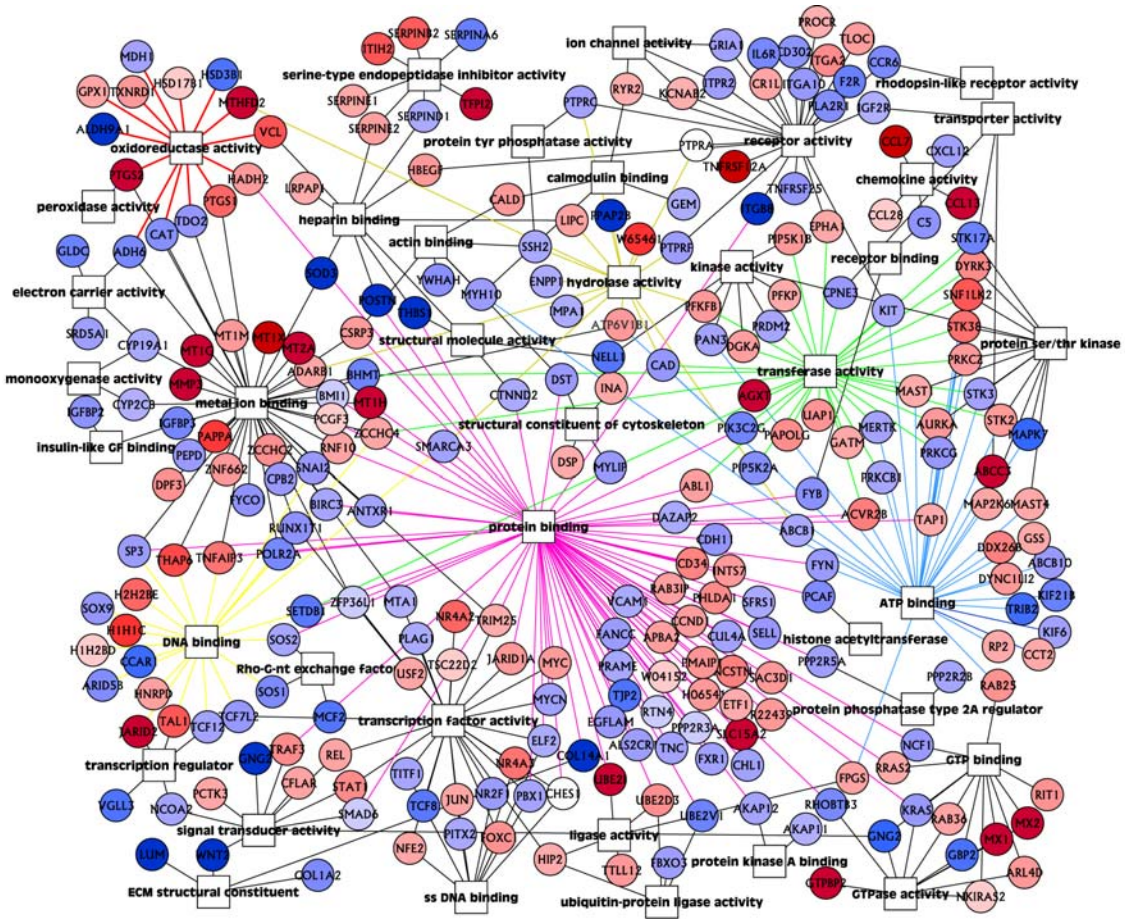

Fig.2.6. The Network of Genes Increased or Decreased in H2O2 Treated Cells. HDFs were treated with 600 μM H_2O_2 for 2 hrs. Microarray analyses were performed using RNA collected 72 hrs after H_2O_2 treatment. The nodes represent genes increasing (red) or decreasing (blue) in H_2O_2 treated cells. The color shades of nodes reflect the degree of changes, with darker color indicating more increase (red) or decrease (blue) than the lighter shade of color. The squares represent gene ontology terms. The colors of the edges enhance the view of corresponding gene ontology groups in the network of proteomic data.

Seven of up-regulated genes were chosen randomly for verification using semi-quantitative RT-PCR. With primer sets specific to ADP-ribosylation factor 4-like (ARF4L), Serine/threonine kinase 15 (Aurora kinase A, AURKA), matrix metallopeptidase 3 (MMP3), Small inducible cytokine A7 (CCL7), Small inducible cytokine subfamily A13 (CCL13), Tumor necrosis factor receptor superfamily member 12A (TNFRSF12A), or TXNRD1, RT-PCR with total RNA show increases in the transcripts of these genes by H_2O_2 treatment (Fig.2.7).

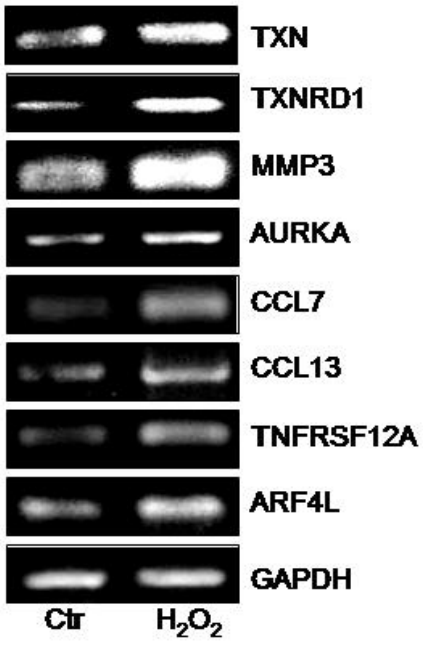

Fig.2.7. Increased mRNA levels of the Genes detected in the H2O2 treated HDFs. HDFs were treated with 600 μM H_2O_2 for 2 hrs. Cells were placed in fresh DMEM containing 10% FBS for 3 days before harvesting. Total RNA (2 μg) was used for reverse transcription (RT) and 3 μl of the 35μl RT reaction mixture was used for each PCR to amplify **ARF4L** (ADP-ribosylation factor 4-like), **AURKA** (Serine/threonine kinase 15), **CCL7** (Small inducible cytokine A7), **CCL13** (Small inducible cytokine subfamily A13), **MMP3** (Matrix metallopeptidase 3), **TXN** (Thioredoxin), **TXNRD1** (Thioredoxin reductase 1), **TNFRSF12A** (Tumor necrosis factor receptor superfamily, member 12A). GAPDH was amplified to show equal amount of RNAs between each sample.

The Overlaps of Proteins and Transcripts Induced by H_2O_2

With the long lists of proteins or genes detected by proteomics or microarray respectively, we have searched for the common outcome between the two platforms of technology. Both LC-MS/MS and cDNA microarray detected the induction of TXNRD1 by H_2O_2 treatment (Table2.2&2.3). This finding was confirmed by RT-PCR and Western blot techniques (Figure2.5&2.7). Among the decreased genes in H_2O_2 treated cells, A kinase anchor protein 12 and NAD malate dehydrogenase 1 were found common between microarray and proteomic outputs (Table2.2&2.3). TXN was found elevated by proteomics but the gene was absent on the microarray chips. RT-PCR analyses show elevated levels of TXN mRNA in H_2O_2 treated cells (Fig.2.7). MMP3 and AURKA are among elevated genes detected by microarray analyses in H_2O_2 treated cells. While proteomics failed to detect these two proteins, Western blots found elevated levels of these two proteins in H_2O_2 treated cells (Fig.2.8). Adding up together, only a short list of genes found to increase or decrease by both microarray and proteomics in H_2O_2 treated cells.

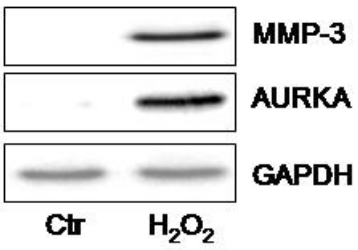

Fig.2.8. Increased Protein levels of AURKA and MMP-3. HDFs were treated with 600 μM H_2O_2 for 2 hrs. Cell lysates were collected 72 hrs after H_2O_2 treatment to perform Western blot analyses to detect MMP3 and AURKA. GAPDH was used as a loading control to show equal amount of proteins between samples.

Discussion:

Using current available technologies, we have intended to address the overlap between transcripts and proteins altered by oxidative stress using HDFs as an experimental system. Even with a low stringency data analysis method of microarray, most genes corresponding to the proteins found unique to H_2O_2 treated cells were not detected for elevated transcripts by microarray analyses. Only TXNRD1 was detected by both LC-MS/MS based proteomics and cDNA microarray technique for elevated expression in H_2O_2 treatment. Two down regulated genes, A kinase anchor protein 12 and NAD malate dehydrogenase 1, were identified as the overlaps between microarray and proteomics. Despite the short list of overlapping genes, transcript or protein network analyses using BioRag and Cytoscape programs point to similar biochemical pathways altered by H_2O_2 treatment.

A cluster of genes or proteins has been found related to oxidoreductase, antioxidants and detoxification enzymes. The finding of elevated expression of TXN and TXNRD1 in H_2O_2 treated cells is consistent with previous reports(190). TXN and TXNRD1 are downstream target genes of AP-1 and/or Nrf-2 transcription factors, both of which are activated by H_2O_2(191-193). TXNRD1 belongs to a family of glutathione reductase-like flavoenzymes, a homodimeric selenium-containing protein that catalyzes NADPH-dependent reduction of TXN disulfide(190, 194, 195). In mammalian cells, two TXNRDs have been found, TXNRD1 located in the cytosol and TXNRD2 located in the mitochondria(190). In addition to TXN, TXNRD1 also catalyzes the reducing reaction of numerous other substrates, including H_2O_2, lipid hydroperoxides, lipoic acid, ascorbyl

free radicals and possibly the tumor suppressor protein p53(190, 196). Both TXNRD1 and TRX contain tandem cysteine residues that are essential for redox regulation of enzymes, signaling molecules and transcription factors(190, 194, 195, 197). Following oxidative stress, TXNRD initiates the reduction and therefore activation of TRX. Activated TRX then relocates from the cytoplasm to the nucleus to turn on the nuclear components of redox-sensitive signaling pathways, for example Ref-1, which then activates transcription factors such as AP-1 and NF-kB(198-201). These transcription factors modulate the expression of downstream target genes important for the gain of repair function against the initial oxidative damage and for development of defense against further insults.

Both microarray and proteomics indicate upregulation of metal binding proteins by H_2O_2 treatment. Up-regulation was observed for 7 genes encoding different isoforms of MTs after H_2O_2 treatment. This finding is consistent with literature reports where MT1A, MT1X, and MT2A have been shown to elevate expression in response to H_2O_2 treatment(202-204). MTs are characterized by their unusually high content of thiols and are capable of binding to iron and preventing the redox cycling of iron(205). As a result, MTs often act as scavengers of ROS, including hydroxyl, phenoxyl, and NO radicals(205, 206). MT mediated cytoprotection serves as a redundant mechanism in addition to TXN/TXNRD in cellular adaptation to an initial insult of oxidative stress.

Fibroblasts produce extracellular matrix to maintain the texture and structure of most organs. In addition, fibroblasts are capable of producing various paracrine factors such as peptide growth factors, cytokines, and chemokines during the processes of tissue

injury and inflammation(207, 208). The expression of several cytokines were found to be elevated by H_2O_2 treatment here: small inducible cytokine A7 (CCL7), small inducible cytokine subfamily A member 13 (CCL13), CC chemokine CCL28 (CCL28), Interleukin 1 beta (IL1B), Interleukin 32 (IL32), Leukemia inhibitory factor (LIF) and Colony stimulating factor 3 (CSF3), indicating HDFs may elicit inflammatory response when they were exposed to sublethal dose of H2O2. Although many of these genes are among the long list of novel finding of oxidative stress response, consistent with our findings, IL1B has been shown induced by H2O2 treatment (209).

Several possibilities explain the short list of overlaps between microarray and proteomics data. The cell lysates used here do not contain secreted proteins, although a number of genes encoding secreted proteins show up in microarray results (for example MMP3 and IGFBP6). Due to the secreted nature of MMP3 and IGFBP6, these proteins are unlikely to be in high abundance in cell lysates and not able to be detected by our current method of proteomics. However IGFBP6 was found elevated in the conditioned media of H_2O_2 treated HDFs using a classical LC-MS/MS that has less sensitivity than current LCQ-Deca XP Plus ion trap mass spectrometer(180). In addition to the absence of secreted proteins for proteomic detection, human 5K cDNA gene chip was used for the microarray technology in this study. Checking the list of genes on these chips, we found that 52% of the proteins detected by LC-MS/MS were absent on the Human 5K cDNA chip (Table 2). For example, TXN was detected in the cell lysate of H_2O_2 treated HDFs by MudPIT analysis but the cDNA sequence of the gene was absent in our microarray slides (Table 2). If we factor in the absence of the genes for 50% detected proteins, the

amount of overlapping genes and proteins detected by microarray and proteomics could be doubled. The human genome encodes about 30,000 transcripts(210, 211). If the cDNA sequences of all these transcripts had been printed for microarray analyses, we expect a 6 fold increase in the number of overlapping genes between proteomics and microarray analyses. By extrapolating our current data, one may predict 18 genes altered at both mRNA and protein levels by H_2O_2 treatment. This number remains far below the assumption that increased mRNAs reflect changes of gene expression at the protein level.

The large gap between the genes expressed at the level of mRNA versus protein may be related to the regulatory mechanism of protein translation under oxidative stress. The process of protein translation is performed by ribosomes and at least 14 eukaryotic initiation factors (eIFs). About 95-97% genes are translated via 5' methyl cap mechanism(212-214). This type of translation requires a large amount of ATP and is generally turned off during stress to conserve energy(213, 215). Only 3-5% genes contain internal ribosomal entry site (IRES), allowing selective protein translation to occur under stress condition(213, 215). Given such a small percentage of genes containing IRES, it is expected that not all the transcripts showing elevated levels are actually translated. Therefore even with improved microarray or proteomic technology, one may find that the overlap between the increases at the level of mRNA versus that of protein remains small.

Proteomics is an evolving technology that demands advancement in instrument sensitivity and versatility(216-218). Improved flexibility in the quantitative nature is also required for comparative proteomics. The detection of quantitative changes is quite

random with current LC-MS/MS based proteomic technologies. Western blot detections of elevated MMP3 and AURKA in H_2O_2 treated cells are good examples suggesting that not all the proteins showing elevated levels can be detected by current technology. The technology requires peptic digestion of a protein mixture. Current mass spectrometers can only detect peptide ions in the range of 300 – 2000 dalton. However, standard tryptic digestion cleaves proteins after Lys or Arg residues and may not generate the peptides within this mass range due to the nature of sequences for certain proteins. Peptide ionization and runing through a mass analyzer compose two additional layers of complexity for successful protein identification. Furthermore, although we have separated the peptide mixtures from cell lysates into 12 fractions by two-dimensional liquid chromatography, additional separation technologies will likely generate less complex peptide mixtures and therefore increase the detection capacity of mass spectrometers. In fact, improving liguid chromatography separation capacity by ues of automatic ultra high pressure, peptide identification capacity should increase about 30%(219). In addition to these mechanical issues of proteomics, many proteins are modified posttranslationally and current available analytical software is limited in detecting posttranslational modifications when the whole proteome of a particular cellular state is profiled. Therefore development of new protein separation technologies, increased capacity of mass spectrometers, and advancement in software tools are essential for profiling the whole proteome depicting a specific state of cells.

Table2.1. Sequence, expected fragment size and annealing temperature (ta) of primers used.

Gene	Sequense	Expected fragment size (bp)	TempA(°C)	GenBank accession number
MMP3	Sense:gcagtttgctcagcctatcc Antisense:gagtgtcggagtccagcttc	214	62	Hs.375129
AURKA	Sense:tgaggagggaactggcatcaa Antisense:gaccacccaaaatctgcaat	208	62	Hs.250822
TXNRD1	Sense:attgccactggtgaaagacc Antisense:accaattttgttggccatgt	185	55	Hs.567352
TXN	Sense:ctgcttttcaggaagccttg Antisense:tgttggcatgcatttgactt	203	53	Hs.435136
CCL7	Sense:atgaaagcctctgcagcact Antisense:ggacagtggctactggtggt	179	64	Hs.251526
CCL13	Sense:atctccttgcagaggctgaa Antisense:cttcagggtgtgagctttcc	165	62	Hs.414629
TNFRSF12A	Sense:ctggctccagaacagaaagg Antisense:gggcctagtgtcaagtctgc	156	62	Hs.355899
ARF4L	Sense:ggggaaccacttgactgaga Antisense:tcttctcggtgttgaagcct	171	62	Hs.183153
GAPDH	Sense:cgtcttcaccatggaga Antisense:cggccatcacgcccacagttt	238	62	Hs.544577

* **MMP3** (Matrix metallopeptidase 3); **AURKA** (Serine/threonine kinase 15); **TXNRD1** (Thioredoxin reductase 1); **TXN** (Thioredoxin); **CCL7** (Small inducible cytokine A7); **CCL13** (Small inducible cytokine subfamily A13); **TNFRSF12A** (Tumor necrosis factor receptor superfamily, member 12A) (); **ARF4L** (ADP-ribosylation factor 4-like); **GAPDH** (Glyceraldehyde-3-phosphate dehydrogenase)

Table 2.2. Proteins found unique to control (Italic) or H2O2-treated HDFs.

Cell lysates were prepared as described in the Methods for MudPIT and MS/MS analyses. The proteins unique to Control group (in italic) or H_2O_2 treated group are listed here. All proteins meet the selection criteria of Xcorr ≥ 1.8 for +1 ions, Xcorr ≥2.5 for +2 ions and Xcorr ≥ 3.5 for +3 ions. The value of Ions exceeds 50% in all cases by Turbo SEQUEST analyses. The column in the table represents 1) Gene symbol. The sign [%] marks the protein whose corresponding cDNAs was not on the list of genes in Human 5k cDNA microarray chip; 2) Gi number; 3) common name of the protein; 4) Xcorr values for +2 peptide ions, means ± standard deviations, unless specifically labeled. The letter *a* indicates Xcorr values for +1 peptide ions, while the letter *c* indicates Xcorr values for +3 peptide ions; 5) The letter *d* indicates the charge of detected peptide ions with the number of detected peptide ions shown in a parenthesis. The letter *e* denotes the peptide sequence if only one peptide ion was detected for the protein. The letter *f* represents the percentage of coverage of detected peptides over total protein sequences.

1) Gene Symbol	2) Gi #	3) Common Name	4) Xcorr (±SD)	5) Charge (Pep#)& Sequence &Coverage
Oxidoreductase/antioxidants/detoxification				
ERO1L[%]	*14250470*	*ERO1-like*	*2.74*	*[d]+2(1), [e]LGAVDESLSEETQK,[f]3.0%*
GSTO1[%]	*4758484*	*glutathione-S-transferase omega 1*	*2.59*	*[d]+2(1), [e]EDPTVSALLTSEK, [f]4.5%*
HADHA	*20127408*	*hydroxyacyl dehydrogenase, subunit A*	*2.79*	*[d]+2(1), [e]TGIEQGSDAGYLCESQK, [f]2.2%*
LDHB[%]	*4557032*	*lactate dehydrogenase B*	*3.41±0.72*	*[d]+2(2), [f]9.3%*
MDH1	*7431153*	*malate dehydrogenase, cytosolic*	*4.38*	*[d]+2(1), [e]VIVVGNPANTNCLTASK, [f]5.1%*
PRDX3	*23308577*	*peroxiredoxin 3 isoform a*	*3.32*	*[d]+2(1), [e]AGTGVDNVDLEAATR, [f]2.8%*
PHGDH	*5802974*	*phosphoglycerate dehydrogenase*	*4.09*	*[d]+2(1), [e]DYGVLLEGSGLALR, [f]5.5%*
ADH5	11496891	alcohol dehydrogenase III5 chi subunit	4.02±1.24	[d]+2(2), [f]9.6%
ASPH[%]	14589860	aspartate beta-hydroxylase isoform c	4.04	[d]+2(1), [e]LGIYDADGDGDFDVDDAK, [f]5.8%
MDH2[%]	21735621	mitochondrial malate dehydrogenase	3.58±1.24	[d]+2(4), [f]18.0%
PDIA6[%]	5031973	Protein disulfide isomerase A6	3.49±0.94	[d]+2(2), [f]6.5%
TXN[%]	135773	thioredoxin	[a]2.98, 2.99±0.49	[d]+1(1), [d]+2(2), [f]37.1%
TXNRD1	34147789	thioredoxin reductase 1	3.11	[d]+2(1), [e]WGLGGTCVNVGCIPK, [f]2.9%
Metabolic enzymes				
ALDOA[%]	*4557305*	*aldolase A*	*4.10±0.14*	*[d]+2(2),[f]10.2%*
ASS[%]	*16950633*	*argininosuccinate synthetase*	*2.53*	*[d]+2(1), [e]FELSCYSLAPQIK, [f]3.2%*
GBE1	*15082371*	*Glucan, branching enzyme 1*	*3.12*	*[d]+2(1), [e]VALILQNVDLPN, [f]1.7%*

GOT2	*12653507*	*Glutamic-oxaloacetic transaminase 2*	*4.11*	*[d]+2(1), [e]FVTVQTISGTGALR, [f]3.3%*
PPIA	*10863927*	*peptidylprolyl isomerase A*	*3.10±0.36*	*[d]+2(2), [f]12.1%*
PPIB	*118090*	*Peptidyl-prolyl cis-trans isomerase B*	*[a]2.14, 3.53*	*[d]+1(1), [d]+2(1),[f]10.1%*
PGK1[%]	*129902*	*Phosphoglycerate kinase 1*	*4.78±0.19*	*[d]+2(2), [f]8.1%*
PKM2[%]	*33286420*	*pyruvate kinase 3 isoform 2*	*3.87±1.01*	*[d]+2(9), [f]22.6%*
PSAP[%]	30235	cerebroside sulfate activator	3.80	[d]+2(1), [e]EIVDSYLPVILDIIK, [f]22.4%
FASN	1345959	Fatty acid synthase	3.91±1.36	[d]+2(2), [f]1.4%
GBA[%]	183012	glucocerebrosidase	3.46	[d]+2(1), [e]PVSLLASPWTSPTWLK, [f]3.0%
GANAB[%]	2274968	Glucosidase II	2.60	[d]+2(1), [e]VPDVLVADPPIAR, [f]1.4%
ECHS1	433413	mitochondrial short-chain enoyl-CoA hydratase	2.98	[d]+2(1), [e]ALNALCDGLIDELNQALK, [f]6.2%
NANS[%]	12056473	N-acetylneuraminic acid phosphate synthase	4.19±0.91	[d]+2(4), [f]2.8%
Receptor activity				
M6PRBP1[%]	*20127486*	*Mannose-6-phosphate receptor binding protein 1*	*3.41*	*[d]+2(1), [e]IATSLDGFDVASVQQQR, [f]3.9%*
TAX1BP3	*11993943*	*Tax interaction protein 1*	*3.99*	*[d]+2(1), [e]VSEGGPAEIAGLQIGDK, [f]13.7%*
GABRB2[%]	12548785	GABA A receptor, beta 2 isoform 1	2.64	[d]+2(1), [e]LDVNKIFYKDIK, [f]2.3%
Transport activity				
ATP1B3	*4502281*	*ATPase, Na+/K+ transporting, beta 3*	*2.67*	*[d]+2(1), [e]LFIYNPTTGEFLGR, [f]5.0%*
ATP5B	*32189394*	*ATP synthase, H+ transporting, mitochondrial F1 complex, beta*	*3.67*	*[d]+2(1), [e]AIAELGIYPAVDPLDSTSR, [f]6.1%*
KPNB1	*19923142*	*karyopherin beta 1*	*2.81±0.12*	*[d]+2(2), [f]3.5%*
Signaling molecules				
ANXA4	*34365437*	*annexin A4*	*3.47*	*[d]+2(1), [e]SETSGSFEDALLAIVK, [f]14.3%*
GNG12[%]	*12229817*	*Guanine nucleotide-binding protein G(I)/G(S)/G(O) gamma-12 subunit*	*3.53*	*[d]+2(1), [e]SDPLLIGIPTSENPFK, [f]22.2%*
RAP1B	*7661678*	*RAS-related protein*	*3.76*	*[d]+2(1), [e]INVNEIFYDLVR, [f]1.6%*

STIP1	*5803181*	*RAP1B stress-induced-phosphoprotein 1*	*3.43*	*[d]+2(1), [e]ALSVGNIDDALQCYSEAIK, [f]3.5%*
ANP32B[%]	5454088	Acidic nuclear phosphoprotein 32 family, member B	3.51	[d]+2(1), [e]SLDLFNCEVTNLNDYR, [f]8.2%
ANXA5[%]	3212603	Annexin V With Proline Substitution By Thioproline	[a]2.05±0.09; 3.82±0.76	[d]+1(3),[d]+2(4), [f]22.5%
CDC42	16357472	cell division cycle 42 isoform 2	2.61	[d]+2(1), [e]TPFLLVGTQIDLR, [f]6.8%
CAP1[%]	33357226	C-Terminal Cap1-Adenylyl Cyclase Associated Protein Chain A	5.03	[d]+2(1), [e]VENQENVSNLVIEDTELK, [f]11.5%
EIF3S5[%]	30584931	eukaryotic translation initiation factor 3, subunit 5 epsilon	3.83	[d]+2(1), [e]VIGLSSDLQQVGGASAR, [f]4.9%
IQGAP1	40674640	IQGAP1 protein	4.03	[d]+2(1), [e]ILAIGLINEALDEGDAQK, [f]1.9%
MVP	5851638	Major vault protein	3.07±0.29	[d]+2(2), [f]20.1%
TBX20[%]	13431875	Putative S100 calcium-binding protein	3.86	[d]+2(1), [e]TEFLSFMNTELAAFTK, [f]15.4%
GDI2	4960030	Rab GDP dissociation inhibitor beta	3.67	[d]+2(1), [e]TDDYLDQPCYETINR, [f]4.2%
SET	1711383	SET protein	3.70	[d]+2(1), [e]IDFYFDENPYFENK, [f]5.1%
GNB1	3387975	signal transducing proteins GS/GI beta-subunit	3.09	[d]+2(1), [e]LLLAGYDDFNCNVWDALK, [f]14.2%
RAB7	1174149	small GTP binding protein Rab7	3.20	[d]+2(1), [e]GADCCVLVFDVTAPNTFK, [f]8.7%
RAP1GAP[%]	34327960	RAP1 GTPase activating protein	2.54	[d]+2(1), [e]GSAIGIGTVEEVVVR, [f]2.2%
Peptidases and Inhibitors				
PPGB[%]	*12653639*	*Protective protein for beta-galactosidase*	*3.22*	*[d]+2(1), [e]DLECVTNLQEVAR, [f]2.7%*
PSMA7[%]	*4506189*	*proteasome subunit, alpha type, 7*	*3.90±0.07*	*[d]+2(2), [f]16.3%*
SERPINB6	*20141722*	*serpin peptidase inhibitor, clade B, member 6*	*2.82*	*[d]+2(1), [e]IAELLSPGSVDPLTR, [f]4.0%*
CTSB[%]	115711	Cathepsin B precursor	3.63	[d]+2(1), [e]NGPVEGAFSVYSDFLLYK, [f]5.3%
PSMA2	4506181	proteasome alpha 2 subunit	3.72	[d]+2(1), [e]AAVPSGASTGIYEALELR, [f]4.1%
Structural				
ACTN4	*12025678*	*actinin, alpha 4*	*3.64±0.93*	*[d]+2(3), [f]4.4%*

ACTR1A	*5031569*	*ARP1 actin-related protein 1 homolog A, centractin alpha*	*4.02±0.97*	*[d]+2(2), [f]8.8%*
Arp11	*12583652*	*Actin-related protein Arp11*	*3.39*	*[d]+2(1), [e]DITYFIQQLLR, [f]5.2%*
ACTB	*16359158*	*beta actin*	*3.65±1.11, [c]4.21*	*[d]+2(4), [d]+3(1),[f]16.0%*
CALD1[%]	*4826657*	*caldesmon 1 isoform 3*	*3.08*	*[d]+2(1), [e]EFDPTITDASLSLPSR, [f]3.3%*
COL6A1[%]	*1360676*	*collagen alpha 1(VI) chain*	*4.93*	*[d]+2(1), [e]LLLFSDGNSQGATPAAIEK, [f]1.8%*
COL6A2	*105706*	*collagen alpha 2(VI) chain*	*4.13*	*[d]+2(1), [e]NLEWIAGGTWTPSALK, [f]6.7%*
COL6A3	*17149807*	*collagen alpha 3 (VI) isoform 3*	*3.29±0.96*	*[d]+2(2), [f]1.0%*
FSCN1[%]	*13623415*	*Fascin 1*	*3.14*	*[d]+2(1), [e]ASAETVDPASLWEY, [f]2.8%*
FER1L3	*10834587*	*Fer-1 like protein 3*	*4.06*	*[d]+2(1), [e]NLVDPFVEVSFAGK, [f]0.7%*
GSN[%]	*17028367*	*Similar to gelsolin*	*3.28±0.02*	*[d]+2(2), [f]10.9%*
RPL18[%]	*4506607*	*ribosomal protein L18*	*2.87*	*[d]+2(1), [e]ILTFDQLALDSPK, [f]6.9%*
RPS8[%]	*4506743*	*ribosomal protein S8*	*3.16*	*[d]+2(1), [e]NCIVLIDSTPYR, [f]5.8%*
TUBA1A[%]	*30584771*	*tubulin alpha 1*	*3.87±0.88; [c]3.76*	*[d]+2(5), [d]+3(1), [f]18.0%*
TPM2[%]	6573280	beta tropomyosin	3.01	[d]+2(1), [e]LVILEGELER, [f]3.5%
CAPZB[%]	13124696	F-actin capping protein beta subunit	2.93	[d]+2(1), [e]GCWDSIHVVEVQEK, [f]5.1%
LAMP1	39645231	LAMP1 protein	5.20	[d]+2(1), [e]FFLQGIQLNTILPDAR, [f]6.5%
MSN	14625824	moesin/anaplastic lymphoma kinase fusion protein	4.74	[d]+2(1), [e]FYPEDVSEELIQDITQR, [f]3.2%
TUBB	56757569	Tubulin beta-1 chain	4.48±0.53	[d]+2(2), [f]7.2%
Protein binding				
AKAP12	*21493022*	*A-kinase anchor protein 12 isoform 1*	*4.50*	*[d]+2(1), [e]LVQNIIQTAVDQFVR, [f]0.8%*
HSPE1	*4008131*	*chaperonin 10*	*4.06*	*[d]+2(1), [e]VLQATVVAVGSGSK, [f]14.1%*
CCT6A	*4502643*	*chaperonin containing TCP1 subunit 6A*	*2.85*	*[d]+2(1), [e]AQLGVQAFADALLIIPK, [f]3.2%*
CTTN[%]	*20357552*	*cortactin isoform a*	*2.65*	*[d]+2(1), [e]YGLFPANYVELR, [f]2.2%*
HSP90AB1[%]	*20149594*	*heat shock protein 90-beta*	*4.08+-0.62*	*[d]+2(3), [f]5.3%*
HSPA2[%]	*13676857*	*heat shock 70kDa protein 2*	*3.40±0.82*	*[d]+2(2), [f]6.1%*
MAP1B[%]	*14165456*	*microtubule-associated protein 1B isoform 2*	*4.07*	*[d]+2(1), [e]NLISPDLGVVFLNVPENLK, [f]0.8%*
RCN1	*4506455*	*reticulocalbin 1 precursor*	*3.42±0.19*	*[d]+2(2), [f]8.5%*
RCN3[%]	*28626510*	*reticulocalbin 3, EF-hand calcium binding*	*4.81*	*[d]+2(1), [e]DIVIAETLEDLDR, [f]4.0%*

		domain		
RNH1[%]	*35844*	*ribonuclease/angiogenin inhibitor*	*3.38±0.69*	[d]*+2(3),* [f]*10.6%*
CAND1[%]	*21361794*	*TIP120 protein*	*3.93*	[d]*+2(1),* [e]*ISGSILNELIGLVR,* [f]*2.5%*
CCT5	24307939	chaperonin containing TCP1, subunit 5	3.25	[d]+2(1), [e]WVGGPEIELIAIATGGR, [f]3.2%
AHNAK[%]	627367	Desmoyokin	3.00±0.26	[d]+2(8), [f]4.2%
FCGR2A[%]	34419635	heat shock 70kDa protein 6	4.02	[d]+2(1), [e]IINEPTAAAIAYGLDR, [f]2.5%
SERPINH1[%]	8574449	rheumatoid arthritis-related antigen RA-A47	3.71±0.07	[d]+2(2), [f]18.6%
VCP[%]	6005942	valosin-containing protein	3.07±0.23	[d]+2(3), [f]7.5%
VAMP3	13543574	Vesicle-associated membrane protein 3	3.48	[d]+2(1), [e]ADALQAGASQFETSAAK, [f]17.0%
DNA/RNA/nucleotide binding				
EIF4A2	*16198386*	*Eukaryotic translation initiation factor 4A, isoform 2*	*2.77*	[d]*+2(1),* [e]*GYDVIAQAQSGTGK,* [f]*3.4%*
HNRPU	*14141161*	*heterogeneous nuclear ribonucleoprotein U isoform b*	*2.12*	[d]*+1(1),* [e]*VSELKEELK,* [f]*1.1%*
HNRPD	*870747*	*heterogeneous nuclear ribonucleoprotein D*	*2.66*	[d]*+2(1),* [e]*IFVGGLSPDTPEEK,* [f]*4.9%*
SERBP1[%]	*7661626*	*PAI-1 mRNA-binding protein*	*3.51*	[d]*+2(1),* [e]*FDQLFDDESDPFEVLK,* [f]*4.0%*
PCBP2	*14141166*	*poly(rC)-binding protein 2 isoform b*	*2.75*	[d]*+2(1),* [e]*AITIAGIPQSIIECVK,* [f]*4.4%*
RPL14[%]	*7513316*	*ribosomal protein L14*	*4.45*	[d]*+2(1),* [e]*LVAIVDVIDQNR,* [f]*5.4%*
CD151	*4506671*	*ribosomal protein P2*	*3.40±0.28*	[d]*+2(2),* [f]*27.8%*
RPS14	*5032051*	*ribosomal protein S14*	*3.14*	[d]*+2(1),* [e]*IEDVTPIPSDSTR,* [f]*8.6%*
septin 11[%]	*33873799*	*Septin11*	*3.44*	[d]*+2(1),* [e]*LTIVDTVGFGDQINK,* [f]*3.1%*
TRIM28	*5032179*	*tripartite motif-containing 28 protein*	*2.57*	[d]*+2(1),* [e]*LDLDLTADSQPPVFK,* [f]*1.8%*
EIF5A[%]	33383425	eukaryotic initiation factor 5A isoform I variant A	4.29	[d]+2(1), [e]NDFQLIGIQDGYLSLLQDSGEVR, [f]12.5%
HNRPA1	133252	Heterogeneous nuclear ribonucleoprotein A1	3.19	[d]+2(1), [e]LFIGGLSFETTDESLR, [f]8.2%
RPL6[%]	16753227	ribosomal protein L6	3.29	[d]+2(1), [e]ASITPGTILIILTGR, [f]5.2%
RPLP0[%]	4432757	ribosomal protein P0	4.30	[d]+2(1), [e]VLALSVETDYTFPLAEK, [f]18.3%
Miscellaneous				
BLOCK 23[%]	*20853684*	*BLOCK 23*	*3.28±0.75*	[d]*+2(2),* [f]*7.9%*

NAP1L2[%]	*30584347*	*Homo sapiens nucleosome assembly protein 1-like 2*	*3.10*	[d]*+2(1),* [e]*LDGLVETPTGYIESLPR,* [f]*4.3%*
VAT1[%]	*18379349*	*vesicle amine transport protein 1(BRCA1)*	*3.38*	[d]*+2(1),* [e]*TVENVTVFGTASASK,* [f]*3.8%*
ATP5A1[%]	34782901	ATP5A1 protein	3.54	[d]+2(1), [e]TGAIVDVPVGEELLGR, [f]3.6%
TMC5[%]	31377679	Transmembrane channel-like 5	[a]1.90	[d]+1(1), [e]NQPRTMEEKR, [f]1.5%

Table 2.3. cDNA Microarray detection of genes changing expression in HDFs with H_2O_2 treatment.

Gene Symbol	Accession	Gene Name	Unigene	Fold of Changes
Oxidoreductase/antioxidants				
GCLM	JC2474	Glutamate-cysteine ligase, modifier subunit	Hs.315562	1.89±0.01
GPX1	AA485362	Glutathione peroxidase 1	Hs.76686	1.74±0.21
GSS	AA463458	Glutathione synthetase	Hs.82327	1.68±0.14
HADH2	AA458661	Hydroxyacyl-Coenzyme A dehydrogenase, type II	Hs.171280	1.99±0.33
LOX	AA453085	Lysyl oxidase	Hs.102267	3.47±2.08
MT1A	H72722	Metallothionein 1A (functional)	Hs.513626	3.74±2.56
MT1E	AA872383	Metallothionein 1E	Hs.534330	3.24±1.66
MT1G	H53340	Metallothionein 1G	Hs.433391	3.90±2.45
MT1H	H77766	Metallothionein 1H	Hs.438462	3.26±1.59
MT1M	AA570216	Metallothionein 1M	Hs.647370	2.89±1.38
MT1X	N80129	Metallothionein 1X	Hs.374950	3.54±2.39
MT2A	AI024402	Metallothionein 2A	Hs.647371	3.47±2.01
MTHFD2	AA480995	Methylenetetrahydrofolate dehydrogenase 2	Hs.469030	3.47±2.72
NAGLU	W07099	N-acetylglucosaminidase, alpha	Hs.50727	1.55±0.06
PTGS1	AA454668	Prostaglandin-endoperoxide synthase 1	Hs.201978	2.50±0.74
PTGS2	AA644211	Prostaglandin-endoperoxide synthase 2	Hs.196384	4.91±4.39
TXNRD1	AA453335	Thioredoxin reductase 1	Hs.654922	2.76±1.88
ADH6	*H68509*	*Alcohol dehydrogenase 6 (class V)*	*Hs.586161*	*-2.32±1.09*
ALDH9A1	*R25818*	*Aldehyde dehydrogenase 9 family, member A1*	*Hs.2533*	*-4.85±5.11*
BBS9	*T58298*	*Bardet-Biedl syndrome 9*	*Hs.372360*	*-1.78±0.23*
CAT	*N77183*	*Catalase*	*Hs.502302*	*-2.18±0.59*
CYP2A6	*T73031*	*Cytochrome P450, subfamily IIA, polypeptide 6*	*Hs.439056*	*-2.36±1.15*
CYP2C8	*N53136*	*Cytochrome P450, subfamily IIC, polypeptide 8*	*Hs.282871*	-1.56±0.05
FMO5	*H52001*	*Flavin containing monooxygenase 5*	*Hs.303476*	*-1.86±0.40*
GLDC	*N78083*	*Glycine dehydrogenase*	*Hs.573072*	*-2.43±0.30*
HSD3B1	*R68803*	*Hydroxy-delta-5-steroid dehydrogenase, 3 beta- and steroid delta-isomerase 1*	*Hs.364941*	*-2.75±1.15*
MDH1	*H83233*	*Malate dehydrogenase 1, NAD (soluble)*	*Hs.526521*	*-1.81±0.26*
NELL1	*W16715*	*NEL-like 1*	*Hs.502145*	*-2.66±0.67*
SOD3	*AA725564*	*Superoxide dismutase 3, extracellular*	*Hs.2420*	*-4.19±0.19*
SRD5A1	*R36874*	*Steroid-5-alpha-reductase, alpha polypeptide 1*	*Hs.552*	*-1.89±0.45*
TDO2	*T72422*	*Tryptophan 2,3-dioxygenase*	*Hs.183671*	*-2.04±0.36*
Metabolic enzymes				

AGXT	N57872	Alanine-glyoxylate aminotransferase	Hs.144567	12.62±13.06
DERA	N74602	2-deoxyribose-5-phosphate aldolase homolog	Hs.39429	1.73±0.16
INPPL1	AA279072	Inositol polyphosphate phosphatase-like 1	Hs.523875	2.35±0.42
UNG2	AA425900	Uracil-DNA glycosylase 2	Hs.3041	1.57±0.06
CAD	*R84263*	*Carbamoyl-phosphate synthetase 2, aspartate transcarbamylase, and dihydroorotase*	*Hs.377010*	*-2.03±0.36*
NM_024843	*N75713*	*Cytochrome b reductase 1*	*Hs.221941*	*-2.61±0.24*
GYS2	*N72934*	*Glycogen synthase 2*	*Hs.82614*	*-1.62±0.04*
SHMT1	*R53294*	*Serine hydroxymethyltransferase 1*	*Hs.513987*	*-2.07±0.81*
UGCGL1	*R98442*	*UDP-glucose ceramide glucosyltransferase-like 1*	*Hs.34180*	*-1.73±0.28*
Transferases				
DNMT1	H09055	DNA-methyltransferase 1	Hs.202672	2.43±0.38
GATM	R61229	Glycine amidinotransferase	Hs.75335	1.68±0.02
GBE1	A46075	Glucan (1,4-alpha-), branching enzyme 1	Hs.436062	1.91±0.44
GALNT2	R00595	UDP-N-acetyl-alpha-D-galactosamine: N-acetylgalactosaminyltransferase 2	Hs.567272	1.89±0.41
UAP1	H78134	UDP-N-acteylglucosamine pyrophosphorylase 1	Hs.492859	2.62±1.30
ZCCHC4	R91215	Zinc finger, CCHC domain containing 4	Hs.278945	1.75±0.25
BHMT	*T58958*	*Betaine-homocysteine methyltransferase*	*Hs.80756*	*-2.41±0.75*
SETDB1	*R12070*	*SET domain, bifurcated 1*	*Hs.516278*	*-2.61±1.55*
ART4	*N70349*	*Translin*	*Hs.13776*	*-1.60±0.07*
Phosphatases				
DUSP5	W65461	Dual specificity phosphatase 5	Hs.2128	2.53±1.38
PPAP2B	*T72119*	*Phosphatidic acid phosphatase type 2B*	*Hs.405156*	*-3.77±3.14*
PPP2R2B	*R55882*	*Protein phosphatase 2, regulatory subunit B (PR 52), beta isoform*	*Hs.193825*	*-1.75±0.17*
PPP2R3A	*N63863*	*Protein phosphatase 2, regulatory subunit B (PR 72), alpha isoform and (PR 130), beta isoform*	*Hs.518155*	*-1.66±0.13*
PPP2R5A	*R59164*	*Protein phosphatase 2, regulatory subunit B, alpha isoform*	*Hs.497684*	*-1.88±0.44*
PTPRC	*H74265*	*Protein tyrosine phosphatase, receptor type, C*	*Hs.192039*	*-1.80±0.42*
PTPRF	*AA598513*	*Protein tyrosine phosphatase, receptor type, F*	*Hs.272062*	*-1.91±0.42*
Peptidases and inhibitors				
ITIH2	R06634	Inter-alpha trypsin inhibitor, H2	Hs.75285	2.67±0.30

		polypeptide		
MMP3	W51794	Matrix metallopeptidase 3	Hs.375129	12.32±8.47
PLAT	AA453728	Plasminogen activator, tissue	Hs.491582	1.86±0.16
PLAU	AA284668	Plasminogen activator, urokinase	Hs.77274	2.24±0.51
PAPPA	R02529	Pregnancy-associated plasma protein A, pappalysin 1	Hs.643599	1.99±0.24
PSME2	H65395	Proteasome activator subunit 2 (PA28 beta)	Hs.434081	1.77±0.09
SERPINE1	N75719	Serine (or cysteine) proteinase inhibitor, clade E, member 1	Hs.414795	1.69±0.17
SERPINE2	N59721	Serpin peptidase inhibitor, clade E, member 2	Hs.38449	1.87±0.01
SERPINI1	AA115876	Serine (or cysteine) proteinase inhibitor, clade I, member 1	Hs.478153	1.98±0.02
TFPI2	AA399473	Tissue factor pathway inhibitor 2	Hs.438231	12.50±13.13
CPB2	*R96561*	*carboxypeptidase B2*	*Hs.512937*	*-2.15±0.79*
CTSE	*H94487*	*Cathepsin E*	*Hs.1355*	*-2.27±0.62*
H04028	*N69322*	*Matrix metalloproteinase 13*	*Hs.2936*	*-2.15±0.76*
MMP13	*AA031513*	*Matrix metalloproteinase 7*	*Hs.2256*	*-2.55±0.42*
MMP7	*H50747*	*Peptidase D*	*Hs.36473*	*-1.95±0.33*
P11	*H04028*	*Protease, serine, 22*	*Hs.997*	*-1.73±0.30*
PEPD	*H90815*	*Serine (or cysteine) proteinase inhibitor, clade A, member 6*	*Hs.532635*	*-2.48±0.87*
SERPINA6	*T62086*	*Serine (or cysteine) proteinase inhibitor, clade D, member 1*	*Hs.474270*	*-1.65±0.13*
USP47	*H63175*	*Ubiquitin specific peptidase 47*	*Hs.567521*	*-2.03±0.38*
Growth factor, cytokines and binding				
AMPH	H06541	Amphiphysin	Hs.592182	2.22±0.74
CCL28	R38459	CC chemokine CCL28	Hs.334633	1.87±0.03
CD34	AA434483	CD34 antigen	Hs.374990	2.21±0.48
CSF3	AI074784	Colony stimulating factor 3	Hs.2233	19.08±2.52
CR1L	T66824	Complement component receptor 1-like	Hs.334019	1.72±0.07
HBEGF	R14663	Diphtheria toxin receptor	Hs.799	2.46±1.15
GTF2IRD1	AA019591	GTF2I repeat domain-containing 1	Hs.647056	2.02±0.23
IGFBP6	AA478724	Insulin-like growth factor binding protein 6	Hs.274313	1.58±0.08
IL1B	AA150507	Interleukin 1, beta	Hs.126256	1.94±0.59
IL32	AA458965	Interleukin 32	Hs.943	1.73±0.04
LIF	R50354	Leukemia inhibitory factor	Hs.2250	3.45±2.74
NRG1	R72075	Neuregulin 1	Hs.453951	2.34±0.74
CCL7	AA040170	Small inducible cytokine A7	Hs.251526	7.15±5.11
CCL13	T64134	Small inducible cytokine subfamily A13	Hs.414629	4.41±2.87
AY114160.1	*N57964*	*Chemokine (C-C motif) receptor 6*	*Hs.46468*	*-2.27±0.57*
CXCL12	*AA447115*	*Chemokine (C-X-C motif) ligand 12*	*Hs.522891*	*-1.85±0.53*
CXCL9	*AA131406*	*Chemokine (C-X-C motif) ligand 9*	*Hs.77367*	*-2.05±0.23*
C5	*N73030*	*Complement component 5*	*Hs.494997*	*-2.1±0.37*
IGFBP1	*AA233079*	*Insulin-like growth factor binding*	*Hs.401316*	*-1.74±0.18*

		protein 1		
IGFBP2	*H79047*	*Insulin-like growth factor binding protein 2*	*Hs.438102*	*-2.11±0.73*
IGFBP3	*AA598601*	*Insulin-like growth factor binding protein 3*	*Hs.450230*	*-2.34±0.24*
IL6R	*T97204*	*Interleukin 6 receptor*	*Hs.135087*	*-2.34±1.12*
MUC1	*AA488073*	*Mucin 1, transmembrane*	*Hs.89603*	*-1.88±0.46*
PGM5P1	*H12279*	*Phosphoglucomutase 5*	*Hs.178400*	*-2.28±1.07*
Receptor activity				
ACVR2B	R68237	ACVR2B: Activin A receptor, type IIB	Hs.517775	2.26±1.02
EPHA1	N90246	EphA1	Hs.89839	1.66±0.16
PTGER4	AA019996	Prostaglandin E receptor 4	Hs.199248	1.72±0.10
LRPAP1	AA486313	Low density lipoprotein-related protein-associated protein 1	Hs.533136	1.62±0.04
RYR2	R15791	Ryanodine receptor 2	Hs.109514	1.57±0.02
PROCR	T47442	Protein C receptor, endothelial	Hs.82353	1.56±0.01
TNFRSF12A	R33355	Tumor necrosis factor receptor superfamily, member 12A	Hs.355899	3.45±1.92
ANTXR1	*H58644*	*Anthrax toxin receptor 1*	*Hs.165859*	*-1.82±0.32*
CCR6	*H60460*	*CD302 antigen*	*Hs.130014*	*-2.12±0.54*
CD302	*AA485795*	*Ephrin-B3*	*Hs.26988*	*-1.91±0.19*
EFNB3	*AA456376*	*Coagulation factor II (thrombin) receptor*	*Hs.482562*	*-2.47±0.76*
GABRP	*AA102670*	*Gamma-aminobutyric acid (GABA) A receptor, pi*	*Hs.26225*	*-1.91±0.33*
GRIA1	*H23378*	*Glutamate receptor, ionotropic, AMPA 1*	*Hs.519693*	*-1.80±0.04*
ITPR2	*AA479093*	*Inositol 1,4,5-triphosphate receptor, type 2*	*Hs.512235*	*-1.88±0.49*
IGF2R	*T62547*	*Insulin-like growth factor 2 receptor*	*Hs.487062*	*-1.56±0.06*
ITGA10	*H44722*	*Integrin, alpha 10*	*Hs.158237*	*-2.01±0.70*
ITGB8	*W56709*	*Integrin, beta 8*	*Hs.592171*	*-3.29±1.22*
KLRC2	*AA191156*	*Killer cell lectin-like receptor subfamily C, member 2*	*Hs.74082*	*-1.71±0.13*
KIT	*N24824*	*V-kit Hardy-Zuckerman 4 feline sarcoma viral oncogene homolog, Kit receptor*	*Hs.479754*	*-1.70±0.14*
PLA2R1	*R91516*	*Phospholipase A2 receptor 1, 180kDa*	*Hs.410477*	*-2.22±0.82*
TNFRSF25	*W76376*	*Tumor necrosis factor receptor superfamily, member 25*	*Hs.462529*	*-2.03±0.58*
Transporters				
ATP6V1B1	R73402	ATPase, H^+ transporting, lysosomal , beta 1	Hs.64173	2.08±0.17
ABCC3	AA429895	ATP-binding cassette, sub-family C, member 3	Hs.463421	3.96±2.68
LIPC	N80949	Lipase, hepatic	Hs.188630	1.82±0.35
SLC15A2	AA425352	Solute carrier family 15 (H+/peptide transporter), member 2	Hs.518089	6.00±4.28

SLC35D1	W16916	Solute carrier family 35 (UDP-glucuronic acid/UDP-N-acetylgalactosamine dual transporter), member D1	Hs.213642	2.26±0.19
SORL1	AA424516	sortilin-related receptor, L(DLR class) A repeats-containing	Hs.368592	2.21±0.40
STARD4	H11369	START domain containing 4, sterol regulated	Hs.93842	1.95±0.02
TAP1	AA487637	Transporter 1, ATP-binding cassette, sub-family B	Hs.352018	1.64±0.03
TLOC1	AA450205	Translocation protein 1	Hs.529591	1.93±0.53
KCNAB2	H14383	Potassium voltage-gated channel, shaker-related subfamily, beta member 2	Hs.440497	1.55±0.01
ABCB1	*AA455911*	*ATP-binding cassette, sub-family B, member 1*	*Hs.489033*	*-1.69±0.26*
ABCB10	*R83875*	*ATP-binding cassette, sub-family B, member 10*	*Hs.17614*	*-1.97±0.39*
SLC6A1	*H61935*	*Solute carrier family 6, member 1*	*Hs.443874*	*-2.09±0.76*
Signaling molecules				
ARL4D	H28952	ADP-ribosylation factor 4-like	Hs.183153	2.80±0.43
CFLAR	N94588	CASP8 and FADD-like apoptosis regulator	Hs.390736	1.79±0.39
GTPBP2	T67069	GTP binding protein 2	Hs.485449	4.07±1.71
LRRFIP2	W30810	Leucine rich repeat (in FLII) interacting protein 2	Hs.475319	2.77±0.90
MX1	AA456886	Myxovirus resistance 1	Hs.517307	4.10±0.74
MX2	AA286908	Myxovirus resistance 2	Hs.926	3.18±0.14
NFKBIA	W55872	I-kappa-Balpha	Hs.81328	2.23±0.83
NKIRAS2	R63172	I-kappa-B-interacting Ras-like protein 2	Hs.632252	1.85±0.28
PHLDA1	AA258396	Pleckstrin homology-like domain, family A, member 1	Hs.484885	2.13±0.49
RAB25	W25368	RAB25, member RAS oncogene family	Hs.632469	2.06±0.47
RAB36	H69004	RAB36, member RAS oncogene family	Hs.369557	1.76±0.05
RAB3IP	W96273	RAB3A interacting protein	Hs.258209	1.89±0.01
RANGAP1	AA026631	Ran GTPase activating protein 1	Hs.183800	1.99±0.33
RIT1	AA027840	Ras-like without CAAX 1	Hs.491234	2.06±0.64
RRAS2	R21415	Related RAS viral (r-ras) oncogene homolog 2	Hs.502004	1.66±0.05
SH3BGR	N52254	SH3 domain binding glutamic acid-rich protein	Hs.473847	4.47±2.12
STC2	R20886	Stanniocalcin 2	Hs.233160	3.91±3.69
TRAF3	AA504259	TNF receptor-associated factor 3	Hs.510528	2.13±0.10
TRH	AA069596	Thyrotropin-releasing hormone	Hs.182231	1.77±0.32
BIRC3	*H48706*	*Baculoviral IAP repeat-containing 3*	*Hs.127799*	*-1.74±0.01*
CEACAM6	*AA054073*	*Carcinoembryonic antigen-related cell adhesion molecule 6*	*Hs.466814*	*-1.81±0.16*

FRZB	*W58032*	*Frizzled-related protein*	*Hs.128453*	*-2.37±0.49*
GBP2	*W77927*	*Guanylate binding protein 2, interferon-inducible*	*Hs.386567*	*-2.77±0.58*
GEM	*AA418077*	*GTP-binding protein overexpressed in skeletal muscle*	*Hs.345139*	*-1.61±0.01*
GNG2	*T80932*	*Guanine nucleotide binding protein (G protein), gamma 2*	*Hs.187772*	*-3.19±1.20*
IQGAP1	*AA598496*	*IQ motif containing GTPase activating protein 1*	*Hs.430551*	*-2.68±1.44*
KRAS	*N95249*	*v-Ki-ras2 Kirsten rat sarcoma viral oncogene homolog*	*Hs.505033*	*-2.21±0.54*
LETM1	*AA417654*	*leucine zipper-EF-hand containing transmembrane protein 1*	*Hs.120165*	*-2.01±0.65*
MCF2	*H05800*	*MCF.2 cell line derived transforming sequence*	*Hs.387262*	*-2.69±0.85*
PLCL1	*AA411387*	*phospholipase C-like 1*	*Hs.153322*	*-2.57±0.57*
PSD3	*R98905*	*Pleckstrin and Sec7 domain containing 3*	*Hs.434255*	*-2.81±1.66*
ARHGEF6	*AA236617*	*Rac/Cdc42 guanine exchange factor 6*	*Hs.522795*	*-1.93±0.23*
RHOBTB3	*N52517*	*Rho-related BTB domain containing 3*	*Hs.445030*	*-2.32±0.93*
SOS1	*H64324*	*Son of sevenless homolog 1*	*Hs.278733*	*-2.27±0.42*
SOS2	*R78735*	*Son of sevenless homolog 2*	*Hs.291533*	*-1.75±0.21*
TSPAN8	*AA045698*	*Tetraspanin 8*	*Hs.170563*	*-1.83±0.17*
Kinase activity				
DGKA	AA456900	Diacylglycerol kinase, alpha	Hs.524488	1.87±0.36
DYRK3	H62028	Dual-specificity tyrosine phosphorylation regulated kinase 3	Hs.164267	2.14±0.92
MAP2K6	H07920	Mitogen-activated protein kinase kinase 6	Hs.463978	1.72±0.03
MAST1	AA479623	Microtubule associated serine/threonine kinase 1	Hs.227489	1.63±0.10
MAST4	AA418846	Microtubule associated serine/threonine kinase family member 4	Hs.133539	1.67±0.04
PCTK3	AA398949	PCTAIRE protein kinase 3	Hs.445402	1.7±0.00
PFKP	R38433	Phosphofructokinase, platelet	Hs.26010	1.65±0.07
PRKCZ	R24258	Protein kinase C, zeta	Hs.496255	1.98±0.45
SNF1LK2	H90161	SNF1-like kinase 2	Hs.555922	2.64±0.59
AURKA	R19158	Serine/threonine kinase 15	Hs.250822	2.62±0.49
STK38	H47863	Serine/threonine kinase 38	Hs.409578	2.39±0.43
FYN	*H91826*	*FYN oncogene related to SRC, FGR, YES*	*Hs.390567*	*-2.42±1.23*
MAPK7	*H39192*	*Mitogen-activated protein kinase 7*	*Hs.150136*	*-2.97±1.55*
MERTK	*AA436591*	*C-mer proto-oncogene tyrosine kinase*	*Hs.306178*	*-1.79±0.07*
PIK3C2G	*T66837*	*Phosphoinositide-3-kinase, class 2, gamma*	*Hs.22500*	*-2.39±0.85*
PIP5K2A	*H93068*	*Phosphatidylinositol-4-phosphate 5-kinase, type II, alpha*	*Hs.588901*	*-2.19±0.57*
PRKCB1	*AA479102*	*Protein kinase C, beta 1*	*Hs.460355*	*-1.73±0.18*
PRKCG	*R89715*	*Protein kinase C, gamma*	*Hs.2890*	*-2.02±0.58*

STK3	*AA464628*	*Serine/threonine kinase 3*	*Hs.492333*	*-1.80±0.23*
STK17A	*H65942*	*Serine/threonine kinase 17a*	*Hs.268887*	*-2.43±0.46*
Structural				
CALD1	N95107	caldesmon 1	Hs.490203	2.01±0.68
DST	H44784	Dystonin	Hs.631992	2.23±0.32
DSP	H90899	Desmoplakin	Hs.519873	1.65±0.03
EVPL	AA029418	Envoplakin	Hs.500635	2.20±0.28
INA	AA448015	Internexin neuronal intermediate filament protein, alpha	Hs.500916	1.70±0.08
VCL	AA486728	Vinculin	Hs.500101	2.70±1.12
A2M	*H06516*	*Alpha-2-macroglobulin*	*Hs.212838*	*-3.07±0.39*
COL14A1	*AA167222*	*Collagen, type XIV, alpha 1*	*Hs.409662*	*-3.16±0.92*
COL1A2	*AA490172*	*Collagen, type I, alpha 2*	*Hs.489142*	*-2.28±1.09*
CTNND2	*H04985*	*Catenin (cadherin-associated protein), delta 2*	*Hs.314543*	*-1.66±0.20*
DST	*W00789*	*Dystonin*	*Hs.485616*	*-1.98±0.03*
FBLN2	*AA452981*	*Fibulin 2*	*Hs.198862*	*-2.7±1.67*
FYCO1	*R11564*	*FYVE and coiled-coil domain containing 1*	*Hs.200227*	*-2.09±0.40*
LUM	*AA453712*	*Lumican*	*Hs.406475*	*-3.47±2.58*
MBP	*H17696*	*Myelin basic protein*	*Hs.551713*	*-2.16±0.51*
MYH10	*AA490477*	*Myosin, heavy polypeptide 10, non-muscle*	*Hs.16355*	*-1.95±0.66*
MYLIP	*AA486836*	*myosin regulatory light chain interacting protein*	*Hs.484738*	*-1.77±0.13*
THBS1	*AA464630*	*Thrombospondin 1*	*Hs.164226*	*-3.53±2.73*
Protein binding				
APBA2	R55789	Amyloid beta precursor protein-binding, family A, member 2	Hs.525718	1.86±0.14
BCL2	W63749	Bcl-2	Hs.150749	1.93±0.52
CCND1	AA487700	Cyclin D1	Hs.523852	1.94±0.31
CCT2	N38959	Chaperonin containing TCP1, subunit 2	Hs.189772	1.67±0.01
INTS7	N80458	DKFZP434B168 protein	Hs.369285	2.21±0.40
ETF1	AA456664	Eukaryotic translation termination factor 1	Hs.483494	1.63±0.10
ITGA2	AA463610	Integrin, alpha 2	Hs.482077	2.13±0.34
ITGB8	R74357	Integrin, beta 8	Hs.592171	1.75±0.28
NCSTN	R96527	Nicastrin	Hs.517249	2.25±0.63
RP2	W00899	Retinitis pigmentosa 2	Hs.44766	1.65±0.07
PCGF3	R06308	Ring finger protein 3	Hs.144309	1.55±0.06
RNF10	H73586	Ring finger protein 10	Hs.442798	1.79±0.40
SAC3D1	W95346	SAC3 domain containing 1	Hs.23642	2.06±0.18
UBE2D3	R91710	Ubiquitin-conjugating enzyme E2D 3	Hs.518773	2.10±0.62
UBE2I	AA487197	Ubiquitin-conjugating enzyme E2I	Hs.302903	3.62±0.12
YWHAH	*N74377*	*14-3-3 protein eta*	*Hs.226755*	*-2.14±0.89*
AKAP12	*AA478542*	*A kinase (PRKA) anchor protein (gravin) 12*	*Hs.371240*	*-1.68±0.13*

PAR3beta	*R99773*	*amyotrophic lateral sclerosis 2 chromosome region, candidate 19*	*Hs.271903*	*-1.90±0.46*
CDH11	*H96738*	*Cadherin 11, type 2, OB-cadherin*	*Hs.116471*	*-2.06±0.74*
CHL1	*R40400*	*Cell adhesion molecule with homology to L1CAM*	*Hs.148909*	*-1.83±0.14*
CUL4A	*R02425*	*Cullin 4A*	*Hs.339735*	*-1.77±0.33*
	AA133797	*Deleted in azoospermia*	*Hs.522868*	*-1.73±0.03*
DAZAP2	*R19889*	*DAZ associated protein 2*	*Hs.369761*	*-1.66±0.01*
EGFLAM	*R08141*	*EGF-like, fibronectin type III and laminin G domains*	*Hs.20103*	*-2.21±0.57*
FANCC	*H62396*	*Fanconi anemia, complementation group C*	*Hs.494529*	*-1.94±0.56*
FYB	*N64862*	*FYN-binding protein*	*Hs.370503*	*-2.13±0.05*
MTMR3	*R11490*	*Nucleoprotein TPR, Translocated promoter region (to activated MET oncogene\)*	*Hs.279640*	*-2.42±1.29*
NAP1L4	*H92347*	*Nucleosome assembly protein 1-like 4*	*Hs.501684*	*-1.67±0.09*
NCF1	*AA459308*	*Neutrophil cytosolic factor 1,*	*Hs.520943*	*-2.08±0.55*
POSTN	*AA598653*	*Periostin, osteoblast specific factor*	*Hs.136348*	*-3.13±2.18*
PRAME	*AA598817*	*Preferentially expressed antigen in melanoma*	*Hs.30743*	*-1.71±0.14*
RTN4	*N68565*	*reticulon 4*	*Hs.429581*	*-1.72±0.02*
SELL	*H00756*	*Selectin L*	*Hs.82848*	*-2.03±0.51*
SNX19	*AA040424*	*Sorting nexin 19*	*Hs.444024*	*-5.93+-6.19*
TJP2	*W31983*	*Tight junction protein 2*	*Hs.50382*	*-2.73±0.99*
TNC	*T69489*	*Tenascin C*	*Hs.143250*	*1.80+-0.02*
UBE2V1	*H69048*	*Ubiquitin-conjugating enzyme E2 variant 1*	*Hs.420529*	*-2.42±0.89*
VCAM1	*H07071*	*Vascular cell adhesion molecule 1*	*Hs.109225*	*-2.50±0.60*
Transcription related				
MPPED2	AA020011	Chromosome 11 open reading frame 8	Hs.289795	1.77±0.23
DPF3	R02268	D4, zinc and double PHD fingers, family 3	Hs.162868	2.07±0.28
FLJ23311	W04152	E2F transcription factor 8	Hs.523526	1.87±0.32
FOXC1	W94714	Forkhead box C1	Hs.348883	2.06±0.18
HIP2	H53038	Huntingtin interacting protein 2	Hs.50308	1.62±0.03
HNRPD	H11069	Heterogeneous nuclear ribonucleoprotein D	Hs.480073	1.84±0.05
JARID1A	AA460756	Jumonji, AT rich interactive domain 1A	Hs.76272	2.37±1.05
JARID2	N73555	Jumonji, AT rich interactive domain 2	Hs.269059	3.62±1.67
JUN	W96155	V-jun avian sarcoma virus 17 oncogene homolog	Hs.525704	1.73±0.23
MYC	W87741	V-myc myelocytomatosis viral oncogene homolog	Hs.202453	1.96±0.20
NFE2	H59000	Nuclear factor, 45kD (NF-E2)	Hs.75643	1.70±0.20
NFIB		nuclear factor I/B	Hs.370359	1.96±0.20
NR4A2	AA598611	Nuclear receptor subfamily 4, group A, member 2	Hs.563344	2.50±0.94
NR4A3	H37761	Nuclear receptor subfamily 4, group A,	Hs.279522	2.37±0.46

		member 3		
REL	N32146	V-rel reticuloendotheliosis viral oncogene homolog	Hs.631886	1.77±0.17
STAT1	AA486367	Signal transducer and activator of transcription 1, 91kD	Hs.470943	2.14±0.48
TAL1	R97066	T-cell acute lymphocytic leukemia 1	Hs.73828	2.64±0.28
TRIM22	AA083407	Tripartite motif-containing 22	Hs.501778	1.60±0.03
TRIM25	N73575	Tripartite motif-containing 25	Hs.528952	1.61±0.06
USF2	AA489017	Upstream transcription factor 2, c-fos interacting	Hs.454534	1.74±0.11
ARID5B	*T77812*	*AT rich interactive domain 5B (MRF1-like)*	*Hs.535297*	*-2.23±0.39*
BMI1	*AA478036*	*B lymphoma Mo-MLV insertion region*	*Hs.496613*	*-1.62±0.15*
ELF2	*AA453714*	*E74-like factor 2*	*Hs.480763*	*-1.60±0.02*
MEF2C	*AA234897*	*MADS box transcription enhancer factor 2C*	*Hs.444409*	*-1.86±0.08*
MTA1	*N71159*	*Metastasis associated 1*	*Hs.525629*	*-1.53±0.02*
MYCN	*R66447*	*V-myc avian myelocytomatosis viral related oncogene, neuroblastoma derived*	*Hs.25960*	*-1.84±0.16*
MYST4	*AA057313*	*MYST histone acetyltransferase 4*	*Hs.35758*	*-3.19±1.02*
NR2F1	*AA452909*	*Nuclear receptor subfamily 2, group F, member 1*	*Hs.519445*	*-1.95±0.33*
PBX1	*H68663*	*Pre-B-cell leukemia transcription factor 1*	*Hs.493096*	*-1.76±0.07*
PCAF	*W00975*	*P300/CBP-associated factor*	*Hs.533055*	*-2.25±0.08*
PITX2	*T64905*	*Paired-like homeodomain transcription factor 2*	*Hs.643588*	*-1.69±0.04*
PLAG1	*AA418251*	*Pleiomorphic adenoma gene 1*	*Hs.14968*	*-1.64±0.04*
POLR2A	*AA479052*	*Polymerase (RNA) II (DNA directed) polypeptide A (220kD)*	*Hs.270017*	*-2.32±1.13*
PRDM2	*W76648*	*PR domain containing 2, with ZNF domain*	*Hs.371823*	*-1.75±0.12*
RUNX1T1	*H37846*	*Runt-related transcription factor 1*	*Hs.368431*	*-2.11±0.60*
SMARCA3	*AA459632*	*SWI/SNF related, matrix associated, actin dependent regulator of chromatin, subfamily a, member 3*	*Hs.3068*	*-1.82±0.16*
SNAI2	*H57309*	*snail homolog 2*	*Hs.360174*	*-2.35±0.61*
SOX9	*AA400739*	*SRY -box 9*	*Hs.647409*	*-2.04±0.15*
SP3	*W32135*	*Sp3 transcription factor*	*Hs.531587*	*-1.95±0.66*
TCF12	*N51828*	*Transcription factor 12*	*Hs.511504*	*-1.80±0.35*
TCF7L2	*N76867*	*Transcription factor 7-like 2*	*Hs.593995*	*-2.02±0.16*
TCF8	*H46553*	*Transcription factor 8*	*Hs.124503*	*-2.62±1.06*
TFAP4	*AA284693*	*Transcription factor AP-4*	*Hs.587500*	*-1.62±0.10*
TITF1	*T60168*	*Thyroid transcription factor 1*	*Hs.94367*	*-1.74±0.16*
ZFP36L1	*AA723035*	*zinc finger protein 36, C3H type-like 1*	*Hs.85155*	*-1.82±0.19*
DNA/RNA/nucleotide binding				
ABL1	R00766	V-abl Abelson murine leukemia viral oncogene homolog 1	Hs.431048	1.88±0.45

ADARB1	AA489331	Adenosine deaminase, RNA-specific, B1	Hs.474018	1.72±0.12
ARF4L	H28952	ADP-ribosylation factor 4-like	Hs.183153	2.80±0.43
DDB2	AA406449	Damage-specific DNA binding protein 2	Hs.651197	1.57±0.09
DDX26B	T99650	DEAD/H (Asp-Glu-Ala-Asp/His) box polypeptide 26B	Hs.496829	2.24±0.97
EIF2B5	R54818	Eukaryotic translation initiation factor 2B, subunit 5	Hs.283551	1.80±0.32
HIST1H1C	T66816	Histone cluster 1, H1c	Hs.7644	3.32±1.36
HIST1H2AC	AA453105	Histone cluster 1, H2ac	Hs.484950	1.96±0.37
HIST1H2BD	N33927	Histone cluster 1, H2bd	Hs.130853	1.88±0.22
HIST2H2BE	AA456695	Histone cluster 2, H2be	Hs.2178	2.14±0.42
MRPL3	H05820	Mitochondrial ribosomal protein L3	Hs.205163	1.77±0.04
PAPOLG	R62241	Poly(A) polymerase gamma	Hs.387471	2.1 ±0.38
PEG10	H51765	Paternally expressed 10	Hs.147492	1.72±0.08
RBM38	AA459588	RNA binding motif protein 38	Hs.236361	1.68±0.16
TOP1	R60160	topoisomerase (DNA) I	Hs.592136	2.05±0.07
ZCCHC2	N54297	Zinc finger, CCHC domain containing 2	Hs.114191	2.10±0.70
ZNF662	N91317	Zinc finger protein 662	Hs.293388	2.33±0.94
ZNF587	H80423	Zinc finger protein 587	Hs.288995	1.81±0.10
FXR1	*N79708*	*Fragile X mental retardation, autosomal homolog 1*	*Hs.478407*	*-1.84±0.46*
IGF2BP2	*W00973*	*Insulin-like growth factor 2 mRNA binding protein 2*	*Hs.35354*	*-2.01±0.32*
KIF21B	*H14513*	*Kinesin family member 21B*	*Hs.169182*	*-2.45±1.27*
KIF6	*N74348*	*Kinesin family member 6*	*Hs.588202*	*-1.84±0.17*
MRPS5	*R26977*	*mitochondrial ribosomal protein S5*	*Hs.355664*	*-2.2±0.93*
SFRS11	*H56944*	*Splicing factor, arginine/serine-rich 11*	*Hs.479693*	*-2.11±0.30*
TIA1	*AA427663*	*TIA1 cytotoxic granule-associated RNA-binding protein*	*Hs.516075*	*-1.99±0.59*
ZFHX4	*N45083*	*Zinc finger homeodomain 4*	*Hs.458973*	*-2.33±0.78*
Miscellaneous				
MMACHC	T67050	DKFZP564I122 protein	Hs.13024	1.87±0.46
DSCR1L2	R27172	Down syndrome critical region gene 1-like 2	Hs.399958	2.13±0.80
DYNC1LI2	AA454959	Dynein, cytoplasmic, light intermediate polypeptide 2	Hs.369068	2.33±0.80
FPGS	R44864	Folylpolyglutamate synthase	Hs.335084	1.81±0.18
DKFZp313A2432	AF527534.1	Hypothetical protein DKFZp313A2432	Hs.349096	2.06±0.75
PFKFB1	T67104	Purinergic receptor P2Y, G-protein coupled, 13	Hs.444304	2.12±0.46
S100A2	AA458884	S100 calcium-binding protein A2	Hs.516484	1.85±0.02
TTLL12	R44546	KIAA0153 protein	Hs.517670	2.71±0.26
TSC22D2	R62373	KIAA0669 gene product	Hs.52526	1.78±0.09
KIAA1571	R68133	KIAA1571 protein	Hs.110489	1.85±0.31
THAP6	N24268	THAP domain containing 6	Hs.479971	2.77±1.42

TNFAIP3	AA476272	Tumor necrosis factor alpha-induced protein 3	Hs.591338	2.36±1.09
UROS	T82469	Uroporphyrinogen III synthase	Hs.501376	1.84±0.27
ADAMTSL4	*R96552*	*ADAMTS-like 4*	*Hs.516243*	*-2.86±1.90*
BAT2D1	*R00395*	*BAT2 domain containing 1*	*Hs.494614*	*-1.74±0.09*
CCAR1	*W05026*	*Cell division cycle and apoptosis regulator 1*	*Hs.49853*	*-2.90±1.81*
CCDC35	*T85902*	*Coiled-coil domain containing 35*	*Hs.135119*	*-1.73±0.16*
DLL1	*R41685*	*Delta-like 1*	*Hs.379912*	*-1.82±0.46*
FBXO3	*T97183*	*F-box protein 3*	*Hs.406787*	*-1.88±0.24*
KIAA0423	*N50014*	*KIAA0423 protein*	*Hs.371078*	*-1.98±0.42*
LDB2	*H74106*	*LIM domain binding 2*	*Hs.23748*	*-2.70±1.60*
MAL	*AA227594*	*Mal, T-cell differentiation protein*	*Hs.80395*	*-1.62±0.01*
PAN3	*R68381*	*PAN3 polyA specific ribonuclease subunit homolog*	*Hs.369984*	*-1.78±0.28*
SAPS3	*R10015*	*SAPS domain family, member 3*	*Hs.503022*	*-1.61±0.03*
SSH2	*R84636*	*Slingshot homolog 2*	*Hs.335205*	*-1.67±0.24*
TBC1D7	*H91404*	*TBC1 domain family, member 7*	*Hs.484678*	*-1.89±0.30*
TRIB2	*AA458653*	*Tribbles homolog 2*	*Hs.467751*	*-2.85±2.04*
VGLL3	*R62289*	*Vestigial like 3*	*Hs.435013*	*-2.73±1.60*
WNT2	*T99653*	*Wingless-type MMTV integration site family member 2*	*Hs.567356*	*-3.14±1.00*

HDFs were treated with 600 μM H_2O_2 for 2 hrs and were placed in fresh culture medium for 72 hr recovery before harvesting RNA for cDNA microarray analyses (see Materials and methods). The data indicate the averages and standard deviations of fold changes from at least two independent experiments. The fold of increase or decrease (negative numbers in italic) for each gene was determined by GeneSpring 5.0 software as statistically significant changes for at least two out of three independent experiments. The column in the table represents (1) Gene symbol, (2) Accession number, (3) common name of the gene, (4) Unigene number, (5) Fold of change for increase and decrease.

CHAPTER III: PROTEOMIC IDENTIFICATION OF INSULIN-LIKE GROWTH FACTOR BINDING PROTEIN-6 INDUCED BY SUBLETHAL H2O2 STRESS FROM HUMAN DIPLOID FIBROBLASTS

Introduction:

Fibroblasts reside in the stromal layer of the skin and actively maintain the integrity and architecture of the tissue by secreting matrix proteases and depositing extracellular matrix proteins. During the process of aging, it is thought that such cells show changes in biochemistry and gene expression patterns. Some of these changes such as alterations in the secretion of degradative enzymes, inflammatory cytokines and growth factors, are related to the senescent phenotype of normal diploid fibroblasts in culture (220-224). These changes can alter the microenvironment, disrupt tissue structures, and cause growth of neighboring premalignant cells (220, 221, 224-229). With HDFs in culture, the senescent phenotype is typically achieved by serial passage (173, 230). However, recent evidence suggests that early passage human diploid fibroblasts (HDFs) respond to a defined dose range of oxidants by entering a state of arrested growth and altered phenotype resembling replicative senescence (176, 178, 231-234).

A large volume of literature supports that oxidative stress contributes to aging and aging associated diseases (235-238). Although aging is the highest risk factor for cancer, cardiovascular disease, and neurodegenerative disease, the mechanism underlying the interplay between oxidative stress, aging and diseases has not been well addressed. Recent experimental evidence supports the hypothesis that induction of the senescent phenotype by oxidants confers a tumor promoting activity of the fibroblasts (225, 239).

Proteins secreted by senescent-like fibroblasts appear to exhibit the ability to promote the growth and colony formation of initiated keratinocytes (239). Uncovering the nature of the proteins secreted by prematurely senescent cells becomes important in understanding the interplay between oxidative stress, aging and aging associated diseases.

Recent advancement in available genomic sequence information has provided an infrastructure for the emerging field of proteomics(240-244). Most commonly used proteomic techniques involve separation of a complex mixture of proteins into less complex subgroups, mass spectrometry analysis of peptides derived from the proteins in each subgroup, and data mining using bioinformatics tools. Often two-dimensional gel electrophoresis has been used for protein separation. However, staining two-dimensional gels only detects abundant proteins that are visible, and the efficiency of protein recovery from the polyacrylamide gel is often a rate-limiting step that prohibits detection of proteins with low abundance. A "shotgun" approach based on the separation capacity of liquid chromatography instrumentation becomes possible if the number of proteins is not overwhelmingly large, such as from a defined subproteome(245, 246). Compared with cell lysates, the subproteome of secreted proteins is less complex and allows meaningful identification of proteins using the shotgun approach. Based on the fact that a mass spectrometer measures a molecule based on its abundance within a mixture of different molecules, methods have been developed not only to identify the nature of proteins in a mixture but also to compare relative levels of a protein between different samples(240, 243, 244, 247-249). Protease digestion of the proteins from conditioned media followed

by analysis of the resulting peptides using ESI-LC-MS/MS allowed us to measure the alteration of secreted protein factors following oxidative stress.

Materials and methods:

Chemicals and Reagents— Chemicals were purchased from Sigma-Aldrich (St. Louis, MO) unless otherwise indicated. Stabilized H_2O_2 (H-1009; Sigma-Aldrich) was used and the concentration of the stock was verified by absorbency at 240 nm.

Maintenance of Cell Culture— HCA_3 human dermal fibroblasts at the population doubling level (PDL) 20 were obtained from Dr. Olivia Periera-Smith. These cells typically reach replicative senescence after PDL 80 and were used for this study at PDL 26-40. HCA3 cells were subcultured weekly in 10 ml of Dulbecco's Modified Eagle's Medium (DMEM) containing 10% (v/v) fetal bovine serum, 50 units/ml penicillin, and 50 μg/ml streptomycin (Life Science Technologies, Grand Island, NY, USA) at a seeding density of 1×10^6 cells per 100-mm Falcon dish. Under these conditions, the cells reached confluence 6-7 days after subculture.

Treatment with H_2O_2 and Various Toxicants— HCA_3 cells were seeded at a density of 2×10^6 per 100-mm dish 5 days before treatment. At the time of H_2O_2 treatment, the cells had reached confluence and the density of cells was $10.48 \pm 0.85\text{x}10^6$. Confluent cells were treated with 600 μM H_2O_2 in 100 mm dish containing 10 ml of medium. This dose is equivalent to ~0.6 pmol H_2O_2 per cell. The dose less than 0.85 pmol/cell has been shown to be non-lethal and induce premature senescence in early passage HDFs (176). For the dose response experiments, cells were treated with H_2O_2 from 150 μM to 600 μM.

After 2 hr incubation in the presence of H_2O_2, cells were placed in fresh DMEM containing 10% (v/v) FBS and were allowed to develop a senescent phenotype in 3 days.

Cis-platin (50 μM), hydroxyurea (50 mM), colchicine (100 μM), L-mimosine (750 μM), rhodamine (1 μM), dithioreitol (1 mM), N-ethylmaleimide (8 μM), and H_2O_2 (250 μM) were used to treat confluent cultures of HCA3 cells for 4hrs. The cells were then placed in fresh DMEM containing 10% (v/v) FBS for 3 days culture. For treatment with retinoic acid (1 μM), confluent cells were incubated in the medium containing these drugs for 3 days without medium change.

Conditioned Medium Preparation— To collect conditioned media of HDFs for proteomic analysis, culture media for HCA3 cells in 100-mm dishes were removed 3 days after H2O2 or other toxicant treatment. The cells were rinsed 2 times in DMEM and were placed in 6 ml of fresh DMEM containing 0% FBS for 3-days culture. The serum free conditioned media were collected, filtered through a 0.45-μm filter to remove cell debris, dialyzed against 0.01N NH4HCO3, and concentrated 100 times down in volume using a speed vacuum concentrator. Protein concentration in the concentrated medium was determined by the Bradford method according to the manufacturer's instruction (BioRad, Richmond, CA).

LC-MS/MS Analysis— The concentrated media were digested overnight with trypsin at a 50:1 ratio, i.e. 1 μg trypsin per 50 μg protein (183). The resulting peptides were analyzed

by a ThermoFinnigan LCQ Classic quadrupole ion trap mass spectrometer (San Jose, CA) equipped with a Michrom MAGIC2002 HPLC (Auburn, CA) and a nanospray ion source (University of Washington). A mixture of peptides equivalent to 7 ng proteins was loaded onto a 10 cm long capillary column with a diameter of 365 □m (O.D) or 100 □m (I.D). The capillary column was generated using a P2000 capillary puller (Sutter Instrument, Novato, CA) and was packed with 5-6 cm of Vydac C18 material. Samples were eluted at a flow rate of 200-300 nanoliter per min into a mass spectrometer using reversed phase solvent conditions. Tandem MS spectra of peptides were analyzed with the Turbo SEQUEST software that assigns peptide sequences to the spectra(244). The software was used to search known human proteins in the non-redundant database from the National Center for Biotechnology Information (NCBI).

Western Blot Analysis— Proteins from conditioned media were separated by SDS polyacrylamide gel electrophoresis using a mini-Protean II electrophoresis apparatus (BioRad, Richmond, CA) run at 90 volts. The separated proteins were transferred to PVDF membranes (Millipore, Bedford, MA) by electrophoresis. The membrane was incubated with antibodies against IGFBP-6 (1:200 dilution; polyclonal, H-70, Santa Cruz Biotechnology), fibronectin (1:2000 dilution, polyclonal, F3648, Sigma-Aldrich), or MMP-2 (1:2000 dilution; polyclonal, AB19015, Chemicon International). The bound antibody was detected using a secondary antibody conjugated with horseradish peroxidase (1:8000, Zymed) for an enhanced chemiluminescence (ECL) reaction.

RNA Isolation and Semiquantitative RT-PCR— Total RNA was extracted from cells with Trizol (Invitrogen, USA) and was used as a template for RT-PCR. Following the reverse transcriptase reaction (RT) using 2 μg of total RNA from each sample, 3 μl of the 35 μl RT reaction mixture was used for each PCR. PCR for IGFBP-6 was carried out in 28 cycles with the primer pair of 5'-GAATCCAGGCACCTCTACCA-3' and 5'-GGTAGAAGCCTCGATGGTCA-3' at 94ºC for 30sec, 62ºC for 30sec and 72ºC for 30sec. Glyceraldehyde-3-phosphate dehydrogenase (GAPDH) was used as a reference gene and as an internal control. PCR for GAPDH was carried out using the primers of 5'-CGTCTTCACCATGGAGA-3' and 5'-CGGCCATACGCCCACAGTTT-3' at 94ºC for 30sec, 55ºC for 30sec, and 72ºC for 30sec for 30 cycles. The PCR products were detected by agarose gel electrophoresis and ethidium bromide staining.

Plasma Collection and Administration of Doxorubicin to Mice— Blood was collected from BL6x129SF1 J mice at 5 to 7 weeks (young) or 16-18 months (old) of age from the abdominal vena cava. Total blood (200 – 300 μl) from an animal was centrifuged at 2000 rpm, 4°C to remove blood cells and sediments. The remaining plasma (40 to 45% of total blood) is clear and transparent. For doxorubicin (Dox) treatment, 5 to 7 week old male (18 – 22 g) mice were treated with Dox via i.p. injection at the dose of 4 mg/kg (10 ml/kg body weight) according to the protocol described by Sun et al(250). The animals were injected twice a week for a total of 10 injections. Control animals were injected with saline at the same volume. The animals were not treated for 2 weeks between the first four injections and the last six injections to allow for recovery of bone marrow depression. The blood from the animals was collected 2 weeks after the last injection.

Results:

Identification of Proteins in Conditioned Media of HDFs by LC-MS/MS

Early passage HCA3 human skin fibroblasts were treated with H_2O_2 and were allowed to develop a stable senescence-like phenotype. To determine the effect of H_2O_2 treatment on protein factors secreted, we compared the profiles of proteins in the conditioned medium from control versus H2O2-treated cells. Serum-free conditioned media were collected for concentration and protease digestion. The resulting peptide mixtures were injected into the ESI-LCMS/MS instrument. A representative total ion current chromatogram from the conditioned medium of control or H2O2-treated cells is shown in Fig.3.1. The mass spectrometer was operated in a data-dependent MS to MS/MS switching mode so that precursor peptide ions detected in a MS survey scan trigger an ion fragmentation for obtaining MS/MS spectra for each of the precursor peptide ions. MS/MS spectra indicate primarily fragment ions originating from either the C terminus (y ion series) or N terminus (b ion series) of a peptide and were searched against a human protein sequence database using the Turbo SEQUEST software. This software searches the entries against all peptide sequences in the database and assigns correlation scores for the probability of matches. The judgment of a confident match is largely based on two parameters: “Xcorr” and “Ions.” Xcorr represents the cross correlation value computed from the experimental MS/MS spectrum when compared with the theoretical candidate peptide MS/MS spectrum, while Ions stands for the number of matched ions in the experimental MS/MS spectrum with the total number of possible sequence ions theoretically predicated for the peptide sequence.

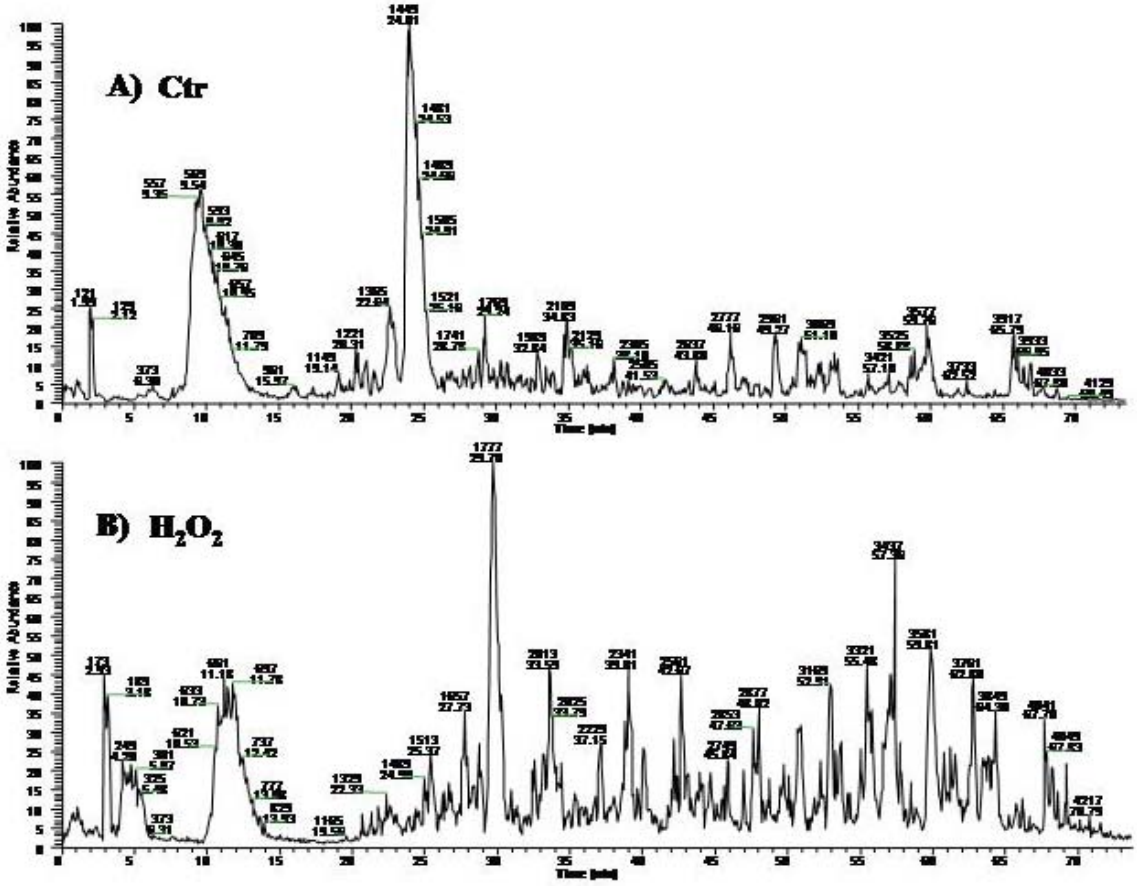

Fig. 3.1. Total ion current chromatogram of conditioned media from control and H2O2-treated HDFs. HCA3 fibroblasts (PDL 26–40) were treated with 600μM (0.6 pmol/cell) H2O2 for 2 h. Cells were allowed to develop a senescent morphology for 3 days before changing medium for conditioned medium collection as described under "Materials and Methods." Concentrated conditioned media were used for overnight tryptic digestion, and an equivalent of 7 μg of proteins were injected into the LC-MS/MS instrument. Each peak represents one parent peptide ion detected by the mass analyzer at each particular time point. The peak height reflects the abundance of the peptide. *A, control (Ctr); B, H2O2 treatment.*

Based on the recommendation of the SEQUEST software, selection criteria for a confident protein identification include Xcorr≥1.8 for +1 ions, Xcorr ≥2.5 for +2 ions, and Xcorr ≥3.5 for +3 ions. In all cases, the value of Ions must be greater than 50%. Table I lists proteins identified by the criteria described above in the conditioned media collected from three independent experiments. The reproducibility of the analytical method is 80–90% between different runs with the same sample (Table 3.2). Several proteins consistently showed up in all three experiments in both control and H2O2-treated groups (Table3.1). These proteins include collagen α1(IV) chain, collagen α2(I) chain, lumican, fibronectin, and MMP-2 (gelatinase A or 72 kDa type IV collagenase). Table II summarizes the scores of Xcorr and Ions and the number of peptides identified for these proteins. IGFBP-6 appeared in the conditioned medium of H2O2-treated cells from all three experiments (Table3.3). The MS/MS spectra and SEQUEST Flicka protein information output on IGFBP-6 identified from three experiments are shown in Fig.3.2, A–D. Each MS/MS spectrum has a high ion-matching ratio. Despite the fact that only one peptide was identified in each experiment for IGFBP-6, the MS/MS spectra and Xcorr and Ions scores all provide high confidence in the detection. This suggests that IGFBP-6 may appear only in the conditioned medium of H2O2-treated cells or that H2O2-treated cells produce more IGFBP-6 than control untreated cells.

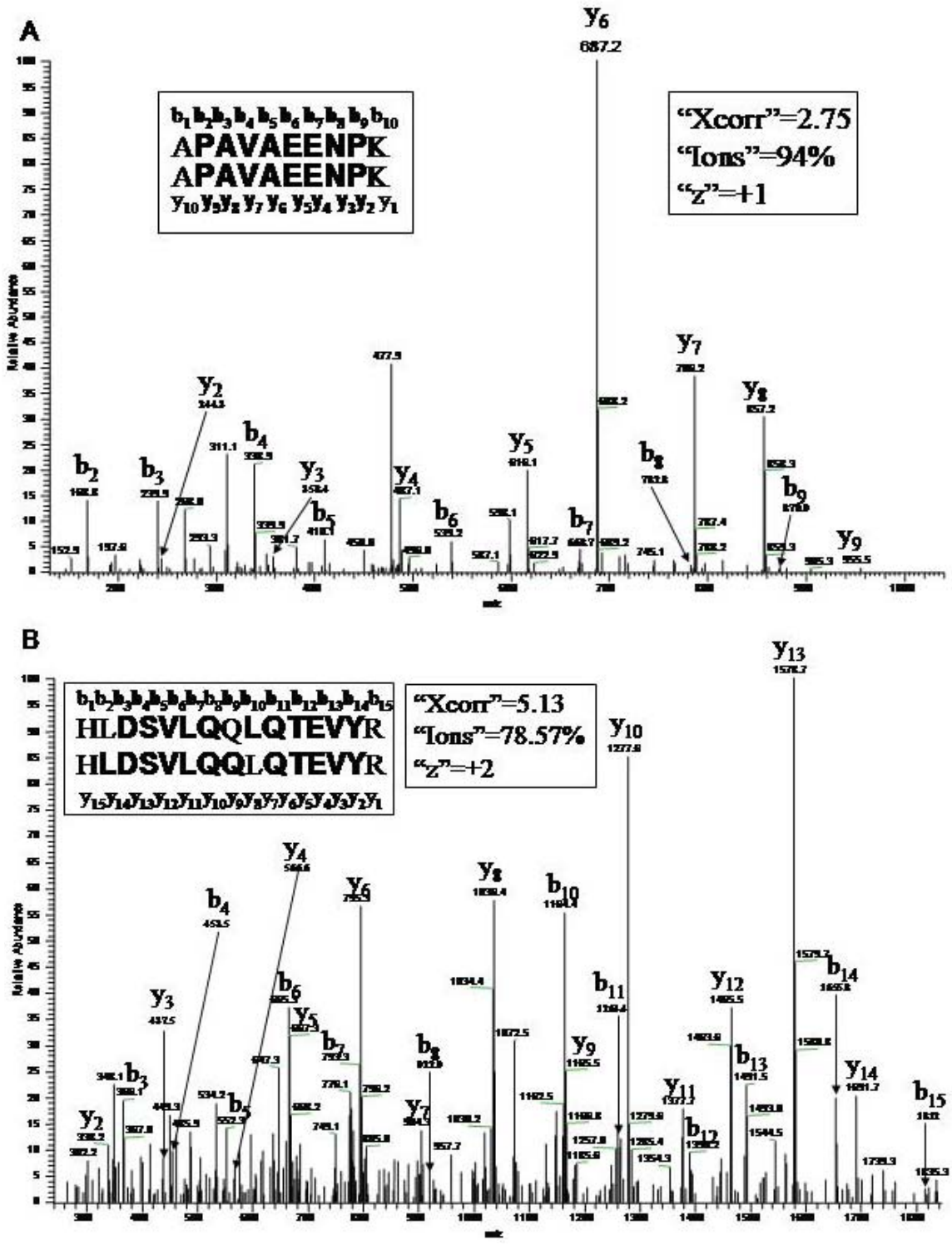
A
APAVAEENPK
APAVAEENPK
"Xcorr"=2.75
"Ions"=94%
"z"=+1
B
HLDSVLQQLQTEVYR
HLDSVLQQLQTEVYR
"Xcorr"=5.13
"Ions"=78.57%
"z"=+2

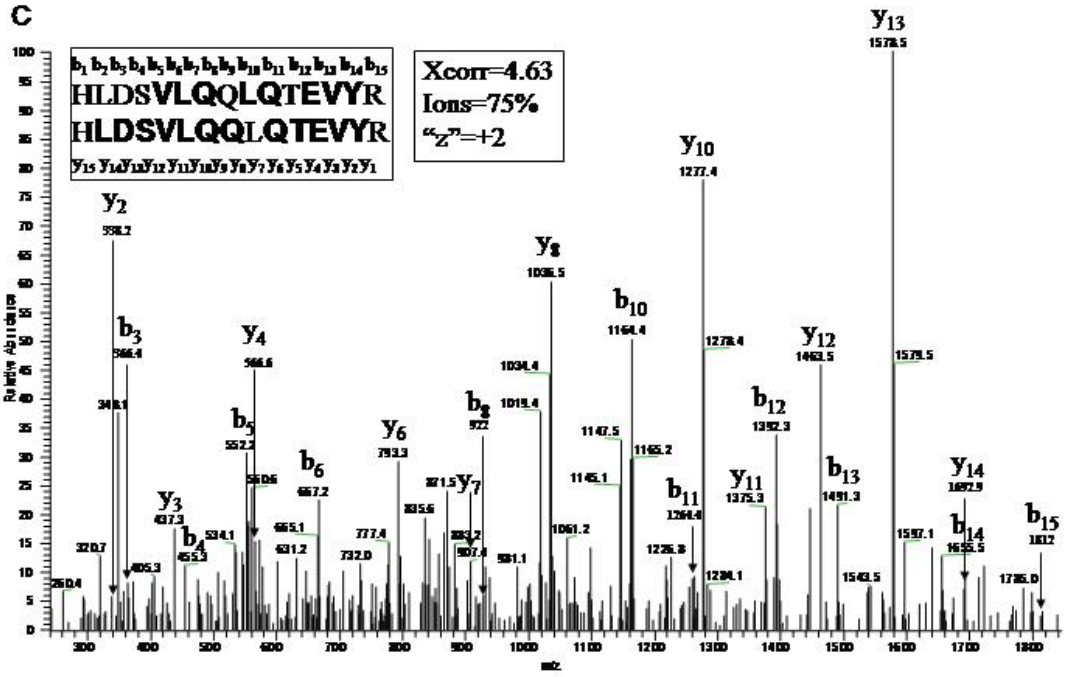

D

Sequest Flicka Protein Information

Insulin-like growth factor binding protein 6 [Homo Sapiens]

gi|11321593|ref|NP_002169.1|

MTPHRLLPPL LLLLALLLAA SPGGALARCP GCGQGVQAGC

PGGCVEEEDG GSPAEGCAEA EGCLRREGQE CGVYTPNCAP

GLQCHPPKDD EAPLRALLLG RGRCLPARAP **AVAEENPKES**

KPQAGTARPQ DVNRRDQQRN PGTSTTPSQP NSAGVQDTEM

GPCRR**HLDSV** **LQQLQTEVYR** GAQTLYVPNC DHRGFYRKRQ

CRSSQGQRRG PCWCVDRMGK SLPGSPDGNG SSSCPTGSSG

Fig. 3.2. MS/MS spectra of IGFBP-6 peptide and SEQUEST Flicka output for detected IGFBP-6 peptides. MS/MS spectra of the IGFBP-6 peptide detected in three independent experiments are shown in *A–C*. The *bold letters* indicate the detected b and y ions matching the predicted ion mass in the database. In *D*, the SEQUEST Flicka protein information page for IGFBP-6 shows the fragments detected.

Induction of IGFBP-6 Expression by H2O2 Treatment

The LC-MS/MS-based shotgun proteomic method led to the identification of IGFBP-6 from H2O2-treated cells and several proteins, including fibronectin and MMP-2, from both control and H2O2-treated cells. To verify these results, we performed Western blot analyses were performed using conditioned media collected from control or H2O2-treated cells. The data indicate that there is no significant difference in the level of MMP-2 and fibronectin in the conditioned media between control and H2O2-treated cells (Fig.3.3). With cell lysates, a minor elevation of fibronectin was detected with H2O2 treatment. MMP-2 was not detected with cell lysates, suggesting that MMP-2 is a secreted protein. IGFBP-6 is known to be O-glycosylated at 5 amino acid residues (Thr126, Ser144, Thr145, Thr146, and Ser152)(251, 252). Western blot analyses of conditioned media showed two bands of IGFBP-6 (Fig.3.3). Presumably the lower molecular weight band represents the non-glycosylated form, and the higher molecular weight band represents the glycosylated form of IGFBP-6. With either form, IGFBP-6 protein showed an elevation in the conditioned medium of H2O2-treated cells (Fig.3.3). IGFBP-6 protein from cell lysates showed a molecular weight between the two forms present in the conditioned medium (Fig.3.3), suggesting that the protein is partially glycosylated. The level of IGFBP-6 protein from cell lysates did not show a dramatic increase with H2O2 treatment. These data demonstrate that we are able to verify the data on IGFBP-6 obtained by LC-MS/MS with Western blot analyses.

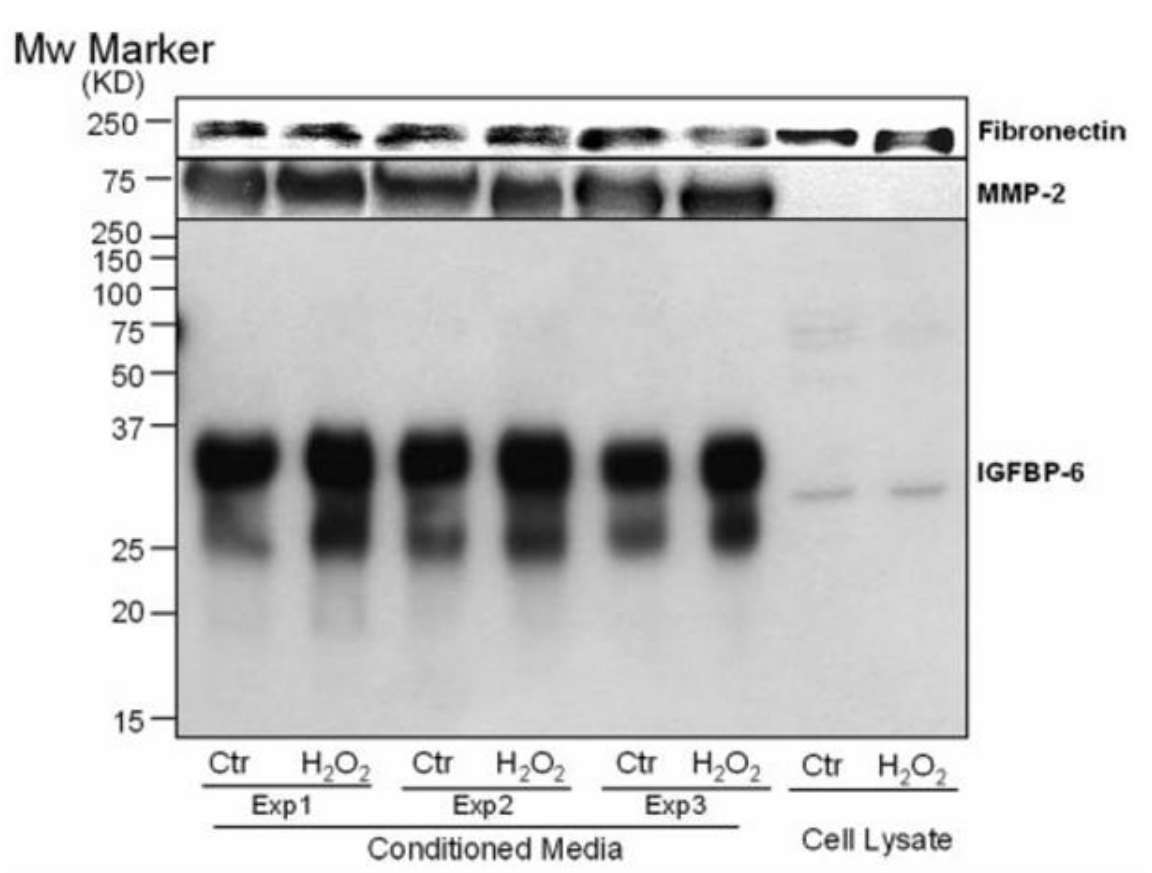

Fig. 3.3. Western blot verification of IGFBP-6, fibronectin, and MMP-2. Conditioned media from control and H2O2-treated cells were collected as described under "Materials and Methods." Following concentration, conditioned media containing 20μg of proteins from three independent experiments were loaded onto an SDS-polyacrylamide gel for electrophoresis followed by Western blot analysis as described under "Materials and Methods." Cell lysates (20μg/lane) were loaded in the same gel for electrophoresis and Western blot. The *numbers* indicate areas corresponding to specific molecular weight markers. *Ctr*, control.

To characterize the induction of IGFBP-6 by H2O2 treatment, we performed dose response studies to measure levels of IGFBP-6 mRNA in cell lysates and to determine levels of IGFBP-6 protein in the conditioned medium. HCA3 cells were treated with 0, 150, 300, 450, or 600 μM H_2O_2. RNA and conditioned media were collected in parallel from the same set of samples. Western blot analyses showed a dose-dependent increase of IGFBP-6 protein, both glycosylated and non-glycosylated forms, in the conditioned medium of H2O2-treated cells (Fig.3.4A). In comparison, no significant changes of fibronectin and MMP-2 at the protein level were detected in the conditioned media of HCA3 cells treated with various doses of H2O2. Consistent with the protein measurement data, semiquantitative RT-PCR showed a dose-dependent increase of IGFBP-6 mRNA with H2O2 treatment (Fig.3.4B).

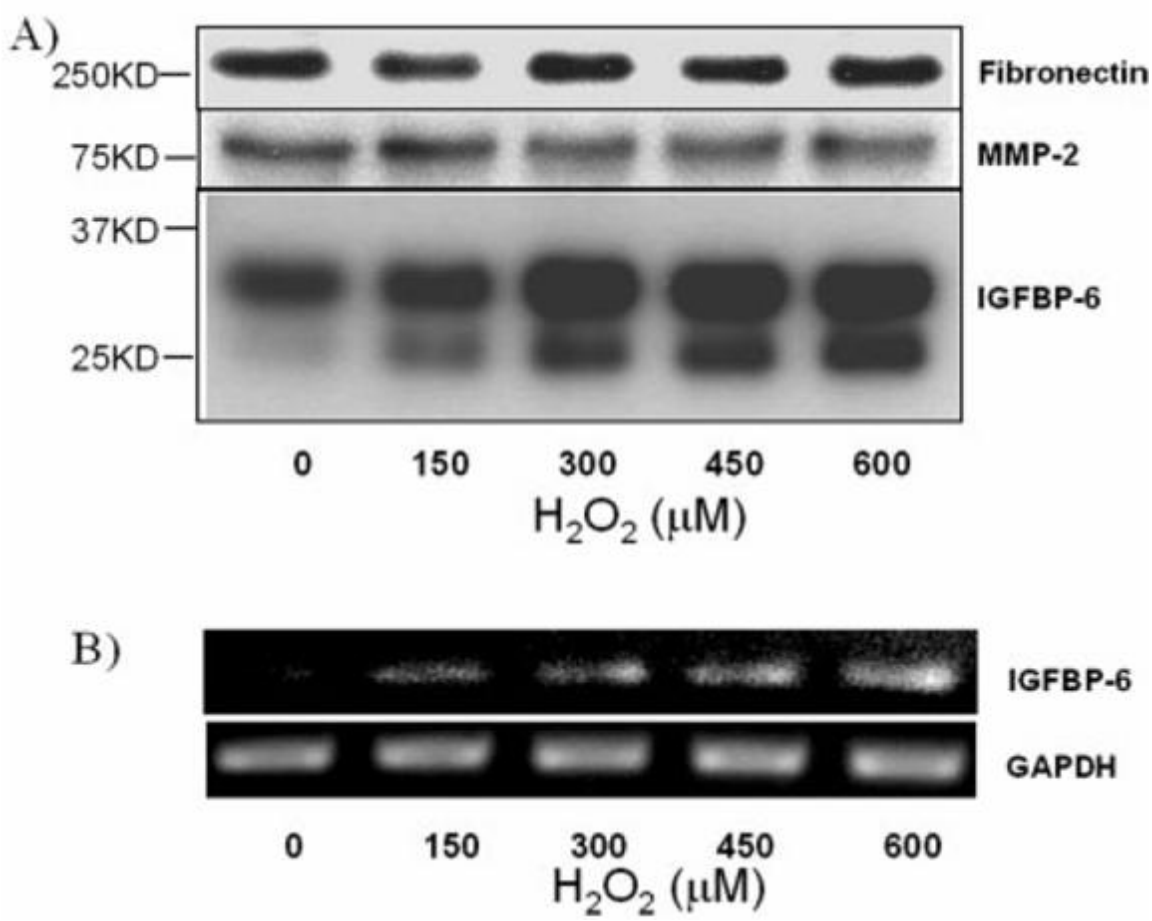

Fig. 3.4. H2O2 dose-dependent induction of IGFBP-6 expression. HCA3 cells were treated with H2O2 at the dose indicated for 2 h and were allowed to recover for 3 days as described under "Materials and Methods." Cells were harvested for RNA extraction at the time of conditioned medium collection. Concentrated conditioned media containing 20μg of proteins were used for Western blot to detect fibronectin, MMP-2, and IGFBP-6 (A). For RT-PCR (B), 2μg of total RNA from each sample were used for RT, and one-tenth of the RT reaction mixture was used for PCR to amplify IGFBP-6. In a parallel PCR using the same RT reaction mixture, GAPDH was amplified to show equal amount of RNAs between each sample.

Using IGFBP-6 as an in Vitro and in Vivo Biomarker of Cellular Injury

We extended our study by asking whether or not IGFBP-6 can serve as a biomarker of oxidative injury. HCA3 cells were treated with a variety of chemicals, including a DNA-damaging agent (cis-platin), DNA polymerase inhibitor (hydroxyurea), microtubule disruptor (colchicine), amino acid analogue (mimosine), mitochondrial uncoupler (rhodamine), and reducing agents (dithiothreitol and N-ethylmaleimide). The nuclear receptor agonist retinoic acid, which has been reported to induce IGFBP-6 expression(253, 254), was included as a comparison. Cells were treated with a sublethal dose of toxins and were allowed to recover for 3 days before collecting the conditioned medium and RNA as described under "Materials and Methods." Western blot analyses indicated that the IGFBP-6 protein in the conditioned media increased to various degrees due to the treatment with different chemicals (Fig.3.5A). Judging from the molecular weight markers, the increased IGFBP-6 from various chemical treatments is mainly the glycosylated form. In contrast, levels of fibronectin or MMP-2 proteins did not appear to change (Fig. 5A). RT-PCR results also indicated up-regulated IGFBP-6 mRNA levels in cells treated with these chemicals (Fig.3.5B). These data suggest that a variety of chemical stresses can induce IGFBP-6.

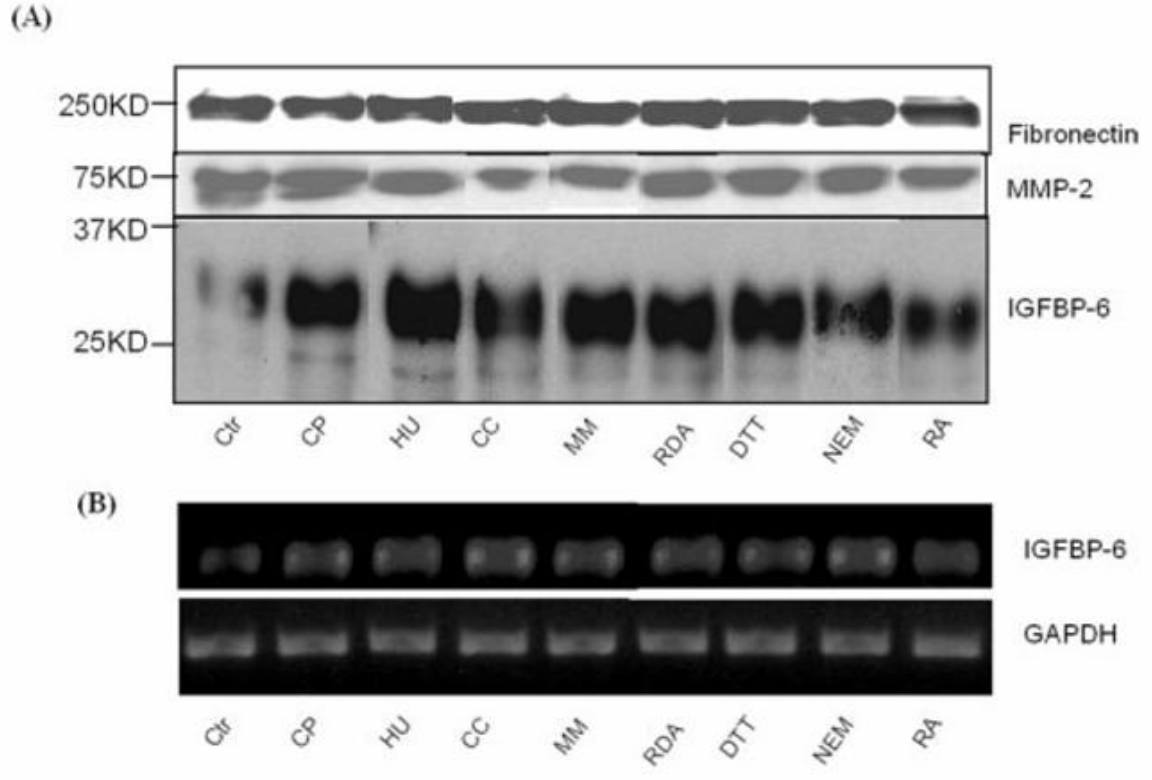

Fig. 3.5. Induction of IGFBP-6 by various chemicals. HCA3 cells (PDL 26–40) were treated for 4 h with cis-platin (50μM, CP), hydroxyurea (50 mM, HU), colchicine (100 _M, CC), L-mimosine (750 _M, MM), rhodamine (1μM, RDA), dithiothreitol (1 mM, DTT), N-ethylmaleimide (8μM, NEM), or H_2O_2 (250μM). The cells were then placed in fresh DMEM containing 10% (v/v) FBS for 3 days of culture. For retinoic acid (1μM) treatment, cells were treated in the drug without medium change for 3 days. Cells were harvested for RNA extraction at the time of conditioned medium collection. Concentrated conditioned media containing 15 μg of protein were used for Western blot to detect fibronectin, MMP-2, and IGFBP-6 (A). Total RNA (2 μg) from each group was used for RT-PCR (B) described in Fig. 4. *Ctr, control.*

Based on the fact that IGFBP-6 is a secreted protein that increases its expression when cells encounter damaging agents, we reason that this protein may serve as a biomarker of cell injury if the increase can be detected in the plasma of individuals. Two animal models were used to test this hypothesis: aging and doxorubincin (Dox) treatment. There is much evidence in support of the fact that oxidative stress contributes to cell degeneration during the process of aging. In comparison, Dox, an antineoplastic drug that is known to produce reactive oxygen species, can induce cardiomyopathy and other types of tissue injury. Plasma was collected from young (5–6 weeks) or old (16 months) mice for Western blot analysis to measure the level of IGFBP-6. The results show that old mice, male or female, exhibited an elevated level of IGFBP-6 in the plasma (Fig.3.6A). The protocol of administering Dox, as described under "Materials and Methods," has been shown to induce cardiomyopathy(250). The plasma of Dox-treated mice showed an elevation of IGFBP-6 (Fig.3.6B). With serum samples from mice, IGFBP-6 appeared to show in one broad band. It is not known whether this band represents the non-glycosylated, glycosylated, or partially glycosylated form. Regardless our data suggest a potential for using plasma levels of IGFBP-6 as a biomarker of tissue degeneration or injury in vivo.

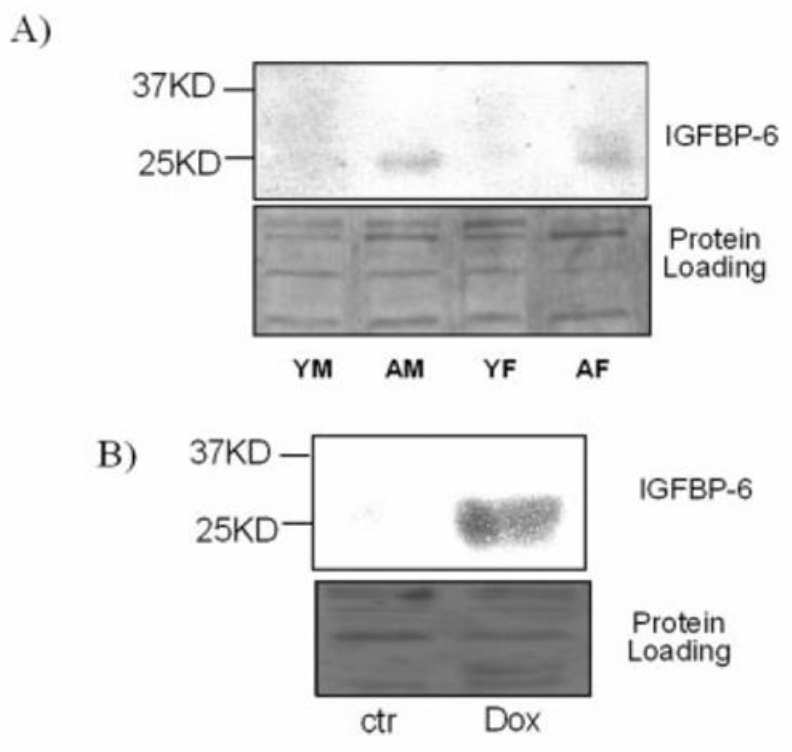

Fig. 3.6. Elevated IGFBP-6 protein levels in the plasma of aging or doxorubicin-treated mice. The blood was collected from BL6 _ 129SF1 J mice at 5–7 weeks (young) or 16–18 months (old) of age. For Dox treatment, 5–7-week-old male mice (18–22 g) were treated with Dox via intraperitoneal injection as described under "Materials and Methods." The plasma containing 20μg of protein was loaded onto an SDS-polyacrylamide gel for electrophoresis and Western blot. An area of silver-stained SDS gel (bottom panels) was included to show equal loading between different groups of samples. *YM, young male; AM, aging male; YF, young female; AF, aging female; ctr, control.*

Discussion:

The shotgun approach of ESI-LC-MS/MS-based proteomics has lead to the discovery that H2O2-induced senescentlike human diploid fibroblasts increase the production of IGFBP-6 protein. The results obtained by this proteomic analysis have been verified by Western blot and semiquantitative RT-PCR analyses. This study sets an example supporting the importance of proteomic techniques in discovering biomarkers, new targets, and novel pathways associated with a particular cellular condition.

Previous studies from our laboratory and others found that senescent or senescent like fibroblasts produce protein factors that stimulate the growth of initiated keratinocytes(225, 239). In theory, proteomic techniques are most suitable for identifying these protein factors and for elucidating the mystery of how many proteins are actually secreted by fibroblasts. Computational analyses of the human genome predict 5235 secreted proteins based on signal peptide sequence analysis(255). Two-dimensional electrophoresis of secreted proteins from adipocytes and osteocytes found about 1000 spots, indicating about 1000 secreted proteins detectable by this method(256, 257). In our experimental system, we have confidently identified 10–20 proteins in the conditioned medium using the shotgun method. Such a low number reflects the limitation of our current instrumentation. The instrument used in this study, a ThermoFinnigan LCQ Classic quadrupole ion trap mass spectrometer, detects peptides at a sensitivity of 200 fmol. With this conventional ion trap, considerable amounts of potentially valuable information are missed when several peptides co-elute, and the instrument is unable to fragment them all efficiently. Much of the emphasis in the proteomic industry involves

improving mass spectrometers in sensitivity, speed, selectivity, dynamic range, and mass accuracy. A linear ion trap is able to collect much more information due to its much faster scanning time. One experiment using a demo model of the ThermoFinnigan linear ion trap LC-MS/MS instrument identified 71 proteins from the conditioned medium of control HDFs. This is a 3–7-fold enhancement in the capacity of protein identification. Two-dimensional linear trap mass spectrometers have recently been developed that offer an increased ion trapping capacity, increased detection sensitivity, and better quality of tandem mass spectra. This type of capillary multidimensional liquid chromatography produces a better separation of complex peptide mixtures with two or more series of orthogonal nano-HPLC columns, allowing the characterization of an entire proteome from cell lysates, which contain 200,000–300,000 proteins(246, 258). The improvement in instrumentation will enhance our capacity to profile secreted proteins toward the level that truly reflects the actual number of secreted proteins from a particular cell type.

Despite the fact that LC-MS/MS analysis can generate data reproducibly for certain proteins, such as fibronectin, MMP-2, and IGFBP-6, we have observed considerable variations in the proteins identified (Table I). Several caveats for the LCMS/MS-based method may explain the observed variations. 1) The principle of the LC-MS/MS instrument analysis involves detection of ions that are most likely abundant. 2) Classical LC-MS/MS is operated under the assumption of “first come and first serve.” Because our current instrument does not have detailed ion separation capacity, the detection is somewhat a process of randomization. 3) The optimal detection range of the mass spectrometer is 700–3000 Da for a peptide. Depending on the completion of

protease cleavage of each protein, a peptide within this mass range may not always appear in a large abundance. 4) The data depicting specific protein identifications are largely dependent on the selection criteria of SEQUEST software. The current setting is quite stringent and therefore filters out the peptide ions that may not meet the level of high confidence. 5) Variations may exist between cells from different passages. Because our three experiments were performed with different passages of cells in culture and HDFs are known to progress toward replicative senescence with each subculture, culture conditions and age of the cells may possibly contribute to variations of proteins in the conditioned medium. Regardless of these caveats, the finding that oxidants and multiple toxicants increase the expression and secretion of IGFBP-6 presents a novel biomarker for diagnosing sublethal cell injury. The data from our animal models of aging and Dox treatment support this biomarker argument. With plasma samples in human studies, a gradual increase in the level of IGFBP-6 up to 2-fold has been documented with increasing age(259). Consistent with this finding, we detected an increased level of IGFBP-6 in the plasma of aged mice.

IGFBP-6 belongs to a family that contains six well characterized members. These members share sequence homologies, contain abundant cysteine residues, and have been found in a variety of biological fluids, including the plasma(260, 261). IGFBP-6 undergoes glycosylation during the process of secretion(251, 252). Our data show two broad bands of IGFBP-6 in Western blots, suggesting non-glycosylated and glycosylated forms, both of which showed elevation in the conditioned medium of H2O2-treated cells. However, an in vivo study showed only one band of IGFBP-6. It is not known whether

the band represents the glycosylated or non-glycosylated form because the glycosylated band seems to be dominant as evidenced by in vitro studies, but the molecular weight of the band from animal serum is close to what is presumably the non-glycosylated form. Species differences also contribute to the complication. Mouse IGFBP-6 appears to have a slightly lower molecular weight than rat IGFBP-6 (251). Regardless, glycosylation appears to play a role in IGFBP-6 protein stability (251, 262). This feature may contribute in part to the increased level of IGFBP-6 protein in addition to transcriptional activation of the IGFBP-6 gene by H2O2. Several nuclear receptor ligands, such as retinoids, vitamin D, and 2,3,7,8-tetrachlorodibenzo-p-dioxin (TCDD)(254, 263, 264), have been shown to induce the expression of IGFBP-6. In contrast, transforming growth factor _ and agents that elevate intracellular cAMP concentration cause decreases in IGFBP-6 expression expression(265). Our finding points to a novel pathway regulating the expression of IGFBP-6 by oxidants and toxicants.

The biological function of IGFBP-6 may vary depending on experimental systems. IGFBP-6 preferentially binds to insulin-like growth factor (IGF)-II rather than to IGF-I. Although IGFBPs can modulate the activity of IGFs through high affinity binding, IGFBPs may also regulate biological processes, such as cell proliferation or growth arrest in an IGF-independent manner, for example through direct cell association. Glycosylation does not appear to affect IGF-II binding but appears to inhibit direct cell association of IGFBP-6(251, 262). Overexpression of IGFBP-6 arbitrarily in non-small cell lung cancer cells activates programmed cell death(266). With TCDD-induced expression of IGFBP-6, a high degree of IGFBP-6 elevation appeared to enhance apoptosis, whereas a reduction

of IGFBP-6 inhibited TCDD from inducing apoptosis in thymoma cells(267). Inactivating the expression of IGFBP-6 in colon cancer cells resulted in a gain of cell proliferation, suggesting that IGFBP-6 may be inhibitory for cell growth(268). Whether IGFBP-6 mediates growth arrest or apoptosis induced by H2O2 treatment remains to be determined.

Table 3.1. List of Proteins Identified From All Three Experiments

	Ctr Fibroblasts	**H_2O_2 Treated Fibroblasts**
Exp. 1	Collagen alpha 1(I) chain	Collagen alpha 1(I) chain
	Collagen alpha 1(VI)chain	Collagen alpha 1(VI) chain
	Collagen alpha 2(I) chain	Collagen alpha 2(I) chain
	Collagen alpha 2(V) chain	Fibronectin
	Fibronectin	Fibulin 1
	Lumican	Lumican
	MMP-2	MMP-2
	Plasma protease C1 inhibitor precursor	TIMP-1
	Beta-2-microglobulin	TIMP-2
		IGFBP-6
		Protein kinase C, Mu type
		Beta-2-microglobulin
Exp. 2	Collagen alpha 1(I) chain	Collagen alpha 1(VI) chain
	Collagen alpha 1(VI) chain	Collagen alpha 2(I) chain
	Collagen alpha 2(I) chain	Fibronectin
	Complement C1r component	Fibulin 1
	Fibronectin	Lumican
	Fibulin 1	MMP-1
	Lumican	MMP-2
	MMP-2	TIMP-1
	TIMP-1	IGFBP-6
	Quiescin Q6	Quiescin Q6
	Superoxide dismutase 3	Clusterin
	Tetranectin (plasminogen binding protein)	Plasminogen activator inhibitor
	Human Complement C1s Protease	Procollagen C-endopeptidase enhancer
	Zinc finger protein 335	Decorin isoform a preproprotein
	Decorin isoform a preproprotein	Complement component 1, s subcomponent
		Vimentin
Exp.3	Collagen alpha 1(I) chain	Collagen alpha 1(I) chain
	Collagen alpha 1(VI) chain	Collagen alpha 1(VI) chain
	Collagen alpha 2(I) chain	Collagen alpha 2(I) chain
	Fibronectin	Fibronectin
	Fibulin 1	Fibulin 1
	Lumican	Lumican
	MMP-1	MMP-1
	MMP-2	MMP-2
	TIMP-1	TIMP-1
	IGFBP-4	TIMP-2
	IGFBP-7	IGFBP-6
	Procollagen C-endopeptidase enhancer	Quiescin Q6
	Complement C1r component precursor	Procollagen C-endopeptidase enhancer
	Autotaxin	Complement C1r component precursor
	Glia-derived nexin precursor	Pigment epithelium-derived factor precursor
	Vimentin	Vimentin

Table 3.2. List of Proteins Identified From Four Runs with the Same Sample

Run 1	**Run 2**
Collagen alpha 2(I) chain	Collagen alpha 1(VI) chain
Lumican	Collagen alpha 2(I) chain
IGFBP-6	Fibronectin
Quiescin Q6	Lumican
	MMP-2
	Quiescin Q6
Run 3	**Run 4**
Collagen alpha 1(VI) chain	Collagen alpha 1(VI) chain
Collagen alpha 2(I) chain	Collagen alpha 2(I) chain
Fibronectin	Fibronectin
Fibulin 1	Fibulin 1
Galectin 3 binding protein	Lumican
IGFBP-6	MMP-2
N-TIMP-1	IGFBP-6
	Quiescin Q6

Note: Red: proteins appeared 4 times out of 4 runs; Purple: proteins appeared 3 times out of 4 runs; Pink: proteins appeared 2 times out of 4 runs; Black: proteins appeared 1 time out of 4 runs.

Table 3.3. Summary of Proteins Consistently Showed Up in All Three Experiments

Proteins Appeared in Both Control and H_2O_2 Groups

Name	Exp#	Group	Xcorr	Ions	#Pep
	1	Ctr	2.66	67.65%	1
		H_2O_2	2.64	50%	1
Collagen alpha1(VI) chain	2	Ctr	3.04±0.51	56.88%±6.84%	5
		H_2O_2	4.30±1.09	60.05%±1.50%	3
	3	Ctr	3.21±0.57	59.42%±7.42%	3
		H_2O_2	4.19±0.88	68.06%±9.72%	3
	1	Ctr	4.01±0.80	63.71%±7.67%	41
		H_2O_2	3.63±0.40	61.20%±8.92%	10
Collagen alpha2(I) chain	2	Ctr	3.54±0.82	56.68%±4.22%	14
		H_2O_2	3.66±0.91	56.88%±8.22%	7
	3	Ctr	3.38±0.51	58.25%±6.29%	6
		H_2O_2	3.72±0.82	57.21%±5.68%	12
	1	Ctr	3.77	57.14%	1
		H_2O_2	3.24±0.63	61.54%±11.81%	3
Fibronectin	2	Ctr	3.07±0.44	60.01%±10.86%	5
		H_2O_2	3.53±0.31	63.07%±15.14%	5
	3	Ctr	3.30±0.51	61.69%±8.07%	7
		H_2O_2	3.17±0.18	61.15%±9.96%	9
	1	Ctr	3.17±0.12	71.35%±19.31%	2
		H_2O_2	3.25	72%	1
Lumican	2	Ctr	3.61±0.86	67.13%±12.08%	5
		H_2O_2	3.49±0.70	65.96%±9.35%	4
	3	Ctr	3.70±1.03	71.99%±8.45%	3
		H_2O_2	3.49±0.73	72.51%±8.94%	5
	1	Ctr	3.17	52.78%	1
		H_2O_2	2.97±0.10	69.00%±19%	2
MMP-2	2	Ctr	3.37±0.65	67.93%±9.47%	3
		H_2O_2	3.17±0.57	62.79%±4.77%	3
	3	Ctr	3.54±0.67	64.95%±7.36%	5
		H_2O_2	3.17±0.34	66.05%±10.64%	8

Proteins Appearing in H_2O_2 Group Alone

Name	Exp#	Group	Xcorr	Ions	#Pep
	1	H_2O_2	2.75	94%	1
IGFBP-6	2	H_2O_2	5.13	79%	1
	3	H_2O_2	4.63	75%	1

CHAPTER IV: PROTEOMIC IDENTIFICATION OF CYSTATIN C AS A CARDIOMYOCYTE BIOMARKER OF OXIDATIVE INJURY

Introduction:

Heart failure represents an end point of many forms of cardiac diseases. A failing heart is incapable of pumping sufficient blood to meet the metabolic need of the body. Despite the current generation of vasodilator and pharmacological agents, patients being diagnosed with heart failure have a poor prognosis in general. On average, one in five patients die within 1 year of heart failure diagnosis (269). Prior to the clinical onset of heart failure symptoms, little is known about individual susceptibility to this irreversible and clinically difficult to treat disease. Non-invasive biomarkers will be valuable in early diagnosis and efficient management of heart failure.

Clinical, epidemiologic, and basic biomedical studies have pointed to oxidative stress as a risk factor for the development and progression of heart failure(40, 44, 270-272). Imperfect coupling of mitochondrial respiration produces reactive oxygen species (ROS) as a byproduct (235, 273, 274). Cardiomyocytes (CMCs), the main cell type composing the myocardium, have the highest content of mitochondria in comparison with any other types of mammalian cells. About 40% cell volume is occupied by mitochondria in CMCs (275). This feature makes CMCs very vulnerable because of huge ROS generation. Ischemia and ischemic reperfusion result in increased generation of ROS in the myocardium. Oxidation and lipid peroxidation products have been detected in failing human hearts and in experimental models of heart failure(40, 44, 273).

The myocardium mainly contains two cell types: CMCs and CFs. During the process of heart failure, while a small proportion of CMCs undergo apoptosis, the majority of CMCs have decreased contractile function and undergo hypertrophy. In contrast, cardiac fibroblasts (CFs) play a critical role in the alignment of CMCs and the texture of the myocardium. Myocardial fibrosis often occurs in association of heart failure and results from changes in the expression of secreted protein factors and extracellular matrix proteins of fibroblasts. Since CMCs are critical for the contractility of the heart, changes to myocyte proteome collectively produce the pathologic phenotype of the diseased heart. Since oxidative stress plays an important role in the pathogenesis of heart failure, we hypothesize that oxidative stress can cause changes in myocyte proteome, resulting in alterations of protein factors released from myocytes into the blood or the culture media, which could be potential indicators useful for early diagnosis of heart failure.

Recent developments in the technology of proteomics allow identification of protein factors secreted by a particular cell type. Most commonly used proteomic techniques involve separation of a complex mixture of proteins into less complex subgroups. A shotgun approach of proteomics takes advantage of the separation capacity of liquid chromatography instrumentation. This approach can be quick and productive given a well defined subproteome(245, 246). Comparing to the whole proteome of a specific cell type, the subproteome of secreted proteins is less complex, allowing meaningful detection of proteins with the shotgun approach of LC-MS/MS based proteomics(180). Once a protein candidate is found from the *in vitro* cell culture system,

the study can be extended to *in vivo* models of heart failure by testing the level of the protein candidate in the circulating system and in the heart tissue.

In an effort to identify CMC cell type specific biomarkers of oxidative injury, CMCs and CFs were isolated from the hearts of 1~3 day old rats and treated with sublethal doses of H2O2 for detection of secreted protein factors in the conditioned media by ESI-LC-MS/MS based shotgun proteomic approach.

Materials and methods:

Tissue Culture— CMCs and CFs were isolated from the hearts of 1-3 day old Sprague-Dawley rats as described previously(192, 193, 276). CMCs were seeded at a density of $2x10^6$ cells per 100-mm dish (Falcon) in low glucose Dulbecco's Modified Eagle Medium (DMEM) containing 10% (v/v) fetal bovine serum (FBS), 50 units/ml penicillin, and 50 μg/ml streptomycin. CFs were cultured in high glucose DMEM with 10% FBS and were subcultured once to eliminate contamination of other cell types. CFs were seeded in 100-mm dish (Falcon) at a density of $2x10^6$ cells per dish for experiments.

Treatment with H_2O_2— At day 5 after seeding, H_2O_2 was added to CMCs or CFs at a final concentration of 300 μM for a 2-hr incubation. The majority of cells survive this dose of H_2O_2 treatment(276, 277). For dose response experiments, CMCs were treated with H_2O_2 ranging from 100 to 400 μM for 2 hrs. Following H_2O_2 treatment, the cells were placed in fresh DMEM containing 10% (v/v) FBS and were cultured for 3 additional days to allow recovery.

Conditioned Media and Cell Lysates Preparation— Serum free conditioned medium was collected as described(180). Three days after H_2O_2 treatment, cells in 100 mm dishes were placed in fresh serum free DMEM after thorough rinsing with DMEM to remove residual serum proteins. After 3 days of culture, the serum-free conditioned media were collected for concentration and dialysis to remove phenol red. To prepare cell lysates, cells were washed twice with ice-cold PBS and scraped in 200 μl of EB lysis buffer [1%

Triton X-100, 10 mM Tris (pH 7.4), 5 mM EDTA, 50 mM NaCl, 50 mM NaF, and freshly added 2 mM DTT, 1 mM Na_2VO_3, 1 mM phenylmethylsulfonyl fluoride, 100 μg/ml leupeptin, and 10 μg/ml aprotinin]. The protein concentrations of the conditioned media and cell lysates were determined using the Bradford method according to the manufacturer's instruction (BioRad, Hercules, CA).

ESI-LC-MS/MS Analysis— The protein mixture from concentrated conditioned media was digested overnight with trypsin at a 50:1 ratio(180, 183). Digested peptides were analyzed using a quadrupole ion trap ThermoFinnigan LCQ DECA XP PLUS (San Jose, CA) equipped with a Michrom Paradigm MS4 HPLC, and a nanospray source based on the design of the University of Washington. Peptides (7 μg total loaded) were eluted from a 15 cm pulled tip capillary column (100 μm I.D. x 360 μm O.D; 3-5 μm tip opening), pulled using a P2000 capillary puller (Sutter Instrument Co., Novato, CA), packed with 7 cm Vydac C18 (Hesperia, CA) material (5 μ, 300Å pore size), using a gradient of 0-65% solvent B (98% methanol/ 2% water/ 0.5% formic acid/ 0.01% triflouroacetic acid) over a 60-min period at a flow rate of 350 nl/min. The LCQ ESI positive mode spray voltage was set at 1.6 kV, with the capillary temperature of 200°C. Dependent data scanning was performed with the Xcalibur v 1.3 software with a default charge of 2, an isolation width of 1.5 amu, an activation amplitude of 35%, activation time of 30 msec, and a minimal signal of 10,000 ion counts(184). Global dependent data settings included a reject mass width of 1.5 amu, dynamic exclusion enabled, exclusion mass width of 1.5 amu, repeat count of 1, repeat duration of 1 min, and exclusion

duration of 5 min. Scan event series included one full scan with mass range 350 – 2000 Da, followed by 3 dependent MS/MS scan of the most intense ions. Turbo SEQUEST™ v 3.1 scores the matches of experimental tandem MS data with theoretical spectra generated from known protein sequences(278). The peak list (dta files) for the search was generated by Xcalibur v1.3. During the search, the tolerance of parent peptide mass error was set at 1.5 amu, with the fragment ion mass tolerance set at 0.5 amu. A preliminary positive peptide match uses the criteria of the correlation factor (Xcorr) greater than 2.5 for doubly-charged peptide ions, delta cross-correlation factor (ΔXcorr) greater than 0.08, minimal one tryptic peptide terminus, and the ratio of experimental over theoretical peptide fragment ions of >50%. For triply- or singly-charged peptide ions, the Xcorr threshold was set at 3.5 or 1.8, respectively(279, 280). Visual examination of the spectra confirms all matched peptides. The spectra were searched against the non-redundant protein database downloaded from NCBI on July 14, 2005, when it contained 2,662,317 entries. DTASelect was subsequently used to filter the SEQUEST output based on above criteria, with the –o function of the software to remove subsets of other proteins(281). Despite the use of the NCBI non-redundant protein database for the search and the –o function of DTASelect, redundancy still exists in the outputs. To further eliminate the redundancy, the DTASelect output file was carefully inspected to remove the peptide hits of non-corresponding species (e.g. the human). When one protein hit was identified with more than one accession number in the DTASelect output, a Gi # from the source species (i.e. the rat) was chosen for data presentation (Table 2).

Western Blot Analysis— Proteins from conditioned media (20 μg), cell lysates (20 μg) or animal plasma (100 μg) were separated by SDS-polyacrylamide gel electrophoresis (15%) before overnight electrophoretic transfer at 30 volts to a polyvinylidene difluoride (PVDF) membrane (Millipore, Bedford, MA). After eliminating non-specific binding with 1 hr incubation in 5% nonfat milk, the PVDF membrane was incubated overnight at 4 °C with the antibody against Cystatin C (1:200 dilution, rabbit polyclonal, Catalog# 06-458, Upstate Biotechnology, NY), ANP (1:3000 dilution, rabbit polyclonal ab14347, Abcam, MA), fibronectin (1:2000 dilution; polyclonal F-3648, Sigma-Aldrich, MO), matrix metalloproteinase 2 (MMP-2, 1:2000 dilution; polyclonal AB19015, Chemicon International, CA), vinculin (1:8000 dilution; mouse monoclonal v9131, Sigma-Aldrich, MO), or GAPDH (1:2000 dilution; polyclonal, ab9485-100, Abcam, MA). The membranes were subsequently incubated 45 minutes in horseradish peroxidase-conjugated secondary antibodies (Zymed Laboratories Inc., South San Francisco, CA; 1:8000) for detection of bound antibodies with enhanced chemiluminescence (ECL) reaction as described previously(192, 276, 282).

RNA Isolation and Semiquantitative RT-PCR— Semiquantitative RT-PCR was performed using 2 μg of total RNA extracted with TriZol (Invitrogen) from each sample for measurement of Cystatin C (rat or mouse) or ANP (mouse) at the mRNA level. Glyceraldehyde-3-phosphate dehydrogenase (GAPDH) was included as an internal control for equal loading. We used the Primer 3 Input Program (http://frodo.wi.mit.edu/cgi-bin/primer3/primer3.cgi) to design PCR primers and to

calculate the optimal PCR annealing temperature (Table 1). PCR products were detected by ethidium bromide staining after agarose gel electrophoresis.

Induction of Cardiomyopathy with Chronic Administration of Doxorubicin to Mice— Five to seven week-old (young) (18–22 g) male BL6/129SF1 J mice were treated with Dox via intraperitoneal injection, twice a week for a total of 10 injections at the dose of 4 mg/kg per injection(180). Control animals were injected with saline at the same volume in parallel. After the first four injections, animals were not injected for 2 weeks to allow recovery of bone marrow depression(250). Cardiac hemodynamic measurements show cardiomyopathy two weeks after the final Dox injection (Terrand et al, manuscript in preparation).

Mouse Model of Myocardial Infarction— The surgical procedure of left anterior descending (LAD) coronary artery occlusion was performed using male BL6/129SF1 J mice (aged 5–7 weeks) as described(283, 284). After induction of anesthesia with Avertin (2.5%), a tracheotomy was performed to ventilate animals through a Harvard Rodent Respirator (Harvard Apparatus, Boston, MA). An anterior thoracotomy was performed to open the pericardium. Upon exposure of the heart, an 8–0 silk suture was tightened around the proximal LAD (1-3 mm from the tip of the left atrium) rapidly. Occlusion of coronary artery results in a visible blanched area in the myocardium distal to the ligation site, serving as an indicator for successful coronary artery ligation. To close the chest cavity by bringing together the second and third ribs with one 6-0 nylon

suture, slight pressure is applied on the chest with the needle holder to reduce the volume of free air in the chest cavity while tying a knot. All layers of muscle and skin are closed with 6-0 continuous absorbable and nylon sutures, respectively. Sham-operated control animals were prepared in a similar manner except the LAD coronary artery was not ligated.

Animal Plasma and Tissue Preparation— As described previously(180), the blood was collected via the abdominal vena cava. The blood from each animal was subsequently centrifuged at 2000 rpm, 4 °C for plasma preparation. To prepare samples for Western blot or RT-PCR analyses, the whole heart was frozen in liquid nitrogen immediately after excision. Hearts were ground into a powder with a pestle and mortar (VWR) in a liquid nitrogen bath. About 1/3 of the powder was dissolved in EB lysis buffer for protein preparation, and 2/3 of the powder was dissolved in TriZol (Invitrogen) for RNA preparation.

STATISTICS:

The student-t test was used for comparisons of means from control versus treated group. One-way analysis of variance (ANOVA) was used to compare groups of means followed by the Bonferroni Correction for multiple samples

Results:

Identification of Proteins in Conditioned Media of CMCs and CFs by ESI-LC-MS/MS

Conditioned media were collected for ESI-LC-MS/MS based proteomics to identify protein factors secreted by CMCs or CFs upon H_2O_2 treatment. The Turbo SEQUEST software searches the experimental tandem MS spectra obtained from LC-MS/MS analyses against a theoretical peptide sequence database. Confident protein identifications rely heavily on two parameters from the SEQUEST output: "Xcorr" and "Ions". Based on the recommendation of the software, while Xcorr≥1.8 for +1 ions, Xcorr≥2.5 for +2 ions and Xcorr≥3.5 for +3 ions, the value of Ions is greater than 50% in all cases (285). The SEQUEST data output was filtered based on these criteria using the DTASelect software, which removes unqualified hits. The DataContrast program was applied to compare DTASelect outputs obtained from CMCs versus CFs with or without H_2O_2 treatment.

Table4.2 lists the proteins identified in the conditioned media of Control (Ctrl) and H_2O_2 treated CMCs or CFs. The Xcorr values were presented as means ± standard deviations (SDs) with the number of detected peptides indicated (Table4.2). For the protein assignment based on a single-peptide match, the sequence of the peptide and the precursor mass or charge were included (Table4.2). Seven proteins appeared common among Ctrl and H_2O_2 treated CMCs and CFs: Biglycan, Collagen alpha 1(III), Collagen alpha 2 (V), Fibronectin 1, Matrix Metalloproteinase 2 (MMP2), Osteonectin, and Procollagen, alpha 2 (I). There were 12 proteins unique to H_2O_2 treated CFs (Table4. 2). Since the goal of this study is to find the secreted protein factors specific to CMCs upon

oxidative stress, we focused on proteins altered in CMCs but not in CFs following H_2O_2 treatment. These proteins include Cystatin C, Follistatin-related protein, actin gamma 2, Complement Component 1s, Myosin Heavy Chain polypeptide 7 (MHC7), MHC6, MHC4, MHC3, a protein similar to MHC2b, a protein similar to Collagen alpha 2(IV) chain and a protein similar to KIAA1512 (Table 4.2).

Figure4.1 shows the MS/MS spectra and the SEQUEST Flicka output of the Cystatin C peptide detected from the conditioned medium of H_2O_2 treated CMCs. Although only one peptide was detected by the Mass Spectrometer, the MS/MS spectrum, "Xcorr" values and "Ions" scores all confer a high confidence in matching this peptide hit with Cystatin C. The discovery of Cystatin C provides a lead in finding CMC cell type specific indicator of oxidative stress injury.

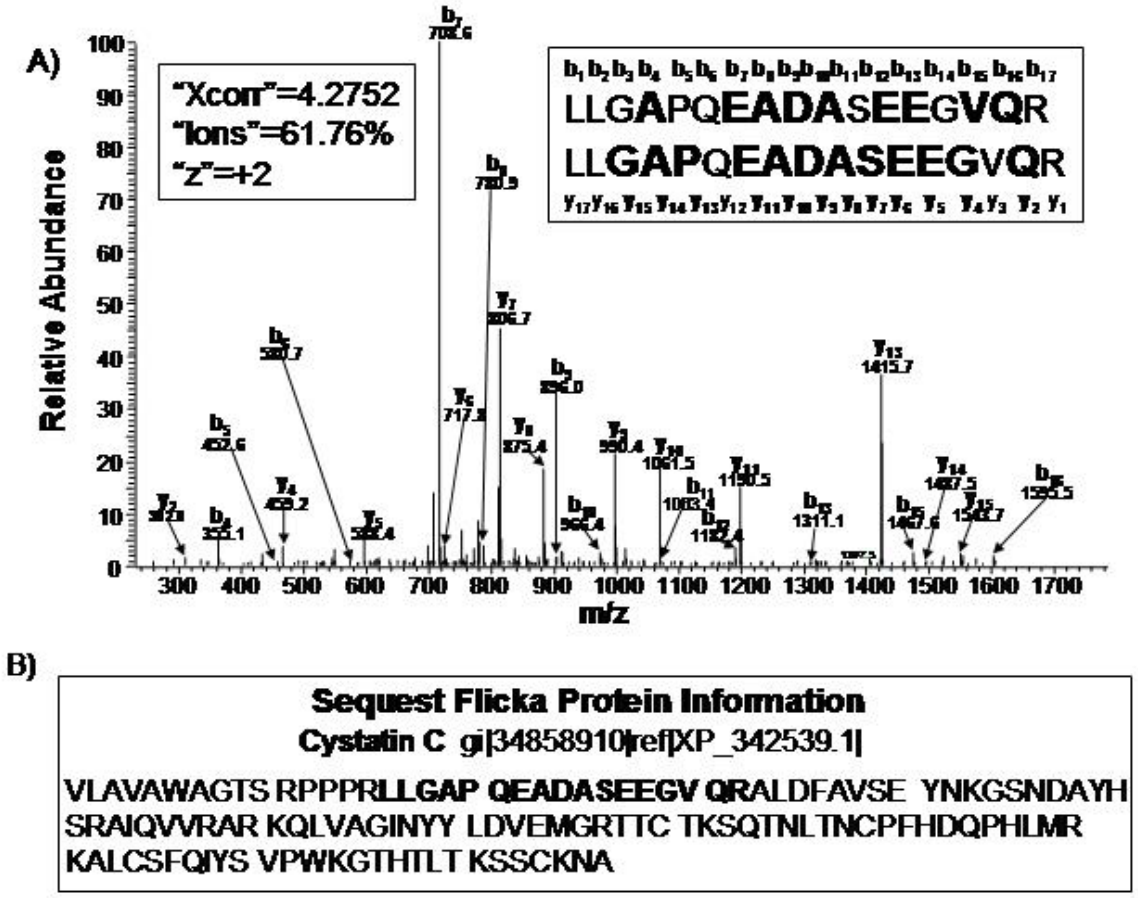

Fig. 4.1. MS/MS Spectrum of the Cystatin C Peptide Detected from the Conditioned Media of H2O2-treated CMCs (A) and SEQUEST Flicka Protein Information for Cystatin C (B). The bolded letters indicate the detected b and y ions matching the predicted ion mass in the database (A). SEQUEST Flicka protein information page for Cystatin C shows the fragment detected by LC-MS/MS (B).

Induction of Cystatin C Expression by H_2O_2 Treatment in CMCs

To verify the finding of Cystatin C induction by H_2O_2 treatment in CMCs, the conditioned media were collected for Western blot analyses. LC-MS/MS analyses indicate that MMP-2 and fibronectin appear in control and H_2O_2 treated CMCs or CFs; allowing us to use these two proteins for comparisons. As expected, Western blot analyses found no significant difference in the level of MMP-2 or fibronectin in the conditioned media between control and H_2O_2 treated CMCs or CFs (Fig4.2A). Consistent with the finding from LC-MS/MS analyses, CFs contain a higher basal level of Cystatin C compared to CMCs but the level of Cystatin C did not change with H_2O_2 treatment in CFs (Fig4.2A). In contrast, an induction of Cystatin C protein was detected in the conditioned medium of H_2O_2 treated CMCs compared to untreated control CMCs (Fig.4.2A).

Atrial Natriuretic Peptide (ANP) has been used as a biomarker of heart failure in many experimental models. ANP, a 28 amino acid peptide, is derived from a 126 amino acid pro hormone (ProANP) due to the cleavage by a serine proteases. The protease also generates a 98 amino acid N-terminal peptide (NT-ANP). An increase of the ProANP or NT-ANP in the circulating system is detectable in patients with left ventricular dysfunction and heart failure(286-290). The level of ProANP and NT-ANP was measured in the conditioned medium of H_2O_2 treated cells for the purpose of comparison with our Cystatin C data. We found that with 20 μg of proteins from the conditioned medium, we could detect elevation of cystatin C but not ANP in its Pro or NT-form.

With 100 μg proteins of conditioned medium, there is a significant elevation of ProANP and NT-ANP in the conditioned medium of H_2O_2 treated CMCs (Fig4.2B).

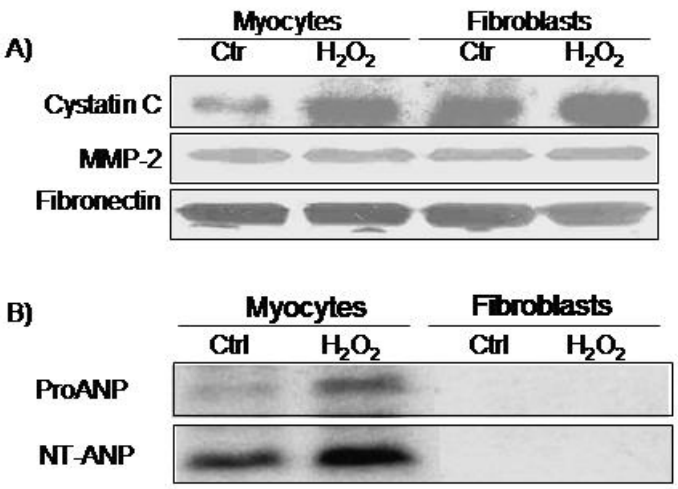

Fig. 4.2. Induction of Cystatin C and ANP by H2O2 in the Conditioned Medium from CMCs but not CFs. CMCs and CFs in 100 mm dishes were treated with 300 μM H_2O_2 for 2 hrs. Cells were placed in fresh DMEM containing 10% FBS for 3 days before being placed in DMEM with 0% FBS for harvesting conditioned medium. Concentrated conditioned medium was used for SDS-PAGE and Western blot analyses to detect Cystatin C, MMP-2 and Fibronectin (A, 15 μg protein/lane), or ProANP and NT-ANP (B, 100 μg protein/lane).

The finding of Cystatin C in the conditioned medium suggests the possibility that H_2O_2 treatment increases the expression of Cystatin C gene. We performed H_2O_2 dose-response studies to determine levels of Cystatin C protein and mRNA in cell lysate. Western blot analyses of cell lysates indicate clear elevation of Cystatin C protein in the lysates of cells treated with 300 or 400 μM H_2O_2 (Fig 3A). With 100 μg proteins from cell lysates, the level of ProANP or NT-ANP reached the highest level with 300 μM H_2O_2 (Fig4.3A). Consistent with the protein data, semiquantitative RT-PCR analyses revealed elevation of Cystatin C mRNA in cells treated with 300 – 400 μM H_2O_2 and optimal induction of ANP with 300 μM H_2O_2 (Fig4.3B). These data suggest that increased secretion of Cystatin C in the conditioned medium results from elevated expression of the Cystatin C gene.

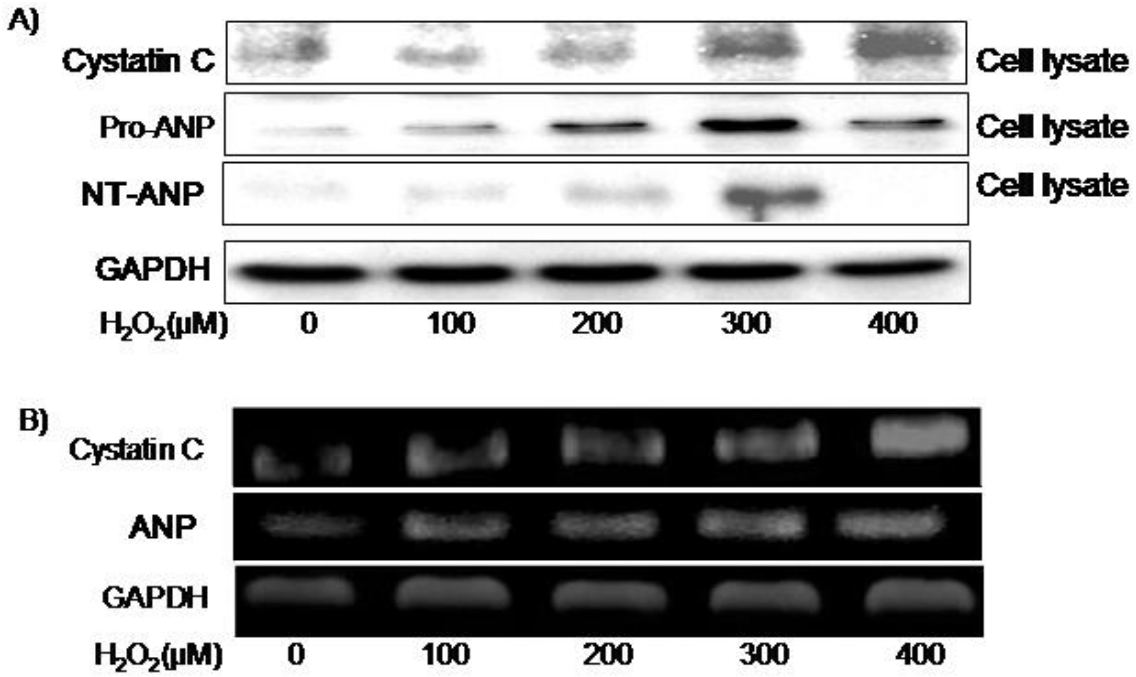

Fig. 4.3. H2O2 Dose-dependent Induction of Cystatin C and ANP in CMCs. CMCs were treated with H_2O_2 at 0 to 400 μM for 2 hrs in 100 mm dishes. Cell lysates and RNA were harvested as described in the Methods. Western blot analysis was used to detect Cystatin C (20 μg protein/lane), ANP (100 μg protein/lane) or GAPDH (20 μg protein/lane) in cell lysates (A). For RT-PCR, 2 μg of total RNA from each sample were used for RT, and one-tenth of the RT reaction mixture was used for PCR to amplify Cystatin C, ANP or GAPDH (C). GAPDH was used as a loading control to show equal amount of proteins or RNA between different groups of samples (C).

Using Cystatin C as an in Vivo Biomarker of Cardiac Injury

Three animal models were used to address whether Cystatin C can serve as an oxidative injury biomarker *in vivo*: aging, Dox induced cardiomyopathy, and coronary artery ligation induced myocardial infarction. Increased levels of oxidative stress have been shown to occur during the process of aging. When the plasma was collected from young (5–7 weeks) or old (16-18 months) female and male mice for Western blot analyses to measure the level of Cystatin C, an elevated level of Cystatin C was found in the plasma of old mice, male and female (Fig.4.4).

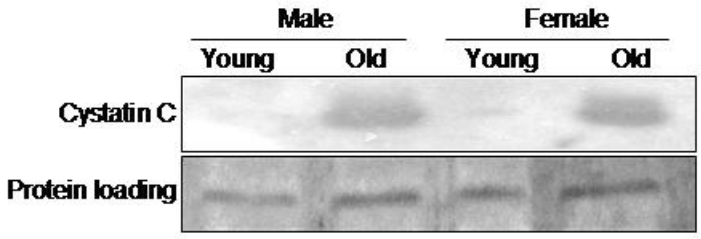

Fig. 4.4. Plasma Cystatin C in Aging Mice. The blood was collected from BL6/129SF1 J mice at 5–7 weeks (young) or 16–18 months (old) of age. The plasma was used for Western blot analysis to detect Cystatin C (100 μg/lane). An area of silver-stained SDS gel around the molecular weight of Cystatin C (*bottom panels*) was included to show equal loading.

Chronic treatment of Dox is known to induce cardiomyopathy and the mechanism of Dox induced cardiomyopathy involves generation of reactive oxygen species(291-294). The protocol of Dox treatment, as described under the "Materials and Methods," has been shown to induce cardiomyopathy(250). Cardiac hemodynamic measurements show cardiomyopathy two weeks after the final Dox injection (Terrand and Chen, manuscript in preparation). Measurements of liver and kidney injury biomarkers indicate the protocol of Dox administration used in this study did not induce liver or kidney injury (Table4.3). With the plasma samples collected from control and Dox-treated mice, Western blot analyses indicate a clear elevation of Cystatin C in the Dox-treated mice (Fig4.5A&B). RT-PCR and Western blot analyses using heart tissue samples show elevated levels of Cystatin C mRNA and protein in animals treated with Dox (Fig4.5C-G), although the changes were less dramatic than the plasma sample. Elevated levels of ANP mRNA were detected in parallel with Cystatin C mRNA in the cardiac tissue from Dox treated mice (Fig4.5E&F). To demonstrate the specificity of Cystatin C induction in the heart, the brain, liver, and kidney tissues were collected from Control and Dox treated mice for Western blot analyses. The assays did not detect elevation of Cystatin C protein in these tissues from Dox treated mice (Fig.4.6). These results support that increased levels of Cystatin C in the circulating system and in the myocardium correlate with cardiomyopathy induced by Dox.

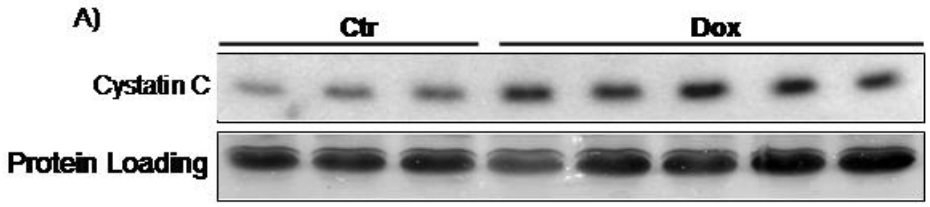
A)
Ctr
Dox
Cystatin C
Protein Loading

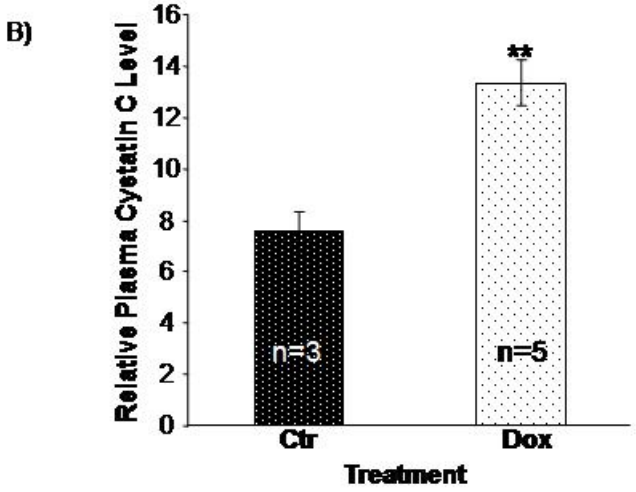
B)
Relative Plasma Cystatin C Level
16
14
12
10
8
6
4
2
0
**
n=3
n=5
Ctr
Dox
Treatment

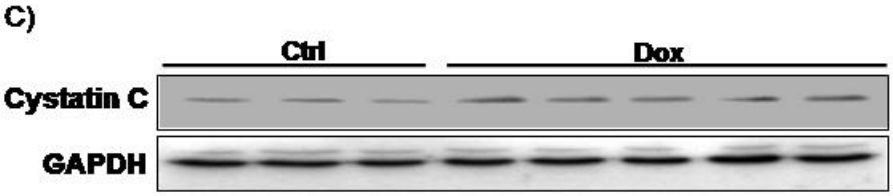
C)
Ctrl
Dox
Cystatin C
GAPDH

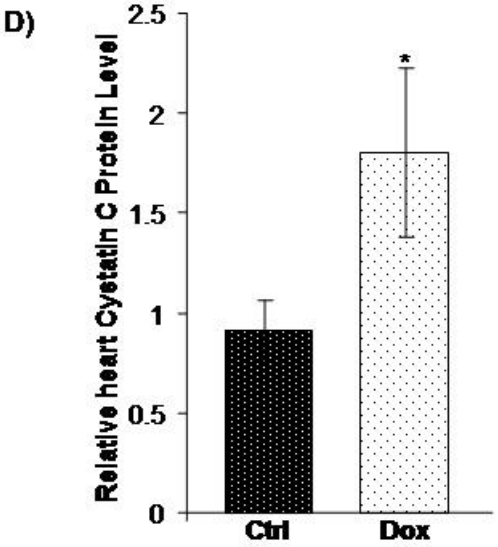
D)
Relative heart Cystatin C Protein Level
2.5
2
1.5
1
0.5
0
*
Ctrl
Dox

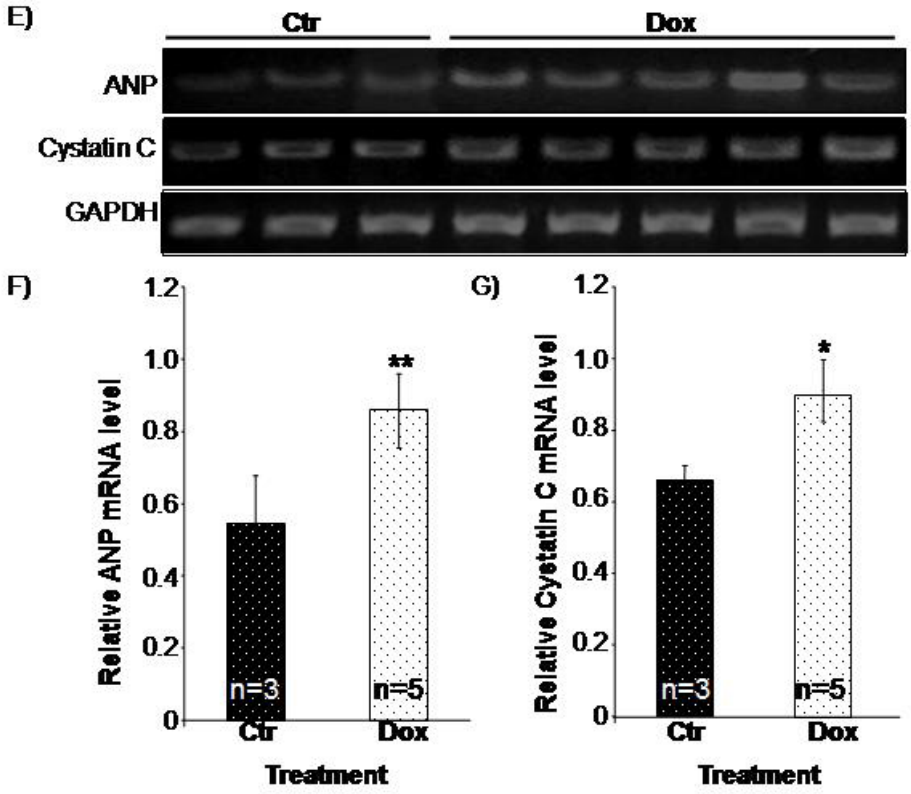

Fig. 4.5. Dox Induced Increases of Cystatin C in the Plasma and the Myocardium. Male BL6/129SF1J mice (5-7 weeks old) were treated with Dox as described in the Methods. The plasma was collected from the control and Dox treated mice 2 weeks after the last Dox injection for measurement of Cystatin C protein levels (A-B). An area of Coomerssie blue-stained SDS gel around the molecular weight of Cystatin C was included to show equal protein loading (A). The heart was collected to detect levels of Cystatin C protein by Western blot (C, D) and levels of Cystatin or ANP mRNA by RT-PCR (E-G). GAPDH was used as a loading control (C, E). The intensities of the bands were quantified using NIH imaging J software and are presented as means ± SE (B, D, F, and G). mRNA levels of ANP and Cystatin C were quantified and normalized to GAPDH based on band intensities using NIH Image J software and are presented as means ± SE (F & G). An asterisk (*) indicates $P<0.05$ while two asterisks (**) indicate $P<0.01$ when means from Dox treated samples are compared to that of control using Student's t test.

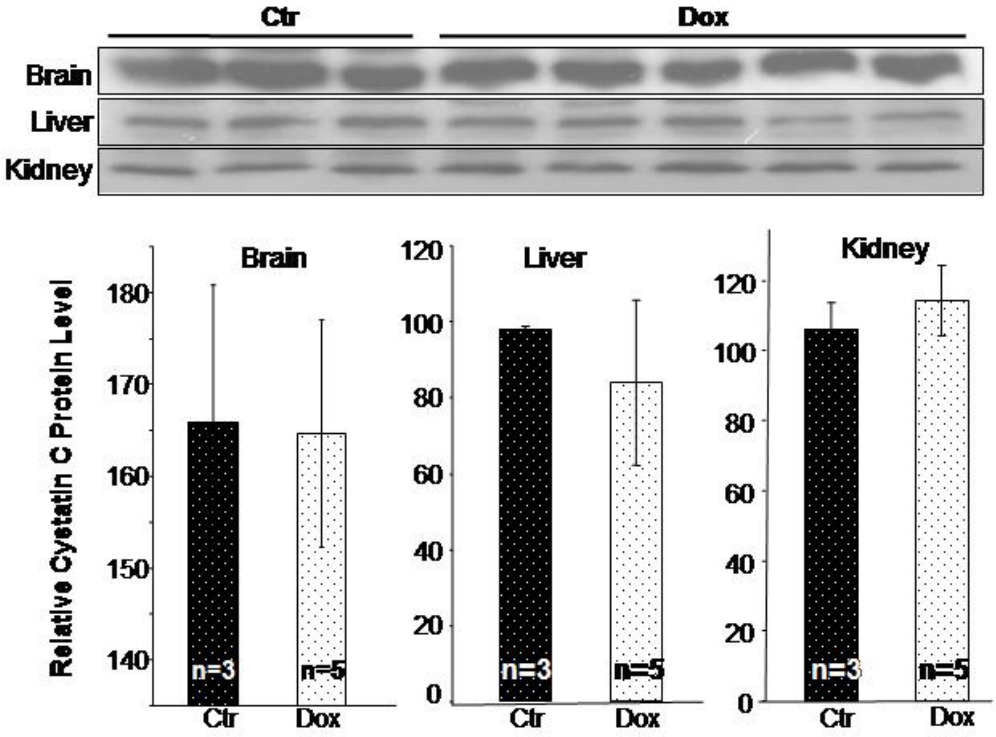

Fig. 4.6. Cystatin C Is Not Elevated in the Brain, Liver or Kidney of Dox Treated Mice. The brain, liver and kidney were harvested from the same set of animals as described in Fig. 6. Tissue homogenates were used for measurements of Cystatin C protein level by Western blot (A). The intensities of the bands were quantified using NIH imaging J software and are presented as means ± SE (B-D).

Since cardiomyopathy typically develops within 10 weeks after the first injection of Dox, this well-defined time frame allows us to address whether elevated Cystatin C can be detected earlier in the time course of cardiomyopathy development. The plasma was collected at 2, 4, 6, and 9 weeks from vehicle and Dox-treated mice for Western blot analysis to detect Cystatin C. Dox treatment causes decreases in animal body weight starting at the 4th week, when the animals show no visible change in locomotion activity. The body weight decreases further in a time-dependent manner as Dox treated animals progress towards cardiomyopathy (Fig.4.7A). Our Western blot analyses indicate an elevated level of Cystatin C in the plasma of mice at 4, 6, and 9 weeks upon Dox treatment (Fig.4.7B). A similar time course of Cystatin C induction was found with analyses of Cystatin C protein in the homogenates of heart tissue (Fig4.7C). These results indicate that Cystatin C elevation can be detected earlier in the time course of heart failure.

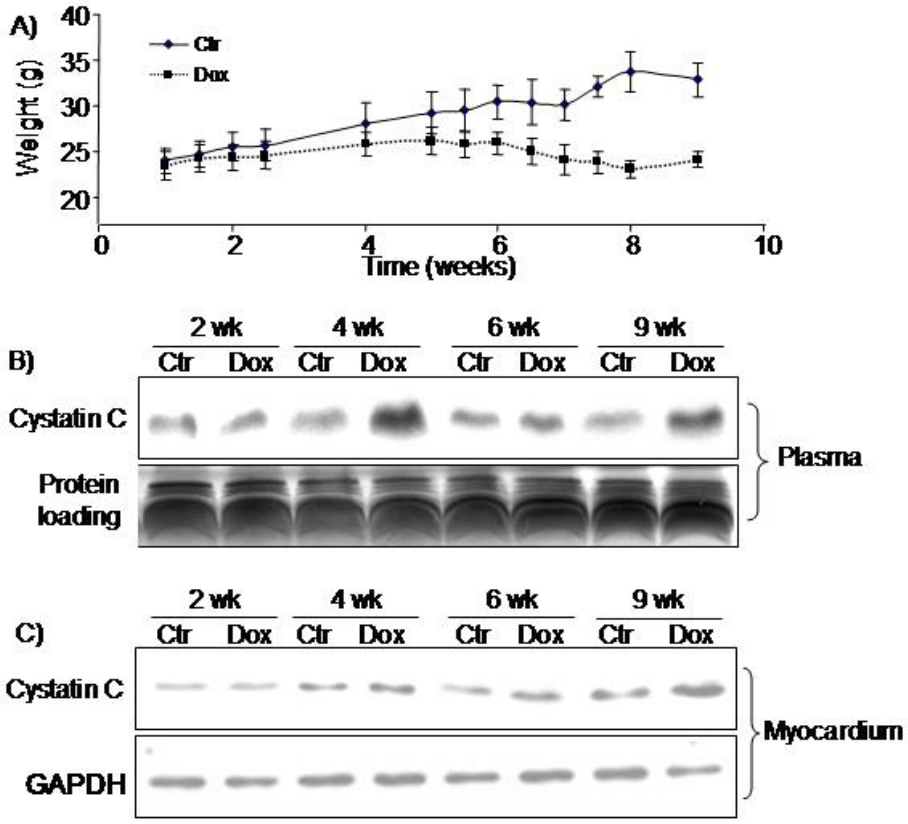

Fig. 4.7. Time-dependent Induction of Cystatin C in the Plasma of Dox-treated Mice. Male BL6/129SF1J mice (5-7 weeks old) were treated with doxorubicin (Dox, i.p) as described in the Method. Weight change in mice upon Dox treatment indicates Dox toxicity starts after the 4th week (A). The plasma (A) and whole heart tissue (B) was collected at weeks 2, 4, 6, and 9 from saline injected Ctrl and Dox treated mice for Western blot analysis of Cystatin C protein levels (B, 100μg protein/lane). An area of Coomassie blue staining corresponding to the molecular weight of Cystatin C was shown to indicate equal protein loading among plasma samples (B). GAPDH was used as an internal loading control (C).

With coronary artery ligation surgery, cardiac specific oxidative injury is induced due to ischemia and myocardial infarction(295). The plasma was collected from control, sham operated, and myocardial infarcted mice at 7 days after the surgery for Western blot analyses. Compared to the control or sham operated mice, there is a significant elevation of Cystatin C protein in the plasma of MI mice (Fig4.8).

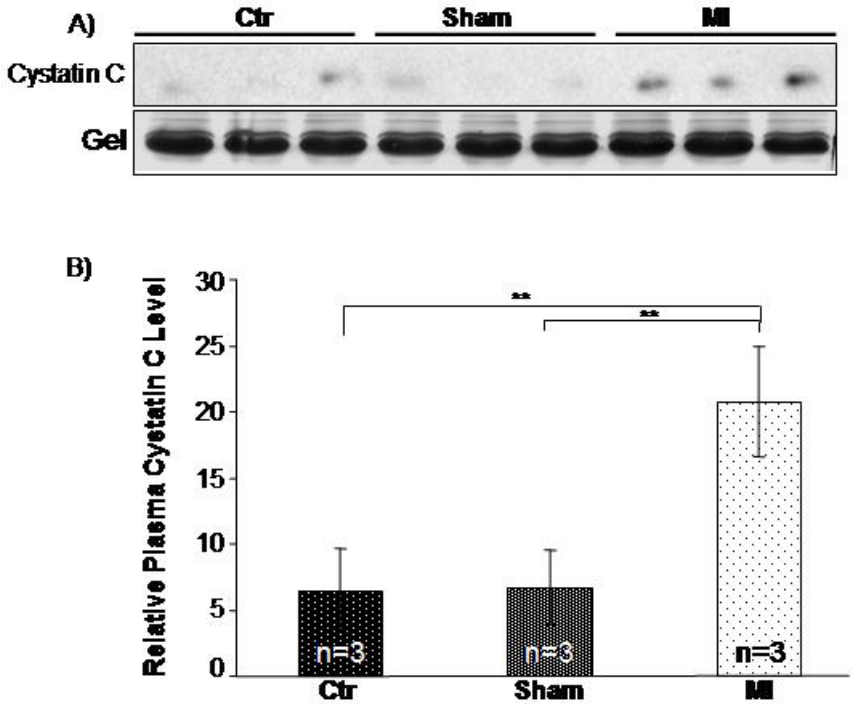

Fig. 4.8. Elevation of Cystatin C in the Plasma of Myocardial Infarcted Mice. Male BL6/129SF1 J mice (aged 5–7 weeks) was used for left anterior descending coronary artery occlusion surgery. The blood was collected from Control (Ctr), Sham operated control (Sham) and myocardial infarcted (MI) mice at 7 days after the surgery. The plasma containing 100 μg of protein was loaded for SDS-PAGE and Western blot analyses to detect Cystatin C (A). An area of Coomassie blue staining corresponding to the molecular weight of Cystatin C was also included to show protein equal loading (A). The intensities of the bands quantified by NIH imaging J software are presented as means ± SE (B). Two asterisks (**) indicate $p<0.05$ when the means of myocardial infaracted mice were compared to that of sham operated or control animals by Student's t-test.

Discussion:

LC-MS/MS based shotgun proteomics has lead to the discovery of Cystatin C in the conditioned media of CMCs treated with H_2O_2. With CMCs in culture, elevation of Cystatin C occurred in cells treated with 300 - 400 μM of H_2O_2 and appeared 5 days after H_2O_2 treatment. With two *in vivo* models of heart failure, Dox treatment induced cardiomyopathy or coronary artery ligation induced myocardial ischemia, elevated levels of Cystatin C was detected in the plasma. These data suggest the potential of using Cystatin C as a non-invasive marker of oxidative stress in association with heart failure.

Cystatin C is a low molecular weight alkaline protein (MW 13,359 Da) belonging to a family of cysteine protease inhibitors(296, 297). As a highly abundant inhibitor of cysteine proteases, Cystatin C is found in most cell types, including cardiac muscle fibers(298-300). The protein is typically secreted by cells and ends up in various biological fluids including urine, blood, saliva, seminal fluid, and cerebrospinal fluid (299, 301). At the cellular level, Cystatin C is an inhibitor regulating the activity of lysosomal cysteine proteases, such as Cathepsins B, H and L (302-304). The activity of these cysteine proteases ultimately participates in regulation of physiological processes such as protein catabolism, antigen presentation, bone reabsorption, and hormone processing (302). In disease states involving tissue remodeling, Cystatin C protects the plasma membrane matrix and extracellular matrix proteins from being cleaved by cysteine proteases. An imbalance between cysteine proteases and Cystatin C contributes to human atherosclerotic and aneurismal aortic lesions (305, 306). Decreased Cystatin C expression in general is associated with an increased incidence of atheroscloersis and the

severity of CVD (305, 307, 308). While deficiency in the activity of cathepsin S, a substrate of Cystatin C, reduces the risk of atherosclerosis (309), increased serum levels of cathepsin L, another substrate of Cystatin C, correlate with coronary artery stenosis (310). Based on these reports, a simplistic explanation for the functional significance of the observed Cystatin C increase in our study is an adaptive mechanism against oxidative stress induced tissue injury and cardiac remodeling associated with cysteine protease activities.

Our data suggest the possibility of using Cystatin C as a diagnostic tool for the early stage of heart failure. Whether serum Cystatin C indeed elevates as a result of cardiac injury in human population remains to be tested in clinical settings. A clinical study performed in Japan has shown that heart failure patients have significantly higher levels of Cystatin C in the circulating system (311). Those with higher levels of circulating Cystatin C have a higher incidence of cardiac disease (311). Sarnak, *et al.* (312) recently reported that high cystatin C concentration in the plasma imposes a risk factor of heart failure in individuals older than 65 years of age. Cystatin C in the blood is usually filtered through the glomeruli, being absorbed in the proximal tubules of the kidney (302, 313-315). Dysfunction of the proximal tubes results in increases in the level of Cystatin C in the circulating system. Several clinical studies have tested Cystatin C as a biomarker of kidney dysfunction in adult, children and elderly populations. A recent study showed that serum Cystatin C is superior to serum creatinine as an indicator of kidney failure involving glomerular filtration (316). With heart failure patients, renal dysfunction implies an adverse prognostic factor (311, 312). Therefore regardless the

source of Cystatin C, elevated serum Cystatin C level may indicate a poor prognosis for patients with symptoms of heart failure.

At present, the natriuretic peptides are the only FDA approved biomarkers for non-invasive diagnosis of heart failure. ANP and BNP are secreted from cardiomyocytes when the heart progresses into failure with various types of inducers, such as hypertension and aortic stenosis. However due to rapid degradation in the plasma, the half life of ANP and BNP is about 3 and 20 minutes, respectively(162, 317). In addition to a short half life, the serum level of BNP is ≤100 pg/ml for normal individuals. In contrast, the concentration of serum Cystatin C for a normal person is in the range of 800-1200 pg/ml (302), about 10 times higher than that of BNP. More importantly, Cystatin C is stable for at least six months when serum samples are kept at -80°C (302, 318). Finney *et al.* (318) found that the blood can be left untreated up to 24 hrs without affecting the detection of Cystatin C. In our experiments, detection of ProANP or NT-ANP by SDS-PAGE and Western-blot requires 5 times more protein from conditioned medium or cell lysates (100 μg protein/lane for Pro or NT-ANP) than detection of Cystatin C (15-20 μg protein/lane) by the same method. With the serum samples that show elevated Cystatin C from Dox treated or myocardial infracted animals, ProANP or NT-ANP could not be detected by Western-blot, indicating a low level or rapid degradation of these proteins in the plasma. These lines of evidence can be translated to the speculation of using Cystatin C as a quick, non-invasive and minimal blood requiring measure of heart failure.

Our study provides experimental evidence suggesting shotgun proteomics as a useful tool for biomarker discovery. The ability to perform analyses with a limited quantity of samples and with a relatively complex mixture were among the advantages of the LC-MS/MS based proteomics technique. The improvement in separation capacity of MS/MS instrument coupled with precision computational sequence database searching software allows meaningful identification of proteins in the subproteome of secreted proteins from the culture media of different cell types. Compared to a previous study from our laboratory using a classical LCQ instrument, which detected about 20 proteins in the conditioned medium of human diploid fibroblasts, we found about 50 proteins in the conditioned medium of CMCs and CFs with a LCQ DECA XP LC-MS/MS system. Although the resolution and the detection sensitivity have been improved with the LCQ DECA XP system, the number of proteins identified by this instrumentation is still far less than what has been predicted based on the consensus signal peptide of secreted proteins from the Human Genome Project. Chen *et al.* (319) predict a putative size of secreted proteome being 5235 proteins. With 2-dimensional gel electrophoresis, about 1000 protein spots were detected from the conditioned medium of adipocytes and osteocytes (257, 320). The low number of secreted proteins detected in our experiments indicates the limitation of our current instrumentation. The technology development in LC-MS/MS industry will eventually lead to the ability to characterize an entire proteome from cell lysates, containing 200,000–300,000 proteins (321-323). Despite current limitation of LC-MS/MS instrumentation, the finding that H_2O_2 treatment increases the

expression and secretion of Cystatin C in CMCs presents a novel candidate for non-invasive diagnosis of oxidative injury in the myocardium.

Table 4.1. Sequence, expected fragment size and annealing temperature (ta) of primers used in the semi-quantitative RT-PCR analysis of mRNA levels

Gene	Sequence	Expected fragment size (bp)	Temp (^{o}C)	GenBank accession number
Cystatin C (rat)	Sense:tggtgagagctcgtaagcag Antisense:gctggattttgtcagggtgt	208	62	Rn.106351
Cystatin C (mouse)	Sense:aaaggcacacactccctgac Antisense:cctgcagcagctcctttact	249	58	Mm.4263
ANP (mouse)	Sense:gtgtacagtgcggtgtccaa Antisense:acctcatcttctaccggcatc	153	62	Mm.19961
GAPDH (rat)	Sense:tgaaggtcggtgtcaacggatttggc Antisense:catgtaggccatgaggtccaccac	223	62	Rn.64496
GAPDH (mouse)	Sense:cctgcaccaccaactgctta Antisense:tcatgagcccttccacaatg	222	62	Mm.379644

Table 4.2. Proteins appearing in the conditioned media of Ctrl and H2O2-treated CMCs and CFs

The conditioned medium was prepared as described in the Methods for LC-MS/MS analysis. The proteins listed here meet the selection criteria of Xcorr ≥ 1.8 for +1 ions, Xcorr ≥2.5 for +2 ions and Xcorr ≥ 3.5 for +3 ions. The values of Ions exceed 50% in all cases per Turbo SEQUEST software. [a] Xcorr values (means±SD); [b]Peptide number; [c]Percent of sequence coverage. If only one peptide is detected, Charge of the peptide[e], and Mass of the Peptide[f] are indicated.

		Cardiomyocytes		Fibroblasts	
gi#	Name	Ctrl Group	H_2O_2-treated Group	Ctrl Group	H_2O_2-treated Group
179433	Biglycan	[a]4.00±0.49; [b]5; [c]17.3%	[a]3.96±0.76; [b]4;)13.3%	[a]4.04±0.87; [b]5; [c]16.2%	[a]4.60±0.82; [b]7; [c]20.1%
543912	Collagen alpha1(III)	[a]3.43±1.00; [b]3; [c]4.1%	[a]3.76; [b]1; [c]1.1% [e]+2; [f]1660.8	[a]3.97±0.60; [b]3; [c]7.5%	[a]3.98±1.03; [b]2; [c]6.6%
34875814	Collagen alpha2(V)	[a]4.40; [b]1; [c]1.4% [e]+2; [f]1782.5	[a]2.88; [b]1; [c]1.3% [e]+2; [f]1749.9	[a]4.13; [b]1; [c]1.4% [e]+2; [f]1779.9	[a]4.54+0.51; [b]2; [c]2.8%
9506703	Fibronectin1	[a]4.27±1.21; [b]12; [c]7.5%	[a]4.38±1.00; [b]16; [c]10.4%	[a]3.74±1.15; [b]2; [c]5.5%	[a]3.59±0.58; [b]3; [c]7.0%
13591991	Matrix metalloproteinas	[a]4.93; [b]1; [c]2.9% [e]+2; [f]2109.3	[a]5.04±0.62; [b]2; [c]5.7%	[a]5.37; [b]1; [c]2.9% [e]2; [f]2138.1	[a]4.37±1.21; [b]3; [c]8.6%
13959575	Osteonectin	[a]3.67±0.87; [b]4; [c]14.0%	[a]3.86±0.93; [b]2; [c]9.0%	[a]3.61±0.93; [b]6; [c]20.9%	[a]3.65±0.69; [b]9; [c]28.5%
16758080	Procollagen, type I alpha 2	[a]3.90±0.95; [b]9; [c]12.0%	[a]3.92±0.73; [b]7; [c]9.5%	[a]3.71±1.29; [b]9; [c]12.0%	[a]4.08±1.0; [b]7; [c]9.5%
11127974	Clusterin	[a]5.33; [b]1; [c]7.8% [e]+2; [f]1889.9	[a]5.52; [b]1; [c]7.8% [e]+2; [f]1889.1		[a]4.22; [b]1; [c]7.8% [e]+2; [f]1887.8
554527	Tropoelastin	[a]3.23; [b]1; [c]5.6% [e]+2; [f]1328.6	[a]3.71; [b]1; [c]5.6% [e]+2; [f]1327.6		[a]4.49; [b]1; [c]12.2% [e]+2; [f]1920.1
13591983	Lumican	[a]5.12; [b]1; [c]5.3% [e]+2; [f]1943.7	[a]4.60; [b]1; [c]5.3% [e]+2; [f]1944.8		

13592133	Beta actin	[a]2.80; [b]1; [c]2.8% [e]+2; [f]1517.4	[a]4.69; [b]1; [c]4.1% [e]+2; [f]1791.1		
27672001	Similar to RIKEN cDNA 1110007F23	[a]5.09; [b]1; [c]7.0% [e]+2; [f]2085.8	[a]4.62; [b]1; [c]7% [e]+2; [f]2086.5		
34854200	Complement component C7 precursor homolog	[a]4.64±0.66; [b]2; [c]4.5%	[a]3.74±1.10; [b]2; [c]3.8%		
34856932	Osteoblast specific factor 2 precursor homolog	[a]4.21±0.56; [b]7; [c]14.4%	[a]4.72±0.62; [b]7; [c]15.2%		
6981278	Natriuretic peptide precursor A	[a]3.11; [b]1; [c]5.9% [e]+2; [f]112.5	[a]2.74; [b]1; [c]5.9% [e]+2; [f]1110.6		
14010871	Dipeptidyl peptidase	[a]4.74; [b]1; [c]4.4% [e]+2; [f]2259.8		[a]2.81; [b]1; [c]2.8% [e]+2; [f]1486.3	[a]4.02; [b]1; [c]4.4% [e]+2; [f]2260.0
19705431	Albumin	[a]2.89; [b]1; [c]2.3% [e]+2; [f]1749.6		[a]2.58; [b]1; [c]2.3% [e]+2; [f]1750.0	
34876253	Nidogen	[a]2.84; [b]1; [c]0.9% [e]+2; [f]1176.4		[a]4.71; [b]1; [c]1.1% [e]+2; [f]1623.5	
9506953	Procollagen C-proteinase enhancer protein	[a]3.25; [b]1; [c]3.0% [e]+2; [f]1418.8			
34864189	Similar to laminin B1	[a]5.21; [b]1; [c]1.0% [e]+2; [f]2170.2			
33340123	Thrombospondin	[a]4.90; [b]1; [c]1.8%, [e]+2; [f]2163.7			
118185	Cystatin C		[a]4.28; [b]1; [c]13.4%, [e]+2; [f]1898.7	[a]4.81; [b]1; [c]13.4%, [e]+2; [f]1769.7	[a]3.45±1.72; [b]2; [c]22.0%
13242265	Follistatin-related protein		[a]4.00; [b]1; [c]5.6% [e]+2; [f]2044.9	[a]4.46±1.13; [b]4; [c]19.9%	[a]4.86±0.89; [b]2; [c]12.1%
6978441	Actin, gamma 2		[a]4.68; [b]1; [c]11.9%,		

			[e]+2; [f]1791.1		
38303991	Complement component 1, s subcomponent		[a]4.38; [b]1; [c]2.0% [e]+2; [f]1785.0		
8393807	Myosin heavy chain, polypeptide 7		[a]4.67±1.75; [b]6; [c]4.5%		
8393804	Myosin heavy chain, polypeptide6		[a]4.60±1.11; [b]6; [c]4.4%		
34870880	Myosin, heavy polypeptide 4		[a]4.51±1.8; [b]4; [c]2.9%		
6981234	Myosin, heavy polypeptide 3		[a]3.24±1.83; [b]2; [c]1.2%		
34870888	Similar to myosin heavy chain 2b		[a]4.67±1.60; [b]5; [c]3.6%		
34879630	Similar to Collagen alpha 2(IV) chain		[a]3.61; [b]1; [c]1.2% [e]+2; [f]1745.9		
34859107	Similar to KIAA1512 protein		[a]1.95; [b]1; [c]0.5% [e]+1; [f]1245.9		
12018262	Cathepsin B preproprotein			[a]3.55; [b]1; [c]7.1% [e]+2; [f]1991.8	[a]5.05; [b]1; [c]7.1% [e]+2; [f]1991.9
14389299	Vimentin			[a]4.17±1.36; [b]3; [c]8.3%	[a]3.64±1.12; [b]4; [c]10.7%
6978677	Procollagen, type II, alpha 1			[a]3.84; [b]1; [c]1.1% [e]+2; [f]1468.8	[a]2.57; [b]1; [c]0.9% [e]+2; [f]1296.9
13540697	NOV protein			[a]2.71; [b]1; [c]4.0% [e]+2; [f]1640.5	
27683465	similar to osteoglycin precursor			[a]5.07; [b]1; [c]5.4% [e]+2; [f]1854.7	
34879634	similar to collagen alpha 1(IV) chain precursor			[a]2.85±0.48; [b]2; [c]1.5%	

38197444	Actn4 protein				[a]4.21; [b]1; [c]1.3% [e]+2; [f]1386.8
27465565	Epididymal secretory protein 1				[a]4.01; [b]1; [c]8.7% [e]+2; [f]1663.5
92907	Hemiferrin				*a)*3.09; *b)*1; *c)*7% [e]+2; [f]1644.7
2072004	Histone H2A				[a]4.32; [b]1; [c]14.6% [e]+2; [f]1931.0
23484951	KED, putative				[a]3.08; [b]1; [c]3.8% [e]+2; [f]2006.8
8393706	Lactate dehydrogenase A				[a]3.36; [b]1; [c]6.3% [e]+2; [f]2291.3
16758210	Nucleobindin				[a]3.80; *b)*1; *c)*3.5% [e]+2; [f]1933.6
13929192	Nucleoside diphosphate kinase				[a]3.07; [b]1; [c]9.9% [e]+2; [f]1880.6
34880944	SM22-alpha homolog				[a])5.30; [b]1; [c]9% [e]+2; [f]2101.3
34872485	Similar to calsyntenin-1 protein				[a]2.73; [b]1; [c]1.6% [e]+2; [f]1937.5
10435300	Tropomyosin 4				[a]3.80; [b]1; [c]7% [e]+2; [f]2341.4
33340123	Thrombospondin 1				[a]5.92; [b]1; [c]1.8% [e]+2; *f)*2163.1

Table 4.3. Laboratory values after doxorubicin treatment in mice

Blood was collected from Ctr and Dox-treated mice and plasma was prepared as described in Methods to do laboratory tests. The data are depicted as means±SD.

	Ctr (n=3)	Dox (n=5)
BUN(8-33mg/dL)	15.7±2.12	10.63±1.37
Creatinine(0.2-0.9mg/dL)	0.15±0.07	0.08±0.05
ALT(17-77U/L)	9.87±12.69	2.83±2.67
AST(54-298U/L)	34.03±16.51	32.43±7.13
Bilirubin(0-0.9mg/dL)	0.23±0.15	0.17±0.21

CHAPTER V: FUNCTIONAL STUDY OF CYSTATIN C IN CARDIAC EXTRACELLULAR MATRIX REMODELING

Introduction:

The cardiac interstitium, which is mainly composed of CFs and proteins produced by CFs, is a dynamic supportive structure for the heart. The myocardial ECM, mainly produced and regulated by CFs, is involved in the process of ventricular hypertrophy and ultimately heart failure (HF)(78).

The myocardial ECM is made up of a fibrillar collagen network, proteoglycans, fibronectin and glycosaminoglycans and contains a diverse array of bioactive signaling molecules(324, 325). The major ECM proteins are type I and III collagens, although type IV, V, and VI collagens, as well as fibronectin and elastin are also present. The fibrillar collagen network ensures the structural integrity of the adjoining myocytes(325), provides the means by which myocyte shortening is translated into ventricular pump function, and is essential for maintaining the alignment of the myofibrils within the myocytes through a collagen-integrin-cytoskeletal myofibril relation(78, 326-332).

A disproportionate increase in synthesis and/or inhibition of degradation of ECM proteins may result in fibrosis. Fibrosis has important functional consequences for the heart. First, increased ECM content stiffens the ventricles and impedes both contraction and relaxation(324). Second, increased collagen content impairs the electrical coupling of cardiomyocytes by separating myocytes with ECM proteins(333). Furthermore, fibrosis results in reduced capillary density and an increased oxygen diffusion distance that can

lead to hypoxia of myocytes(334). Thus, fibrosis profoundly affects myocyte metabolism and performance and ultimately ventricular function(335).

Enzymes such as matrix metalloproteinases (MMPs), a family of proteolytic enzymes for ECM degradation, and tissue inhibitors of MMPs (TIMPs) have been shown to be involved in the process of cardiac remodeling (78, 336, 337). Several MMPs (MMP-1, MMP-2, MMP-3, MMP-9, MMP-13 and MMP-14), which have been found in the myocardium, can degrade the components of myocardial ECM such as fibrillar collagens (type I, II and III), gelatin, fibronectin, laminin and vitronectin. All MMPs are inhibited by specific TIMPs. Four different TIMPs (TIMP-1, TIMP-2, TIMP-3 and TIMP-4) have been identified and have been shown to bind to activated MMPs in a 1:1 stoichiometric ratio. Increased levels of MMP-2, MMP-3, MMP-9 and MMP-13 have been identified in the myocardium of patients with heart failure. Several studies have reported the roles of MMPs and TIMPs in the development of cardiac remodeling by using transgenic mice and knockout mice. MMP-1-overexpressing mice showed loss of cardiac interstitial collagen correlating with cardiac dysfunction(330). In contrast, targeted deletion of MMP-9 attenuated LV enlargement and decreased collagen accumulation in the infarcted region after MI(338). TIMP-1 prevented cardiac rupture but impaired scar formation and revascularization after MI. TIMP-1 deficient mice showed LV enlargement and the reduction in myocardial fibrillar collagen(339).

Cysteine proteinases, such as Cathepsin B (CTB), a 30 kDa bilobal protein(340), has has not been well studied in cardiac disease. CTB can degrade ECM directly(341, 342) or indirectly via activating prourokinase (pro-uPA) and subsequently the proteolytic

cascade downstream of urokinase (uPA)(343). Increased expression, membrane association and secretion of CTB have been observed in various human tumors, including brain, colorectal, lung and prostate(344, 345). Overexpression of CTB has also been observed in rheumatoid arthritis(346) and osteoarthritis (347). However, the involvement of CTB, and their endogenous inhibitors, such as Cystatin C, in myocardial ECM remodeling has not been well studied.

Cystatin C is a potent endogenous inhibitor of Cathepsin B, H and L(302-304, 348, 349). Functionally, in disease states involving tissue remodeling, Cystatin C protects the plasma membrane matrix and ECM proteins from being cleaved by cysteine proteases. An imbalance between cysteine proteases and Cystatin C contributes to human atherosclerotic and aneurismal aortic lesions(305, 350). These observations suggest that Cystatin C may play important roles in cardiac ECM remodeling. However, the precise functional significance of Cystatin C in cardiac ECM remodeling is not yet understood.

In the myocardium, CFs produce ECM proteins, MMPs, growth factors, and cytokines, thus they play a central role in the regulation of ECM. In this study, the coronary artery ligation induced MI mouse model was applied to characterize the induction of Cystatin C in the infarcted area and the accumulation of ECM proteins. For the in Vitro study, we applied neonatal cardiac fibroblasts, overexpressed and treated cells with Cystatin C, to investigate the pathophysiologic roles of Cystatin C in cardic ECM remodeling.

Materials and methods:

Materials— Cystatin C protein (ab7653) was purchased from Abcam, Inc (Cambridge, MA, USA). Restriction enzymes and other DNA modifying enzymes were from New England Biolabs, Inc. (Ipswich, MA, USA).

Tissue Culture— Cardiac Fibroblasts (CFs) were isolated from the hearts of 1-3 day old Sprague-Dawley rats as described previously (192, 193, 293). CFs were cultured in high glucose Dulbecco's Modified Eagle Medium (DMEM) containing 10% (v/v) fetal bovine serum (FBS), 50 units/ml penicillin, and 50 μg/ml streptomycin. CFs were subcultured once to eliminate contamination of other cell types. CFs were seeded in 6-well plates (Falcon) at a density of $0.3x10^6$ cells/well for experiments.

Treatment with Cystatin C— At day 3 after seeding, CFs were starved with 0.5% FBS/DMEM for overnight, treated with Cystatin C ranging from 0nM to 10nM. Cells were harvested at 24 hrs after Cystatin C treatment.

DNA constructs and cell transfections— Cystatin C cDNA was isolated by reverse transcription-PCR (RT-PCR) from rat CFs and inserted between KpnI and XbaI sites in pcDNA4/HisMax© vector (Invitrogen) creating pcDNA-Cystatin C. The pcDNA4/HisMax© vector drives transcription of the inserted cDNA by the strong cytomegalovirus promoter and also contains the ampicillin resistance gene driven by the SV40 promoter. Transient transfection of rat CFs was done with Fugene 6 (Roche).

Briefly, pcDNA-Cystatin C construct was incubated with Fugene 6 in serum-free DMEM medium for at least 15 minutes before adding to cells. Following 24-hr incubation (37°C, 5% CO_2), cells were placed in fresh 0.5% FBS/DMEM for overnight and then harvested for Western-blot, RT-PCR and Cell number analyses.

Western Blot Analysis— Proteins from cell lysates (20 μg) or heart tissue (40 μg) were separated by SDS-polyacrylamide gel electrophoresis (15%) before overnight electrophoretic transfer at 30 volts to a polyvinylidene difluoride (PVDF) membrane (Millipore, Bedford, MA). After eliminating non-specific binding with a minimal 1 hr incubation in 5% nonfat milk, the PVDF membrane was incubated overnight at 4 °C with the antibody against Cystatin C (1:200 dilution, rabbit polyclonal, Catalog# 06-458, Upstate Biotechnology, NY), CTB (1:200, rabbit polyclonal, Catalog# 06-480, Upstate Biotechnology, NY), FN (Fibronectin) (1:2000 dilution; polyclonal F-3648, Sigma-Aldrich, MO), CAI (Collagen I) (1:200 dilution, goat polyclonal, SC-8784, Santa Cruz Biotechnicology, CA), CAIII (Collagen III) (1:200 dilution, goat polyclonal, SC-8781, Santa Cruz Biotechnicology, CA) and Vinculin (1:8000 dilution; mouse monoclonal v9131, Sigma-Aldrich, MO). The membranes were subsequently incubated 45 minutes in horseradish peroxidase-conjugated secondary antibodies (Zymed Laboratories Inc., South San Francisco, CA; 1:8000) for detection of bound antibodies with enhanced chemiluminescence (ECL) reaction as described previously (192, 276, 282).

RNA Isolation and Semiquantitative RT-PCR— Semiquantitative RT-PCR was performed using 2 μg of total RNA extracted with TriZol (Invitrogen) from each sample for measurement of Cystatin C, CAI, CAIII and FN. Glyceraldehyde-3-phosphate dehydrogenase (GAPDH) was included as an internal control for equal loading. We used the Primer 3 Input Program (http://thaisnp.biotec.or.th/cgi-bin/primer3/primer3_www.cgi) to design PCR primers and to calculate the optimal PCR annealing temperature (Table 1). PCR products were detected by ethidium bromide staining after agarose gel electrophoresis.

Cell number analysis by Trypan blue staining— Cell suspension and Trypan Blue solution were placed into a 1.5 ml centrifuge tube at a 1:1 ratio (50ul:50ul). With a cover-slip in place, ~10 μl of the trypan blue-cell suspension was transfered to a chamber on the hemocytometer. This is done by carefully touching the edge of the cover-slip with the pipette tip and allowing the chamber to fill by capillary action. Do not overfill or underfill the chambers. Under a microscope, cells were counted in the 1mm center square and the four corner squares. The cell concentration per ml (and the total number of cells) was determined using the following calculations:

Cells per ml = the average count per square x the dilution factor x 10^4

Total cell number = cells per ml x the original volume of fluid from which cell sample was removed.

CTB activity assay— Cells or heart tissue were lysed with CTB activity buffer (88 mM KH2PO4, 12 mM Na2HPO4, 1.33 mM EDTA, 2.7 mM DTT, 0.03% Brij 35, PH5.8). In a 96 well plate, 5 µl of cell lysate was combined with 240 µl of CTB activity buffer and 5 µl of the substrate stock solution of Z-Arg-Arg-AMC (CTB Substrate III, Fluorogenic, Cat. No. 219392, EMD Biosciences, Inc., CA) in 80 mM in DMSO. Samples were stored at room temperature for 2~3 hr with gentle rocking to allow full activation in this buffer. Fluorescence was recorded on a fluorometer set at excitation 380 nm and emission at 440 nm to determine the enzyme activity.

Mouse Model of MI— The surgical procedure of left anterior descending coronary artery (LAD) occlusion using male BL6/129SF1 J mice (aged 5–7 weeks) was performed as described(283, 284). Mice were maintained four to a cage in a climate-controlled room on a 12-hour light/dark cycle (lights on at 6:00 AM). All experimental protocols were approved by the Institutional Animal Care and Use Committee of the University of Arizona.

After induction of anesthesia with Avertin (2.5%), a tracheotomy was performed and the animal was ventilated on a Harvard Rodent Respirator (Harvard Apparatus, Boston, MA). An anterior thoracotomy was performed to open the pericardium. Upon rapid deterioration of the heart, an 8–0 silk suture was tightened around the proximal LAD (1-3 mm from the tip of the left atrium). Coronary artery ligation was confirmed via visible blanched cardiac tissue distal to the ligation site. The chest cavity is closed by bringing together the second and third ribs with one 6-0 nylon suture. While tying a knot, slight pressure is applied on the chest with the needle holder to reduce the volume of free

air in the chest cavity. All layers of muscle and skin are closed with 6-0 continuous absorbable and nylon sutures, respectively.

Evans Blue Staining and Heart Tissue Preparation— 24 hrs after coronary artery occlusion surgery, the coronary arteries were perfused for 5 mins via the ascending part of the aorta with 2% Evans Blue solution before rapid excision of the hearts. The non-infarcted area (N-Inf) and infarcted area (Inf) were isolated from the myocardial infarction heart and frozen in liquid nitrogen immediately after excision. To prepare samples for Western blot or enzyme activity analyses, heart tissue were grinded into a powder form with a pestle and mortar (VWR) in a liquid nitrogen bath. The powder was dissolved in EB lysis buffer for protein preparation, or in CTB activity assay buffer for CTB activity analysis.

STATISTICS:

The student-t test was used for two mean comparisons. One-way analysis of variance (ANOVA) was used to compare groups of means followed by the Bonferroni Correction for multiple samples

Results:

Cystatin C Induction and CTB Inhibition in the Infarcted Area after MI

To localize and measure expression level of Cystatin C and CTB in the heart after MI, coronary artery ligation induced MI mouse model was used. Fig5.1A shows the position of the suture and the size of the infarcted area (pale zone) after 2% Evans blue staining at 24 hr after coronary artery occlusion surgery. The non-infarcted area (N-Inf) and infarcted area (Inf) were isolated from the myocardium at 24 hr after coronary artery ligation surgery for Western blot and CTB activity analyses. Compared to the non-infarcted area, there was a significant elevation of Cystatin C protein in the infarcted area (Fig5.1B&C). In parallel, the cleavage of CTB protein level was decreased in the infarcted area compared to the non-infarcted area as shown in the reduced level of mature 40 KD CTB (Fig5.1D&F), with a corresponding accumulation of ProCTB in the infarcted area (Fig5.1D&E). Compared to the non-infarcted area, the CTB activity was decreased in the infarcted area as well (Fig5.1G).

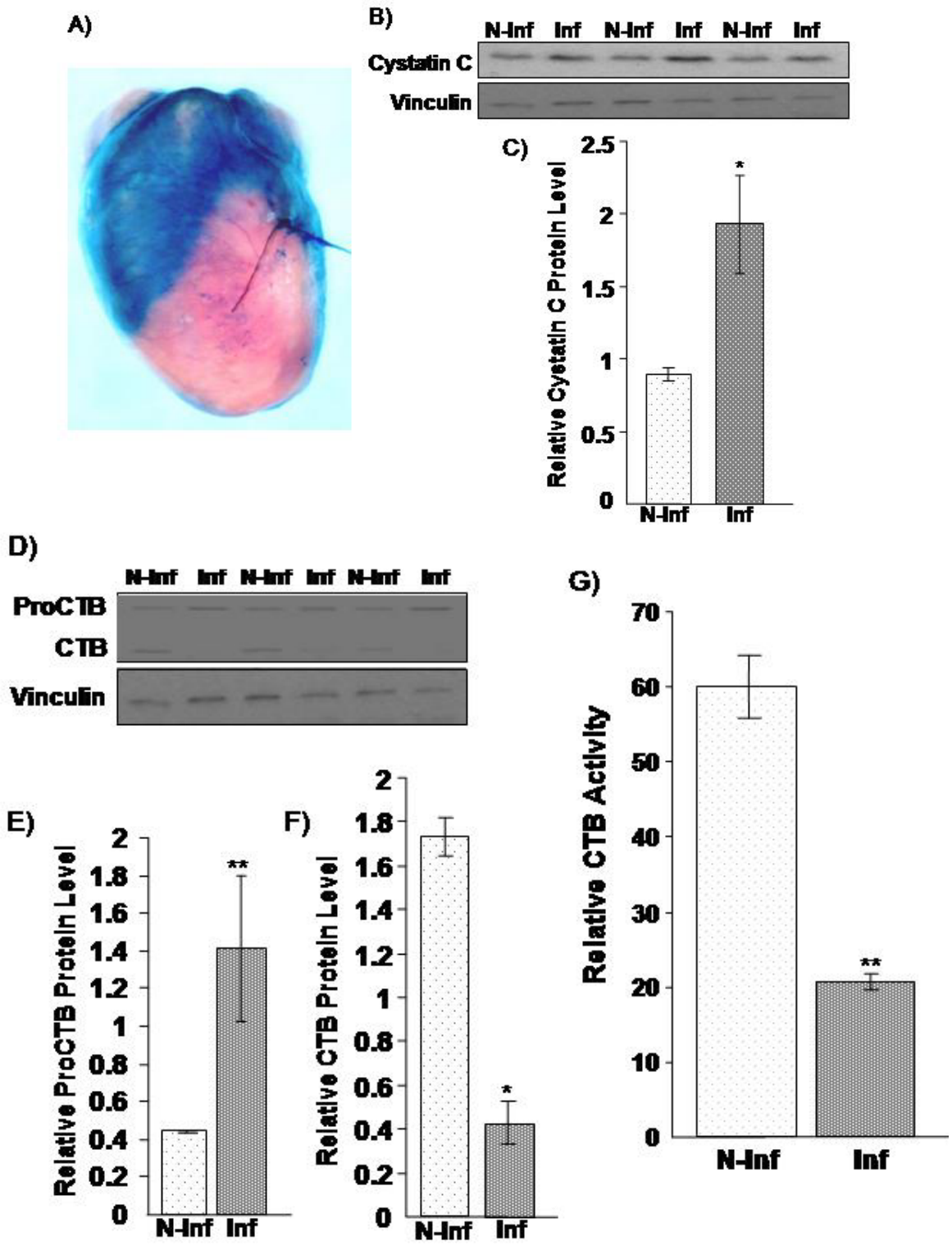
A)
B)
N-Inf Inf N-Inf Inf N-Inf Inf
Cystatin C
Vinculin
C)
Relative Cystatin C Protein Level
2.5
2
1.5
1
0.5
0
*
N-Inf Inf
D)
N-Inf Inf N-Inf Inf N-Inf Inf
ProCTB
CTB
Vinculin
E)
Relative ProCTB Protein Level
2
1.8
1.6
1.4
1.2
1
0.8
0.6
0.4
0.2
0
**
N-Inf Inf
F)
Relative CTB Protein Level
2
1.8
1.6
1.4
1.2
1
0.8
0.6
0.4
0.2
0
*
N-Inf Inf
G)
Relative CTB Activity
70
60
50
40
30
20
10
0
**
N-Inf Inf

Fig. 5.1. Induction of Cystatin C and Inhibition of CTB in the Infarcted Area after MI Male BL6/129SF1 J mice (aged 5–7 weeks) was used for left anterior descending coronary artery ligation surgery. A) 24 hr after MI operation: position of the suture, and the size of the infarcted area (pale zone) after 2% Evans Blue staining via the ascending part of the aorta. The non-infarcted area (N-Inf) and infarcted area (Inf) were isolated from the myocardial infarction heart and frozen in liquid nitrogen immediately after excision. The heart tissue containing 60 μg of protein was loaded for SDS-PAGE and Western blot analyses to detect Cystatin C (B). The membrane was stripped by Restore™ Western Blot Stripping Buffer (Cat# 20159, PIERCE, IL) to detected CTB (D). Vinculin was used as an internal loading control (B&D). The intensities of the bands quantified by NIH imaging J software and normalized with Vinculin are presented as means ± SE (C&E&F)). To perform CTB activity assay, 5 μl of tissue lysate was combined with 240 μl of CTB activity buffer and 5 μl of the substrate stock solution of Z-Arg-Arg-AMC, and incubated for 2~3 hrs at room temperature with gentle rocking to allow full activation. Fluorescence was recorded on a fluorometer set at excitation 380 nm and emission at 440 nm to determine the enzyme activity (G). Two asterisks (**) indicate $p<0.01$, one asterisks (*) indicate $p<0.05$ when the means of infaracted area was compared to that of non-infarcted area by Student's t-test.

ECM Protein Accumulation in the Infarcted Area after MI

Western Blots for CAI, CAIII, and FN were performed with the heart tissue (non-infarcted area and infarcted area) dissected from the myocardium at 24 hr after coronary artery occlusion surgery. The results indicate the elevation of CAI, CAIII and FN protein levels in the infarcted area (Figr5.2A-D)

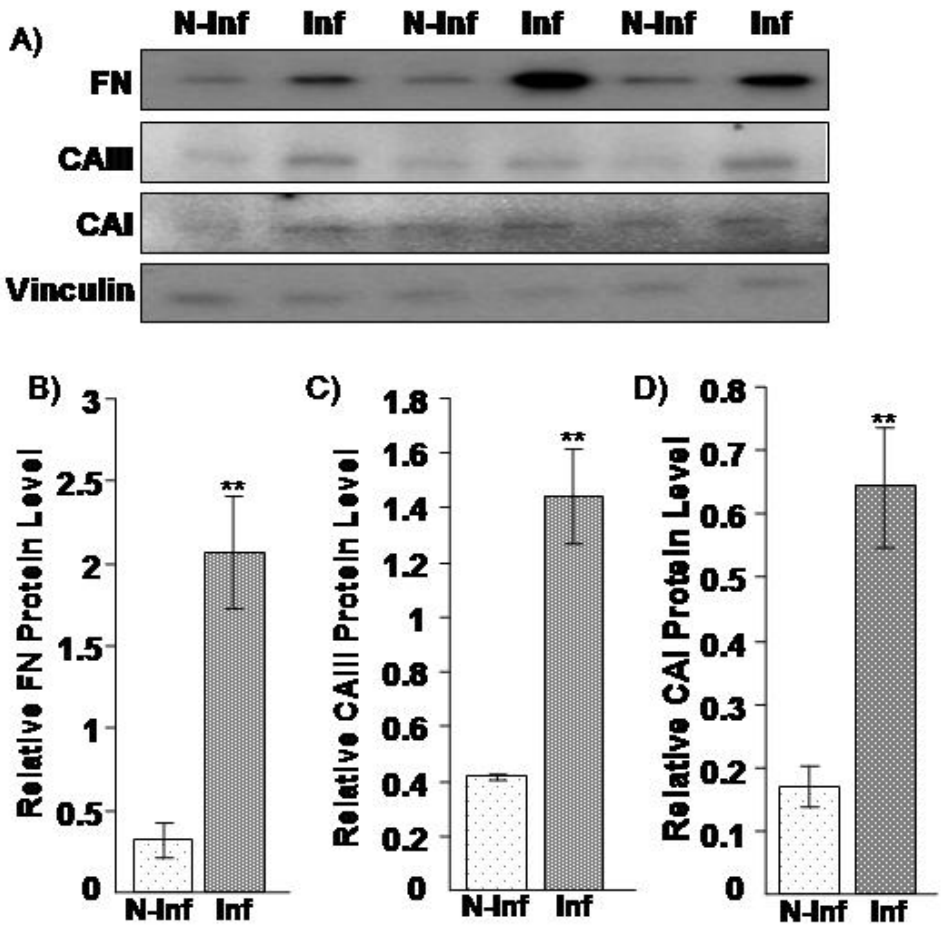

Fig. 5.2. Increased protein levels of CAI, CAIII and FN in the Infarcted Area after MI. 24 hr after MI operation, the non-infarcted area (N-Inf) and infarcted area (Inf) were isolated from the myocardial infarction heart and frozen in liquid nitrogen immediately after excision. The heart tissue containing 60 μg of protein was loaded for SDS-PAGE and Western blot analyses to detect CAI, CAIII and FN (A). Vinculin was used as an internal loading control (A). The intensities of the bands quantified by NIH imaging J software and normalized with Vinculin are presented as means ± SE (B-D). Two asterisks (**) indicate $p<0.01$ when the means of infaracted area was compared to that of non-infarcted area by Student's t-test.

Cystatin C over-expression in CFs

An in vitro study was carried out to confirm the effect of Cystatin C elevation on cardiac ECM remodeling. pcDNA-Cystatin C constructs were transiently transfected into CFs. 24 hrs after transfection, the cells were harvested in EB buffer for Western-blot analysis or in Trizol (Invitrogen) for RT-PCR analysis. The Western-blot results indicate that Cystatin C overexpression in CFs can cause elevations of ECM proteins, CAI, CAIII and FN (Fig5.3.A). To see if this induction is due to transcriptional regulation, RT-PCR analysis was performed with total RNA extracted from cells. The results indicate that the mRNA levels of CAI, CAIII and FN are not affected by Cystatin C over-expression (Fig.5.3B). Since fibroblast proliferation plays an important role in cardiac remodeling, we examined the alteration of cell number upon cystatin C plasmid transfection. The results indicate that Cystatin C overexpression did not affect cell growth (Fig5.3C).

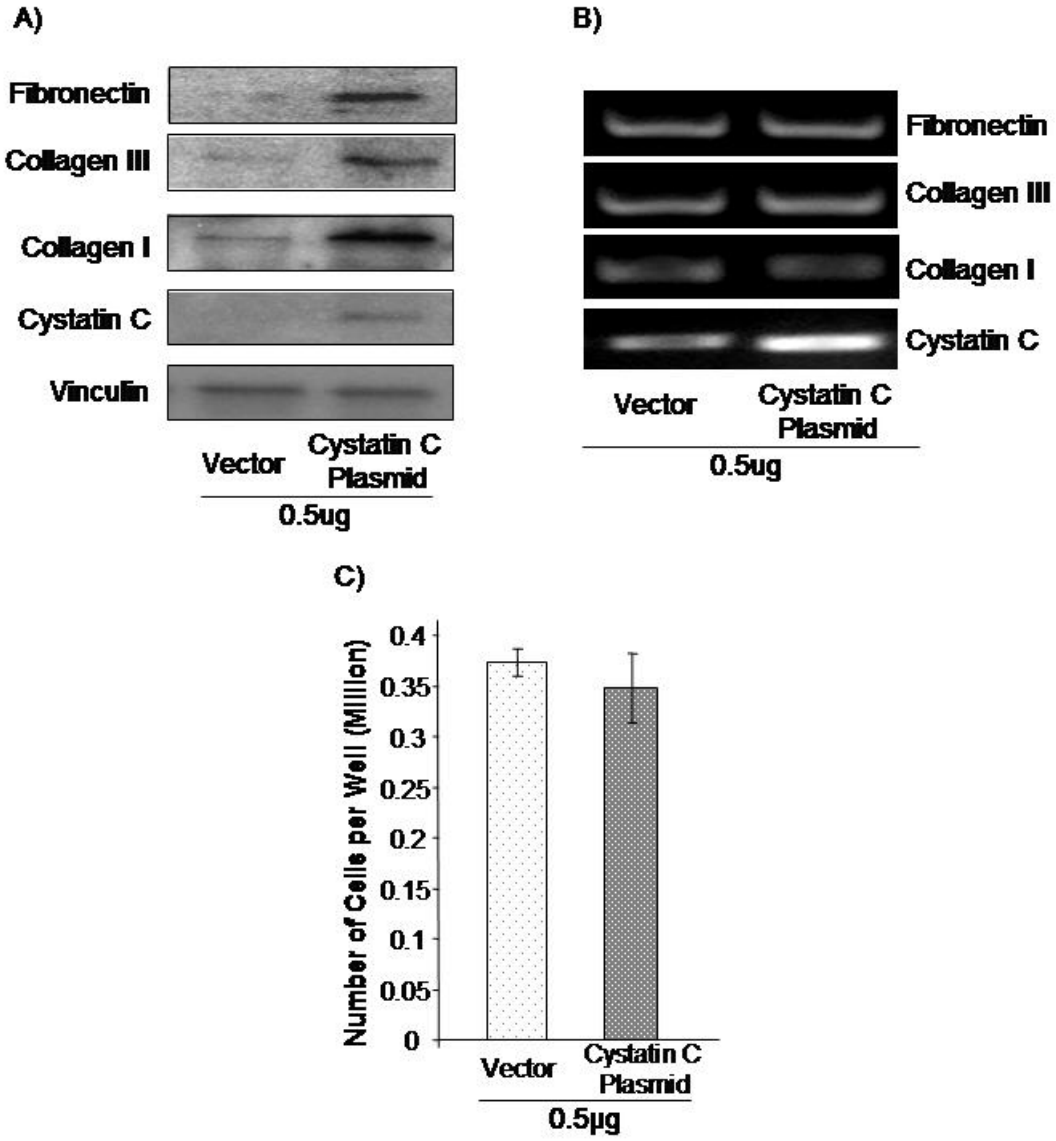

Fig. 5.3. Increased CAI, CAIII and FN protein level, but not mRNA level in CFs upon pcDNA-Cystatin C transfection. The cell number was not affected by pcDNA-Cystatin C transfection.

CFs were seeded in 6-well plates (Falcon) at a density of $0.3x10^6$ cells/well. 0.5ug/well of pcDNA-Cystatin C constructs were transiently transfected into CFs. 24 hrs after transfection, the cells were harvested in EB buffer for Western-blot analysis to detect CAI, CAIII, FN and Cystatin C, and Vinculin was used as an internal loading control (Fig.3A); were harvested in Trizol to perform RT-PCR analysis for CAI, CAIII and Cystatin C (Fig.3B); and were trypsinized to perform cell number analysis by Trypan blue staining (Fig.3C).

CFs treated with Cystatin C

To see if Cystatin C plays a role in cardiac ECM remodeling, we also treated CFs with Cystatin C protein. At 24 hr after treatment, the cells were harvested for Western-blot analyses or in Trizol (Invitrogen) for RT-PCR analysis The Western-blot results indicate that Cystatin C treatment can cause CAI, CAIII and FN elevation in CFs (Fig5.4.A). To eliminate the possibility that this induction is due to transcriptional regulation, RT-PCR analysis was performed with total RNA extracted from cells. The results indicate that the mRNA levels of CAI, CAIII and FN are not affected by Cystatin C treatment (Fig.5.4B). The cell number was not affected by Cystatin C treatment (Fig.5.4C).

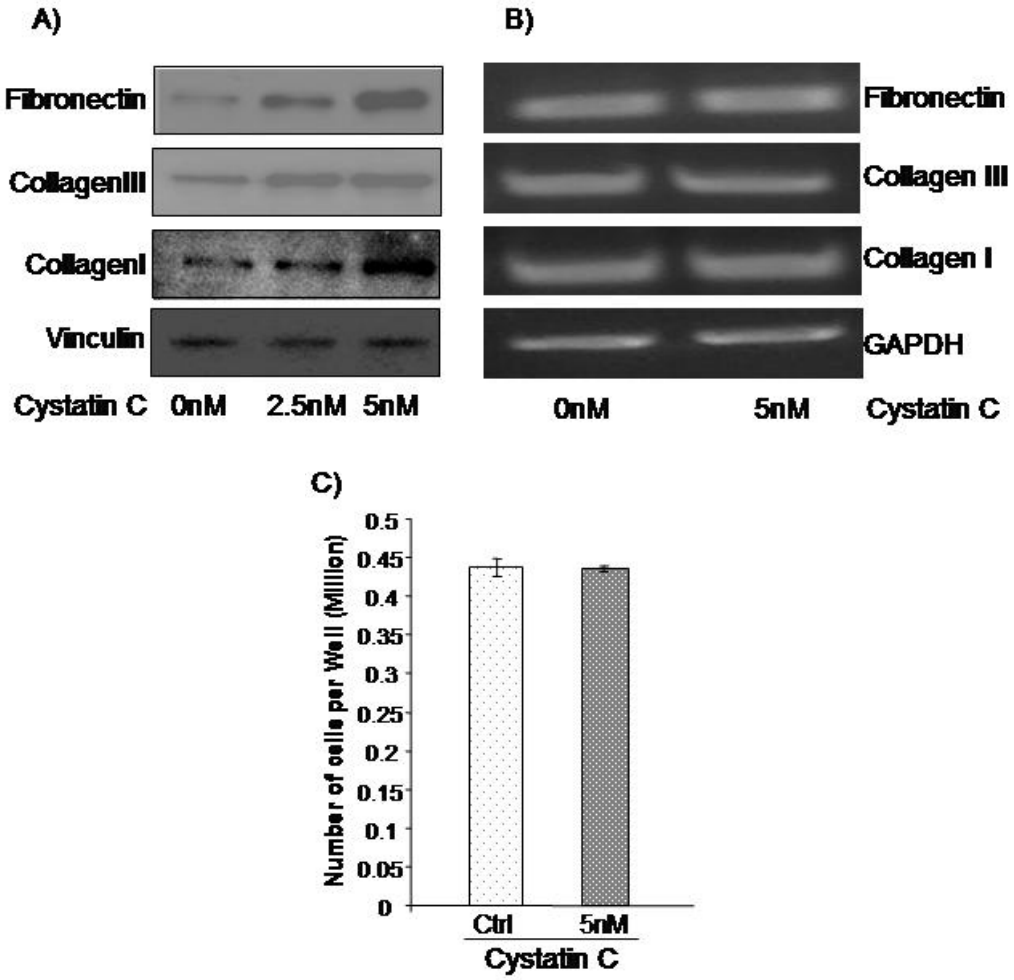

Fig. 5.4. Increased CAI, CAIII and FN protein level, but not mRNA level in CFs upon Cystatin C treatment. The cell number was not affected by Cystatin C treatment.

At day 3 after seeding in 6-well plates, CFs were starved with 0.5% FBS/DMEM for overnight, treated with Cystatin C ranging from 0nM to 5nM. 24 hrs after Cystatin C treatment, cells were harvested in EB buffer for Western-blot analysis to detect CAI, CAIII and FN, and Vinculin was used as an internal loading control (Fig.4A); were harvested in Trizol to perform RT-PCR analysis for CAI, CAIII, and FN, and GAPDH was used as a loading control (Fig.4B); and were trypsinized to perform cell number analysis by Trypan blue staining (Fig.4C).

To see if the ECM protein elevation is due to inhibition of CTB, Western Blot was performed for CTB with the cell lysates collected from Ctrl and Cystatin C treated CFs. The results indicate that there is a decreased level of CTB protein with a 5nM of Cystatin C treatment and a corresponding accumulation of ProCTB (Fig.5.5A). The CTB activity was inhibited due to Cystatin C treatment (Fig.5.5B).

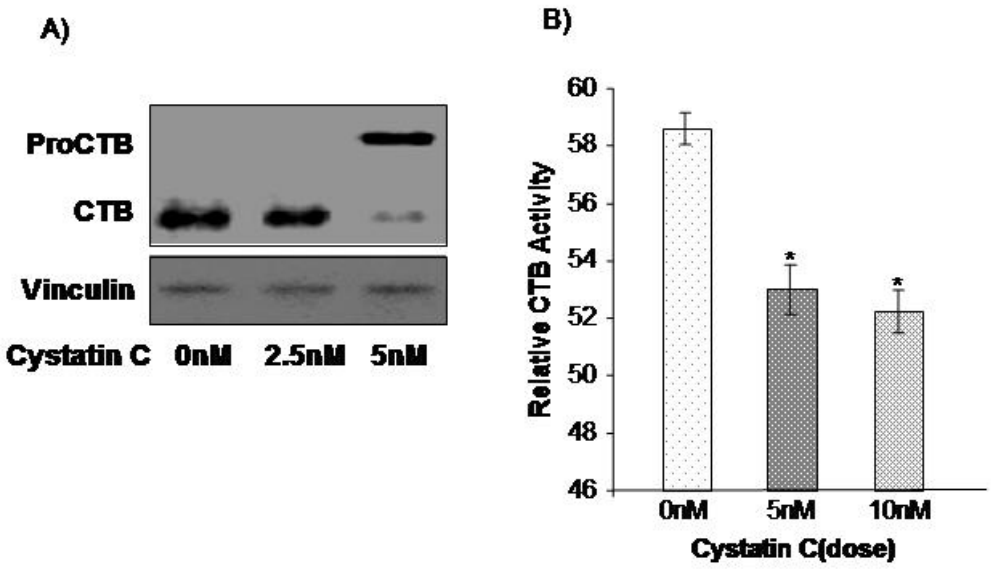

Fig. 5.5. Decreased CTB protein level and activity in CFs upon Cystatin C treatment Three days after seeding, CFs were starved with 0.5% FBS/DMEM for overnight, treated with Cystatin C ranging from 0nM to 10nM. 24 hrs after Cystatin C treatment, cells were harvested in EB buffer for Western-blot analysis to detect CTB (Fig.5A), and were harvested in CTB activity buffer to perform CTB activity assay (Fig.5B).

Discussion:

In this study, with coronary artery ligation induced MI mouse model, we discovered that Cystatin C was increased in the ischemic area of the heart, compared to the non-ischemic area. Increased levels of ECM proteins (CAI, CAIII and FN) were detected in the ischemic area as well. However, a reduced level of CTB was detected in this area. The mechanism of Cystatin C induced ECM accumulation was addressed in vitro. Overexpression and treatment of Cystatin C result in increased level of ECM proteins (CAI, CAIII and FN) in CFs. The CTB protein and activity levels were decreased in CFs with Cystatin C treatment. These data indicate that Cystatin C can cause ECM accumulation, the mechanism of which maybe due to CTB inhibition. This study, for the first time, established Cystatin C could be a potential fibrotic factor during the process of myocardial remodeling.

Our previous studies have shown that Cystatin C protein was markedly elevated in the plasma of coronary artery ligation induced MI mice (Xie and Chen, manuscript submitted). The in vivo data from this study showed the induction of Cystatin C protein in the infarcted area of the heart (Fig.5.2B&C), indicating Cystatin C may play a role in the cardiac remodeling after MI. Remodeling of the myocardium is the major mechanism for heart failure and associated mortality after MI. The myocardium expressed several matrix proteins, including collagens, FN, and laminin. CAI, CAIII, and collagen IV are the predominant collagens in the myocardium(351). FN is the most abundant non collagenous protein(351) and plays important roles in development, adhesion and wound healing and is upregulated in the heart with mechanical overload(352). The ECM

provides the environment for cells to migrate, grow and differentiate(353). As such, the matrix is an integral regulator of cell and tissue function. While the cardiac myocyte occupies the majority of myocardial volume, the cardiac fibroblasts are the most abundant non-myocyte cell type in the myocardium and regulate ECM levels through at least three mechanisms. The first is through the synthesis and deposition of matrix molecules; the second is through matrix degradation and turnover by the production and release of MMPs; and the third is by maintaing mechanical tension on the collagen network(354). Under normal conditions, synthesis and degradation of the ECM is a tightly regulated process. During left ventricle remodeling, however, an increase in synthesis and/or decrease in degradation of ECM is/are associated with development of fibrosis. The increased accumulation of collagen I-III that occurs in the hypertensive heart and heart failure has been associated mostly to fibrosis(352, 355, 356). It has been reported that heart failure patients have significantly higher levels of Cystatin C in the circulating system(357). On the other hand, those with higher levels of circulating Cystatin C have a higher incidence of cardiac disease (357). Sarnak, *et al.* recently reported that high cystatin C concentration in the plasma imposes a risk factor of heart failure in individuals older than 65 years of age (358). Because reparative fibrosis is an essential component of healing of the infarct zone after MI, the finding of increased levels of CAI, CAIII and FN in the infarcted area may be related to wound healing (Fig.5.2A&B). This ECM induction could be due to decreased degradation directly or indirectly by CTB, since decreased CTB protein level and activity were detected in the

infarcted area after MI (Fig5.1D-G). The inhibition of CTB could result from induction of Cystatin C (Fig.5.1B&C) in the infarcted area.

Cystatin C is an inhibitor of CTB, which is distributed widely in various tissues, including cardiac muscle fibers (298-300, 359, 360) and is involved in regulation of local inflammation(361), tumor invasion and metastasis(362). It has been reported that CTB can degrade ECM, such as type IV collagen, laminin and FN, directly(341, 342) or indirectly by activating pro-uPA and subsequently the proteolytic cascade downstream of uPA in human tumor cells (343). Cardiac fibrosis arises from complex interactions between CMCs and nonmyocytes (the majority of which are CFs), in which several locally produced regulatory factors may possibly be involved(363-365). Our previous study has shown that Cystatin C expression level was increased in CMCs, but not CFs after H_2O_2 treatment. CFs are known to synthesize fibronectins, vitronectin, collagen types I, III and V, collagenases, among many other ECM and ECM related proteins(351, 366). Our data indicate that stimulation of CFs with Cystatin C resulted in increased CAI, CAIII and FN accumulation, and decreased protein level and activity of CTB. These observations indicate Cystatin C may serve as a cardiomyocyte-derived fibrotic factor acting on cardiac fibroblasts during the process of ventricular remodeling.

Table 5.1. Sequence, expected fragment size and annealing temperature (ta) of primers used in the semi-quantitative RT-PCR analysis of mRNA levels

Gene (rat)	Sequence	Expected fragment size (bp)	Temp (^{o}C)	GenBank accession number
CollagenI	**Sense:**tgctgccttttctgttcctt **Antisense:**aaggtgctgggtagggaagt	179	56	Rn.2953
CollagenIII	**Sense:**gtccacgaggtgacaaaggt **Antisense:**catcttttccaggaggtcca	189	56	Rn.3247
Fibronectin	**Sense:**gaaaggcaaccagcagagtc **Antisense:**ctggagtcaagccagacaca	230	56	Rn.1604
Cystatin C	**Sense:**tggtgagagctcgtaagcag **Antisense:**gctggattttgtcagggtgt	208	62	Rn.106351
GAPDH	**Sense:**tgaaggtcggtgtcaacggatttggc **Antisense:**catgtaggccatgaggtccaccac	223	62	Rn.64496

CHAPTER VI: SUMMARY STATEMENTS

Cardiovascular disease (CVD) is the number one killer in the United States. Heart failure is the end point of many forms of CVD. Numerous lines of evidence indicate a role of oxidative stress in initiation and progression of heart failure. The overall goal of the dissertation is to identify novel indicators of cardiac specific oxidative injury. Such indicators or potential biomarkers will be useful for early diagnosis or efficient management of heart failure, and for uncovering novel molecular pathways regulating myocardial remodeling. We have found the techniques most suitable for finding novel targets mediating oxidative injury. Using ESI-LC-MS/MS based proteomic approach, we discovered a novel cardiomyocyte specific indicator of oxidative injury, i.e. cystatin C. We have investigated the functional role of cystatin C in cardiac ECM remodeling.

The data presented in this dissertation support the hypothesis that alterations of secreted protein factors from CMCs under oxidative stress could be potential non-invasive indicators useful for early diagnosis or management of heart failure. The first study demonstrated that ESI-LC-MS/MS analysis of conditioned media is the most suitable way to identify proteins secreted by cells, which could serve as non-invasive indicators of diseases. The second study demonstrated the use of ESI-LC-MS/MS based shotgun approach of proteomics for the discovery of Cystatin C as an indicator of cardiomyocyte specific oxidative injury *in vitro* and *in vivo*. The third study demonstrated that increased level of Cystatin C can cause increased accumulation of ECM proteins, CAI, CAIII and FN, in CFs and in the myocardium of infarcted area, the mechanism of which could be due to inhibition of CTB.

Based on the work of this dissertation, the following model is proposed (Fig.6.1). Under stressed condition, the CMCs will develop a hypertrophic phenotype, resulting in increased production and secreation of Cystatin C from CMCs. On one hand, Cystatin C could be used as an indicator of CMC injury in vitro and in vivo and could also serve as a potential biomarker for early diagnosis of heart failure. On the other hand, Cystatin C could act on CFs, result in increased ECM accumulation through inhibition of CTB. This study established the involvement of cysteine protease (CTB) and its inhibitor (Cystatin C) in the process of cardiac ECM remodeling.

Cystatin C has been found to be an independent risk factor for the development of heart failure in older adults (367). More recently, Arimoto and colleagues(368) showed that patients with high cystatin C level have a higher incidence of cardiac event than those with a normal cystatin C level. However, the sensitivity, specificity and predictive values of Cystatin C have to be validated clinically before applying Cystatin C as an early diagnostic marker of heart failure.

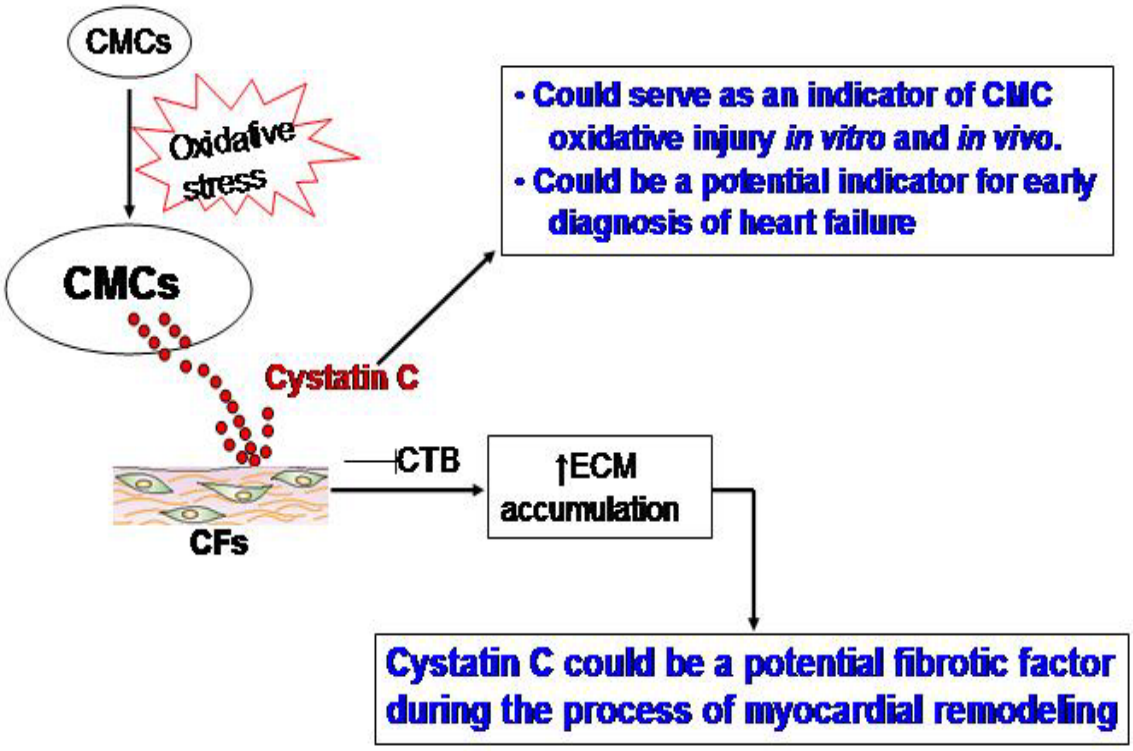

Fig.6.1. Proposed scheme for oxidative stress induced Cystatin C induction in CMCs and it's mechanism of action in myocardial ECM remodeling

ABBREVIATIONS:

ANP: Atrial Natriuretic Peptide;

BNP: Brain Natriuretic Peptide

CAI: Collagen I

CAIII: Collagen III

CFs: Cardiac Fibroblasts;

CMCs: Cardiomyocytes;

CTB: Cathepsin B

CVD: Cardiovascular disease;

Dox: Doxorubicin;

ECM: Extracellular matrix;

FN: Fibronectin

HDFs: Human diploid fibroblasts

Inf: Infarcted area

MMP matrix metalloproteinase

MI: Myocardial Infarction;

MudPIT: Multidimensional Protein Identification Technology

N-Inf: Non-infarcted area

ProCTB: Procathepsin B

ROS: Reactive Oxygen Species

TIMP: Tissue Inhibitor of Metalloproteinases.

REFERENCES

1. Rosamond W, Flegal K, Friday G, Furie K, Go A, Greenlund K, et al. Heart Disease and Stroke Statistics--2007 Update. A Report From the American Heart Association Statistics Committee and Stroke Statistics Subcommittee. Circulation. 2006 December 28, 2006:CIRCULATIONAHA.106.179918.

2. Minino AM HM, Smith BL. Deaths: preliminary data for 2004. Natl Vital Stat Rep 2006 Jun 28;54(19):1-49.

3. HC Stary AC, S Glagov, JR Guyton, W Insull Jr, ME Rosenfeld, SA Schaffer, CJ Schwartz, WD Wagner and RW Wissler A definition of initial, fatty streak, and intermediate lesions of atherosclerosis. A report from the Committee on Vascular Lesions of the Council on Arteriosclerosis, American Heart Association. Arteriosclerosis and Thrombosis 1994;14:840-56.

4. Organization. WH. Arterial hypertension and ischemic heart disease. . WHO Tech Report, Geneva,. 1962;231:18.

5. Aronow WS. Guest Editorial: What Is the Appropriate Treatment of Hypertension in Elders? J Gerontol A Biol Sci Med Sci. 2002 August 1, 2002;57(8):M483-6.

6. Aronow WS. Should the NCEP III Guidelines Be Changed in Elderly and Younger Persons at High Risk for Cardiovascular Events? J Gerontol A Biol Sci Med Sci. 2005 May 1, 2005;60(5):591-2.

7. Bybee KA, Wright RS, Williams BA, Murphy JG, Holmes DR, Kopecky SL. Effect of concomitant or very early statin administration on in-hospital mortality and reinfarction in patients with acute myocardial infarction. The American Journal of Cardiology. 2001;87(6):771-4.

8. Stenestrand U, Wallentin L, for the Swedish Register of Cardiac Intensive C. Early Statin Treatment Following Acute Myocardial Infarction and 1-Year Survival. JAMA. 2001 January 24, 2001;285(4):430-6.

9. Davies K. Oxidative stress: the paradox of aerobic life.
. Biochem Soc Symp. 1995;61:1-31.

10. S. Miwa MDB. Mitochondrial matrix reactive oxygen species production is very sensitive to mild uncoupling. Biochem Soc 2003;31:1300–1.

11. Genova ML, Pich MM, Biondi A, Bernacchia A, Falasca A, Bovina C, et al. Mitochondrial Production of Oxygen Radical Species and the Role of Coenzyme Q as an Antioxidant. Experimental Biology and Medicine. 2003 May 1, 2003;228(5):506-13.

12. B. Halliwell JG. Role of free radicals and catalytic metal ions in human disease: an overview. Methods Enzymol. 1990;186:1-85.

13. Lloyd RV, Hanna PM, Mason RP. The Origin of the Hydroxyl Radical Oxygen in the Fenton Reaction. Free Radical Biology and Medicine. 1997;22(5):885-8.

14. Kukreja RC HM. The oxygen free radical system: from equations through membrane-protein interactions to cardiovascular injury and protection. Cardiovasc Res 1992 Jul;26(7):641-55.

15. Singal PK, Khaper N, Palace V, Kumar D. The role of oxidative stress in the genesis of heart disease. Cardiovascular Research. 1998;40(3):426-32.

16. Dhalla NS TR, Netticadan T. . Role of oxidative stress in cardiovascular diseases. J Hypertens 2000 Jun;18(6):655-73.

17. ML Hess NM. Molecular oxygen: friend and foe. The role of the oxygen free radical system in the calcium paradox, the oxygen paradox and ischemia/reperfusion injury. J Mol Cell Cardiol. 1984 Nov;16(11):969-85.

18. Suzuki YJ, Ford GD. Redox Regulation of Signal Transduction in Cardiac and Smooth Muscle. Journal of Molecular and Cellular Cardiology. 1999;31(2):345-53.

19. Kevin LG, Novalija E, Stowe DF. Reactive Oxygen Species as Mediators of Cardiac Injury and Protection: The Relevance to Anesthesia Practice. Anesth Analg. 2005 November 1, 2005;101(5):1275-87.

20. Davies K. Oxidative stress: the paradox of aerobic life.
. Biochem Soc Symp 1995;61:1-31.

21. Ide T, Tsutsui H, Kinugawa S, Utsumi H, Kang D, Hattori N, et al. Mitochondrial Electron Transport Complex I Is a Potential Source of Oxygen Free Radicals in the Failing Myocardium. Circ Res. 1999 August 20, 1999;85(4):357-63.

22. Sawyer DB, Siwik DA, Xiao L, Pimentel DR, Singh K, Colucci WS. Role of Oxidative Stress in Myocardial Hypertrophy and Failure. Journal of Molecular and Cellular Cardiology. 2002;34(4):379-88.

23. Seshiah PN, Weber DS, Rocic P, Valppu L, Taniyama Y, Griendling KK. Angiotensin II Stimulation of NAD(P)H Oxidase Activity: Upstream Mediators. Circ Res. 2002 September 6, 2002;91(5):406-13.

24. Xia Y, Tsai A-L, Berka V, Zweier JL. Superoxide Generation from Endothelial Nitric-oxide Synthase. A Ca2+/CALMODULIN-DEPENDENT AND

TETRAHYDROBIOPTERIN REGULATORY PROCESS. J Biol Chem. 1998 October 2, 1998;273(40):25804-8.

25. Xia Y, Roman LJ, Masters BSS, Zweier JL. Inducible Nitric-oxide Synthase Generates Superoxide from the Reductase Domain. J Biol Chem. 1998 August 28, 1998;273(35):22635-9.

26. Griendling KK, Sorescu D, Ushio-Fukai M. NAD(P)H Oxidase : Role in Cardiovascular Biology and Disease. Circ Res. 2000 March 17, 2000;86(5):494-501.

27. Zorov DB, Filburn CR, Klotz L-O, Zweier JL, Sollott SJ. Reactive Oxygen Species (ROS)-induced ROS Release: A New Phenomenon Accompanying Induction of the Mitochondrial Permeability Transition in Cardiac Myocytes. J Exp Med. 2000 October 2, 2000;192(7):1001-14.

28. Nordberg J, Arner ESJ. Reactive oxygen species, antioxidants, and the mammalian thioredoxin system. Free Radical Biology and Medicine. 2001;31(11):1287-312.

29. Kirkman HN, Gaetani GF. Catalase: A Tetrameric Enzyme with Four Tightly Bound Molecules of NADPH. PNAS. 1984 July 15, 1984;81(14):4343-7.

30. Kirkman HN, Rolfo M, Ferraris AM, Gaetani GF. Mechanisms of Protection of Catalase by NADPH. KINETICS AND STOICHIOMETRY. J Biol Chem. 1999 May 14, 1999;274(20):13908-14.

31. Ursini F MM, Brigelius-Flohé R, Aumann KD, Roveri A, Schomburg D, Flohé L. Diversity of glutathione peroxidases. Methods Enzymol. 1995;252:38-53.

32. de Haan JB, Bladier C, Lotfi-Miri M, Taylor J, Hutchinson P, Crack PJ, et al. Fibroblasts derived from Gpx1 knockout mice display senescent-like features and are susceptible to H2O2-mediated cell death. Free Radical Biology and Medicine. 2004;36(1):53-64.

33. Conrad M, Jakupoglu C, Moreno SG, Lippl S, Banjac A, Schneider M, et al. Essential Role for Mitochondrial Thioredoxin Reductase in Hematopoiesis, Heart Development, and Heart Function. Mol Cell Biol. 2004 November 1, 2004;24(21):9414-23.

34. Yu BP. Cellular defenses against damage from reactive oxygen species. Physiol Rev. 1994 January 1, 1994;74(1):139-62.

35. Fridovich I. Superoxide Anion Radical (Obardot 2), Superoxide Dismutases, and Related Matters. J Biol Chem. 1997 July 25, 1997;272(30):18515-7.

36. Dhalla AK, Singal PK. Antioxidant changes in hypertrophied and failing guinea pig hearts. Am J Physiol Heart Circ Physiol. 1994 April 1, 1994;266(4):H1280-5.

37. Dhalla AK, Hill MF, Singal PK. Role of oxidative stress in transition of hypertrophy to heart failure. J Am Coll Cardiol. 1996 August 1, 1996;28(2):506-14.

38. Kinugawa S, Tsutsui H, Hayashidani S, Ide T, Suematsu N, Satoh S, et al. Treatment With Dimethylthiourea Prevents Left Ventricular Remodeling and Failure After Experimental Myocardial Infarction in Mice : Role of Oxidative Stress. Circ Res. 2000 September 1, 2000;87(5):392-8.

39. Ghatak A, Brar MJS, Agarwal A, Goel N, Rastogi AK, Vaish AK, et al. Oxy free radical system in heart failure and therapeutic role of oral vitamin E. International Journal of Cardiology. 1996;57(2):119-27.

40. Keith M, Geranmayegan A, Sole Md FMJ, Kurian Bsc R, Robinson Bsc A, Omran Md AS, et al. Increased Oxidative Stress in Patients With Congestive Heart Failure. Journal of the American College of Cardiology. 1998;31(6):1352-6.

41. Diaz-Velez CR, Garcia-Castineiras S, Mendoza-Ramos E, Hernandez-Lopez E. Increased malondialdehyde in peripheral blood of patients with congestive heart failure. American Heart Journal. 1996;131(1):146-52.

42. Mallat Z, Philip I, Lebret M, Chatel D, Maclouf J, Tedgui A. Elevated Levels of 8-iso-Prostaglandin F2{alpha} in Pericardial Fluid of Patients With Heart Failure : A Potential Role for In Vivo Oxidant Stress in Ventricular Dilatation and Progression to Heart Failure. Circulation. 1998 April 28, 1998;97(16):1536-9.

43. McMurray J, McLay J, Chopra M, Bridges A, Belch JJF. Evidence for enhanced free radical activity in chronic congestive heart failure secondary to coronary artery disease. The American Journal of Cardiology. 1990;65(18):1261-2.

44. Singh N, Dhalla AK, Seneviratne C, Singal PK. Oxidative stress and heart failure. Molecular and Cellular Biochemistry. 1995;147(1):77-81.

45. Ellis GR, Anderson RA, Lang D, Blackman DJ, Morris RHK, Morris-Thurgood J, et al. Neutrophil superoxide anion-generating capacity, endothelial function and oxidative stress in chronic heart failure: effects of short- and long-term vitamin C therapy. Journal of the American College of Cardiology. 2000;36(5):1474-82.

46. F Liao AA, J H Qiao, H Allayee, A M Fogelman, and A J Lusis. Genetic evidence for a common pathway mediating oxidative stress, inflammatory gene induction, and aortic fatty streak formation in mice. J Clin Invest 1994 August;94(2):877–84.

47. GT Rowe NM, M Caplan, ML. Hess Hydrogen peroxide and hydroxyl radical mediation of activated leukocyte depression of cardiac sarcoplasmic reticulum. Participation of the cyclooxygenase pathway. Circ Res. 1983 Nov;53(5):584-91.

48. Xu KY, Zweier JL, Becker LC. Hydroxyl Radical Inhibits Sarcoplasmic Reticulum Ca2+-ATPase Function by Direct Attack on the ATP Binding Site. Circ Res. 1997 January 1, 1997;80(1):76-81.

49. Xie YW, Kaminski PM, Wolin MS. Inhibition of Rat Cardiac Muscle Contraction and Mitochondrial Respiration by Endogenous Peroxynitrite Formation During Posthypoxic Reoxygenation. Circ Res. 1998 May 4, 1998;82(8):891-7.

50. Kwon SH, Pimentel DR, Remondino A, Sawyer DB, Colucci WS. H2O2 regulates cardiac myocyte phenotype via concentration-dependent activation of distinct kinase pathways. Journal of Molecular and Cellular Cardiology. 2003;35(6):615-21.

51. Li J-M, Gall NP, Grieve DJ, Chen M, Shah AM. Activation of NADPH Oxidase During Progression of Cardiac Hypertrophy to Failure. Hypertension. 2002 October 1, 2002;40(4):477-84.

52. Date M-o, Morita T, Yamashita N, Nishida K, Yamaguchi O, Higuchi Y, et al. The antioxidant N-2-mercaptopropionyl glycine attenuates left ventricular hypertrophy in in vivo murine pressure-overload model. J Am Coll Cardiol. 2002 March 6, 2002;39(5):907-12.

53. Higuchi Y, Otsu K, Nishida K, Hirotani S, Nakayama H, Yamaguchi O, et al. Involvement of Reactive Oxygen Species-mediated NF- [kappa] B Activation in TNF- [alpha] -induced Cardiomyocyte Hypertrophy. Journal of Molecular and Cellular Cardiology. 2002;34(2):233-40.

54. Pimentel DR, Amin JK, Xiao L, Miller T, Viereck J, Oliver-Krasinski J, et al. Reactive Oxygen Species Mediate Amplitude-Dependent Hypertrophic and Apoptotic Responses to Mechanical Stretch in Cardiac Myocytes. Circ Res. 2001 August 31, 2001;89(5):453-60.

55. Nakamura K, Fushimi K, Kouchi H, Mihara K, Miyazaki M, Ohe T, et al. Inhibitory Effects of Antioxidants on Neonatal Rat Cardiac Myocyte Hypertrophy Induced by Tumor Necrosis Factor-{alpha} and Angiotensin II. Circulation. 1998 August 25, 1998;98(8):794-9.

56. Amin JK, Xiao L, Pimental DR, Pagano PJ, Singh K, Sawyer DB, et al. Reactive Oxygen Species Mediate Alpha-adrenergic Receptor-stimulated Hypertrophy in Adult Rat Ventricular Myocytes. Journal of Molecular and Cellular Cardiology. 2001;33(1):131-9.

57. Hunter JJ, Chien KR. Signaling Pathways for Cardiac Hypertrophy and Failure. N Engl J Med. 1999 October 21, 1999;341(17):1276-83.

58. Irani K. Oxidant Signaling in Vascular Cell Growth, Death, and Survival : A Review of the Roles of Reactive Oxygen Species in Smooth Muscle and Endothelial Cell Mitogenic and Apoptotic Signaling. Circ Res. 2000 August 4, 2000;87(3):179-83.

59. Sabri A HH, Lucchesi PA. Regulation of hypertrophic and apoptotic signaling pathways by reactive oxygen species in cardiac myocytes. Antioxid Redox Signal 2003 Dec;5(6):731-40.

60. Ghosh MC WX, Li S, Klee C. Regulation of calcineurin by oxidative stress. Methods Enzymol. 2003;366:289-304.

61. Buttke TM SP. Oxidative stress as a mediator of apoptosis. Immunol Today 1994 Jan;15(1):7-10.

62. von Harsdorf R, Li P-F, Dietz R. Signaling Pathways in Reactive Oxygen Species–Induced Cardiomyocyte Apoptosis. Circulation. 1999 June 8, 1999;99(22):2934-41.

63. MacLellan WR, Schneider MD. Death by Design : Programmed Cell Death in Cardiovascular Biology and Disease. Circ Res. 1997 August 19, 1997;81(2):137-44.

64. Haunstetter A, Izumo S. Apoptosis : Basic Mechanisms and Implications for Cardiovascular Disease. Circ Res. 1998 June 15, 1998;82(11):1111-29.

65. Veinot JP, Gattinger DA, Fliss H. Early apoptosis in human myocardial infarcts. Human Pathology. 1997;28(4):485-92.

66. Anversa P LP, Zhang X, Olivetti G, Capasso JM. Ischaemic myocardial injury and ventricular remodelling. Cardiovasc Res. 1993 Feb;27(2):145-57.

67. Antonio Abbate GGLB-ZAB. Pathophysiologic role of myocardial apoptosis in post-infarction left ventricular remodeling. Journal of Cellular Physiology. 2002;193(2):145-53.

68. Weber KT, Sun Y, Katwa LC, Cleutjens JP, Zhou G. Connective tissue and repair in the heart. Potential regulatory mechanisms. Ann NY Acad Sci. 1995 March 1, 1995;752(1):286-99.

69. Spinale FG, Coker ML, Bond BR, Zellner JL. Myocardial matrix degradation and metalloproteinase activation in the failing heart: a potential therapeutic target. Cardiovascular Research. 2000;46(2):225-38.

70. Nagase H, Woessner JF, Jr. Matrix Metalloproteinases. J Biol Chem. 1999 July 30, 1999;274(31):21491-4.

71. Rajagopalan S, Meng XP, Ramasamy S, Harrison DG, Galis ZS. Reactive Oxygen Species Produced by Macrophage-derived Foam Cells Regulate the Activity of Vascular Matrix Metalloproteinases In Vitro . Implications for Atherosclerotic Plaque Stability. J Clin Invest. 1996 December 1, 1996;98(11):2572-9.

72. Siwik DA, Pagano PJ, Colucci WS. Oxidative stress regulates collagen synthesis and matrix metalloproteinase activity in cardiac fibroblasts. Am J Physiol Cell Physiol. 2001 January 1, 2001;280(1):C53-60.

73. Inoue N, Takeshita S, Gao D, Ishida T, Kawashima S, Akita H, et al. Lysophosphatidylcholine increases the secretion of matrix metalloproteinase 2 through the activation of NADH/NADPH oxidase in cultured aortic endothelial cells. Atherosclerosis. 2001;155(1):45-52.

74. Grote K, Flach I, Luchtefeld M, Akin E, Holland SM, Drexler H, et al. Mechanical Stretch Enhances mRNA Expression and Proenzyme Release of Matrix Metalloproteinase-2 (MMP-2) via NAD(P)H Oxidase-Derived Reactive Oxygen Species. Circ Res. 2003 June 13, 2003;92(11):80e-6.

75. Coker ML, Thomas CV, Clair MJ, Hendrick JW, Krombach RS, Galis ZS, et al. Myocardial matrix metalloproteinase activity and abundance with congestive heart failure. Am J Physiol Heart Circ Physiol. 1998 May 1, 1998;274(5):H1516-23.

76. Thomas CV, Coker ML, Zellner JL, Handy JR, Crumbley AJ, III, Spinale FG. Increased Matrix Metalloproteinase Activity and Selective Upregulation in LV Myocardium From Patients With End-Stage Dilated Cardiomyopathy. Circulation. 1998 May 5, 1998;97(17):1708-15.

77. Li YY, Feldman AM, Sun Y, McTiernan CF. Differential Expression of Tissue Inhibitors of Metalloproteinases in the Failing Human Heart. Circulation. 1998 October 27, 1998;98(17):1728-34.

78. Spinale FG. Matrix Metalloproteinases: Regulation and Dysregulation in the Failing Heart. Circ Res. 2002 March 22, 2002;90(5):520-30.

79. Thom T, Haase N, Rosamond W, Howard VJ, Rumsfeld J, Manolio T, et al. Heart Disease and Stroke Statistics--2006 Update: A Report From the American Heart Association Statistics Committee and Stroke Statistics Subcommittee. Circulation. 2006 February 14, 2006;113(6):e85-151.

80. Biomarkers Definitions Working Group: Arthur J. Atkinson Jr MD WACP, MDS Victor G. DeGruttola ScD, David L. DeMets PhD, Gregory J. Downing DO, PhD, Daniel F. Hoth MD, John A. Oates MD, Carl C. Peck MD, Robert T. Schooley MD, Bert A. Spilker PhD, MD, Janet Woodcock MD and Scott L. Zeger PhD. Biomarkers and surrogate endpoints: Preferred definitions and conceptual framework. Clinical Pharmacology & Therapeutics. 2001;69:89–95.

81. Nick Fox JHG. Biomarkers and Surrogates. NeuroRx. 2004 April;1(2):181.

82. JS Alpert KT, E Antman, JP Bassand. Myocardial infarction redefined--A consensus document of The Joint European Society of Cardiology/American College of Cardiology Committee for the Redefinition of Myocardial Infarction. Eur Heart J. 2000 September 2, 2000;21(18):1502-13.

83. Daggubati S, Parks JR, Overton RM, Cintron G, Schocken DD, Vesely DL. Adrenomedullin, endothelin, neuropeptide Y, atrial, brain, and C-natriuretic prohormone peptides compared as early heart failure indicators. Cardiovascular Research. 1997;36(2):246-55.

84. Barrans JD, Allen PD, Stamatiou D, Dzau VJ, Liew C-C. Global Gene Expression Profiling of End-Stage Dilated Cardiomyopathy Using a Human Cardiovascular-Based cDNA Microarray. Am J Pathol. 2002 June 1, 2002;160(6):2035-43.

85. Boheler KR, Volkova M, Morrell C, Garg R, Zhu Y, Margulies K, et al. Sex- and age-dependent human transcriptome variability: Implications for chronic heart failure. PNAS. 2003 March 4, 2003;100(5):2754-9.

86. Kääb S, Barth AS, Margerie D, Dugas M, Gebauer M, Zwermann L, et al. Global gene expression in human myocardium—oligonucleotide microarray analysis of regional diversity and transcriptional regulation in heart failure. Journal of Molecular Medicine. 2004;V82(5):308-16.

87. Kittleson MM, Minhas KM, Irizarry RA, Ye SQ, Edness G, Breton E, et al. Gene expression in giant cell myocarditis: Altered expression of immune response genes. International Journal of Cardiology. 2005;102(2):333-40.

88. Steenman M, Chen YW, Le Cunff M, Lamirault G, Varro A, Hoffman E, et al. Transcriptomal analysis of failing and nonfailing human hearts. Physiol Genomics. 2003 January 15, 2003;12(2):97-112.

89. Steenman M, Lamirault G, Le Meur N, Le Cunff M, Escande D, Leger JJ. Distinct molecular portraits of human failing hearts identified by dedicated cDNA microarrays. European Journal of Heart Failure. 2005;7(2):157-65.

90. Tan F-L, Moravec CS, Li J, Apperson-Hansen C, McCarthy PM, Young JB, et al. The gene expression fingerprint of human heart failure. PNAS. 2002 August 20, 2002;99(17):11387-92.

91. Yung CK, Halperin VL, Tomaselli GF, Winslow RL. Gene expression profiles in end-stage human idiopathic dilated cardiomyopathy: altered expression of apoptotic and cytoskeletal genes. Genomics. 2004;83(2):281-97.

92. Hwang J-J, Allen PD, Tseng GC, Lam C-W, Fananapazir L, Dzau VJ, et al. Microarray gene expression profiles in dilated and hypertrophic cardiomyopathic end-stage heart failure. Physiol Genomics. 2002 July 12, 2002;10(1):31-44.

93. Blaxall BC, Tschannen-Moran BM, Milano CA, Koch WJ. Differential gene expression and genomic patient stratification following left ventricular assist device support. Journal of the American College of Cardiology. 2003;41(7):1096-106.

94. Chen MM, Ashley EA, Deng DXF, Tsalenko A, Deng A, Tabibiazar R, et al. Novel Role for the Potent Endogenous Inotrope Apelin in Human Cardiac Dysfunction. Circulation. 2003 September 23, 2003;108(12):1432-9.

95. Chen Y, Park S, Li Y, Missov E, Hou M, Han X, et al. Alterations of gene expression in failing myocardium following left ventricular assist device support. Physiol Genomics. 2003 August 15, 2003;14(3):251-60.

96. Hall JL, Grindle S, Han X, Fermin D, Park S, Chen Y, et al. Genomic profiling of the human heart before and after mechanical support with a ventricular assist device reveals alterations in vascular signaling networks. Physiol Genomics. 2004 May 19, 2004;17(3):283-91.

97. Kittleson MM, Minhas KM, Irizarry RA, Ye SQ, Edness G, Breton E, et al. Gene expression analysis of ischemic and nonischemic cardiomyopathy: shared and distinct genes in the development of heart failure. Physiol Genomics. 2005 May 11, 2005;21(3):299-307.

98. Margulies KB, Matiwala S, Cornejo C, Olsen H, Craven WA, Bednarik D. Mixed Messages: Transcription Patterns in Failing and Recovering Human Myocardium. Circ Res. 2005 March 18, 2005;96(5):592-9.

99. Anderson L. Candidate-based proteomics in the search for biomarkers of cardiovascular disease. J Physiol (Lond). 2005 February 15, 2005;563(1):23-60.

100. Stanley BA GR, Cotter RJ, Van Eyk JE. Heart disease, clinical proteomics and mass spectrometry. Dis Markers 2004;20(3):167-78.

101. Ping P. Identification of Novel Signaling Complexes by Functional Proteomics. Circ Res. 2003 October 3, 2003;93(7):595-603.

102. Klose J SH. Gel isoelectric focusing of mouse lactate dehydrogenase: heterogeneity of the isoenzymes A4 and X4. Biochem Genet 1975 Oct;13(9-10):707-20.

103. O'Farrell PZ, Goodman HM. Resolution of simian virus 40 proteins in whole cell extracts by two-dimensional electrophoresis: Heterogeneity of the major capsid protein. Cell. 1976;9(2):289-98.

104. Andersen JS, Lam YW, Leung AKL, Ong S-E, Lyon CE, Lamond AI, et al. Nucleolar proteome dynamics. Nature. 2005;433(7021):77-83.

105. Gramolini AO KT, Liu P, MacLennan DH, Emili A. . Analyzing the cardiac muscle proteome by liquid chromatography-mass spectrometry-based expression proteomics. Methods Mol Biol 2007;357:15-31.

106. Kislinger T, Rahman K, Radulovic D, Cox B, Rossant J, Emili A. PRISM, a Generic Large Scale Proteomic Investigation Strategy for Mammals. Mol Cell Proteomics. 2003 February 1, 2003;2(2):96-106.

107. Kislinger T EA. Going global: protein expression profiling using shotgun mass spectrometry. Curr Opin Mol Ther 2003 Jun;5(3):285-93.

108. Chen EI, Hewel J, Felding-Habermann B, Yates JR, III. Large Scale Protein Profiling by Combination of Protein Fractionation and Multidimensional Protein Identification Technology (MudPIT). Mol Cell Proteomics. 2006 January 1, 2006;5(1):53-6.

109. Koller A, Washburn MP, Lange BM, Andon NL, Deciu C, Haynes PA, et al. From the Cover: Proteomic survey of metabolic pathways in rice. PNAS. 2002 September 3, 2002;99(18):11969-74.

110. Le Roch KG, Johnson JR, Florens L, Zhou Y, Santrosyan A, Grainger M, et al. Global analysis of transcript and protein levels across the Plasmodium falciparum life cycle. Genome Res. 2004 November 1, 2004;14(11):2308-18.

111. Schirmer EC, Florens L, Guan T, Yates JR, III, Gerace L. Nuclear Membrane Proteins with Potential Disease Links Found by Subtractive Proteomics. Science. 2003 September 5, 2003;301(5638):1380-2.

112. Rodeheffer RJ. Measuring plasma B-type natriuretic peptide in heart failure: Good to go in 2004? Journal of the American College of Cardiology. 2004;44(4):740-9.

113. Hartmann F, Packer M, Coats AJS, Fowler MB, Krum H, Mohacsi P, et al. Prognostic Impact of Plasma N-Terminal Pro-Brain Natriuretic Peptide in Severe Chronic Congestive Heart Failure: A Substudy of the Carvedilol Prospective Randomized Cumulative Survival (COPERNICUS) Trial. Circulation. 2004 September 28, 2004;110(13):1780-6.

114. Gardner RS, Ozalp F, Murday AJ, Robb SD, McDonagh TA. N-terminal pro-brain natriuretic peptide: A new gold standard in predicting mortality in patients with advanced heart failure. Eur Heart J. 2003 October 1, 2003;24(19):1735-43.

115. Weber T AJ, Eber B. . The diagnostic and prognostic value of brain natriuretic peptide and aminoterminal (nt)-pro brain natriuretic peptide. Curr Pharm Des 2005;11(4):511-25.

116. Fisher C, Berry C, Blue L, Morton JJ, McMurray J. N-terminal pro B type natriuretic peptide, but not the new putative cardiac hormone relaxin, predicts prognosis in patients with chronic heart failure. Heart. 2003 August 1, 2003;89(8):879-81.

117. Ng LL GS, Jennings SC, Loke I, O'Brien RJ. . Diagnosis of heart failure using urinary natriuretic peptides. Clin Sci (Lond) 2004 Feb;106(2):129-33.

118. Winters CJ, Sallman AL, Baker BJ, Meadows J, Rico DM, Vesely DL. The N-terminus and a 4,000-MW peptide from the midportion of the N- terminus of the atrial natriuretic factor prohormone each circulate in humans and increase in congestive heart failure. Circulation. 1989 September 1, 1989;80(3):438-49.

119. Cohn JN LT, Olivari MT, Garberg V, Lura D, Francis GS, Simon AB, Rector T. . Plasma norepinephrine as a guide to prognosis in patients with chronic congestive heart failure. N Engl J Med 1984 Sep 27;311(13):819-23.

120. Benedict CR, Shelton B, Johnstone DE, Francis G, Greenberg B, Konstam M, et al. Prognostic Significance of Plasma Norepinephrine in Patients With Asymptomatic Left Ventricular Dysfunction. Circulation. 1996 August 15, 1996;94(4):690-7.

121. Anand IS, Fisher LD, Chiang Y-T, Latini R, Masson S, Maggioni AP, et al. Changes in Brain Natriuretic Peptide and Norepinephrine Over Time and Mortality and Morbidity in the Valsartan Heart Failure Trial (Val-HeFT). Circulation. 2003 March 11, 2003;107(9):1278-83.

122. Sato Y, Kataoka K, Matsumori A, Sasayama S, Yamada T, Ito H, et al. Measuring serum aminoterminal type III procollagen peptide, 7S domain of type IV collagen, and cardiac troponin T in patients with idiopathic dilated cardiomyopathy and secondary cardiomyopathy. Heart. 1997 November 1, 1997;78(5):505-8.

123. Setsuta K, Seino Y, Takahashi N, Ogawa T, Sasaki K, Harada A, et al. Clinical significance of elevated levels of cardiac troponin T in patients with chronic heart failure. The American Journal of Cardiology. 1999;84(5):608-11.

124. Perna ER, Macin SM, Parras JI, Pantich R, Farias EF, Badaracco JR, et al. Cardiac troponin T levels are associated with poor short- and long-term prognosis in patients with acute cardiogenic pulmonary edema. American Heart Journal. 2002;143(5):814-20.

125. Del Carlo CH, O'Connor CM. Cardiac troponins in congestive heart failure. American Heart Journal. 1999;138(4):646-53.

126. Hudson MP, O'Connor CM, Gattis WA, Tasissa G, Hasselblad V, Holleman CM, et al. Implications of elevated cardiac troponin t in ambulatory patients with heart failure: a prospective analysis. American Heart Journal. 2004;147(3):546-52.

127. Perna ER, Macin SM, Cimbaro Canella JP, Alvarenga PM, Rios NG, Pantich R, et al. Minor myocardial damage detected by troponin T is a powerful predictor of long-term prognosis in patients with acute decompensated heart failure. International Journal of Cardiology. 2005;99(2):253-61.

128. Sato Y, Taniguchi R, Nagai K, Makiyama T, Okada H, Yamada T, et al. Measurements of cardiac troponin T in patients with hypertrophic cardiomyopathy. Heart. 2003 June 1, 2003;89(6):659-60.

129. Missov E, Calzolari C, Pau B. Circulating Cardiac Troponin I in Severe Congestive Heart Failure. Circulation. 1997 November 4, 1997;96(9):2953-8.

130. Harrington D, Clark AL, Chua TP, Anker SD, Poole-Wilson PA, Coats AJS. Effect of reduced muscle bulk on the ventilatory response to exercise in chronic congestive heart failure secondary to idiopathic dilated and ischemic cardiomyopathy. The American Journal of Cardiology. 1997;80(1):90-3.

131. Horwich TB, Patel J, MacLellan WR, Fonarow GC. Cardiac Troponin I Is Associated With Impaired Hemodynamics, Progressive Left Ventricular Dysfunction, and Increased Mortality Rates in Advanced Heart Failure. Circulation. 2003 August 19, 2003;108(7):833-8.

132. Takeshi Niizeki YT, Takanori Arimoto, Tatsuya Takahashi, Hidenobu Okuyama, Noriaki Takabatake, Naoki Nozaki, Osamu Hirono, Yuichi Tsunoda, Tetsuro Shishido, Hiroki Takahashi, Yo Koyama, Akira Fukao and Isao Kubota. Combination of Heart-Type Fatty Acid Binding Protein and Brain Natriuretic Peptide Can Reliably Risk Stratify Patients Hospitalized for Chronic Heart Failure. Circ J. 2005;69(8):922-7.

133. Niizeki T TY, Arimoto T. Serum heart-type fatty acid binding protein predicts cardiac events in elderly patients with chronic heart failure. . J Cardiol. 2005;46(1):9–15.

134. Sugiura T, Takase H, Toriyama T, Goto T, Ueda R, Dohi Y. Circulating Levels of Myocardial Proteins Predict Future Deterioration of Congestive Heart Failure. Journal of Cardiac Failure. 2005;11(7):504-9.

135. Hansen MS, Stanton EB, Gawad Y, Packer M, Pitt B, Swedberg K, et al. Relation of circulating cardiac myosin light chain 1 isoform in stable severe congestive heart failure to survival and treatment with flosequinan. The American Journal of Cardiology. 2002;90(9):969-73.

136. George J, Patal S, Wexler D, Roth A, Sheps D, Keren G. Circulating matrix metalloproteinase-2 but not matrix metalloproteinase-3, matrix metalloproteinase-9, or tissue inhibitor of metalloproteinase-1 predicts outcome in patients with congestive heart failure. American Heart Journal. 2005;150(3):484-7.

137. Lubos E, Schnabel R, Rupprecht HJ, Bickel C, Messow CM, Prigge S, et al. Prognostic value of tissue inhibitor of metalloproteinase-1 for cardiovascular death among patients with cardiovascular disease: results from the AtheroGene study. Eur Heart J. 2006 January 2, 2006;27(2):150-6.

138. Spinale FG, Coker ML, Heung LJ, Bond BR, Gunasinghe HR, Etoh T, et al. A Matrix Metalloproteinase Induction/Activation System Exists in the Human Left Ventricular Myocardium and Is Upregulated in Heart Failure. Circulation. 2000 October 17, 2000;102(16):1944-9.

139. Sundstrom J, Evans JC, Benjamin EJ, Levy D, Larson MG, Sawyer DB, et al. Relations of plasma total TIMP-1 levels to cardiovascular risk factors and echocardiographic measures: the Framingham heart study. Eur Heart J. 2004 September 1, 2004;25(17):1509-16.

140. Vasan RS, Sullivan LM, Roubenoff R, Dinarello CA, Harris T, Benjamin EJ, et al. Inflammatory Markers and Risk of Heart Failure in Elderly Subjects Without Prior Myocardial Infarction: The Framingham Heart Study. Circulation. 2003 March 25, 2003;107(11):1486-91.

141. Cesari M, Penninx BWJH, Newman AB, Kritchevsky SB, Nicklas BJ, Sutton-Tyrrell K, et al. Inflammatory Markers and Onset of Cardiovascular Events: Results From the Health ABC Study. Circulation. 2003 November 11, 2003;108(19):2317-22.

142. Weinberg EO, Shimpo M, De Keulenaer GW, MacGillivray C, Tominaga S-i, Solomon SD, et al. Expression and Regulation of ST2, an Interleukin-1 Receptor Family

Member, in Cardiomyocytes and Myocardial Infarction. Circulation. 2002 November 11, 2002:01.CIR.0000038705.69871.D9.

143. Weinberg EO, Shimpo M, Hurwitz S, Tominaga S-i, Rouleau J-L, Lee RT. Identification of Serum Soluble ST2 Receptor as a Novel Heart Failure Biomarker. Circulation. 2003 February 11, 2003;107(5):721-6.

144. Limas CJ HC, Iakovou J, Kroupis C, Haidaroglou A, Cokkinos DV. . Prognostic significance of soluble interleukin-2 receptor levels in patients with dilated cardiomyopathy. Eur J Clin Invest 2003;33(6):443-8.

145. Van Kooten C BJ. CD40-CD40 ligand: a multifunctional receptor-ligand pair. Adv Immunol. 1996;61:1-77.

146. Wagner DH Jr SR, Suttles J. . Role of the CD40-CD40 ligand interaction in CD4+ T cell contact-dependent activation of monocyte interleukin-1 synthesis. Eur J Immunol 1994 Dec;24(12):3148-54.

147. Yin W-H, Chen J-W, Jen H-L, Chiang M-C, Huang W-P, Feng A-N, et al. The prognostic value of circulating soluble cell adhesion molecules in patients with chronic congestive heart failure. European Journal of Heart Failure. 2003;5(4):507-16.

148. Stumpf C, Lehner C, Eskafi S, Raaz D, Yilmaz A, Ropers S, et al. Enhanced levels of CD154 (CD40 ligand) on platelets in patients with chronic heart failure. European Journal of Heart Failure. 2003;5(5):629-37.

149. Hokamaki J, Kawano H, Yoshimura M, Soejima H, Miyamoto S, Kajiwara I, et al. Urinary biopyrrins levels are elevated in relation to severity of heart failure. J Am Coll Cardiol. 2004 May 19, 2004;43(10):1880-5.

150. Nonaka-Sarukawa M, Yamamoto K, Aoki H, Takano H, Katsuki T, Ikeda U, et al. Increased urinary 15-F2t-isoprostane concentrations in patients with non-ischaemic congestive heart failure: a marker of oxidative stress. Heart. 2003 August 1, 2003;89(8):871-4.

151. Jortani SA VRJ. Digoxin and its related endogenous factors. Crit Rev Clin Lab Sci 1997 Jun;34(3):225-74.

152. Balzan S, Neglia D, Ghione S, D'Urso G, Baldacchino MC, Montali U, et al. Increased circulating levels of ouabain-like factor in patients with asymptomatic left ventricular dysfunction. European Journal of Heart Failure. 2001;3(2):165-71.

153. Nagele H, Bahlo M, Klapdor R, Schaeperkoetter D, Rodiger W. CA 125 and its relation to cardiac function. American Heart Journal. 1999;137(6):1044-9.

154. Kouris NT, Zacharos ID, Kontogianni DD, Goranitou GS, Sifaki MD, Grassos HE, et al. The significance of CA125 levels in patients with chronic congestive heart failure. Correlation with clinical and echocardiographic parameters. European Journal of Heart Failure. 2005;7(2):199-203.

155. Ng LL, Loke IW, O'Brien RJ, Squire IB, Davies JE. Plasma urocortin in human systolic heart failure. Clin Sci. 2004 Apr , 2004;106(4):383-8.

156. Jougasaki M, Wei C-M, McKinley LJ, Burnett JC, Jr. Elevation of Circulating and Ventricular Adrenomedullin in Human Congestive Heart Failure. Circulation. 1995 August 1, 1995;92(3):286-9.

157. Nishikimi T, Saito Y, Kitamura K, Ishimitsu T, Eto T, Kangawa K, et al. Increased plasma levels of adrenomedullin in patients with heart failure. J Am Coll Cardiol. 1995 November 15, 1995;26(6):1424-31.

158. Nagaya N, Nishikimi T, Uematsu M, Yoshitomi Y, Miyao Y, Miyazaki S, et al. Plasma adrenomedullin as an indicator of prognosis after acute myocardial infarction. Heart. 1999 May 1, 1999;81(5):483-7.

159. S. TALWAR IBS, P. F. DOWNIE, R. J. O'BRIEN, J. E. DAVIES and L. L. NG. Elevated circulating cardiotrophin-1 in heart failure: relationship with parameters of left ventricular systolic dysfunction. Clinical Science 2000;99:83–8.

160. Mitrovic V. SIRIUS II: Safety and efficacy of an intravenous placebo controlled randomised infusion of ularitide in a prospective
double-blind study in patients with symptomatic, decompensated chronic heart failure. . Program and abstracts, European Society of Cardiology Congress, Stockholm,
Sweden 2005 September 3–7(Hot line I: Heart failure/cardiac function.).

161. Latini R, Masson S, Anand I, Salio M, Hester A, Judd D, et al. The comparative prognostic value of plasma neurohormones at baseline in patients with heart failure enrolled in Val-HeFT. Eur Heart J. 2004 February 2, 2004;25(4):292-9.

162. Lee DS, Vasan, R. S. . Novel markers for heart failure diagnosis and prognosis. . Current Opinion in Cardiology. 2005;20:201-10.

163. Dalle-Donne I, Rossi R, Colombo R, Giustarini D, Milzani A. Biomarkers of Oxidative Damage in Human Disease. Clin Chem. 2006 April 1, 2006;52(4):601-23.

164. Jenner P. Oxidative stress in Parkinson's disease. Annals of Neurology. 2003;53(S3):S26-S38.

165. Sayre LS, MA; Perry G. Chemistry and biochemistry of oxidative stress in neurodegenerative disease. Current medicinal chemistry. 2001 Jun;8(7):721-38.

166. Miller ER, III, Pastor-Barriuso R, Dalal D, Riemersma RA, Appel LJ, Guallar E. Meta-Analysis: High-Dosage Vitamin E Supplementation May Increase All-Cause Mortality. Ann Intern Med. 2005 January 4, 2005;142(1):37-46.

167. Florens L WM. Proteomic analysis by multidimensional protein identification technology. Methods Mol Biol 2006;328:159-75.

168. Paoletti AC, Zybailov B, Washburn MP. Principles and applications of Multidimensional Protein Identification Technology. Expert Review of Proteomics. 2004;1(3):275-82.

169. Mauri P, Scarpa A, Nascimbeni AC, Benazzi L, Parmagnani E, Mafficini A, et al. Identification of proteins released by pancreatic cancer cells by multidimensional protein identification technology: a strategy for identification of novel cancer markers. FASEB J. 2005 May 4, 2005:04-3000fje.

170. Washburn MP, Wolters D, Yates JR. Large-scale analysis of the yeast proteome by multidimensional protein identification technology. Nat Biotech. 2001;19(3):242-7.

171. Breci L HP. Two-dimensional nanoflow liquid chromatography-tandem mass spectrometry of proteins extracted from rice leaves and roots. Methods Mol Biol 2007;355:249-66.

172. HAYFLICK L. THE LIMITED IN VITRO LIFETIME OF HUMAN DIPLOID CELL STRAINS. Exp Cell Res 1965 Mar;37:614-36.

173. Cristofalo VJ, and Pignolo, R. J. . Replicative senescence of human fibroblast-like cells in culture. Physiol Rev. 1993;73:617–38.

174. Patil CK, Mian IS, Campisi J. The thorny path linking cellular senescence to organismal aging. Mechanisms of Ageing and Development. 2005;126(10):1040-5.

175. Campisi J. Senescent Cells, Tumor Suppression, and Organismal Aging: Good Citizens, Bad Neighbors. Cell. 2005;120(4):513-22.

176. Chen Q, and Ames, B. N. . Senescence-like growth arrest induced by hydrogen peroxide in human diploid fibroblast F65 cells. Proc Natl Acad Sci U S A. 1994; 91:4130–4.

177. Chen Q, Liu, J., and Merrett, J. . Apoptosis or senescence-like growth arrest: influence of cell cycle position, p53, p21 and bax in H2O2
response of normal human fibroblasts. Biochem J. 2000;347:543–51.

178. Chen Q, Prowse, K., Tu, V., and Linskens, M. , . Uncoupling the senescent phenotype from telomere shortening in oxidant-treated fibroblasts. Exp Cell Res. 2001;265:294–303.

179. Chen Q, Ames B. Senescence-Like Growth Arrest Induced by Hydrogen Peroxide in Human Diploid Fibroblast F65 Cells
10.1073/pnas.91.10.4130. PNAS. 1994 May 10, 1994;91(10):4130-4.

180. Xie L, Tsaprailis, G., Chen, Q. M. . Proteomic Identification of Insulin-like Growth Factor Binding Protein-6 Induced by Sublethal H2O2 Stress from Human Diploid Fibroblasts. Mol Cell Proteomics. 2005;4:1861-73.

181. CHEN QM. Replicative Senescence and Oxidant-Induced Premature Senescence: Beyond the Control of Cell Cycle Checkpoints. Ann NY Acad Sci. 2000 June 1, 2000;908(1):111-25.

182. Q M Chen JL, and J B Merrett. Apoptosis or senescence-like growth arrest: influence of cell-cycle position, p53, p21 and bax in H2O2 response of normal human fibroblasts. Biochem J 2000 April 15;347(Pt 2):543–51.

183. Shevchenko A, Wilm, M., Vorm, O., Mann, M. . Mass spectrometric sequencing of proteins silver-stained polyacrylamide gels. . Analytical Chemistry. 1996;68:850-8.

184. Andon NL, Hollingworth, S., Koller, A., Greenland, A. J., Yates, J. R., 3rd, Haynes, P. A. . Proteomic characterization of wheat amyloplasts using identification of proteins by tandem mass spectrometry. Proteomics. 2002;2:1156-68.

185. Andon NL ED, Yates JR, Haynes PA. High-throughput functional affinity purification of mannose binding proteins from Oryza sativa. PROTEOMICS. 2003 Jul;3(7):1270-8.

186. Yates JR 3rd EJ, McCormack AL, Schieltz D. Method to correlate tandem mass spectra of modified peptides to amino acid sequences in the protein database. Analytical Chemistry. 1995 Apr 15;67(8):1426-36.

187. Watts GS, Futscher BW, Isett R, Gleason-Guzman M, Kunkel MW, Salmon SE. cDNA Microarray Analysis of Multidrug Resistance: Doxorubicin Selection Produces Multiple Defects in Apoptosis Signaling Pathways. J Pharmacol Exp Ther. 2001 November 1, 2001;299(2):434-41.

188. Crowley-Weber CL, Payne CM, Gleason-Guzman M, Watts GS, Futscher B, Waltmire CN, et al. Development and molecular characterization of HCT-116 cell lines resistant to the tumor promoter and multiple stress-inducer, deoxycholate
10.1093/carcin/23.12.2063. Carcinogenesis. 2002 December 1, 2002;23(12):2063-80.

189. Tabb DL, McDonald WH, Yates JR. DTASelect and Contrast: Tools for Assembling and Comparing Protein Identifications from Shotgun Proteomics. J Proteome Res. 2002;1(1):21-6.

190. Mustacich D PG. Thioredoxin reductase. Biochem J. 2000 Feb 15;346 Pt 1:1-8.

191. Sen CK, Packer L. Antioxidant and redox regulation of gene transcription. FASEB J. 1996 May 1, 1996;10(7):709-20.

192. Coronella-Wood J, Terrand, J., Sun, H., Chen, Q. M. . c-Fos phosphorylation induced by H2O2 prevents proteasomal degradation of c-Fos in cardiomyocytes. . Journal of Biological Chemistry. 2004; 279:33567-74.

193. Purdom-Dickinson S, Lin, Y., Dedek, M., Johnson, J., Chen, Q. . Induction of Antioxidant and Detoxification Response by Oxidants in Cardiomyocytes: Evidence from Gene Expression Profiling and Activation of the Nrf2 Transcription Factor. J Mol Cell Biol. 2006:in press.

194. Becker K, Gromer S, Schirmer RH, Muller S. Thioredoxin reductase as a pathophysiological factor and drug target. Eur J Biochem. 2000 October 15, 2000;267(20):6118-25.

195. Arner ESJ, Holmgren A. Physiological functions of thioredoxin and thioredoxin reductase. Eur J Biochem. 2000 October 15, 2000;267(20):6102-9.

196. Casso D, Beach D, Casso D, Beach D. A mutation in a thioredoxin reductase homolog suppresses p53-induced growth inhibition in the fission yeastSchizosaccharomyces pombe. Molecular and General Genetics MGG. 1996;252(5):518-29.

197. Powis G, Kirkpatrick DL, Angulo M, Baker A. Thioredoxin redox control of cell growth and death and the effects of inhibitors. Chemico-Biological Interactions. 1998;111-112:23-34.

198. Wei SJ, Botero A, Hirota K, Bradbury CM, Markovina S, Laszlo A, et al. Thioredoxin Nuclear Translocation and Interaction with Redox Factor-1 Activates the Activator Protein-1 Transcription Factor in Response to Ionizing Radiation. Cancer Res. 2000 December 1, 2000;60(23):6688-95.

199. Karimpour S LJ, Lin LL, Rene LM, Lagunas L, Ma X, Karra S, Bradbury CM, Markovina S, Goswami PC, Spitz DR, Hirota K, Kalvakolanu DV, Yodoi J, Gius D. Thioredoxin reductase regulates AP-1 activity as well as thioredoxin nuclear localization via active cysteines in response to ionizing radiation. Oncogene. 2002 Sep 12;21(41):6317-27.

200. Hirota K, Matsui M, Iwata S, Nishiyama A, Mori K, Yodoi J. AP-1 transcriptional activity is regulated by a direct association between thioredoxin and Ref-1. PNAS. 1997 April 15, 1997;94(8):3633-8.

201. Schenk H, Klein M, Erdbrugger W, Droge W, Schulze-Osthoff K. Distinct Effects of Thioredoxin and Antioxidants on the Activation of Transcription Factors NF-{kappa}B and AP-1. PNAS. 1994 March 1, 1994;91(5):1672-6.

202. Tate DJ MM, Newsome DA. . Expression of metallothionein isoforms in human chorioretinal complex. Curr Eye Res 2002 Jan;24(1):12-25.

203. Dalton T, Palmiter RD, Andrews GK. Transcriptional induction of the mouse metallothionein-I gene in hydrogen peroxide-treated Hepa cells involves a composite major late transcription factor/antioxidant response element and metal response promoter elements. Nucl Acids Res. 1994 November 25, 1994;22(23):5016-23.

204. Andrews GK. Regulation of metallothionein gene expression by oxidative stress and metal ions. Biochemical Pharmacology. 2000;59(1):95-104.

205. Kang YJ. Metallothionein Redox Cycle and Function. Experimental Biology and Medicine. 2006 October 1, 2006;231(9):1459-67.

206. Sato M, Bremner I. Oxygen free radicals and metallothionein. Free Radical Biology and Medicine. 1993;14(3):325-37.

207. Smith RS, Smith TJ, Blieden TM, Phipps RP. Fibroblasts as sentinel cells. Synthesis of chemokines and regulation of inflammation. Am J Pathol. 1997 August 1, 1997;151(2):317-22.

208. Buckley CD, Pilling D, Lord JM, Akbar AN, Scheel-Toellner D, Salmon M. Fibroblasts regulate the switch from acute resolving to chronic persistent inflammation. Trends in Immunology. 2001;22(4):199-204.

209. Haddad JJ. Redox regulation of pro-inflammatory cytokines and I[kappa]B-[alpha]/NF-[kappa]B nuclear translocation and activation. Biochemical and Biophysical Research Communications. 2002;296(4):847-56.

210. Lander EL, LM; Birren, B; Nusbaum, C; Zody, MC; Baldwin, J; Devon, K; Dewar, K; Doyle, M; FitzHugh, W; Funke, R; Gage, D; Harris, K; Heaford, A; Howland, J; Kann, L; Lehoczky, J; LeVine, R; McEwan, P; McKernan, K; Meldrim, J; Mesirov, JP; Miranda, C; Morris, W; Naylor, J; Raymond, C; Rosetti, M; Santos, R; Sheridan, A; Sougnez, C; Stange-Thomann, N; Stojanovic, N; Subramanian, A; Wyman, D; Rogers, J; Sulston, J; Ainscough, R; Beck, S; Bentley, D; Burton, J; Clee, C; Carter, N; Coulson, A; Deadman, R; Deloukas, P; Dunham, A; Dunham, I; Durbin, R; French, L; Grafham, D;

Gregory, S; Hubbard, T; Humphray, S; Hunt, A; Jones, M; Lloyd, C; McMurray, A; Matthews, L; Mercer, S; Milne, S; Mullikin, JC; Mungall, A; Plumb, R; Ross, M; Shownkeen, R; Sims, S; Waterston, RH; Wilson, RK; Hillier, LW; McPherson, JD; Marra, MA; Mardis, ER; Fulton, LA; Chinwalla, AT; Pepin, KH; Gish, WR; Chissoe, SL; Wendl, MC; Delehaunty, KD; Miner, TL; Delehaunty, A; Kramer, JB; Cook, LL; Fulton, RS; Johnson, DL; Minx, PJ; Clifton, SW; Hawkins, T; Branscomb, E; Predki, P; Richardson, P; Wenning, S; Slezak, T; Doggett, N; Cheng, JF; Olsen, A; Lucas, S; Elkin, C; Uberbacher, E; Frazier, M; Gibbs, RA; Muzny, DM; Scherer, SE; Bouck, JB; Sodergren, EJ; Worley, KC; Rives, CM; Gorrell, JH; Metzker, ML; Naylor, SL; Kucherlapati, RS; Nelson, DL; Weinstock, GM; Sakaki, Y; Fujiyama, A; Hattori, M; Yada, T; Toyoda, A; Itoh, T; Kawagoe, C; Watanabe, H; Totoki, Y; Taylor, T; Weissenbach, J; Heilig, R; Saurin, W; Artiguenave, F; Brottier, P; Bruls, T; Pelletier, E; Robert, C; Wincker, P; Smith, DR; Doucette-Stamm, L; Rubenfield, M; Weinstock, K; Lee, HM; Dubois, J; Rosenthal, A; Platzer, M; Nyakatura, G; Taudien, S; Rump, A; Yang, H; Yu, J; Wang, J; Huang ,G; Gu, J; Hood, L; Rowen, L; Madan, A; Qin, S; Davis, RW; Federspiel, NA; Abola, AP; Proctor, MJ; Myers, RM; Schmutz, J; Dickson, M; Grimwood, J; Cox, DR; Olson, MV; Kaul, R; Raymond, C; Shimizu, N; Kawasaki, K; Minoshima, S; Evans, GA; Athanasiou, M; Schultz, R; Roe, BA; Chen, F; Pan, H; Ramser, J; Lehrach, H; Reinhardt, R; McCombie, WR; de la Bastide, M; Dedhia, N; Blocker, H; Hornischer, K; Nordsiek, G; Agarwala, R; Aravind, L; Bailey, JA; Bateman, A; Batzoglou, S; Birney, E; Bork, P; Brown, DG; Burge, CB; Cerutti, L; Chen, HC; Church, D; Clamp, M; Copley, RR; Doerks, T; Eddy, SR; Eichler, EE; Furey, TS; Galagan, J; Gilbert, JG; Harmon, C; Hayashizaki, Y; Haussler, D; Hermjakob, H; Hokamp, K; Jang, W; Johnson, LS; Jones, TA; Kasif, S; Kaspryzk, A; Kennedy, S; Kent, WJ; Kitts, P; Koonin, EV; Korf, I; Kulp, D; Lancet, D; Lowe, TM; McLysaght, A; Mikkelsen, T; Moran, JV; Mulder, N; Pollara, VJ; Ponting, CP; Schuler, G; Schultz, J; Slater, G; Smit, AF; Stupka, E; Szustakowski, J; Thierry-Mieg, D; Thierry-Mieg, J; Wagner, L; Wallis, J; Wheeler, R; Williams, A; Wolf, YI; Wolfe, KH; Yang, SP; Yeh, RF; Collins, F; Guyer, MS; Peterson, J; Felsenfeld, A; Wetterstrand, KA; Patrinos, A; Morgan, MJ; de Jong, P; Catanese, JJ; Osoegawa, K; Shizuya, H; Choi, S; Chen; YJ; International Human Genome Sequencing Consortium. Initial sequencing and analysis of the human genome. Nature. 2001;409(6822):860-921.

211. Venter JC, Adams MD, Myers EW, Li PW, Mural RJ, Sutton GG, et al. The Sequence of the Human Genome. Science. 2001 February 16, 2001;291(5507):1304-51.

212. Gebauer F, Hentze MW. MOLECULAR MECHANISMS OF TRANSLATIONAL CONTROL. Nature Reviews Molecular Cell Biology. 2004;5(10):827-35.

213. Merrick WC. Cap-dependent and cap-independent translation in eukaryotic systems. Gene. 2004;332:1-11.

214. Thomas Preiss MWH. Starting the protein synthesis machine: eukaryotic translation initiation. BioEssays. 2003;25(12):1201-11.

215. Holcik M, Sonenberg N. TRANSLATIONAL CONTROL IN STRESS AND APOPTOSIS. Nature Reviews Molecular Cell Biology. 2005;6(4):318-27.

216. Qian W-J, Jacobs JM, Liu T, Camp DG, II, Smith RD. Advances and Challenges in Liquid Chromatography-Mass Spectrometry-based Proteomics Profiling for Clinical Applications. Mol Cell Proteomics. 2006 October 1, 2006;5(10):1727-44.

217. Joerg Reinders ULJMYWAS. Challenges in mass spectrometry-based proteomics. PROTEOMICS. 2004;4(12):3686-703.

218. Smith R. Trends in mass spectrometry instrumentation for proteomics. Trends Biotechnol 2002 Dec;20(12 Suppl):S3-7.

219. Motoyama A, Venable JD, Ruse CI, Yates JR. Automated Ultra-High-Pressure Multidimensional Protein Identification Technology (UHP-MudPIT) for Improved Peptide Identification of Proteomic Samples. Anal Chem. 2006;78(14):5109-18.

220. Campisi J. Aging and cancer: the double-edged sword of replicative senescence. . J Am Geriatr Soc. 1997;45:482–8.

221. Campisi J. The role of cellular senescence in skin aging. Journal of Investigative Dermatology Symposium Proceedings. 1998;3(1):1-5.

222. Saad MJ, Velloso, L. A., and Carvalho, C. R. . Angiotensin II induces tyrosine phosphorylation of insulin receptor substrate 1 and its association with phosphatidylinositol 3-kinase in rat heart. Biochem J. 1995;310:741–4.

223. Shelton DN, Change, E., Whittier, P. S., Choi, D., and Funk, W. D. , . Microarray analysis of replicative senescence. Curr Biol. 1999;9:939–45.

224. Campisi J. Cancer and ageing: rival demons? Nat Rev Cancer. 2003; 3:339–49.

225. Krtolica A, Parrinello, S., Lockett, S., Desprez, P. Y., and Campisi, J., . Senescent fibroblasts promote epithelial cell growth and tumorigenesis: a link between cancer and aging. Proc Natl Acad Sci U S A. 2001;98:12072–7.

226. Fusenig NE, and Boukamp, P. . Multiple stages and genetic alterations in immortalization, malignant transformation, and tumor progression of human skin keratinocytes. Mol Carcinog. 1998;23:144–58.

227. Olumi AF, Grossfeld, G. D., Hayward, S. W., Carroll, P. R., Tlsty, T. D.,, and Cunha GR. Carcinoma-associated fibroblasts direct tumor progression of initiated human prostatic epithelium. . Cancer Res. 1999;59:5002–11.

228. Rinehart CA, and Torti, V. R. . Aging and cancer: the role of stromal interactions with epithelial cells. . Mol Carcinog. 1997;18:187–92.

229. DePinho RA. The age of cancer. Nature 2000;408:248–54.

230. Smith JR, and Pereira, S. O. . Replicative senescence: implications for in vivo aging and tumor suppression. Science. 1996;273:63–7.

231. Chen QM, Bartholomew, J. C., Campisi, J., Acosta, M., Reagan, J. D.,, and Ames BN. Molecular analysis of H2O2-induced senescentlike growth arrest in normal human fibroblasts: p53 and Rb control G1
arrest but not cell replication. Biochem J 1998;332:43–50.

232. Chen Q, Liu J, Merrett J. Apoptosis or Senescence-Like Growth Arrest: Influence of Cell Cycle Position, p53, p21 and bax in H2O2 Response of Normal Human Fibroblasts. Biochem J. 2000;347:543-51.

233. Chen QM. Replicative Senescence and Oxidant Induced Premature Senescence: Beyond the Control of Cell Cycle Checkpoints. Ann N Y Acad Sci. 2000;908:111-25.

234. Chen QM, Tu VC, Catania J, Burton M, Toussaint O, Dilley T. Involvement of Rb family proteins, Focal Adhesion Proteins and De Novo Protein Synthesis in Senescent Morphogenesis Induced by Hydrogen Peroxide. J Cell Science. 2000;113:4087-97.

235. Beckman KB, Ames BN. The free radical theory of aging matures. Physiological Reviews. 1998;78(2):547-81.

236. Golden TR, Hinerfeld, D. A., and Melov, S. . Oxidative stress and aging: beyond correlation. Aging Cell. 2002;1:117–23.

237. Cadenas E, and Davies, K. J. . Mitochondrial free radical generation, oxidative stress, and aging. Free Radic Biol Med. 2000;29:222–30.

238. Sohal RS, Mockett, R. J., and Orr, W. C. . Mechanisms of aging: an appraisal of the oxidative stress hypothesis. Free Radic Biol Med. 2002;33:575–86.

239. Dilley TK, Bowden, G. T., and Chen, Q. M. . Novel mechanisms of sublethal oxidant toxicity: induction of premature senescence in human
fibroblasts confers tumor promoter activity. . Exp Cell Res. 2003;290:38–48.

240. Yates JR, III Mass spectrometry and the age of the proteome. . J Mass Spectrom. 1998;33:1–19.

241. Liebler DC. Proteomic approaches to characterize protein modifications:new tools to study the effects of environmental exposures. Environ Health Perspect. 2002;110:3–9.

242. Pandey A, Mann, M. . Proteomics to study genes and genomes. . Nature 2000;405:837-46.

243. Yates JR, III , . Mass spectrometry. From genomics to proteomics. Trends Genet. 2000;16:5–8.

244. Yates JR, 3rd. . Mass spectral analysis in proteomics. Annual Review of Biophysics & Biomolecular Structure. 2004;33:297-316.

245. McDonald WH, Yates, J. R., 3rd. . Shotgun proteomics: integrating technologies to answer biological questions. . Current Opinion in Molecular Therapeutics. 2003;5:302-9.

246. Link AJ, Eng, J., Schieltz, D. M., Carmack, E., Mize, G. J., Morris, D. R., Garvik, B. M., Yates, J. R., 3rd. . Direct analysis of protein complexes using mass spectrometry. Nature Biotechnology. 1999;17:676-82.

247. Pasa-Tolic L, Harkewicz, R., Anderson, G. A., Tolic, N., Shen, Y., Zhao, R.,, Thrall B, Masselon, C., and Smith, R. D. , . Increased proteome coverage for quantitative peptide abundance measurements based upon
high performance separations and DREAMS FTICR mass spectrometry. J Am Soc Mass Spectrom. 2002;13:954–63.

248. Yates JR, III, Link, A. J., and Schieltz, D. . Direct analysis of proteins in mixtures. Application to protein complexes. . Methods Mol Biol. 2000;146:17–26.

249. Gygi SP, Rist, B., and Aebersold, R. . Measuring gene expression by quantitative proteome analysis. Curr Opin Biotechnol. 2000;11:396–401.

250. Sun X, Zhou, Z., Kang, Y. J. . Attenuation of doxorubicin chronic toxicity in metallothionein-overexpressing transgenic mouse heart. Cancer Research. 2001;61:3382-7.

251. Bach LA. Insulin-like growth factor binding protein-6: the “forgotten” binding protein? Horm Metab Res. 1999;31:226–34.

252. Bach LA, Thotakura, N. R., and Rechler, M. M. . Human insulin-like growth factor binding protein-6 is O-glycosylated. Biochem Biophys

Res Commun. 1992;186:301–7.

253. Dailly YP, Zhou, Y., Linkhart, T. A., Baylink, D. J., and Strong, D. D. , . Structure and characterization of the human insulin-like growth factor binding protein (IGFBP)-6 promoter: identification of a functional retinoid response element. Biochim Biophy Acta. 2001;1518:145–51.

254. Chambery D, De Galle, B., Ehrenborg, E., and Babajko, S. . Multihormonal regulation of IGFBP-6 expression in human neuroblastoma cells. Growth Horm IGF Res 2000;10:349–59.

255. Chen Y, Yu, P., Luo, J., Jiang, Y. . Secreted protein prediction system combining CJ-SPHMM, TMHMM, and PSORT. Mammalian Genome 2003;14:859-65.

256. Kratchmarova I, Kalume, D. E., Blagoev, B., Scherer, P. E., Podtelejnikov, A. V., Molina, H., Bickel, P. E., Andersen, J. S., Fernandez, M. M., Bunkenborg, J., Roepstorff, P., Kristiansen, K., Lodish, H. F., Mann, M., Pandey, A. . A proteomic approach for identification of secreted proteins during the differentiation of 3T3-L1 preadipocytes to adipocytes. Molecular & Cellular Proteomics. 2002;1:213-22.

257. Kubota K, Wakabayashi, K., Matsuoka, T. . Proteome analysis of secreted proteins during osteoclast differentiation using two different methods: two-dimensional electrophoresis and isotope-coded affinity tags analysis with two-dimensional chromatography. Proteomics 2003;3:616-26.

258. Wolters DA, Washburn, M. P., Yates, J. R., 3rd. . An automated multidimensional protein identification technology for shotgun proteomics. . Analytical Chemistry. 2001;73:5683-90.

259. Van Doorn J, Ringeling, A. M., Shmueli, S. S., Kuijpers, M. C., Hokken-, Koelega AC, van Buul-Offers, S. C., and Jansen, M. . Circulating levels of human insulin-like growth factor binding protein-6 (IGFBP-6) in health and disease as determined by radioimmunoassay. Clin Endocrinol. 1999;50:601–9

260. Hwa V, Oh, Y., and Rosenfeld, R. G. . The insulin-like growth factorbinding protein (IGFBP) superfamily. Endocr Rev. 1999;20:761–87.

261. Kelley KM, Schmidt, K. E., Berg, L., Sak, K., Galima, M. M., Gillespie, C.,, Balogh L, Hawayek, A., Reyes, J. A., and Jamison, M. . Comparative endocrinology of the insulin-like growth factor-binding protein. J Endocrinol 2002;175:3–18.

262. Marinaro JA, Neumann, G., Russo, V., Leeding, K., and Bach, L. A. , . O-glycosylation of insulin-like growth factor (IGF) binding protein-6 maintains high IGF-II

binding affinity by decreasing binding to glycosaminoglycans and susceptibility to proteolysis. Eur J Biochem. 2000;267:5378–86.

263. Drivdahl RH, Loop, S. M., Andress, D. L., and Ostenson, R. C. . IGF-binding proteins in human prostate: expression and regulation by 1,25-dihydroxyvitamin D3. Prostate 1995; 26:72–9

264. Park JH, Lee, S. W., Kim, I. T., Shin, B. S., Cheong, S. W., Cho, U. H., Huh, M. J., and Oh, G. S. . TCDD-up-regulation of IGFBP-6 and IL-5R α subunit genes in vivo and in vitro. Molecules Cells. 2001 12:372–9.

265. Martin JL, Coverley, J. A., and Baxter, R. C. . Regulation of immunoreactive insulin-like growth factor binding protein-6 in normal and transformed human fibroblasts. J Biol Chem. 1994;269:11470–7.

266. Sueoka N, Lee, H.-Y., Wiehle, S., Cristiano, R. J., Fang, B., Ji, L., Roth,, J. A. H, W. K., Cohen, P., and Kurie, J. M. . Insulin-like growth factor binding protein-6 activates programmed cell death in non-small cell lung cancer cells. . Oncogene. 2000;19:4432–6.

267. Park JH, Hahn, E. J., Kong, J. H., Cho, H. J., Yoon, C. S., Cheong, S. W.,, Oh GS, and Youn, H. J. . TCDD-induced apoptosis in EL-4 cells deficient of the aryl hydrocarbon receptor and down-regulation of IGFBP-
6 prevented the apoptotic cell death. Toxicol Lett. 2003;145:55–68.

268. Kim EJ, Schaffer, B. S., Kang, Y. H., Macdonald, R. G., and Park, J. H., . Decreased production of insulin-like growth factor-binding protein (IGFBP)-6 by transfection of colon cancer cells with an antisense IGFBP-6 cDNA construct leads to stimulation of cell proliferation. J Gastroenterol Hepatol. 2002; 17: 563–70.

269. Thom T, Haase N, Rosamond W, Howard VJ, Rumsfeld J, Manolio T, et al. Heart disease and stroke statistics--2006 update: a report from the American Heart Association Statistics Committee and Stroke Statistics Subcommittee. Circulation. 2006;113(6):14.

270. Dhalla AK, Hill MF, Singal PK. Role of oxidative stress in transition of hypertrophy to heart failure. Journal of the American College of Cardiology. 1996;28(2):506-14.

271. Hoeschen R. Oxidative stress and cardiovascular disease. Can J Cardiol. 1997 Nov;13(11):1021-5.

272. Nakamura K, Kusano KF, Matsubara H, Nakamura Y, Miura A, Nishii N, et al. Relationship Between Oxidative Stress and Systolic Dysfunction in Patients With Hypertrophic Cardiomyopathy. Journal of Cardiac Failure. 2005;11(2):117-23.

273. Sawyer DB, Colucci WS. Mitochondrial Oxidative Stress in Heart Failure : "Oxygen Wastage" Revisited. Circ Res. 2000 February 4, 2000;86(2):119-20.

274. Inoue MS, Eisuke F.; Nishikawa Manabu; Park Ah-Mee; Kira Yukimi; Imada Isuke; Utsumi Kozo. Mitochondrial generation of reactive oxygen species and its role in aerobic life. . Current Medicinal Chemistry. 2003;10:2495-505.

275. Barth E, Stammler, G., Speiser, B., Schaper, J. . Ultrastructural quantitation of mitochondria and myofilaments in cardiac muscle from 10 different animal species including man. Journal of Molecular & Cellular Cardiology. 1992;24:669-81.

276. Purdom S, Chen, Q. M. . Epidermal growth factor receptor-dependent and -independent pathways in hydrogen peroxide-induced mitogen-activated protein kinase activation in cardiomyocytes and heart fibroblasts. Journal of Pharmacology & Experimental Therapeutics. 2005;312:1179-86.

277. Chen Q, Tu, V., Wu, Y., Bahl, J. . Hydrogen Peroxide Dose Dependent Induction of Cell Death or Hypertrophy in Cardiomyocytes. Arch Biochem Biophys. 2000;373:242-8.

278. Eng JK, McCormack, A. L., Yates, J. R. I. . An Approach to Correlate Tandem Mass Spectral Data of Peptides with Amino Acid Sequences in a Protein Database. J Am Soc Mass Spectrom. 1994;5:976-89.

279. Cooper B, Eckert, D., Andon, N. L., Yates, J. R., Haynes, P. A. . Investigative proteomics: identification of an unknown plant virus from infected plants using mass spectrometry. . Journal of the American Society for Mass Spectrometry. 2003;14:736-41.

280. Washburn MP, Wolters, D., Yates, J. R., 3rd. . Large-scale analysis of the yeast proteome by multidimensional protein identification technology. Nature Biotechnology 2001;19:242-7.

281. Tabb DL, McDonald, W. H., Yates, J. R., 3rd. . DTASelect and Contrast: tools for assembling and comparing protein identifications from shotgun proteomics. Journal of Proteome Research 2002;1:21-6.

282. Tu V, Chen, Q. . Distinct Roles of ERKs and p38 MAPK in Oxidant Induced Cardiomyocyte Hypertrophy. Cardiovasc Tox. 2003;3:119-33.

283. Michael LH, Entman, M. L., Hartley, C. J., Youker, K. A., Zhu, J., Hall, S. R., Hawkins, H. K., Berens, K., Ballantyne, C. M. . Myocardial ischemia and reperfusion: a murine model. . American Journal of Physiology 1995;269:H2147-54.

284. Tarnavski O, McMullen, J. R., Schinke, M., Nie, Q., Kong, S., Izumo, S. . Mouse cardiac surgery: comprehensive techniques for the generation of mouse models of human diseases and their application for genomic studies. . Physiological Genomics 2004;16:349-60.

285. Xie L, Tsaprailis G, Chen QM. Proteomic Identification of Insulin-like Growth Factor Binding Protein-6 Induced by Sublethal H2O2 Stress from Human Diploid Fibroblasts. Mol Cell Proteomics. 2005;4(9):1861-73.

286. Lee S-C, Stevens, T. L., Sandberg, S. M., Heublein, D. M., Nelson, S. M., Jougasaki, M., Redfield, M. M., Burnett, J., John C. . The potential of brain natriuretic peptide as a biomarker for New York Heart Association class during the outpatient treatment of heart failure. . Journal of Cardiac Failure. 2002;8:149-54.

287. Jortani SA, Prabhu, S. D., Valdes, R., Jr. . Strategies for Developing Biomarkers of Heart Failure. Clin Chem. 2004;50:265-78.

288. McDonagh TA, Robb, S. D., Murdoch, D. R., Morton, J. J., Ford, I., Morrison, C. E., Tunstall-Pedoe, H., McMurray, J. J., Dargie, H. J. . Biochemical detection of left-ventricular systolic dysfunction. . Lancet 1998;351:9-13.

289. Vesely DL. Atrial natriuretic hormones originating from the N-terminus of the atrial natriuretic factor prohormone. Clinical & Experimental Pharmacology & Physiology. 1995;22:108-14.

290. Rosenzweig A, Seidman, C. E. . Atrial natriuretic factor and related peptide hormones. Annual Review of Biochemistry. 1991;60:229-55.

291. Keizer HG, Pinedo, H. M., Schuurhuis, G. J., Joenje, H. . Doxorubicin (adriamycin): a critical review of free radical-dependent mechanisms of cytotoxicity. Pharmacology & Therapeutics. 1990;47:219-31.

292. Singal PK, Li, T., Kumar, D., Danelisen, I., Iliskovic, N. . Adriamycin-induced heart failure: mechanism and modulation. Molecular & Cellular Biochemistry. 2000;207:77-86.

293. Chen Q, Alexander, D., Sun, H., Xie, L., Lin, Y., Terrand, J., Morrissy, S., Purdom, S. . Corticosteroids Inhibit Cell Death Induced by Doxorubicin in Cardiomyocytes: Induction of Anti-apoptosis, Antioxidant and Detoxification Genes. Mol Pharm. 2005;67:1861-73.

294. Wallace KB. Doxorubicin-induced cardiac mitochondrionopathy. Pharmacology & Toxicology. 2003;93:105-15.

295. Grill HP, Zweier, J. L., Kuppusamy, P., Weisfeldt, M. L., Flaherty, J. T. . Direct measurement of myocardial free radical generation in an in vivo model: effects of postischemic reperfusion and treatment with human recombinant superoxide dismutase. Journal of the American College of Cardiology. 1992;20:1604-11.

296. Newman DJ. Cystatin C. . Annals of Clinical Biochemistry. 2002;39:89-104.

297. Brown WM, Dziegielewska, K. M. . Friends and relations of the cystatin superfamily--new members and their evolution. . Protein Science. 1997;6:5-12.

298. Abrahamson M, Olafsson, I., Palsdottir, A., Ulvsback, M., Lundwall, A., Jensson, O., Grubb, A. . Structure and expression of the human cystatin C gene. Biochemical Journal. 1990;268:287-94.

299. Cole T, Dickson, P. W., Esnard, F., Averill, S., Risbridger, G. P., Gauthier, F., Schreiber, G. . The cDNA structure and expression analysis of the genes for the cysteine proteinase inhibitor cystatin C and for beta 2-microglobulin in rat brain. European Journal of Biochemistry. 1989;186:35-42.

300. Barka T, van der Noen, H. . Expression of the cysteine proteinase inhibitor cystatin C gene in rat heart: use of digoxigenin-labeled probes generated by polymerase chain reaction directly for in situ and northern blot hybridizations. . Journal of Histochemistry & Cytochemistry. 1993;41:1863-7.

301. Tavera C, Prevot D, Girolami JP, Leung-Tack J, Colle A. Tissue and biological fluid distribution of cysteine proteinases inhibitor: rat cystatin C. Biological Chemistry Hoppe Seyler. 1990;371:187-92.

302. Mussap M, Plebani, M. . Biochemistry and clinical role of human cystatin C. Critical Reviews in Clinical Laboratory Sciences. 2004;41:467-550.

303. Anastasi A, Brown, M. A., Kembhavi, A. A., Nicklin, M. J., Sayers, C. A., Sunter, D. C., Barrett, A. J. . Cystatin, a protein inhibitor of cysteine proteinases. Improved purification from egg white, characterization, and detection in chicken serum. . Biochemical Journal. 1983;211:129-38.

304. Mason RW, Sol-Church, K., Abrahamson, M. . Amino acid substitutions in the N-terminal segment of cystatin C create selective protein inhibitors of lysosomal cysteine proteinases. . Biochemical Journal. 1998;330:833-8.

305. Sukhova GK, Wang, B., Libby, P., Pan, J. H., Zhang, Y., Grubb, A., Fang, K., Chapman, H. A., Shi, G. P. . Cystatin C deficiency increases elastic lamina degradation and aortic dilatation in apolipoprotein E-null mice. Circulation Research. 2005;96:368-75.

306. Shi GP, Sukhova GK, Grubb A, Ducharme A, Rhode LH, Lee RT, et al. Cystatin C deficiency in human atherosclerosis and aortic aneurysms.[see comment]. Journal of Clinical Investigation. 1999;104(9):1191-7.

307. Bengtsson E, To, F., Hakansson, K., Grubb, A., Branen, L., Nilsson, J., Jovinge, S. . Lack of the cysteine protease inhibitor cystatin C promotes atherosclerosis in apolipoprotein E-deficient mice. Arteriosclerosis, Thrombosis & Vascular Biology. 2005; 25:2151-6.

308. Eriksson P, Deguchi, H., Samnegard, A., Lundman, P., Boquist, S., Tornvall, P., Ericsson, C. G., Bergstrand, L., Hansson, L. O., Ye, S., Hamsten, A. . Human evidence that the cystatin C gene is implicated in focal progression of coronary artery disease. Arteriosclerosis, Thrombosis & Vascular Biology. 2004;24:551-7.

309. Sukhova GK, Zhang, Y., Pan, J. H., Wada, Y., Yamamoto, T., Naito, M., Kodama, T., Tsimikas, S., Witztum, J. L., Lu, M. L., Sakara, Y., Chin, M. T., Libby, P., Shi, G. P. . Deficiency of cathepsin S reduces atherosclerosis in LDL receptor-deficient mice. Journal of Clinical Investigation. 2003;111:897-906.

310. Liu J, Sukhova, G. K., Yang, J. T., Sun, J., Ma, L., Ren, A., Xu, W. H., Fu, H., Dolganov, G. M., Hu, C., Libby, P., Shi, G. P. . Cathepsin L expression and regulation in human abdominal aortic aneurysm, atherosclerosis, and vascular cells. Atherosclerosis. 2006;184:302-11.

311. Arimoto TT, Yasuchika Niizeki, Takeshi Takabatake, Noriaki Okuyama, Hidenobu Fukui, Akio Tachibana, Hidetada Nozaki, Naoki Hirono, Osamu Tsunoda, Yuichi. Cystatin C, a Novel Measure of Renal Function, Is an Independent Predictor of Cardiac Events in Patients With Heart Failure. Journal of Cardiac Failure. 2005 2005/10;11(8):595-601.

312. Sarnak MJ, Katz R, Stehman-Breen CO, Fried LF, Jenny NS, Psaty BM, et al. Cystatin C concentration as a risk factor for heart failure in older adults. Annals of Internal Medicine. 2005;142(7):497-505.

313. Randers E, Erlandsen, E. J. . Serum cystatin C as an endogenous marker of the renal function--a review. . Clinical Chemistry & Laboratory Medicine. 1999;37:389-95.

314. Dworkin LD. Serum cystatin C as a marker of glomerular filtration rate. Current Opinion in Nephrology & Hypertension. 2001;10:551-3.

315. Reed CH. Diagnostic applications of cystatin C. . British Journal of Biomedical Science. 2000;57:323-9.

316. Dharnidharka VR, Kwon, C., Stevens, G. . Serum cystatin C is superior to serum creatinine as a marker of kidney function: a meta-analysis. American Journal of Kidney Diseases. 2002;40:221-6.

317. Munagala VK, Burnett, J. C., Jr., Redfield, M. M. . The natriuretic peptides in cardiovascular medicine. . Current Problems in Cardiology. 2004;29:707-69.

318. Finney HN, David J. Gruber, Walter Merle, Peter Price, Christopher P. . Initial evaluation of cystatin C measurement by particle-enhanced immunonephelometry on the Behring nephelometer systems (BNA, BN II). Clin Chem 1997;43:1016-22.

319. Chen Y, Yu P, Luo J, Jiang Y. Secreted protein prediction system combining CJ-SPHMM, TMHMM, and PSORT. Mammalian Genome. 2003;14(12):859-65.

320. Kratchmarova I, Kalume DE, Blagoev B, Scherer PE, Podtelejnikov AV, Molina H, et al. A proteomic approach for identification of secreted proteins during the differentiation of 3T3-L1 preadipocytes to adipocytes. Molecular & Cellular Proteomics. 2002;1(3):213-22.

321. Wolters DA, Washburn MP, Yates JR, 3rd. An automated multidimensional protein identification technology for shotgun proteomics. Analytical Chemistry. 2001;73(23):5683-90.

322. Yates JR, 3rd. Mass spectral analysis in proteomics. Annual Review of Biophysics & Biomolecular Structure. 2004;33:297-316.

323. Pandey A, Mann M. Proteomics to study genes and genomes. Nature. 2000;405(6788):837-46.

324. Brown RD, Ambler SK, Mitchell MD, Long CS. THE CARDIAC FIBROBLAST: Therapeutic Target in Myocardial Remodeling and Failure. Annual Review of Pharmacology and Toxicology. 2005;45(1):657-87.

325. Brad SB, Karl TW. Cardiac Fibrosis as a Cause of Diastolic Dysfunction. Herz. 2002;27(2):92-8.

326. Sackner-Bernstein J. The myocardial matrix and the development and progression of ventricular remodeling. Curr Cardiol Rep 2000 Mar;2(2):112-9.

327. Burlew BS WK. Connective tissue and the heart. Functional significance and regulatory mechanisms. Cardiol Clin 2000 Aug;18(3):435-42.

328. Weber KT PR, Janicki JS, Gadodia G, Lakier JB. Inadequate collagen tethers in dilated cardiopathy. Am Heart J 1988 Dec;116(6 Pt 1):1641-6.

329. Cleutjens JP, Verluyten MJ, Smiths JF, Daemen MJ. Collagen remodeling after myocardial infarction in the rat heart. Am J Pathol. 1995 August 1, 1995;147(2):325-38.

330. Kim HE, Dalal SS, Young E, Legato MJ, Weisfeldt ML, D'Armiento J. Disruption of the myocardial extracellular matrix leads to cardiac dysfunction. J Clin Invest. 2000 October 1, 2000;106(7):857-66.

331. Keller RS, Shai S-Y, Babbitt CJ, Pham CG, Solaro RJ, Valencik ML, et al. Disruption of Integrin Function in the Murine Myocardium Leads to Perinatal Lethality, Fibrosis, and Abnormal Cardiac Performance. Am J Pathol. 2001 March 1, 2001;158(3):1079-90.

332. Kato S, Spinale FG, Tanaka R, Johnson W, Cooper Gt, Zile MR. Inhibition of collagen cross-linking: effects on fibrillar collagen and ventricular diastolic function. Am J Physiol Heart Circ Physiol. 1995 September 1, 1995;269(3):H863-8.

333. Swynghedauw B. Molecular Mechanisms of Myocardial Remodeling. Physiol Rev. 1999 January 1, 1999;79(1):215-62.

334. Hani NS, Victor GS, Michael L, Sidney G. Progression of heart failure: A role for interstitial fibrosis. Molecular and Cellular Biochemistry. 1995;147(1):29-34.

335. Schnee JM, Hsueh WA. Angiotensin II, adhesion, and cardiac fibrosis. Cardiovascular Research. 2000;46(2):264-8.

336. Fedak PWM, Altamentova SM, Weisel RD, Nili N, Ohno N, Verma S, et al. Matrix remodeling in experimental and human heart failure: a possible regulatory role for TIMP-3. Am J Physiol Heart Circ Physiol. 2003 February 1, 2003;284(2):H626-34.

337. Peterson JT, Li H, Dillon L, Bryant JW. Evolution of matrix metalloprotease and tissue inhibitor expression during heart failure progression in the infarcted rat. Cardiovascular Research. 2000;46(2):307-15.

338. Ducharme A, Frantz S, Aikawa M, Rabkin E, Lindsey M, Rohde LE, et al. Targeted deletion of matrix metalloproteinase-9 attenuates left ventricular enlargement and collagen accumulation after experimental myocardial infarction. J Clin Invest. 2000 July 1, 2000;106(1):55-62.

339. Roten L, Nemoto S, Simsic J, Coker ML, Rao V, Baicu S, et al. Effects of Gene Deletion of the Tissue Inhibitor of the Matrix Metalloproteinase-type 1 (TIMP-1) on Left Ventricular Geometry and Function in Mice. Journal of Molecular and Cellular Cardiology. 2000;32(1):109-20.

340. Mort JS, Buttle DJ. Cathepsin B. The International Journal of Biochemistry & Cell Biology. 1997;29(5):715-20.

341. Buck MR KD, Day NA, Honn KV, Sloane BF. Degradation of extracellular-matrix proteins by human cathepsin B from normal and tumour tissues. Biochem J ;:. 1992 Feb 15;282 ((Pt 1)):273-8.

342. Sameni M MK, Sloane BF. . Imaging proteolysis by living human breast cancer cells. Neoplasia 2000 Nov-Dec;2(6):496-504.

343. Kobayashi H, Schmitt M, Goretzki L, Chucholowski N, Calvete J, Kramer M, et al. Cathepsin B efficiently activates the soluble and the tumor cell receptor-bound form of the proenzyme urokinase-type plasminogen activator (Pro-uPA). J Biol Chem. 1991 March 15, 1991;266(8):5147-52.

344. Yan S SM, Sloane BF. . Cathepsin B and human tumor progression. Biol Chem 1998 Feb;379(2):113-23.

345. Koblinski JE, Ahram M, Sloane BF. Unraveling the role of proteases in cancer. Clinica Chimica Acta. 2000;291(2):113-35.

346. Sohar N HH, Sohar I. Lysosomal peptidases and glycosidases in rheumatoid arthritis. Biol Chem ;():. 2002 May;383(5):865-9.

347. Baici A HD, Lang A, Merlin C, Kissling R. . Cathepsin B in osteoarthritis: zonal variation of enzyme activity in human femoral head cartilage. Ann Rheum Dis 1995 Apr;54(4):281-8.

348. Bjorck L, Akesson P, Bohus M, Trojnar J, Abrahamson M, Olafsson I, et al. Bacterial growth blocked by a synthetic peptide based on the structure of a human proteinase inhibitor. Nature. 1989;337(6205):385-6.

349. Marks N, Berg MJ, Makofske RC, Danho W. Synthetic domains of cystatins linked to enkephalins are novel inhibitors of brain cathepsins L/B. Peptides. 1990;11(4):679-82.

350. Shi GP, Sukhova, G. K., Grubb, A., Ducharme, A., Rhode, L. H., Lee, R. T., Ridker, P. M., Libby, P., Chapman, H. A. . Cystatin C deficiency in human atherosclerosis and aortic aneurysms.[see comment]. Journal of Clinical Investigation 1999;104:1191-7.

351. Bashey RI DM, Insinga F, Jimenez SA. Growth properties and biochemical characterization of collagens synthesized by adult rat heart fibroblasts in culture. J Mol Cell Cardiol 1992 Jul;24(7):691-700.

352. Villarreal FJ DW. Cardiac hypertrophy induced changes in mRNA levels for TGFb-1, fibronectin and collagens. Am J Physiol Cell Physiol. 1992;262:H1861–H6.

353. Scott-Burden T. Extracellular Matrix: The Cellular Environment. News Physiol Sci. 1994 June 1, 1994;9(3):110-5.

354. Kanekar S, Hirozanne T, Terracio L, Borg TK. Cardiac Fibroblasts: Form and Function. Cardiovascular Pathology. 1998;7(3):127-33.

355. Weber KT, Sun Y, Tyagi SC, Cleutjens JPM. Collagen Network of the Myocardium: Function, Structural Remodeling and Regulatory Mechanisms. Journal of Molecular and Cellular Cardiology. 1994;26(3):279-92.

356. Robert V, Silvestre J-S, Charlemagne D, Sabri A, Trouve P, Wassef M, et al. Biological Determinants of Aldosterone-Induced Cardiac Fibrosis in Rats. Hypertension. 1995 December 1, 1995;26(6):971-8.

357. Arimoto TT, Yasuchika Niizeki, Takeshi Takabatake, Noriaki Okuyama, Hidenobu Fukui, Akio Tachibana, Hidetada Nozaki, Naoki Hirono, Osamu Tsunoda, Yuichi. . Cystatin C, a Novel Measure of Renal Function, Is an Independent Predictor of Cardiac Events in Patients With Heart Failure. Journal of Cardiac Failure. 2005;11:595-601.

358. Sarnak MJ, Katz, R., Stehman-Breen, C. O., Fried, L. F., Jenny, N. S., Psaty, B. M., Newman, A. B., Siscovick, D., Shlipak, M. G., Cardiovascular Health, S. . Cystatin C concentration as a risk factor for heart failure in older adults. Annals of Internal Medicine. 2005;142:497-505.

359. Abrahamson M, Barrett AJ, Salvesen G, Grubb A. Isolation of six cysteine proteinase inhibitors from human urine. Their physicochemical and enzyme kinetic properties and concentrations in biological fluids. J Biol Chem. 1986 August 25, 1986;261(24):11282-9.

360. Barrett AJ, Davies ME, Grubb A. The place of human [gamma]-trace (cystatin C) amongst the cysteine proteinase inhibitors. Biochemical and Biophysical Research Communications. 1984;120(2):631-6.

361. Leung-Tack J, Tavera C, Gensac MC, Martinez J, Colle A. Modulation of phagocytosis-associated respiratory burst by human cystatin C: Role of the N-terminal tetrapeptide Lys---Pro---Pro---Arg. Experimental Cell Research. 1990;188(1):16-22.

362. Barrett AJ FH, Grubb A, Isemura S, Jarvinen M, Katunuma N, Machleidt W, Muller-Esterl W, Sasaki M, Turk V. . Nomenclature and classification of the proteins

homologous with the cysteine-proteinase inhibitor chicken cystatin. Biochem J 1986 May 15;236(1):312.

363. Weber KT, Brilla CG. Pathological hypertrophy and cardiac interstitium. Fibrosis and renin- angiotensin-aldosterone system. Circulation. 1991 June 1, 1991;83(6):1849-65.

364. Butt RP, Laurent GJ, Bishop JE. Mechanical Load and Polypeptide Growth Factors Stimulate Cardiac Fibroblast Activity. Annals of the New York Academy of Sciences. 1995;752(1):387-93.

365. Harada M, Itoh H, Nakagawa O, Ogawa Y, Miyamoto Y, Kuwahara K, et al. Significance of Ventricular Myocytes and Nonmyocytes Interaction During Cardiocyte Hypertrophy : Evidence for Endothelin-1 as a Paracrine Hypertrophic Factor From Cardiac Nonmyocytes. Circulation. 1997 November 18, 1997;96(10):3737-44.

366. Suresh C. Tyagi KL, Darius Pikes, Alton Marcello, Vibhas S. Mujumdar, Lane M. Smiley, Charles K. Moore. Stretch-induced membrane type matrix metalloproteinase and tissue plasminogen activator in cardiac fibroblast cells. Journal of Cellular Physiology. 1998;176(2):374-82.

367. Sarnak MJ, Katz R, Stehman-Breen CO, Fried LF, Jenny NS, Psaty BM, et al. Cystatin C Concentration as a Risk Factor for Heart Failure in Older Adults. Ann Intern Med. 2005 April 5, 2005;142(7):497-505.

368. Arimoto T, Takeishi Y, Niizeki T, Takabatake N, Okuyama H, Fukui A, et al. Cystatin C, a Novel Measure of Renal Function, Is an Independent Predictor of Cardiac Events in Patients With Heart Failure. Journal of Cardiac Failure. 2005;11(8):595-601.